

**Mechanisms, distribution, and subsurface implications
of clastic injectites**

Sarah Louise Cobain

Submitted in accordance with the requirements for the degree of
Doctor of Philosophy

The University of Leeds
School of Earth and Environment

June 2016

Declaration of Authorship

The candidate confirms that the work submitted is her own, except where work which has formed part of jointly-authored publications has been included. The contribution of the candidate and the other authors to this work has been explicitly indicated below. The candidate confirms that appropriate credit has been given within the thesis where reference has been made to the work of others.

The work in **Chapter 4** reproduces a manuscript that was published in *GSA Bulletin*.

Cobain, S. L., Peakall, J., and Hodgson, D. M. (2015) Indicators of propagation direction and relative depth in clastic injectites: Implications for laminar versus turbulent flow processes. *Geological Society of America Bulletin*, 127(11-12), 1816-1830.

Data were collected in the field by Sarah Cobain. All data were processed, interpreted, presented and the conceptual model designed by Sarah Cobain. Ideas were shaped and developed during discussion with co-authors.

This copy has been supplied on the understanding that it is copyright material and that no quotation from the thesis may be published without proper acknowledgement

© 2016 The University of Leeds and Sarah Louise Cobain

The right of Sarah Louise Cobain to be identified as Author of this work has been asserted by her in accordance with the Copyright, Designs and Patents Act 1988.

Acknowledgements

Firstly, I would like to express my sincere gratitude to my supervisors Dave Hodgson and Jeff Peakall for their continuous support, patience, motivation and enthusiasm over the years. I especially appreciate all the opportunities I was given during my PhD, fieldwork across several continents, attending conferences and field assisting.

I would like to express gratitude to the farmers in Laingsburg and Tanqua for allowing us access to their land, without them, fieldwork would not have been possible. I am very grateful to Michelle Shiers and Colleen Kurcinka who assisted me / embraced my insanity in the field.

Thanks also goes to the Petech team at Statoil for making Aberdeen feel like home; Simone Silcock, Pete McFadzean, Sven Østmo and Ruairidh Macdonald, you made me fall in love with the Granite City.

Many thanks go to my fellow Stratigraphy Group members (past and present): Emma Morris, Yvonne Spsychala, Menno Hofstra, Janet Richardson, Andrea Ortiz-Karpf, Hannah Brooks, Luz Gomis, Chris Stevenson, Bonita Barret-Crosdil, Miquel Poyatos More, Aurelia Privat. Thanks also to Michelle Shiers, Catherine Russell, and Cathy Burns. This incredible and diverse cohort of people has made my PhD experience one I will never forget, or possibly even top.

There is one place, that without which, many a lively discussion on paper edits would not have happened over the years: Fanny's ale house. More science than is possibly healthy has been debated over those tables.

So much thanks has to go to my flatmate of the last three years, Rachael, who was always there to provide a glass or bottle of wine when it was needed. And to my family, thanks for all your love and support, you've never once doubted I could do this.

And finally, to Ashley, I don't know how I would have gotten through these last two years without you. Your continuous support and love has been my anchor and I am eternally grateful.

This research was funded by a Natural Environment Research Council PhD studentship (Ref. number NE/J016950/1) with Statoil as a CASE partner.

Abstract

Understanding how clastic injectites form is important, as they are increasingly being recognised as significant components of sedimentary basin-fills, but are not predicted by standard sedimentary facies models. This study focuses on exhumed examples of injectites from the Karoo Basin, South Africa, and utilises a multidisciplinary approach to investigate clastic injectites across a variety of scales.

Small-scale analysis of injectites allows a classification of fracture patterns preserved on sill and dyke margins. These are used to interpret propagation direction through brittle, fine grained sediments under a laminar flow regime at depth in closed fracture networks. In contrast, shallow injectites, where they do not extrude, are identified by; fewer dykes, less stratigraphy crosscut, lower volume of injected material, and in some cases burrows on injectite margins—suggesting exploitation of injectite networks close to the surface.

These insights are applied to larger-scale (100s m to km) analysis, where extensive outcrop and well constrained paleogeography permits the injectite geometry to be related to parent sandstone facies and architecture. The influence of fluid flow pre-, syn- and post-injection is investigated across multiple scales. A model for the predictive distribution of injectites is proposed, which highlights the close association of basin-floor stratigraphic traps and sub-seismic clastic injectites. The outcrop data permits construction of forward seismic models demonstrate injectite architecture is scale invariant, which supports the use of outcrop-scale data in seismic-scale interpretations.

The integration of outcrop panels, well log data, forward seismic models and subsurface seismic sections has aided the identification of injectites in the subsurface and therefore the ability to discriminate between clastic injectites and parent sandbodies. The increased predictability in the location and character of injectites allows subsurface uncertainty in the impact of clastic injectites on hydrocarbon reservoirs to be reduced.

Thesis Structure

Title.....	i
Declaration of authorship.....	ii
Acknowledgements.....	iii
Abstract.....	iv
Table of Contents.....	v
List of Tables.....	x
List of Figures.....	xi
Nomenclature.....	xiv
Preface.....	xv

Table of Contents

1 Thesis context, significance and structure.....	1
1.1 Thesis rationale and objectives.....	1
1.2 Thesis structure.....	4
2 Outcrop and subsurface expression of clastic injectites.....	7
2.1 Introduction to clastic injectites	7
2.2 Components of a clastic injectite system	7
2.2.1 Parent body.....	8
2.2.2 Dykes.....	8
2.2.3 Sills	8
2.3 Internal and external sedimentary features	10
2.3.1 External	11
2.3.2 Internal.....	12
2.4 Comparison to igneous intrusions	13
2.5 Vertical exaggeration	14
2.6 Summary	15
3 Injectite formation: physical and forward modelling.....	16
3.1 Injectite formation	16
3.2 Physical modelling.....	16
3.2.1 Box modelling and flow dynamics	17
3.2.2 Fracture morphology and propagation.....	19
3.3 Forward modelling	23
3.4 Summary	24

4	Indicators of propagation direction and relative depth in clastic injectites: implications for laminar versus turbulent flow processes.....	25
4.1	Introduction.....	25
4.2	Sources of overpressure, trigger mechanisms, and fracture propagation: current understanding	26
4.3	Geological background	28
4.4	Recognition of injectites in the field.....	30
4.5	Methodology and dataset	31
4.6	External structures and morphology.....	34
4.6.1	Smooth surfaces	34
4.6.2	Blistered surfaces	35
4.6.3	Plumose ridges	35
4.6.4	Ridged margins	36
4.6.5	Mudstone clasts.....	38
4.6.6	Stepped sills.....	40
4.6.7	Summary of spatial distribution of injectite margin structures	40
4.7	Discussion	42
4.7.1	Determining injection propagation direction using margin structures.....	42
4.7.2	Estimating injection depth.....	44
4.7.3	Flow processes during injection	47
4.8	Conclusions.....	51
5.	An integrated model of clastic injectites and basin floor lobe complexes: implications for stratigraphic trap plays.....	53
5.1.	Introduction.....	53
5.2.	Geological Setting.....	54
5.3.	Methodology and dataset	55
5.4.	Outcrop data.....	57
5.4.1.	Bizansgat; Tanqua Depocentre.....	57
5.4.2.	Zoutkloof; Laingsburg Depocentre	62
5.4.3.	Slagtersfontein; Laingsburg Depocentre	66
5.4.4.	Comparison of study areas	68
5.5.	Discussion	69
5.5.1.	Injectite emplacement in the Karoo Basin: mechanisms and controls	69
5.5.2.	Possible trigger mechanisms	71
5.5.3.	An integrated model of injectites in basin-floor lobes.....	73

5.5.4.	Stages of fluid flow associated with injectites	76
5.5.5.	Implications for hydrocarbon extraction	79
5.6.	Conclusions	80
6.	Genesis and morphology of clastic injectites in a Palaeocene North Sea case study: constraints on parent sand and formative depth.....	81
6.1.	Introduction	81
6.2.	Geological setting.....	81
6.2.1.	Case study stratigraphy, North Sea.....	81
6.3.	Methodology.....	82
6.3.1.	Seismic mapping	82
6.4.	Results and analysis	85
6.4.1.	Seismic mapping	85
6.5.	Discussion.....	89
6.5.1.	Source of North Sea case study injectites.....	89
6.5.2.	Timing of Mariner injectites.....	91
6.5.3.	Implications for hydrocarbon exploration	91
6.6.	Conclusions	92
7.	Forward seismic modelling of exhumed clastic injectites: the importance of scale invariance	93
7.1.	Introduction	93
7.2.	Geological setting.....	94
7.2.1.	Karoo Basin, South Africa.....	94
7.3.	Methodology.....	95
7.3.1.	Outcrop	95
7.3.2.	Synthetic seismic.....	98
7.4.	Results and analysis	105
7.4.1.	Injectite morphologies	105
7.5.	Discussion.....	109
7.5.1.	Scale invariance and clastic injectites	109
7.5.2.	Implications for hydrocarbon exploration	110
7.6.	Conclusions	110
8.	Injecting life into the deep biosphere: a new macrofaunal limit	112
8.1.	Introduction	112
8.2.	Geological setting.....	113

8.3.	Outcrop observations	115
8.3.1.	Site 1: Unit E, Geelbeck.....	115
8.3.2.	Site 2: Unit D, Slagtersfontein West	116
8.3.3.	Site 3: Unit C, Slagtersfontein East	116
8.3.4.	Outcrop summary.....	117
8.4.	Interpretation	119
8.5.	Discussion	119
8.5.1.	Modelling survival times.....	120
8.5.2.	Model assumptions	120
8.5.3.	Implications	123
8.6.	Conclusions.....	126
9.	Mechanisms, distribution, and subsurface implications of clastic injectites: A synthesis	
	127	
9.1.	Introduction.....	127
9.2.	What are the physical differences in clastic injectites formed at shallow and deep burial depths, and at what depth does this transition occur?	128
9.2.1.	Near surface injectite architecture.....	128
9.2.2.	Shallow injectite architecture.....	132
9.2.3.	Deep injectite architecture	133
9.2.4.	Comparison of injectites as a function of depth	135
9.3.	What factors control injectite architecture?	137
9.3.1.	Large-scale controls.....	137
9.3.2.	Small-scale controls	146
9.3.3.	Fluid flow	147
9.3.4.	Depth as a control	150
9.4.	Are clastic injectites (palaeo-)geographically predictable in deep-marine settings?	151
9.4.1.	Slope injectites.....	151
9.4.2.	Lobe injectites.....	152
9.4.3.	Model.....	153
9.5.	What clastic injectite characteristics affect reservoir quality?	154
9.5.1.	Fluid flow pre-, syn-, and post-injection.....	154
9.5.2.	Four-way traps.....	156
9.5.3.	Sub-seismic predictability.....	156
9.5.4.	Sediment reworking and carbon reduction.....	156
9.6.	Conclusions.....	157

9.7. Suggestions for future research.....	158
Appendix A – Logs and Panels.....	186
Appendix B – Spreadsheet data.....	200

List of Tables

Table 4.1 Parameters used in order to calculate flow velocity and Reynolds number of fluid flow of clastic injections in the Karoo Basin.....	48
Table 4.2 Flow Reynolds numbers for grain concentrations of 54%, 47% and 40% in sill apertures ranging from 0.1 m to 1.3 m.....	50
Table 6.1 2D seismic profiles were taken at intervals of 50 m along both ILs and XLs for quantitative analysis of 14 bowl structures.....	88
Table 7.1 Final values used for sandstone when modelling in RokDoc. Values were taken from a brine filled sand in well 9/11A-6.....	101

List of Figures

Figure 1.1	Illustration to depict four data chapters and how each addresses the stated research questions.....	4
Figure 2.1	Common injectite geometries identified in both outcrop and seismic data.	9
Figure 2.2	Conical injectites showing characteristic V-shape from the Faroe-Shetland basin; arrows mark the top injectite	10
Figure 2.3	External features described on injectite margins.	11
Figure 2.4	A) Graded layering in clastic dyke. B) Banding from horizontal flow in injectite >15 m thick.....	12
Figure 2.5	Example of vertically exaggerated seismic section.....	15
Figure 3.1	Example of sand box model experiments.....	19
Figure 3.2	Types of fracture morphology	21
Figure 3.3	Various styles of plumose morphology.....	22
Figure 3.4	Example of forward seismic model.....	24
Figure 4.1	Plot of vertical and horizontal stress regimes in a tectonically relaxed basin....	26
Figure 4.2	Temporal development (time steps 1-4) of injectite fractures	27
Figure 4.3	Palaogeographic extent of the Paraná Basin and Karoo Basin in Gondwana during the Late Permian.....	29
Figure 4.4	Schematic sketch showing Karoo Basin as a retro arc foreland basin in front of the palaeo-Pacific plate subduction zone	29
Figure 4.5	A) GoogleEarth image of SW Karoo Basin. B) Summary log. C) Typical example of sill at outcrop. D) Typical example of small dyke and sills at outcrop.	30
Figure 4.6	Outcrop photo panel highlighting injectites between A5 and A6	32
Figure 4.7	Representative photographs depicting typical margin structures	33
Figure 4.8	A) Schematic block diagram depicting joint faces and features on a plumose fracture (adapted from Fossen, 2010). B) Three time phases depicting formation of a single plumose fracture. C) Three time phases depicting formation of parallel ridges with hackles...	37
Figure 4.9	A) Sill-to-dyke transition zone. B) Sill with an <i>in situ</i> mud clast.....	38
Figure 4.10	A) Three time phases showing the formation of a stepped sill as an injectite propagates. B) Schematic diagram showing spatial distribution of internal and external injectite structures.....	41
Figure 4.11	Recognition criteria for distinguishing between laminar and turbulent flow in clastic injectites.....	46
Figure 5.1	SW Karoo Basin with Tanqua and Laingsburg depocentres	56

Figure 5.2	Palaeogeography of Fan 3	58
Figure 5.3	Bizansgat outcrop – correlation panels and injectite margin structures	59
Figure 5.4	Bizansgat outcrop – injectite geometries and orientations.	60
Figure 5.5	A) Palaeogeography of subunit C1. B) Palaeogeography of subunit C2.....	64
Figure 5.6	Zoutkloof outcrop and injectites.	65
Figure 5.7	Slagtersfontein outcrop and injectites	67
Figure 5.8	Schematic diagram to indicate areas of injection in a deep marine system.....	74
Figure 5.9	Simplified map view illustrations of the orientation of parent sand and injectites at the three study sites.....	75
Figure 5.10	Fluid flow associated with stages of clastic injection	77
Figure 6.1	North Sea Basin showing present day distribution of Palaeocene-Lower Eocene sandstone in yellow.....	82
Figure 6.2	Mapped area of North Sea case study	83
Figure 6.3	Well log ties to seismic interpretation	86
Figure 6.4	Geometric properties and vertical position of the mapped sands	87
Figure 6.5	A) Section taken through bowls 8a and 8b in the case study area. B) Simplified interpretation of depleted parent sand and resultant injected sand.	89
Figure 6.6	Temporal model of parent sand depleting as injectites form	90
Figure 6.7	A) 3D reservoir modelling process for a single geological model (adapted from Bentley and Smith 2008). B) Same model with sub-seismic injectites providing vertical connectivity between reservoir units.....	92
Figure 7.1	Locality of Tanqua and Laingsburg depocentres, SW Karoo Basin.....	96
Figure 7.2	Outcrop panels used in forward seismic modelling with examples of outcrop expression of injectites.....	97
Figure 7.3	Initial test model of simple injectite geometries.....	99
Figure 7.4	A) and B) Well logs A and B used in forward modelling,	100
Figure 7.5	Same input: V-shaped cone fed by dyke, but varying the wavelet frequency and angle of offset.....	101
Figure 7.6	Initial models of outcrop panel Zoutkloof in RokDoc.....	102
Figure 7.7	Initial models of outcrop panel Geelbeck in RokDoc	103
Figure 7.8	Outcrop to RokDoc synthetic seismic workflow.....	104
Figure 7.9	Recognised injectite geometry types 1-6.	107
Figure 7.10	Recognised injectite morphotypes 1-6 in synthetic seismic	108
Figure 8.1	Location map of Laingsburg depocentre and outcrop sites 1-3, South Africa ..	113

Figure 8.2	Summary stratigraphic log of Laingsburg depocentre, letters A-G refer to Units A-G (Flint <i>et al.</i> , 2011).....	114
Figure 8.3	A) Cross-section panel for outcrop sites with several stratigraphic logs taken from South to North B) Example of typical bioturbation seen on the base of Unit E2 (see C). C) Outcrop photograph demonstrating how source sand connects to and feeds injectites, intruded into mudstone.....	115
Figure 8.4	Typical examples of bioturbation found on clastic injectite margins	117
Figure 8.5	Bioturbation examples from injectites related to Units C and D	118
Figure 8.6	Oxygen depletion graph.....	121
Figure 8.7	Model showing evolution of bioturbation from lobes to injectites.....	125
Figure 9.1	Near surface injectites.	130
Figure 9.2	Shallow injectites.	131
Figure 9.3	Plumose fracture patterns preserved on injectite margins	134
Figure 9.4	Deep injectites	136
Figure 9.5	Formation of conical injectites through time phases T1-3	141
Figure 9.6	Injectite feeder evolution for conical and wing-like injectites.	142
Figure 9.7	Two ways in which forced folding occurs due to injectite emplacement	144
Figure 9.8	Remobilisation and injection due to propagating polygonal faults.....	145
Figure 9.9	Small-scale controls on injectite propagation.	147
Figure 9.10	Fluid flow associated with stages of clastic injection	149
Figure 9.11	Simple model for how depth of injection impacts scale and geometry of injectites where principal stress is vertical.....	151
Figure 9.12	Schematic diagram to indicate likely sites of injection.....	154

Nomenclature

A fracture aperture (m)

g acceleration due to gravity (ms^{-2})

U velocity (ms^{-1})

$C_{D,o}$ drag coefficient for a solitary particle in relative motion with an infinite fluid (non-dimensional)

D_s clast diameter; the diameter of a sphere with the same volume as the particle (m)

D_p the diameter of a circle of the same area as the projected profile of the particle in its most stable orientation (m)

n an exponent, a function of particle shape

ϕ solid volume fraction

ρ density (kg m^{-3})

μ kinematic viscosity (Pa s)

Subscripts

s solid

f fluid

pf pseudo fluid

L larger particle

S small particle

Preface

This theses comprises four chapters that were prepared for publication in international peer-reviewed journals. At time of submission the status of the manuscripts is as follows:

Chapter 4: **Cobain, S.L.**, Peakall, J., Hodgson, D.M., 2015, Indicators of propagation direction and relative depth in clastic injectites: Implications for laminar versus flow processes. *GSA Bulletin*, 127, 1816-1830.

Author Contributions:

- Cobain, S.L. – Main author. Responsible for data collection, processing, collation and interpretation, and writing of the manuscript.
- Peakall, J. - In depth discussion and detailed review of the manuscript
- Hodgson, D.M. – In depth discussion and detailed review of the manuscript

Chapter 5: **Cobain, S.L.**, Hodgson, D.M., Peakall, J., Shiers, M.N., *Revise and resubmit*, A holistic model of clastic injectites and basin floor lobe complexes: implications for fluid flow. *Basin Research*.

Author Contributions:

- Cobain, S.L. – Main author. Responsible for data collection, processing, collation and interpretation, and writing of the manuscript.
- Hodgson, D.M. – In depth discussion and detailed review of the manuscript
- Peakall, J. – In depth discussion and detailed review of the manuscript
- Shiers, M.N. – Discussion and manuscript review

Chapter 6: **Cobain, S.L.**, Østmo, S., Silcock, S.Y., Hodgson, D.M., Peakall, J., *in review*, Forward seismic modelling of exhumed clastic intrusions to reduce uncertainty in Palaeogene injectites in the Northern North Sea: the importance of scale invariance. *Marine and Petroleum Geology*.

Author Contributions:

- Cobain, S.L. – Main author. Responsible for data collection, processing, collation and interpretation, and writing of the manuscript.
- Østmo, S. – Taught main author use of modelling software. Manuscript discussion.
- Silcock, S.Y. – In depth discussion of the manuscript and software limitations.
- Hodgson, D.M. – In depth discussion and detailed review of the manuscript
- Peakall, J. – Discussion and detailed manuscript revision

Chapter 7: **Cobain, S.L.**, Hodgson, D.M., Peakall, J., Wignall, P., Cobain, M.R.D., *in prep.* A new macrofaunal limit: injecting life into the deep biosphere. To be submitted to *Science*.

Author Contributions:

- Cobain, S.L. – Main author. Responsible for data collection, processing, collation and interpretation, and writing of the manuscript.
- Hodgson, D.M. – In depth discussion and detailed review of the manuscript
- Peakall, J. – In depth discussion and detailed review of the manuscript
- Wignall, P. – Discussion and manuscript review
- Cobain, M.R.D. – Equation analysis and discussion

“Hail hail to the good times, Cos rock has got the right of way”

-AC/DC

1 Thesis context, significance and structure

1.1 Thesis rationale and objectives

Exhumed sandstone dykes and sills, referred to generically as clastic injectites, have been reported from many outcrops (Hiscott, 1979; Archer, 1984; Keighley and Pickerill, 1994; Jonk *et al.*, 2003; Scott *et al.*, 2009; Kane, 2010; Ross *et al.*, 2014; Ito *et al.*, 2016; Hurst *et al.*, 2016). First recognised in the 19th century (Murchison, 1827; Diller, 1890; Woodworth, 1895) as small-scale features (10's m in length, <2 m in width), initially being regarded as a geological curiosity. Interest and understanding of clastic injectites has increased significantly over the last two decades, driven by their recognition in the subsurface as important, and frequently large-scale features (100s m to km), during exploration and production of hydrocarbon reservoirs. However, the relationship between small scale, sub-seismic injectite geometries and architectures, and seismic-scale examples remains poorly understood (Duranti and Hurst, 2004; Huuse *et al.*, 2007, 2010). This has led to an increase in outcrop investigations to better constrain the pre-requisite conditions, processes, and products of clastic injection. This in turn, has enhanced predictive geometric modelling, in addition to characterising physical properties of clastic injectite networks (Ravier *et al.*, 2015).

There are still many aspects of clastic injectite formation that are poorly understood. Research undertaken for this thesis aims to address the following questions, which are returned to and addressed in Chapter 8:

Question 1: *What are the physical differences in clastic injectites formed at shallow and deep burial depths, and at what depth does this transition occur?*

Rationale: Commonly, at outcrop or in seismic data the depth of injection is hard to resolve. Where injectites reach the surface it can be possible to give a definitive depth of burial prior to injection (Obermeier, 1998; Hurst *et al.*, 2006; Jonk *et al.*, 2007; Vigorito *et al.*, 2008; Ross *et al.*, 2013). However, when injectites do not reach the palaeosurface their depth of injection is more difficult to define. Clastic injectites are known to form different geometries when injected at shallow depths (Jolly and Lonergan, 2002; Duranti and Hurst, 2004; Jonk *et al.*, 2005b) or after deep burial (Jolly and Lonergan, 2002; Vigorito *et al.*, 2008; Vigorito and Hurst, 2010). The current “shallow” and “deep” injectite classifications are broad categories that overlap

substantially. For example, Duranti and Hurst (2004) define shallow as <100 m, whereas Jonk *et al.* (2005b) define shallow as <400 m.

Establishing recognition criteria for the identification of injectite morphology in both outcrop and seismic data, or of surface indicators at different depths, could help constrain the depth of burial at time of injection. This can be applied to improve understanding of the pre-requisite conditions and trigger mechanism prior to injection, and inform the likely rheology of the host rock during injection. Constraining the depth of burial prior to injection can also be used to build 4D fluid flow models in regards to timing in hydrocarbon exploration and production. The depth, and therefore timing, of injection is key to evaluating fluid flow pathways and reservoir charge.

Question 2: *What factors control injectite architecture?*

Rationale: The complexity and variation within and across injectite networks suggests more than one or two principal factors control injectite architecture (Parize and Friès, 2003; Jackson, 2007; Mourgues *et al.*, 2012; Cobain *et al.*, 2015; Wheatley, 2016). The processes involved in injectite emplacement have been of interest for over a century (Newsom, 1903; Jenkins, 1930), and more recently focus has been on the mechanisms that control both large and small-scale architecture types (Jolly and Lonergan, 2002; Gallo and Woods, 2004; Cartwright *et al.*, 2008; Ito *et al.*, 2016). Emphasis has been towards understanding the conditions required for hydraulic fracturing (Cosgrove, 2001; Jolly and Lonergan, 2002) and how a fluidised flow can fill the fracture and cause them to propagate (Cosgrove, 2001; Hurst and Cartwright, 2007; Hurst *et al.*, 2011). Other factors to have been postulated that control injectite architecture include: host rock rheology, and heterogeneity, the volume and architecture of the parent sand, the trigger mechanism, basin tectonic setting, fluid flow regime and pore fluid composition, grain size of fluidised material, and depth of injection.

Gaining a more comprehensive understanding of how different factors interact to control injectite architecture requires detailed analysis of intrinsic (e.g. flow type) and extrinsic (e.g. host lithology, tectonic stresses) influences, in addition to understanding small-scale factors (e.g. host strata heterogeneities during fracture propagation). Understanding these controls and how they ultimately affect injectite propagation and morphology brings us closer to understanding the formative process in clastic injection.

Question 3: *Are clastic injectites (palaeo-)geographically predictable in deep-marine settings?*

Rationale: Identification of clastic injectites in the subsurface can be challenging. Often, the resolution of seismic data is too low for individual injectites to be identified, or if dykes are steeply inclined then they may not be imaged (Jackson *et al.*, 2011). As a result, interpretation of injectites in the subsurface is biased toward large-scale intrusion complexes (Schwab *et al.*, 2015), often sourced from slope settings (Parize and Friès, 2003; Duranti and Hurst, 2004; Huuse *et al.*, 2005a; Diggs, 2007; Duranti, 2007; Frey-Martínez *et al.*, 2007; Hamberg *et al.*, 2007; Jackson, 2007; Jonk *et al.*, 2007; Surlyk *et al.*, 2007; Vigorito *et al.*, 2008; Kane, 2010; Svendsen *et al.*, 2010; Szarawarska *et al.*, 2010; Jackson *et al.*, 2011; Løseth *et al.*, 2013; Morton *et al.*, 2014). Yet those of a sub-seismic-scale may still have the potential to be laterally extensive for several km (Cobain *et al.*, 2015), and therefore impact reservoir quality and connectivity. Understanding how and why injectites form where they do would mean increased predictability on a sub-seismic-scale.

Using well constrained outcrop data to establish palaeogeographical settings, parent sand architecture and host stratigraphy for injectites in deep marine settings can permit a model to be developed to improve prediction for injectite distributions. This model could be used to help reduce uncertainty in the subsurface distribution of sub-seismic, and steep or bed-parallel injectites in different parts of basin-fills.

Question 4: *What clastic injectite characteristics affect reservoir quality?*

Rationale: It is widely acknowledged that clastic injectites can have major impacts on hydrocarbon exploration and development in deep-marine systems by forming fluid migration pathways (e.g. Dixon *et al.*, 1995; Jolly and Lonergan, 2002) or acting as reservoirs in their own right (Schwab *et al.*, 2015; Hurst *et al.*, 2016). Yet details, such as grain packing, pore-scale properties, post depositional reworking and volumetrics (Lonergan and Cartwright, 1999; Duranti *et al.*, 2002) are rarely investigated or included in the building of geocellular reservoir models. It is the smaller-scale details that, without core data, are absent from subsurface datasets. Application, therefore, of detailed outcrop analysis across a range of injectite geometries and known injection depths is crucial in analysing and building realistic subsurface reservoir models.

Figure 1.1 demonstrates how particular aspects of Chapters 4 – 7 address these research questions.

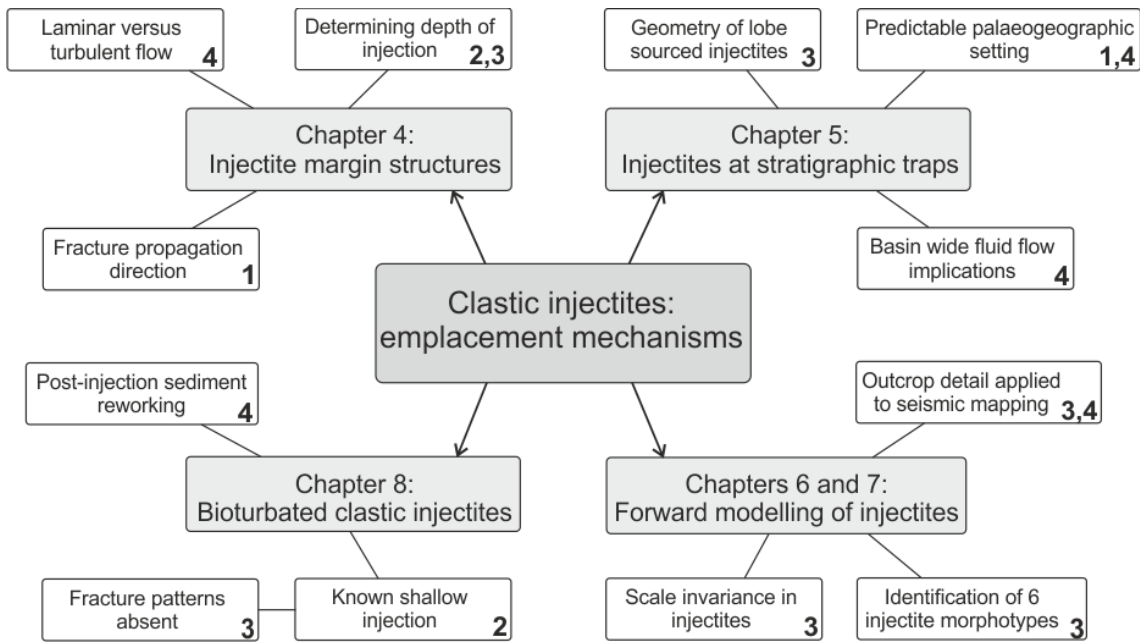


Figure 1.1 Illustration to depict four data chapters and how each addresses the stated research questions. Numbers in bold on lower right of boxes refer to research question number.

1.2 Thesis structure

This thesis begins with an introduction to clastic injectite expression at outcrop and in the subsurface and discusses similarities in geometry and architecture to igneous intrusions (Chapter 2). This is followed by a review of injectite formation, and physical and forward modelling (Chapter 3). Four subsequent chapters (Chapters 4-7) present results of independent research, each comprising individual rationale, discussion and conclusions, one of which is published, two are in review, and the final one is almost at submission stage. The thesis concludes with a synthesis of the mechanisms, distribution and subsurface implications of clastic injectites (Chapter 8) that addresses each research question posed in Section 1.1.

Chapter 2: *Outcrop and subsurface expression of clastic injectites.* This chapter summarises the components in clastic injectite networks including smaller-scale internal and external structures. The geometry of clastic injectites is then compared to that of igneous intrusions and the use of vertical exaggeration in subsurface data is explored.

Chapter 3: *Injectite formation: physical and forward modelling.* This chapter describes the process of injectite formation theory. Physical modelling of box injectite and fracture propagation is then described. Finally, the use of forward modelling of sedimentary outcrops in seismic interpretation and facies analysis is discussed.

Chapter 4: *Indicators of propagation direction and relative depth in clastic injectites: implications for laminar versus turbulent flow processes.* Published in GSA Bulletin. This chapter analyses surface features on the margins of clastic injectites in the Karoo Basin, South Africa to develop a model for injectite emplacement that considers fracture propagation mechanics as well as internal flow processes during injection.

Chapter 5: *A holistic model of clastic injectites and basin floor lobe complexes: implications for fluid flow.* Submitted to Basin Research. This chapter presents examples of injectites from the Laingsburg and Tanqua depocentres, Karoo Basin, South Africa. The architecture of injectites is characterised in relation to the palaeogeography of the parent sand units. This allows for a holistic model of clastic injectites in basin-floor settings to be presented with discussion on how basin-wide fluid flow is affected pre-, syn-, and post-injection.

Chapter 6: *Relationship between clastic injectites and parent sand depletion of Palaeocene sands in the Northern North Sea.* This chapter presents a North Sea case study example of clastic injectites, mapped using a high resolution broadband dataset, and associated potential area of depletion of the underlying source unit.

Chapter 7: *Forward seismic modelling of exhumed clastic injectites: the importance of scale invariance.* This chapter We use geometric data from exhumed injectites, and forward seismic modelling techniques, to assess to what degree injectites are scale invariant and to improve understanding of the complicated, and sometimes chaotic, expression of clastic injectites.

Chapter 8: *A new macrofaunal limit: injecting life into the deep biosphere.* In preparation for submission to Science. This chapter demonstrates that macrofauna lived in injectites several metres below the sediment surface at 3 separate outcrop sites in the Karoo Basin, South Africa. Conservative estimates are made for the length of time before oxygen depletion occurs in order to show plausibility of macrofauna survival post injection.

Chapter 9: *Mechanisms, distribution, and subsurface implications of clastic injectites: A synthesis.* This chapter provides an extended discussion that addresses the key research questions presented in Chapter 1. Findings from research presented in Chapters 4-7 are collated and synthesised to answer these questions.

2 Outcrop and subsurface expression of clastic injectites

2.1 Introduction to clastic injectites

The most commonly cited environment for injectites to occur at outcrop and in seismic are deep-marine settings (Jolly and Lonergan, 2000), and in particular deep-marine channel-fills and other deposits associated with submarine slope settings (Parize and Friès, 2003; Duranti and Hurst, 2004; Huuse *et al.*, 2005a; Diggs, 2007; Duranti, 2007; Frey-Martinez *et al.*, 2007; Hamberg *et al.*, 2007; Jackson *et al.*, 2007; Jonk *et al.*, 2007; Surlyk *et al.*, 2007; Vigorito *et al.*, 2008; Kane, 2010; Svendsen *et al.*, 2010; Szarawarska *et al.*, 2010; Jackson *et al.*, 2011; Løseth *et al.*, 2013; Monnier *et al.*, 2014; Morton *et al.*, 2014). However, they are also found in many other sedimentary environments such as lacustrine (Moretti and Sabato, 2007), sub-glacial deposits (e.g. Von Brunn and Talbot, 1986), shallow marine deposits (e.g. Boehm and Moore, 2002, Scott *et al.*, 2009), alluvial floodplains (e.g. Guhman and Pederson, 1992; Bezerra *et al.*, 2005), arid settings (Ross *et al.*, 2014) and many others.

2.2 Components of a clastic injectite system

Sand injectite complexes have 3 main components; 1) the primary depositional body or parent unit, 2) intrusive bodies including sills roughly concordant with bedding, and 3) dykes which crosscut stratigraphy, and may feed seabed extrusions (Vigorito *et al.*, 2008) (Fig. 2.1). Injectites have been documented across a wide range of scales from >1 km in length and 10s – 100s m thick, most often recognised in seismic (e.g. Dixon, 1995; Duranti and Hurst, 2004; Hurst *et al.*, 2005; Huuse *et al.*, 2004; Andresen *et al.*, 2009) to centimetre scale, seen in core and at outcrop (e.g. Keighley and Pickerill, 1994; Jonk *et al.*, 2003; Scott *et al.*, 2009; Kane, 2010). Larger intrusions, mainly identified in seismic sections, can cross-cut 100's m stratigraphy and may be laterally extensive for many kilometres. In contrast, those seen at outcrop are usually limited by the extent of the outcrop itself (Kane, 2010), which may be why they are usually only reported on a smaller scale. Few examples exist of seismic scale injection complexes at outcrop; those that do are possibly able to bridge the gap between the two (Surlyk *et al.*, 2007; Vigorito *et al.*, 2008; Vigorito and Hurst, 2010).

2.2.1 Parent body

Parent units are often sandbodies of a primary deposition that partially to completely liquefy, become fluidised and feed clastic injectites. The majority of studies on parent sand architecture are from subsurface data (Cartwright, 2010; Szarawarska *et al.*, 2010; Jackson *et al.*, 2011), although even in seismic data the parent sand may be difficult to identify where injectites are not in direct contact (Huuse *et al.*, 2005a). At outcrop, parent sands are often more difficult to constrain due to exposure (Surlyk *et al.*, 2007; Vigorito *et al.*, 2008; Kane, 2010).

2.2.2 Dykes

Dykes are discordant with host strata, can be of any scale from mm to 10s m thick and crosscut 100s m stratigraphy (Jonk *et al.*, 2003; Huuse *et al.*, 2005a; Szarawarska *et al.*, 2010), they are usually categorised into low (<20°) or high (>35°) angled (Hurst *et al.*, 2011). Dykes commonly bifurcate, taper and/or are ptymatically folded, which is widely considered to be due to post injection differential compaction (Hillier and Cosgrove, 2002; Hubbard *et al.*, 2007; Satur and Hurst, 2007), and larger dykes are often associated with deeper intrusions and often feed or terminate in sills (Jolly and Lonergan, 2002).

2.2.3 Sills

Sills are mainly concordant with bedding, occasionally stepping up and down stratigraphy (Truswell, 1972; Hiscott, 1979; Obermeier *et al.*, 2005; Hillier and Cosgrove, 2002; Diggs, 2007; Lonergan *et al.*, 2007; Vigorito *et al.*, 2008; Vétel and Cartwright, 2010). As with dykes, sills are common on all scales from mm to 10's m thick (Vigorito *et al.*, 2008; Vétel and Cartwright, 2010; Vigorito and Hurst, 2010) and can be laterally continuous (both in outcrop and seismic) for >1 km (Duranti and Mazzini, 2005; Huuse *et al.*, 2005a; Vigorito *et al.*, 2008). In both seismic and outcrop it is common to see lateral changes in thickness of sills, though small-scale changes are only apparent at outcrop (Hiscott, 1979; Diggs, 2007).

Another common feature, typically observed in 2D and 3D seismic sections, are wing-like or saucer-shaped structures (Polteau *et al.*, 2008; Jackson *et al.*, 2011) and cone sheets (Cartwright *et al.*, 2008; Andresen *et al.*, 2009), where steeply dipping dykes feed large bodied and laterally extensive sills which then pinch out at inclined angles forming wings (Fig. 2.2). These conical- or saucer-shaped intrusions can themselves vary in shape. They can form a flat-based saucer with the centre concordant with host strata and then inclined margins or wings at the edges, or form

apical cones where none of the intrusion is host concordant and sides are steeply dipping directly from the apex (Cartwright *et al.*, 2008).

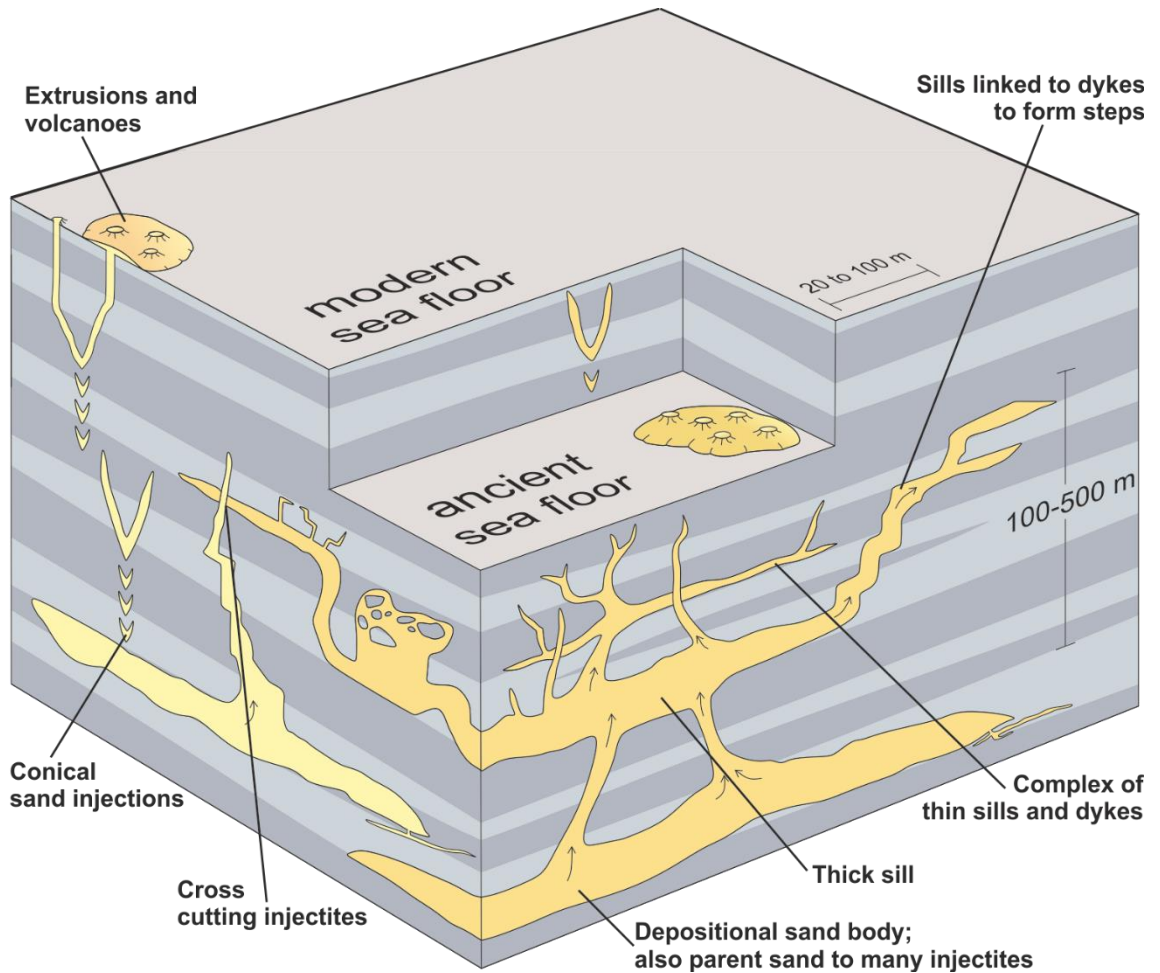


Figure 2.1 Some common injectite geometries identified in both outcrop and seismic data. Modified after Hurst and Cartwright (2007).

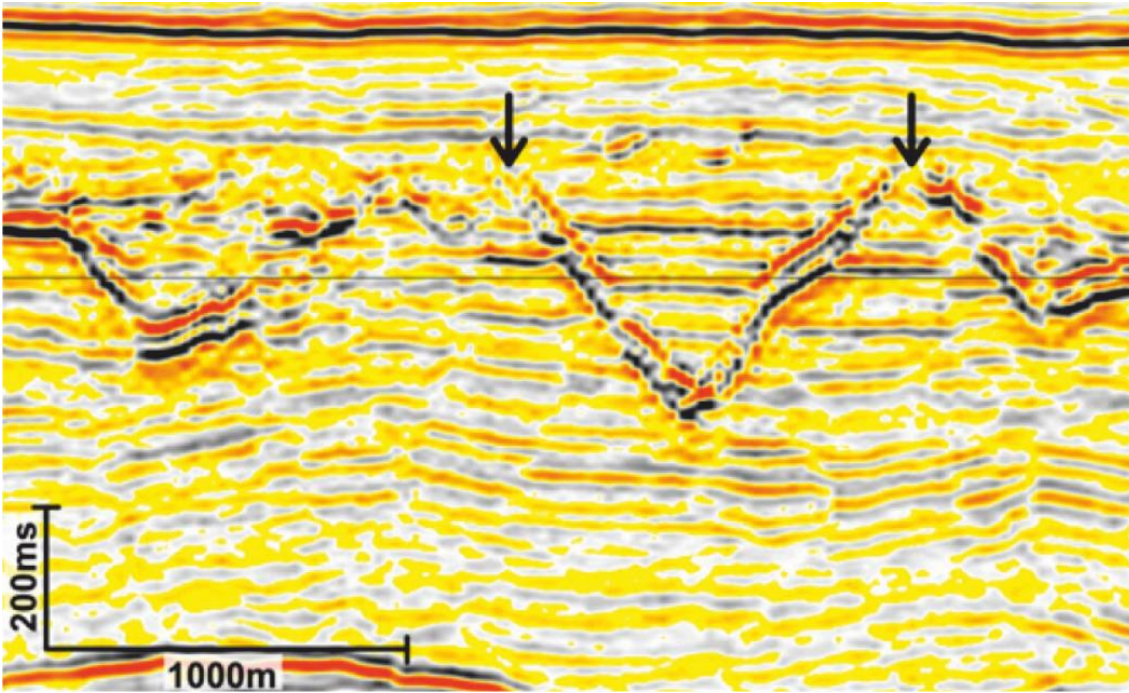


Figure 2.2 Conical injectites showing characteristic V-shape from the Faroe-Shetland basin; arrows mark the top injectite. From Cartwright *et al.* (2008).

2.3 Internal and external sedimentary features

Internal and external sedimentary structures associated with clastic injectites are both widely documented in the literature (Peterson, 1968; Hiscott, 1979; Keighley and Pickerill, 1994; Boehm and Moore, 2002; Curtis and Riley, 2003; Hurst *et al.*, 2003, 2011; de Vallejo *et al.*, 2005; Vigorito *et al.*, 2008; Scott *et al.*, 2009; Groenenberg *et al.*, 2010; Kane, 2010; Vétel and Cartwright, 2010). Internal structures are usually indicative of the type of flow during or during the waning stages of sand emplacement, whereas external structures, observed on sill and dyke margins are a record of the interaction between injecting sand and host muds/mudstone.

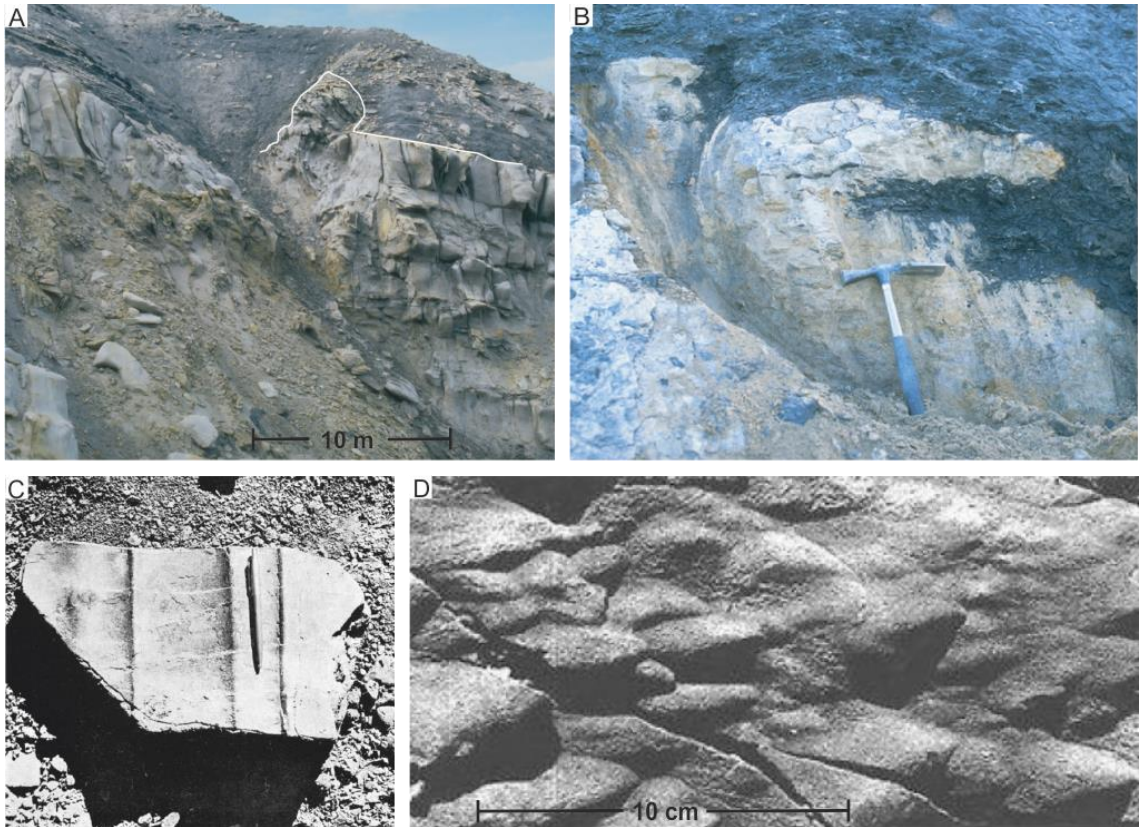


Figure 2.3 External features described on injectite margins. A + B) Scours on injectite tops. Katedralen member, Gåseelv (A) and Katedralen (B), Jameson Land, Greenland. From Surlyk *et al.* (2007). C) Linear structures resembling groove casts (pencil for scale), Sacramento Valley, California. From Peterson (1968). D) Flute casts on injectite margin. From Keighley and Pickerill (1994).

2.3.1 External

All contacts between injection margins and host strata are sharp (Hurst *et al.*, 2003) and any structures preserved are either caused by the flow of fluidised sand or a preservation of the fracture morphology of the mudstone. Indications towards this process of fluidisation and injection of sand into hydraulic fractures include the preserved structures on the margins of dykes and sills (Scott *et al.*, 2009). Individual surface structures can be >1 m in length and relief ranges from mm to cm, and this can be on the top or base margins of injectites, or both (Hurst *et al.*, 2011). As well as being found on margins of intrusions these external features are seen on the margins of large mudstone clasts or rafts contained within the injectites (Hurst *et al.*, 2003). Common external features include: i) scours, attributed to erosional processes, that are positive relief features that cut into host mudstone and can be up to several metres in length (Fig. 2.3A); ii) scallops that erode upward, from sills, up to 5 m into overlying mudstone and can extend

laterally for up to 10 m (Hurst *et al.*, 2003, Surlyk *et al.*, 2007) (Fig. 2.3B); iii) drag lines (Fig. 2.3C) that represent groove marks seen in any other flow/depositional setting; and, iv) flutes, widely documented cm to dm in length (Peterson, 1968; Keighley and Pickerill, 1994; Hillier and Cosgrove, 2002; Kane, 2010) and are attributed to erosion (Kane, 2010) and therefore forcible injection (Fig. 2.3D).

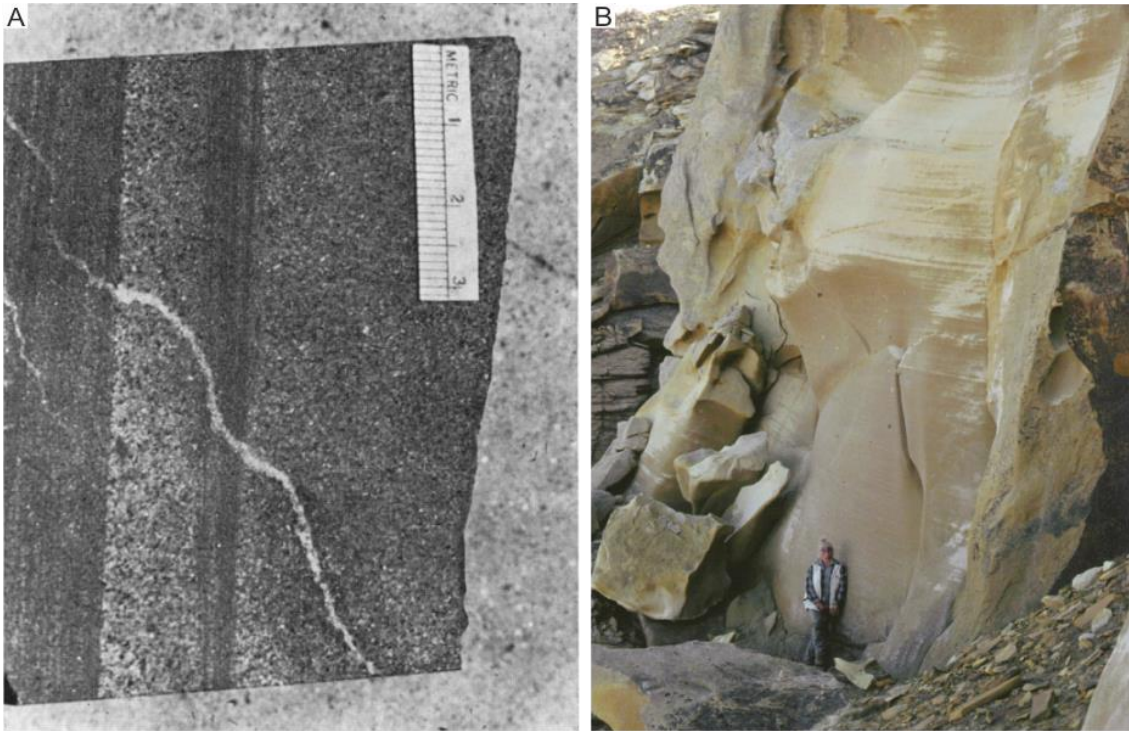


Figure 2.4 A) Graded layering in clastic dyke, grading is perpendicular to dyke walls. From Peterson (1968). B) Banding from horizontal flow in injectite >15 m thick. Katedralen Member, Jameson Land, Greenland. From Surlyk *et al.* (2007).

2.3.2 Internal

Internal structures are indicative of flow processes and can often resemble flow structures seen in fluvial and marine deposits (Hurst *et al.*, 2011). Most intrusions appear structureless (Peterson, 1968), but where internal structures do occur they can include laminations, banding, clasts and grading. Laminations are caused by segregation of grains where there is a range of grain-size or grain-properties (Hubbard *et al.*, 2007; Macdonald and Flecker, 2007), like those seen in open-channel and gravity flow deposits (Fig 2.4B). The degree of preferred orientation varies (Peterson, 1968) depending on flow behaviour at the time of deposition and degree of post-depositional compaction. Laminations remain parallel to each other and thicknesses of

individual lamina will always remain constant (Hurst *et al.*, 2003). Banding (Fig. 2.4A) is characterised by well-defined, individual layers, parallel to the injection margins with grain-size varying between bands. Layers vary in thickness from <1 mm to several cm and may be both present and absent in a single injection (Peterson, 1968; Hurst *et al.*, 2003; Kane, 2010). They may laterally extend for up to 15 m and undulate on wavelengths of several metres, not necessarily parallel with injectite walls (Hurst *et al.*, 2003; Sherry *et al.*, 2012). Clasts of host rock are usually orientated parallel to the dyke margin and range in length from <1 mm to >1 m (Peterson, 1968; Surlyk *et al.*, 2007; Sherry *et al.*, 2012). Clast edges can be from angular to smooth; large clasts (>3 m long) are termed rafts and are often rounded (Hurst *et al.*, 2003). Clasts are more abundant close to the injectite margin, are not always locally derived, and are transported before deposition; this includes large rafts (Sherry *et al.*, 2012). Grading is seen perpendicular to the walls/margins of the injection and may occur as a single graded layer or multiple layers. There appears to be no preferential direction for grading, it occurs both normal and inverse to flow direction (Hubbard *et al.*, 2007).

2.4 Comparison to igneous intrusions

Clastic injectites are comparable in many aspects to igneous intrusions in sedimentary basins at outcrop, in the subsurface, and in experimental modelling. Affinities in their characteristics include geometry, architecture, surface features, and processes of rock fracture and injection propagation (Polteau *et al.*, 2008) and can be related to heterogeneities in the basin-fill such as bedding. As with clastic injectites, igneous sills and dykes occur at a range of scales from mm to km. The two main types of cone- or saucer-shaped intrusions that have been described in studies of clastic injectites are also seen in igneous intrusions; V-shaped conical intrusions that are fed by a dyke at the apex, and flat based, saucer-shaped intrusions where the base is concordant with host strata, feeding into inclined wings that either taper out or extrude (Cartwright *et al.*, 2008; Polteau *et al.*, 2008). This style of intrusion architecture is thought to be controlled by the host stratigraphy rather than the injecting material (Polteau *et al.*, 2008) providing evidence that host strata has a control on geometries compared to the injecting medium whether it be igneous or clastic (Cartwright *et al.*, 2008, Polteau *et al.*, 2008).

Experimental modelling of magmatic intrusions into sedimentary, brittle strata (Mathieu *et al.*, 2008; Galland *et al.*, 2009) reveals many of the same results as that of clastic intrusions produced through sandbox modelling (Cobbold and Castro, 1999; Nichols *et al.*, 2006; Rodrigues *et al.*,

2009; Mourgues *et al.*, 2012). All experiments result in a feeder dyke or conduit that supplies fluidised material or 'magma' to an inverted cone or saucer shaped intrusive body. As well as having similarities, Mourgues *et al.* (2012) noted some differences: igneous intrusions can only migrate a relatively short distance as the viscous fluids cannot migrate through pores, and fluid pressure remains within the intrusion itself. Whereas with clastic intrusions, fluids can permeate through pores into surrounding or host rock, ultimately affecting the stress field around the intrusive body.

Outcrop and core studies have reported a range of erosional structures including flutes and striae on the margins of clastic dykes and sills (Peterson, 1968; Keighley and Pickerill, 1994; Hurst *et al.*, 2003, 2011; Bezerra *et al.*, 2005; Vigorito *et al.*, 2008; Scott *et al.*, 2009; Groenenberg *et al.*, 2010; Kane, 2010) (section 2.3, Fig. 2.3). It is arguable to what extent these can be compared to those found on igneous dykes and sills. External markings on intrusions of igneous origin tend to be less varied, with some striations, erosional grooves and 'hot slickenlines' (Varga *et al.*, 1998) compared to flutes marks, scours, groove marks, frondescent marks etc. in clastic intrusions. Many external structures found on clastic intrusions are interpreted to be a preservation of fracture morphology of the host rock (Hillier and Cosgrove, 2002; Kane, 2010) whereas only erosional and flow features are preserved on igneous sill and dyke margins (Polteau *et al.*, 2008).

2.5 Vertical exaggeration

It is standard practice to use vertically exaggerated seismic reflection data when interpreting geological structures and stratigraphy (Stewart, 2011, 2012). In fact 74% of published seismic data from 2006-2010 had no label or indication of its vertical exaggeration (Stewart, 2011). The geometries and architectures of clastic injections are apparent due to vertical exaggeration. However, it appears that this has been overlooked in many published sections. For example, sills look much thicker than in reality, this can have significant implications when being compared to feeder dykes, which would only appear longer and keep a constant thickness. One of the most commented on geometries of sand intrusions in seismic sections are wing-like features (Jackson, 2007), however when vertically exaggerated, the angle of wing-like features is greatly increased (Fig. 2.5). Interpretations are affected when wing-like and saucer-shaped geometries are compared to magmatic intrusions of different vertical exaggeration (Mourgues *et al.*, 2012) when in fact there may be a huge difference or no comparison at all.

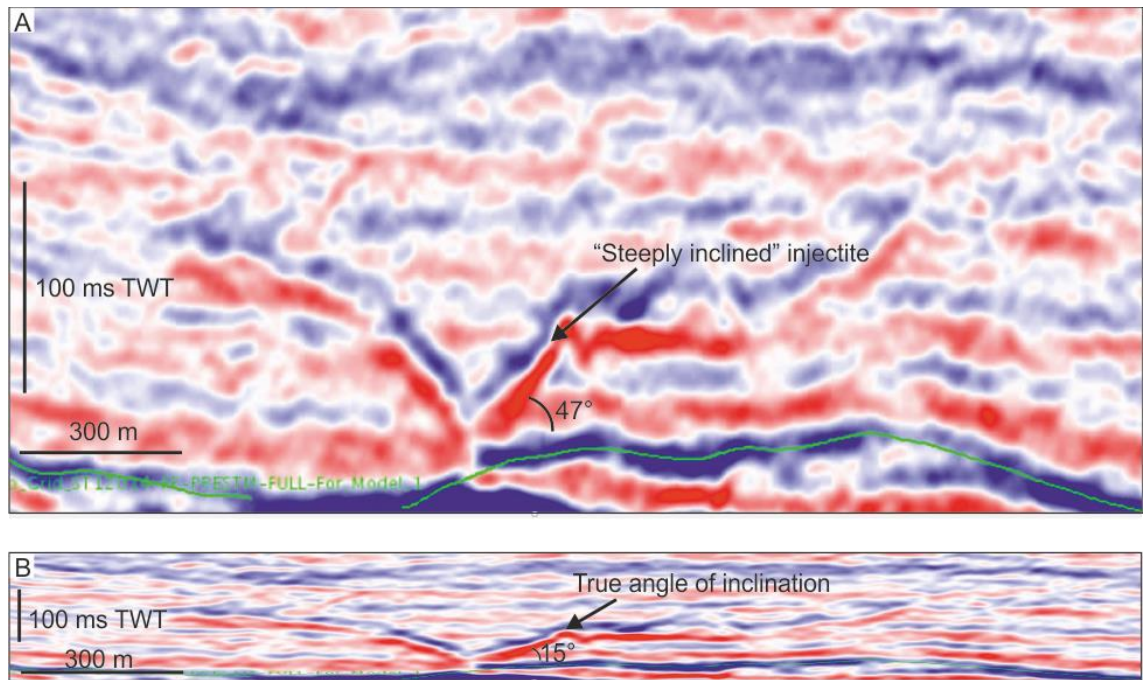


Figure 2.5 A) Example of vertically exaggerated seismic section from a case study in the Northern North Sea with a steep apparent dip of the injectite. B) Same section as (A) with no vertical exaggeration, apparent dip angle of the injectite is greatly reduced.

2.6 Summary

Clastic injectite research has been driven by increased recognition in the subsurface during hydrocarbon exploration in the last two decades. Injectite complexes can be broadly categorised into the parent sand unit, which feeds a network of sills and dykes. Sedimentary structures observed both internally and on the margins of the sills and dykes provide insight into the types of flow processes that occur during fluidisation and deposition. However, there are still ambiguities in defining the style of injectites produced from different flow types, i.e. laminar versus turbulent flow regimes.

Clastic injectites pose similar geometries to igneous intrusions in sedimentary basins, therefore it is possible to compare intrusion mechanisms and external factors affecting injectite morphology. The majority of these similarities are identified on seismic profiles, however vertical exaggeration in these profiles poses additional difficulties; unit thicknesses, angle of inclination, and volumes of sand are manipulated when vertical exaggeration is applied.

3 Injectite formation: physical and forward modelling

3.1 Injectite formation

Injectites are considered to be the products of natural hydraulic fracturing processes (Lorenz *et al.*, 1991; Cosgrove, 2001; Jolly and Lonergan 2002; Cobain *et al.*, 2015) requiring a pressure differential between the source of the injecting sediment and the tip of a developing fracture to sustain propagation (Lorenz *et al.*, 1991). The pre-requisite conditions for clastic injections to form are well known and generally agreed upon. The over- and underlying lithology must seal a parent sand, acting as an impermeable barrier, and this then enables pore pressure within the parent unit to increase during burial and compaction, becoming higher than that of the surrounding strata (Lorenz *et al.*, 1991; Cosgrove, 2001; Jolly and Lonergan 2002). Overpressure forms within a bed when a sealing lithology of low-permeability, usually mudstone, prevents the escape of pore fluids during compaction, or during earthquake induced shaking, resulting in the pore fluid pressure becoming higher than the surrounding hydrostatic pressure (Maltman, 1994). Entrapped pore fluids can cause the sediment to remain unconsolidated, even at great depth, and thus have the potential to fluidise. Finally, a trigger is needed to cause the sealing lithology to hydraulically fracture and the parent sand to fluidise, migrating into the newly formed fractures and forming injectites (Jolly and Lonergan, 2002). Where host rock is cohesive, sheet intrusions occur in the form of dykes, sills or cones; where host sediments are cohesionless (usually at more shallow depths), pipes form that feed extrusions onto the surface (Maltman, 1994; Ross *et al.*, 2011).

3.2 Physical modelling

Physical modelling of clastic injectites can be separated into: i) box modelling of injectite architecture during formation in sedimentary basins (e.g. Rodrigues *et al.* 2009), ii) studies of flow dynamics in conduits (e.g. Nichols *et al.*, 1994; Nichols, 1995; Ross *et al.*, 2011), and iii) modelling of the fracture processes that occur at the tip of a propagating hydraulic fracture (e.g. Müller and Dahm, 2000).

3.2.1 Box modelling and flow dynamics

In order to model naturally occurring geological processes and maintain kinematic and geometric accuracy, the principles of dimensionless scaling must be applied (Hubbert, 1937). Sandbox modelling has been a standard method of modelling tectonics and associated processes including fluidisation (Hubbert, 1951; Karig and Hou, 1992; Cobbold and Castro, 1999; Murdoch and Slack, 2002; Nichols *et al.*, 2006; Rodrigues *et al.*, 2009; Mourgues *et al.*, 2012). These models all use dimensionless scaling, however there are variables that need to be addressed in order for the experiments to replicate natural processes as closely as possible. For example many sandbox models (Mourgues and Cobbold, 2003; Nichols *et al.*, 2006; Rodrigues *et al.*, 2009; Gressier *et al.*, 2010) use compressed air as injectite pore fluid yet its behavioural properties may be greatly different to that of the water/hydrocarbons they are trying to model.

Sand injectites were first studied using box modelling by Rodrigues *et al.* (2009) who reproduced structures geometrically similar to injectites in the Tampen Spur area of the North Sea (Fig. 3.1). However, previous fluidisation experiments (Nichols *et al.*, 1994; Nichols, 1995; Cobbold and Castro, 1999; Ross *et al.*, 2011) had also produced sand intrusions in the form of sills, pipes and extrusions although this had not necessarily been the primary aim of experimentation. Rodrigues *et al.* (2009) drove compressed air through layers of sand, glass microspheres, silica and diatomite powder until the non-cohesive sand and glass microspheres overpressured causing the cohesive powders to hydraulically fracture, and the non-cohesive sediments to fluidise and inject upwards. Different thicknesses of sand were used in each model with similar results. Initially, the state of stress was lithostatic and increased during the experiment by pumping compressed air upwards through the layers of sediment until non-cohesive layers fluidised and sediment was transported to the surface through vents (Rodrigues *et al.*, 2009). The sand was then dampened and cut for observation. This experiment used air to simulate pore fluids, but it is far more compressible than water, and was only introduced from below; in nature pore fluid pressure would increase by being expelled from the mudstone/cohesive sediments from above as well as below, as they compacted. Although Rodrigues *et al.* (2009) were able to produce a range of injectites including sills, laccoliths and conical injections (Fig. 3.1), they were all produced at near surface pressures with sediment compaction restricted to several centimetres of overburden at the most. As a result, most of the intrusions were coupled with extrusions. The experiment did not allow the process of the injection formation to be observed or monitored, or the pressures to be measured; only the architectural results could be studied. However the experiment did show that sediments became fluidised and then injected, and as a

result the source layer is sediment-depleted afterwards, which has not previously been commented on or taken into consideration when studying, or modelling from, seismic sections or outcrop. Rodrigues *et al.* (2009) also managed to replicate some examples of injectite zones or layers found in nature; with hydraulic fracturing of the basal layers, followed by doming of the uppermost layers and extrusions on the surface.

Other physical experiments related to clastic injectite modelling are those of shallow magma emplacement into sedimentary basins; methods and host rock materials and pressures are generally the same, the only difference being the rheological properties of injected material. Galland *et al.* (2009) simulated magma (molten, low-viscosity oil) intruding into brittle crust (silica flour); vertical dykes formed in the deepest layers (4-5 cm) whereas cone sheets were produced at shallower depths (1-3 cm). Geometries of intrusions produced were very similar to those replicating clastic intrusions: a vertical dyke or conduit feeding a cone sheet which is responsible for doming of the upper surface of the host sediments, and finally extrusion/eruption of injected fluid where the conical fracture reaches the surface. Another set of experiments replicating magmatic intrusions used silicone putty injected into diatomite powder (Gressier *et al.*, 2010), with compressed air as the pore fluid. As with sandbox modelling of clastic dykes and sills, the results of replicating shallow magma emplacement show that with a greater overpressure, sills are formed at a greater depth (Kavanagh *et al.*, 2006).

Although clastic dykes and sills appear to have been successfully modelled in physical experiments, there is a notable absence of any physical experiments that produce clastic injections under high pressure to simulate emplacement at depth. Laccoliths and sills that are reproduced (Cobbold and Castro, 1999; Nichols *et al.*, 2006; Mourgues *et al.*, 2012) are accompanied by extrusions, and are produced at atmospheric/lithostatic pressures with only a few centimetres of overburden and compressed air as a pore fluid instead of water. In all of the above experiments, the cohesive sediment was hydraulically fractured due to overpressure caused by an increase in compressed air. These models do not involve deliberate triggers; Moretti *et al.* (1999) do model seismites through a shaking table acting as an earthquake simulator to trigger liquefaction and fluidisation. It is widely speculated that clastic injections are caused by a range of trigger mechanisms including seismic shaking and high rates of deposition (Truswell, 1972; Boehm and Moore, 2002; Jolly and Lonergan, 2002; Obermeier *et al.*, 2005; Hurst *et al.*, 2011). Yet these are another variable that have rarely been taken into consideration when experimentally fluidising or causing hydraulic fracture to occur.

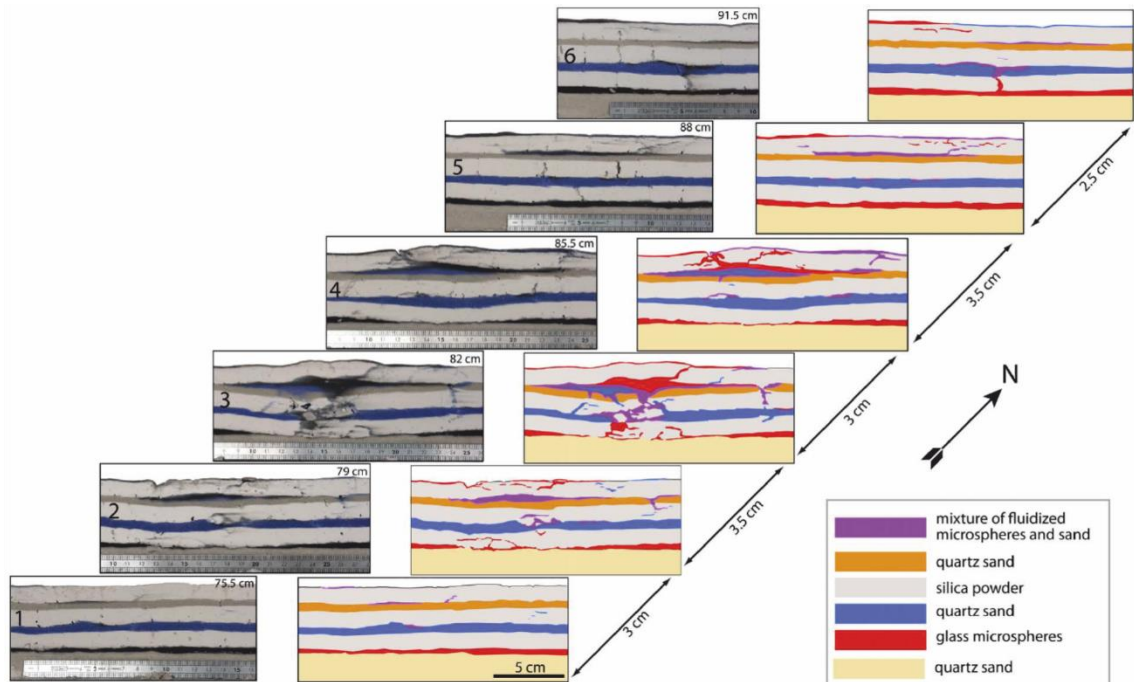


Figure 3.1 Example of sand box model experiments (Rodrigues *et al.*, 2009). Photographs and line drawings of black glass microspheres and blue quartz sand filling fractures within silica.

3.2.2 Fracture morphology and propagation

The margins of clastic injectites preserve the nature of the contact between intrusive body and host rock. This has been interpreted as the preservation of host rock fracturing prior to or during injection (Cosgrove, 1995). Morphologies caused by fracturing reflect the fracture process (Müller and Dahm, 2000) and therefore give indications to the specific properties of the host rock or sediment at time of fracture as well as propagation with regards velocity, direction etc. (Woodworth, 1895). Physical modelling of the formation of various fractures provides insights into how clastic injectites propagate through a host medium.

Fracture morphology types

Several fracture types are produced when cohesive or partially lithified sediment hydraulically fractures: i) striae occur in assemblages together; they are linear grooves and indicate shear fracturing parallel to the direction of the groove surface, ii) river line patterns are generated by mixed mode loading effects, and these show how apparent propagation direction can be

misleading (Hull, 1996) (Fig. 3.2A), iii) hackle marks also appear grouped and are linear highs but are not parallel to one another (Lutton, 1970) (Fig. 3.2B), iv) steps can occur at any point, though they are usually more prominent towards the edges or fringe of a fracture — they are an offset of the main fracture along other smaller fractures (Lutton, 1970) (Fig. 3.2B) —, and v) rib marks are usually curved ridges and troughs, arranged concentrically around the point of origin of the fracture (Fig. 3.2C).

Fracture modelling

Lab tests studying the propagation of fractures suggests that the formation and origin of microfractures during different stages of deformation start in stress concentrations of small and pre-existing flaws in the rock then propagate as a mode I fracture perpendicular to the minimal principal compressive stress (Lorenz *et al.*, 1991). Even if stresses across bodies or whole beds of rock are uniform, small-scale stresses at the tip of a propagating fracture may be between the source bed or body and the tip of the propagating fracture itself. Once the difference in pressure begins to balance the fracture freezes and sand no longer injects (Lorenz *et al.*, 1991).

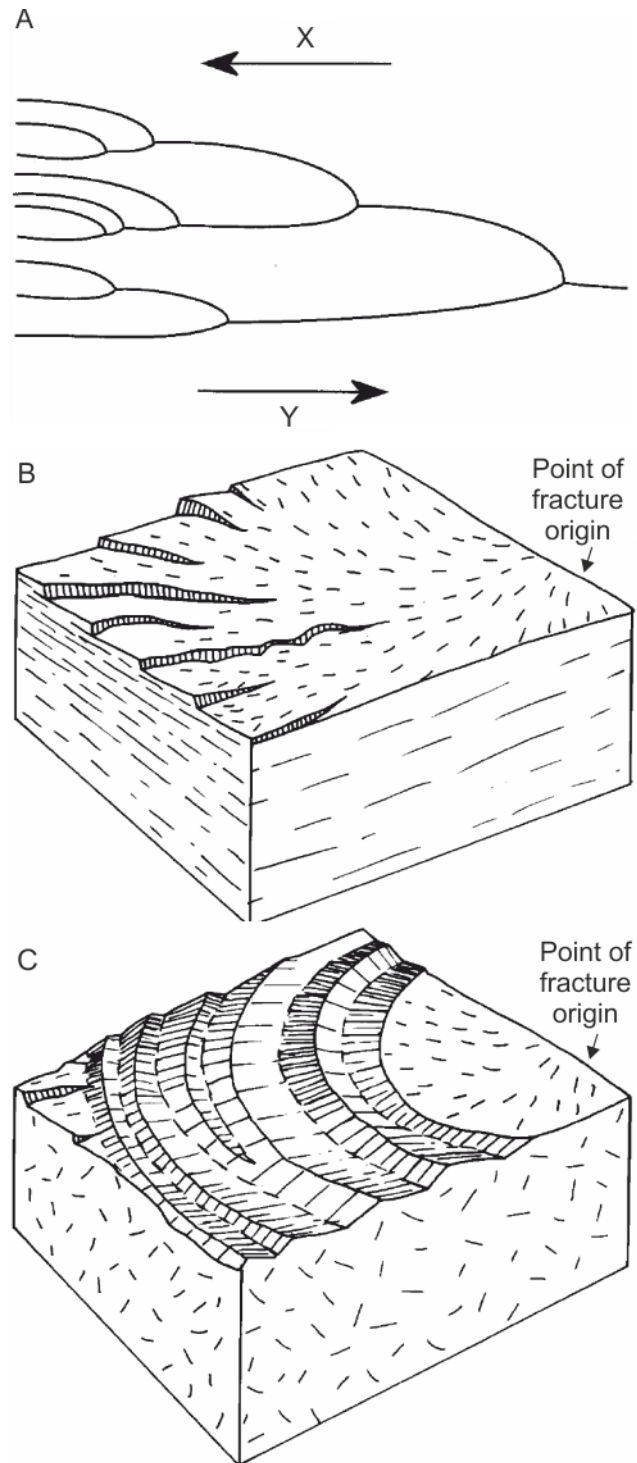


Figure 3.2 Types of fracture morphology. A) River line pattern. Direction of crack propagation originally assumed to be X (Djordjevic et al., 1996). Actual fracture propagation direction is Y (Hull, 1996). B) Hackle marks and steps in a plumose arrangement. C) Rib marks in concentric arrangement. B + C from Lutton (1971).

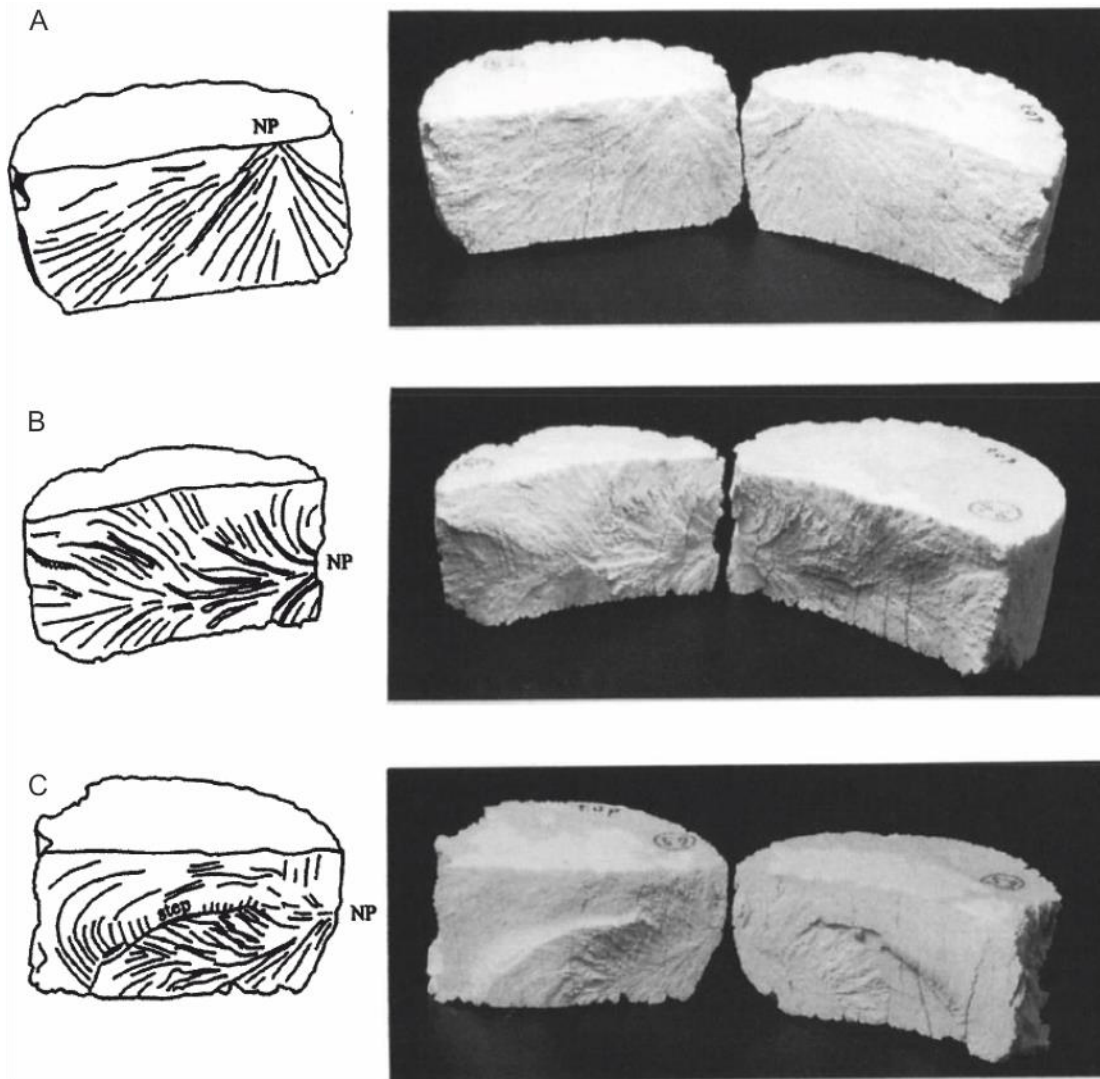


Figure 3.3 Various styles of plumose morphology (NP = nucleation point). Specimen diameter 65mm. From Müller and Dahm (2000).

Experiments have shown that rupture velocity decreases following a decrease of tensile stress due to the increase in water concentration. Rupture velocity also decreases with increasing depth in vertical fractures (which would produce dykes). It is more difficult to gain an understanding of horizontal rupture velocity (sills) via experimentation (Müller and Dahm, 2000) (Fig. 3.3). In the fringe zone of the cracks, rupture velocities are lower, which coincides with topographic relief being higher (Müller and Dahm, 2000), although topographic amplitudes do depend on more than rupture velocity. However, in these experiments by Müller and Dahm (2000), the cause for velocity decrease is general stress decrease due to the propagation of the fracture, whereas with clastic injection, fracture propagation is continuously driven by the influx of fluidised sand. Müller and Dahm (2000) have shown that both plumose structures give

propagation direction and that vertical fractures tend to propagate laterally from a source point rather than propagating directly downwards (Fig. 3.3). This is important when considering small- and large-scale clastic injection in both seismic and outcrop sections. Although apparent downwards propagation geometries in 2D section are more likely to be a result of a laterally migrated sheet of sand (e.g. Kane 2010). With an understanding of the rupture velocity of tensile cracks and the different fracture morphologies associated with different fracture speeds it may be possible to estimate sand injection velocities from sill and dyke margin morphologies at outcrop as well as overall propagation direction. However, many variables would have to be taken into consideration such as pressure due to depth and the extent of consolidation due to burial etc.

3.3 Forward modelling

Forward seismic modelling of geological outcrops creates a seismic profile of the units and features present; the approach was first applied in the late 1980's (Rudolph, 1989). The main basis for implementing the forward modelling approach of outcrop data is to improve hydrocarbon exploration by improving not only interpretation of seismic profiles through reservoirs (Armitage and Stright, 2010), but also using this to increase predictability of reservoir architecture and connectivity (Falivene *et al.*, 2010). When integrated with outcrop, seismic and wellbore data, forward modelling can aid in building both regional and more locally detailed depositional models of basins and their hydrocarbon reservoirs to better understand their architecture, connectivity and distribution (Hodgetts and Howell, 2000). Properly calibrated deep-water outcrops can provide constrained geometric and architectural data to fill the gaps between wells or stochastic modelling uncertainties below the resolution of seismic data (Hodgetts and Howell, 2000) (Fig. 3.4).

More recent studies into the applicability of forward modelling to distinguish particular channel internal architecture and facies distribution have shown that this is beyond the scope of even the highest frequency seismic (Falivene *et al.*, 2010). Differentiating between sandstone-filled or debrite-filled channels within channel complexes is problematic, with debrite-filled channels producing a slightly more chaotic seismic reflection and a less obvious amplitude contrast at the base (Falivene *et al.*, 2010).

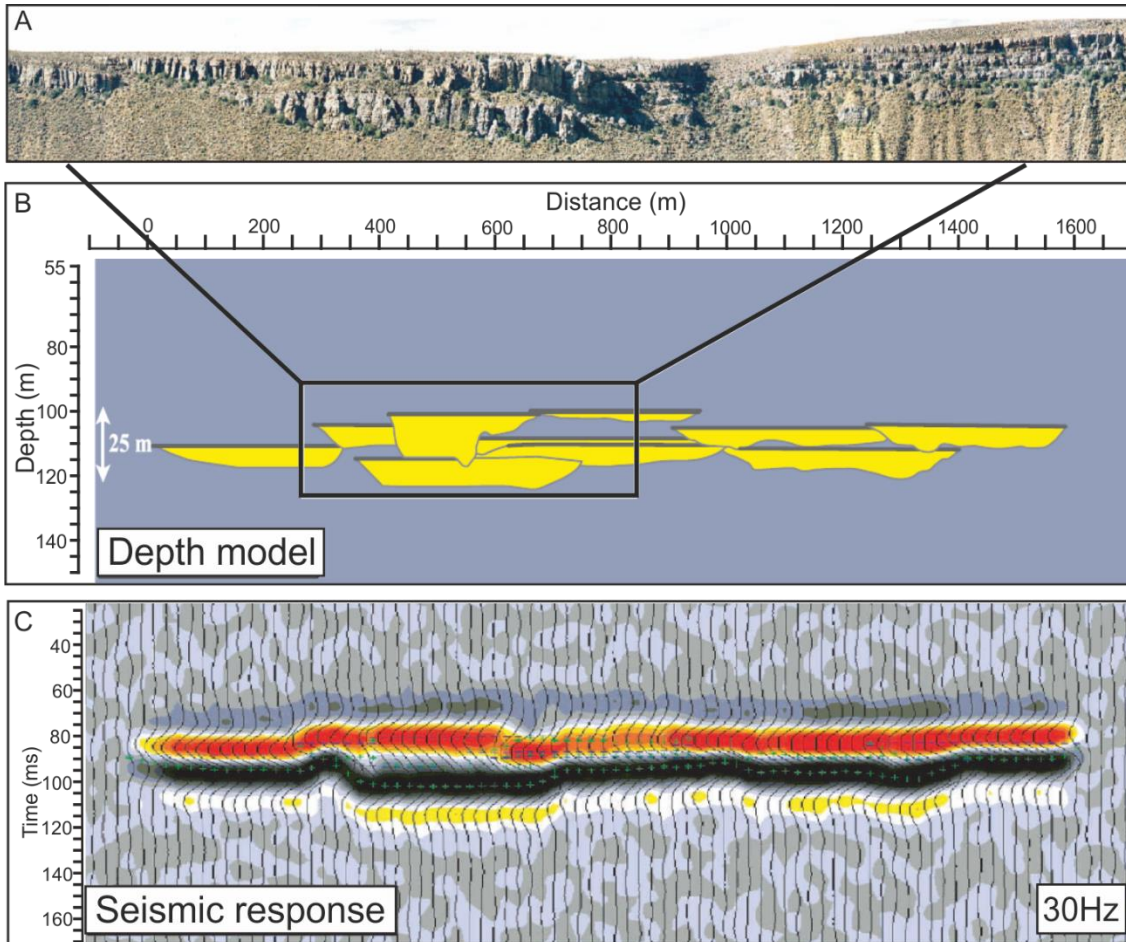


Figure 3.4 Example of forward seismic model. A) Outcrop photo, Karoo Basin, South Africa. B) Depth model for the outcrop using density and velocity properties from deep-water reservoirs, Gulf of Mexico. C) Seismic response for a 30 Hz wavelet. Adapted from Sullivan *et al.* (2004).

3.4 Summary

Clastic injectites form through a process of natural hydraulic fracturing with fluidised clastic sediment infilling and propagating the fracture through a pressure differential between fracture tip and source of fluidised material. This process has been modelled through a combination of sand box experiments simulating injectite geometries mapped in the subsurface and through fracture propagation experiments determining how specific fracture types form.

An additional method of understanding outcrop expression of deposits in reflection seismic data is to forward model two dimensional outcrop architectural panels. This enables facies and geometric complexity to be added to seismic interpretations, and for different frequencies to be imaged.

4 Indicators of propagation direction and relative depth in clastic injectites: implications for laminar versus turbulent flow processes

4.1 Introduction

Clastic injectites have been documented in many sedimentary environments (see Hurst *et al.*, 2011; Ross *et al.*, 2011, and references therein). Interest in injectites has increased as their significance for petroleum systems has been realised: they can serve as hydrocarbon reservoirs (e.g., Schwab *et al.*, 2015) as well as dramatically change reservoir architecture and form fluid migration pathways in a broad range of reservoirs (e.g. Dixon *et al.*, 1995; Jolly and Lonergan, 2002). In the subsurface, reflection seismic data can help to constrain the large-scale architecture, and in some cases the propagation direction of injection complexes (Hurst *et al.*, 2003; Huuse *et al.*, 2004; Cartwright *et al.*, 2008; Vigorito *et al.*, 2008; Szarawarska *et al.*, 2010; Jackson *et al.*, 2011), but flow direction and relative depth of formation are hard to interpret, even with the addition of core and outcrop analogues. Despite their importance, many of the underlying formation processes remain poorly understood, such as the mode of propagation and nature of sediment transport processes within these conduits. In particular, there has been considerable discussion on the nature of fluid flow during injection, especially whether flows are laminar or turbulent (Peterson, 1968; Taylor, 1982; Obermeier, 1996; Duranti, 2007; Hubbard *et al.*, 2007; Hurst *et al.*, 2011; Ross *et al.*, 2014).

This chapter reports detailed observations on the morphology and distribution of a wide array of structures on the margins of exhumed clastic injectites. These observations are then integrated with the existing literature, including that pertaining to igneous dyke and sill emplacement, to develop a model that considers the mechanisms and internal flow processes in operation during sand injection. We thus address the following fundamental questions: i) Can injection propagation direction be determined using margin structures? ii) Can injection depth be estimated? and iii) What flow processes occur during injection? These questions support a discussion on sand injectite emplacement mechanisms, including the current debate on laminar versus turbulent flow and how this controls differences in injectite geometries and surface features.

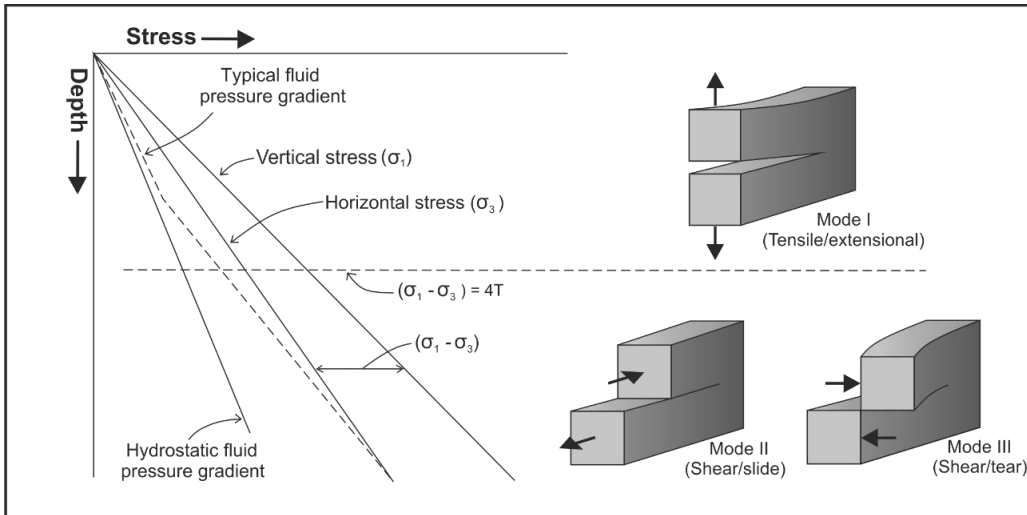


Figure 4.1 Plot of vertical and horizontal stress regimes in a tectonically relaxed basin. Differential stress increases with depth; at a depth where applied shear stress exceeds four times the tensile strength of the host rock, the type of fracture changes from extensional to shear. Mode I, II, and III type fractures correlated with relative depth of formation. Adapted from Cosgrove (2001).

4.2 Sources of overpressure, trigger mechanisms, and fracture propagation: current understanding

The most commonly invoked triggering mechanisms for clastic injectites are seismicity (Obermeier, 1996; Boehm and Moore, 2002; Obermeier *et al.*, 2005), overpressuring by rapid fluid migration into parent sands (Davies *et al.*, 2006), rapid burial (Truswell, 1972; Allen, 2001) or instability of overlying sediments (Jonk, 2010). Seismicity, and overpressure by rapid burial or unstable overlying sediments are associated with relatively shallow and often localised injection (Hurst *et al.*, 2011; Bureau *et al.*, 2014). Deeper, and in many cases, larger scale injectites are thought to be related to compaction, and/or the migration of fluids from a deeper source into a sealed sandstone body causing an increase in pore pressure (Vigorito and Hurst, 2010; Bureau *et al.*, 2014). Therefore at depth, in a seismically quiescent basin, pore fluid overpressure from compaction and/or migrating fluids can act as both the primer and the trigger for clastic injection.

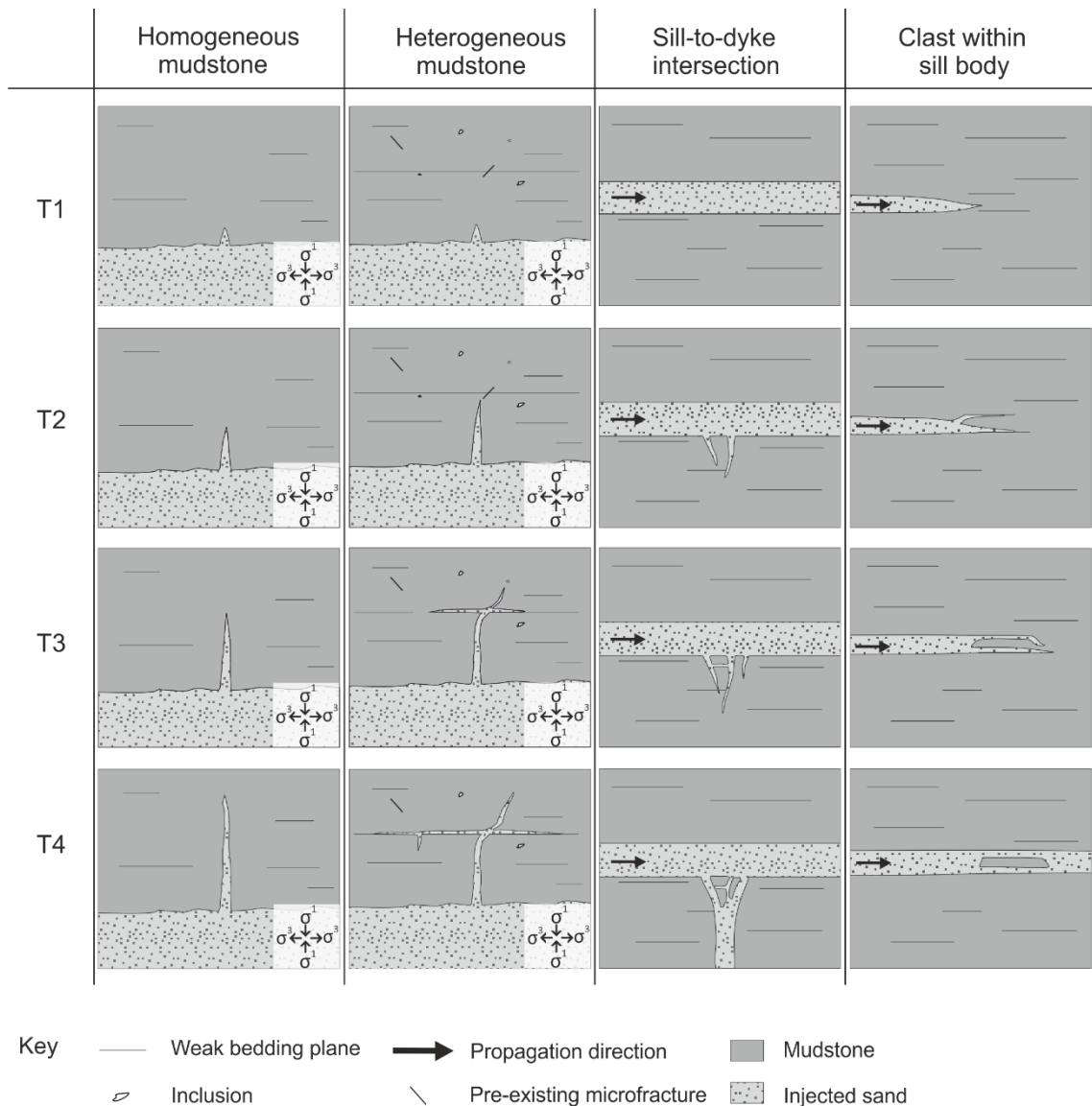


Figure 4.2 Temporal development (time steps 1-4) of injectite fractures, showing simple fracture propagation in homogeneous and heterogeneous mudstones, fracture development at a sill-to-dyke intersection and the formation of associated clasts, and the propagation of horizontal fractures leading to a large clast within a sill body.

Once triggered, clastic sills and dykes fill natural hydraulic fractures (Lorenz *et al.*, 1991; Cosgrove, 2001; Jolly and Lonergan, 2002; Jonk, 2010) opening in a mode I propagation (Fig. 4.1) normal to the plane of least compressive stress (Delaney *et al.*, 1986). Once opened, fracture propagation is maintained by a constant differential of pore fluid pressure between the source bed and the tip of the propagating fracture. When the difference in pressure begins to balance, the fracture ceases to propagate and injection stops (Lorenz *et al.*, 1991; Jonk, 2010). Initial failure can result from the development of a single critical fracture involving only a few primary

flaws such as impurities, grain boundaries, inclusions or microcracks (Aubertin and Simon, 1997) (Fig. 4.2: heterogeneous mudstone). The opening of a macroscopic crack, originating at one or more of these flaws, occurs when the stress intensity breaches the limit of the strength of the rock (Charlez, 1991). On a larger scale, even if stresses across bodies or whole beds of rock are uniform, small scale stresses due to flaws or impurities at the tip of a propagating fracture may be uneven causing irregularities in fracture direction and geometries (Lorenz *et al.*, 1991; Aubertin and Simon, 1997) (Fig. 4.2: heterogeneous mudstone). Ben-Zion and Morrissey (1995) have shown that a fracture propagating through a heterogeneous medium (Fig. 4.2) continually interacts with random asperities and diverges as heterogeneities in the fracture energy are incorporated. Here, observations of features on the margins or exhumed injectites hosted in deep-marine deposits in the Karoo Basin are used in conjunction with fracture mechanics to interpret propagation direction and flow processes.

4.3 Geological background

The Karoo Basin has long been interpreted as a retro-arc foreland basin that formed on the southern margin of the Gondwana palaeocontinent behind a magmatic arc and fold-and-thrust belt (Johnson, 1991; Visser & Praekelt, 1996; Catuneanu *et al.*, 1998; Johnson *et al.*, 2006). However, more recent studies suggest subsidence during the Permian was driven by mantle flow and foundering of basement blocks coupled to subduction of the palaeo-Pacific Plate to the south, pre-dating the Cape Orogeny (Tankard *et al.*, 2009) (Figs. 4.3 and 4.4). The deep-water stratigraphy of the Laingsburg depocentre, SW Karoo Basin, South Africa comprises a 1.8 km thick shallowing-upwards succession passing from distal basin floor (Vischkuil Formation, van der Merwe *et al.*, 2010), through proximal basin-floor (Laingsburg Formation; Sixsmith *et al.*, 2004) and channelised submarine slope (Fort Brown Formation; Di Celma *et al.*, 2011), to shelf-edge and shelf-delta deposits (Waterford Formation, Jones *et al.*, 2013) (Fig. 4.5A and 4.5B). The Laingsburg and Fort Brown Formations comprise seven sand-prone units (Units A to G) separated by regional mudstones, which signify shutdown of clastic input (Flint *et al.*, 2011). Unit A (Laingsburg Formation) is further divided into 6 sub-units (A1-A6), each bound by mudstones, which in turn relate to a regional shutdown of clastic input (Sixsmith *et al.*, 2004; Pr lat and Hodgson, 2013). The present study uses observations from an injectite-prone, 12 m thick mudstone unit between units A5 and A6 at the Buffels River, Laingsburg (Fig. 4.5B) where the source sand for clastic injectites is the underlying Unit A5, identified where dykes connect directly with sandstone beds. Figures 4.5C and D shows the typical outcrop expression of the clastic sills and dykes.

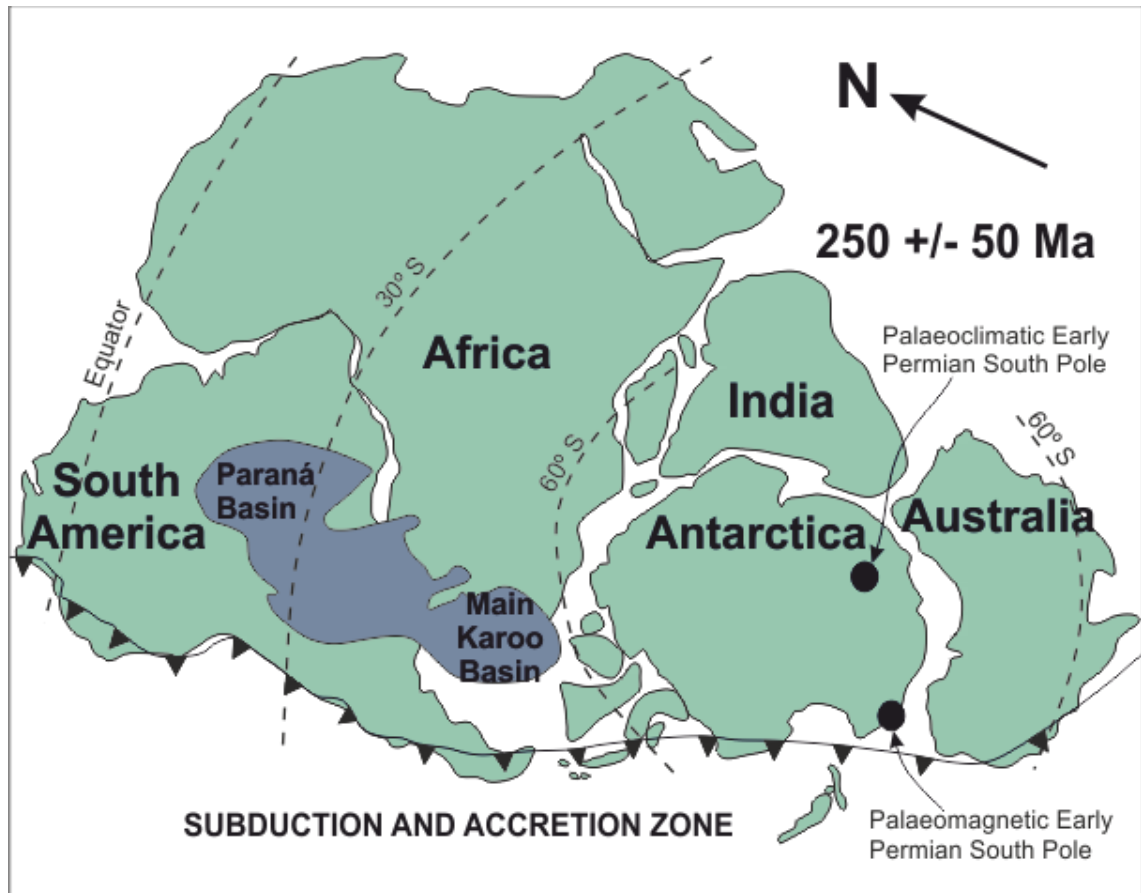


Figure 4.3 Palaeogeographic extent of the Paraná Basin and Karoo Basin in Gondwana during the Late Permian (modified from Faure and Cole, 1999).

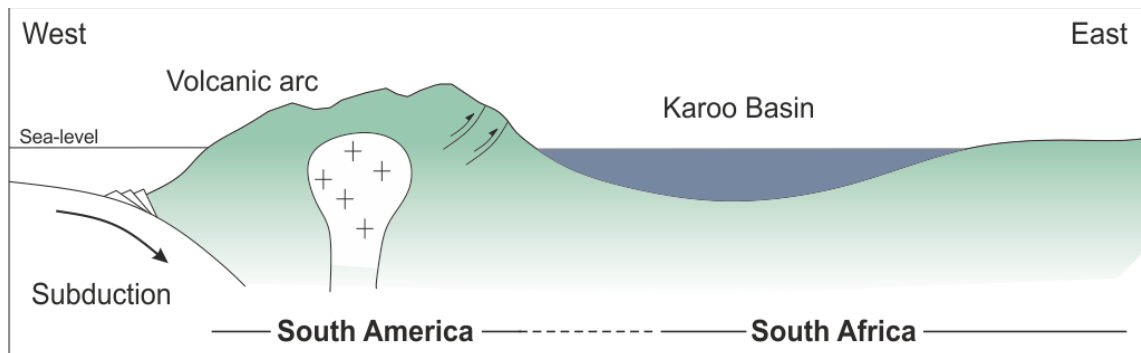


Figure 4.4 Schematic sketch showing Karoo Basin as a retro arc foreland basin in front of the palaeo-Pacific plate subduction zone (after Visser and Praekelt, 1996).

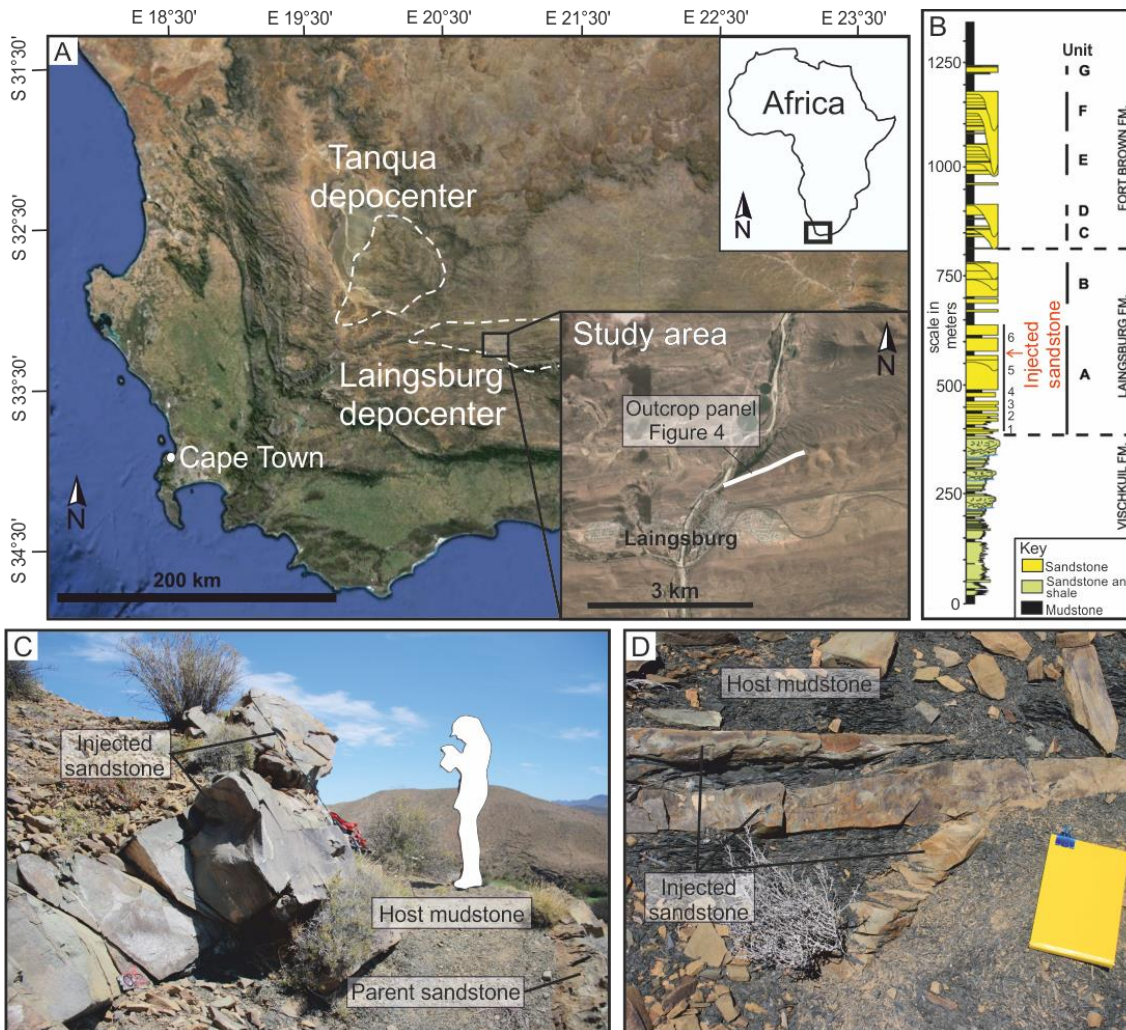


Figure 4.5 A) GoogleEarth image of SW Karoo Basin with Tanqua and Laingsburg depocentres outlined and study area enlarged. B) Summary log and highlighted stratigraphic position of clastic injectites (Flint *et al.*, 2011). C) Typical example of sill at outcrop. D) Typical example of small dyke and sills at outcrop.

4.4 Recognition of injectites in the field

Clastic injections in the Karoo Basin are fine grained, well sorted sandstones, much like the parent sandstones. Dykes are discordant with host strata, often at angles between 10-35°, though vertical dykes are also present, and range from <1 cm to several 10s cm in thickness and can be traced up to 20 m from the parent sand. Sills are concordant with host strata, although locally they step through stratigraphy to form stepped sills, and range from a few centimetres to 1.3 m in thickness, and 100's m in length. Recognition criteria for clastic sills include the presence of distinctive features on top and base margins (Figs. 4.6 and 4.7), and the absence of

depositional sedimentary structures, such as planar or ripple cross-laminations, or grain-size grading, although a faint banding is sometimes present towards top and base margins. In addition, injectites exposed in the Karoo Basin weather a distinctive colour and style aiding field identification.

4.5 Methodology and dataset

Injectites were mapped at cm-scale (Fig. 4.6B) along a 500 m long, 12 m thick south-west to north-east trending exposure of a regional mudstone interval that separates sandstone-prone units A5 and A6 of the Laingsburg Formation at Buffels River, Laingsburg, which are interpreted as submarine lobe complexes (Prélat and Hodgson, 2013). Detailed sedimentologic and stratigraphic observations include logged sections, photographs and dip and strike data (Fig. 4.6C). Eighteen logs were collected using the top of unit A5 and base of unit A6 as datums as the mudstone in between has a constant thickness of 12 m across the entire panel.

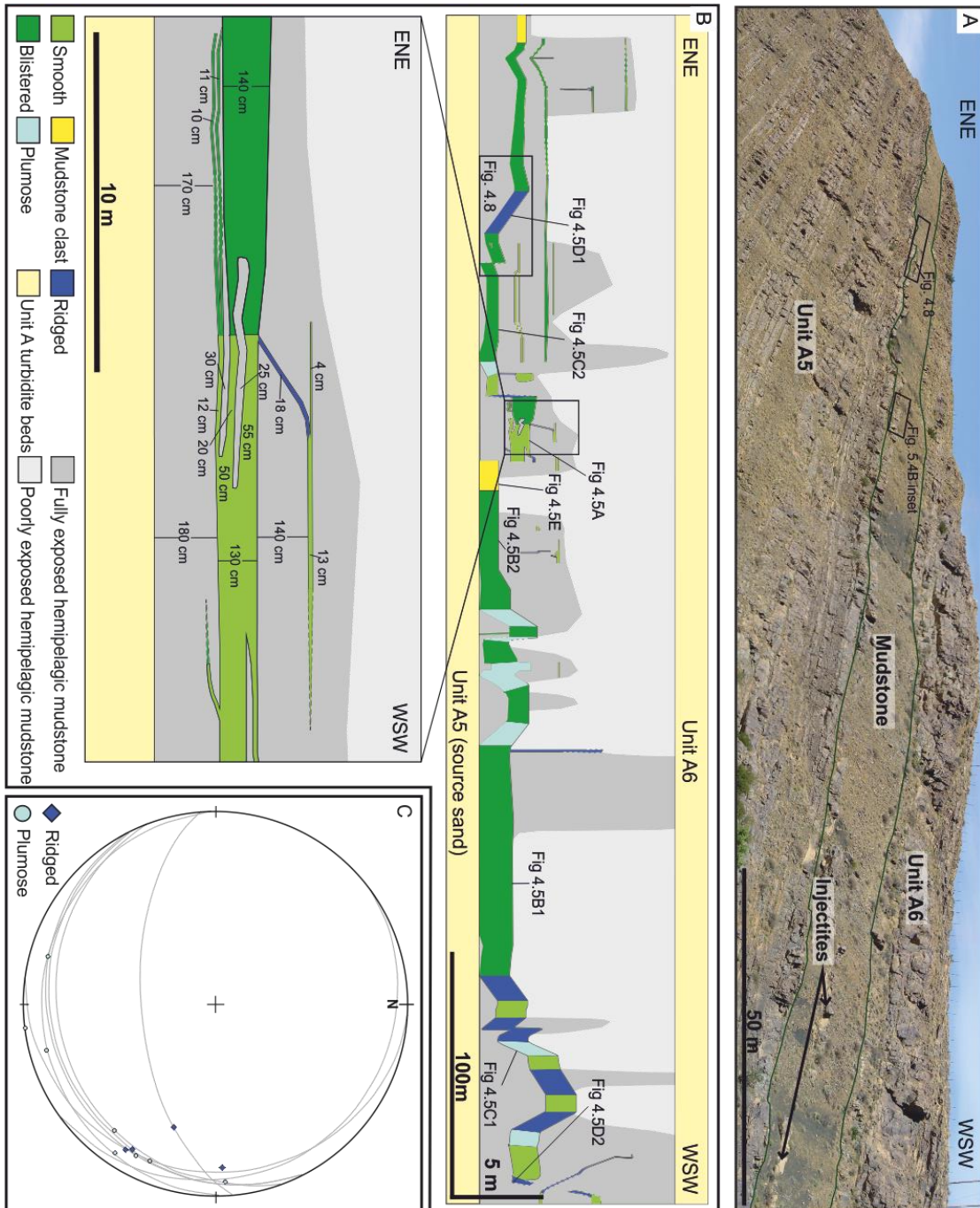


Figure 4.6 A) Outcrop photo panel highlighting injectites between lobe complexes A5 and A6. B) Panel used to correlate injectites showing the distribution of margin structures. Detailed panel in Appendix A.1, outcrop measurements in Appendix B.2. The inset shows the detailed distribution of injectites, with thicknesses and the distribution of margin structures. C) Stereonet with restored dykes, and plumose fracture and parallel ridge propagation data. Lineations are restored orientation of ridges and plumose fractures. Using the hackles (ridges) and fanning direction (plumose) the overall propagation direction was to the North and West, consequently there is a component of propagation from left to right in the figure, and another component coming out of the page towards the viewer.

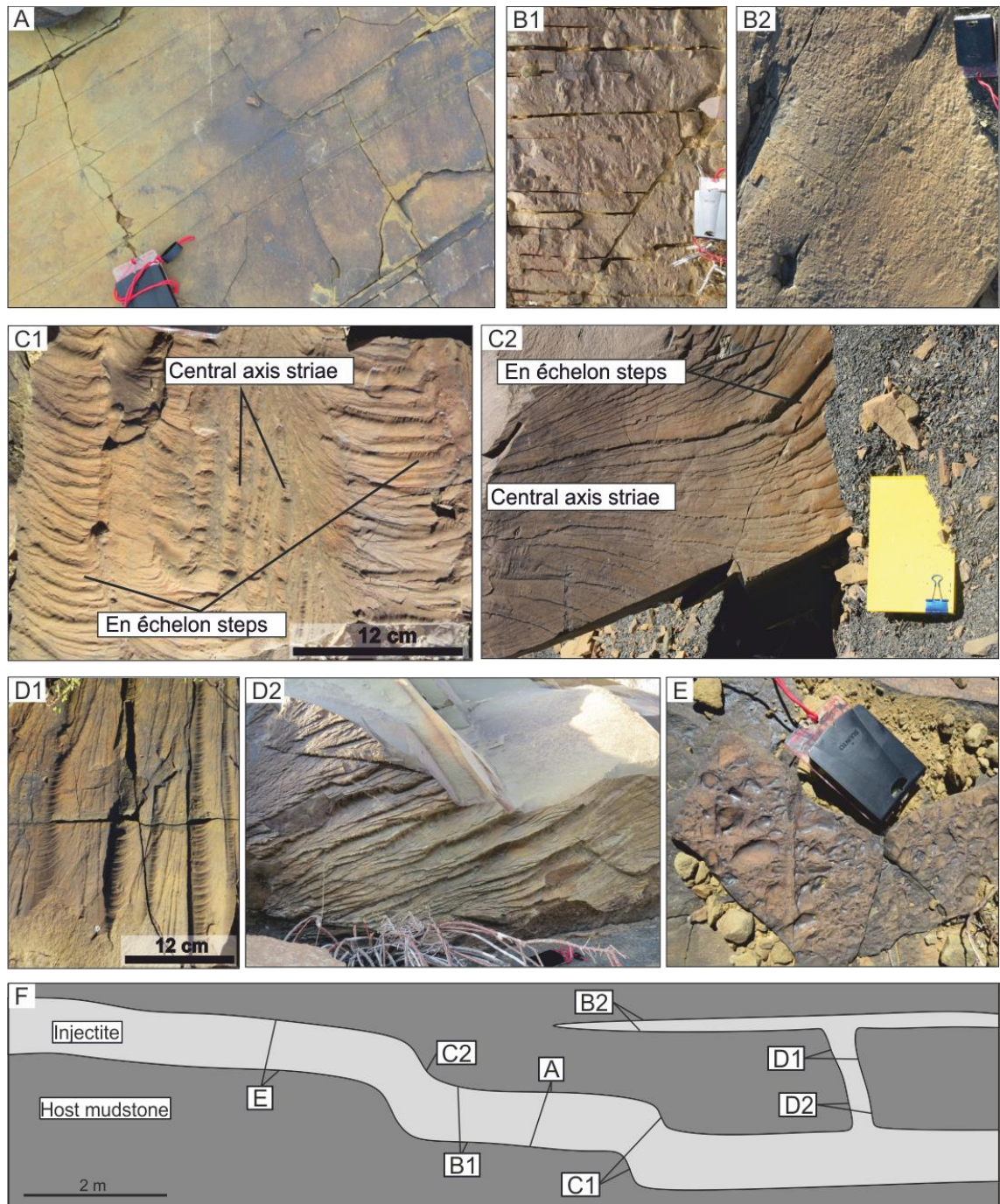


Figure 4.7 Representative photographs depicting typical margin structures associated with clastic injectites in the Karoo Basin, South Africa. A) Smooth, structureless surface. B1 and B2) Blistered surfaces, B1 showing the largest typical blisters, and B2 the smallest. C1 and C2) Two very different styles of plumose fracture, all indicating fracture direction. D1 and D2) Parallel ridges, all on sub-vertical injectites and with secondary hackle marks superimposed. E) Margin surface where mudstone clasts have been eroded out; clasts are up to several cm in diameter and are sometimes rounded. F) Cartoon of typical cross-section through injectite with positions of margin photos in relation to injectite geometry.

4.6 External structures and morphology

Several different structures have previously been identified on the margins of exhumed clastic sills and dykes. Features include flute-like marks, grooves, rills, lobate scours, frondescent marks and gutter marks (Peterson, 1968; Keighley and Pickerill, 1994; Parize and Friès, 2003; Surlyk *et al.*, 2007; Kane, 2010; Hurst *et al.*, 2011). Relief of such features ranges from millimetres to several metres in scale eroding into host stratigraphy. Small clasts of shale have been documented along dyke margins in outcrop (e.g. Diller, 1890), with laminations within clasts parallel to those of the host stratigraphy (Newsom, 1903; Parize *et al.*, 2007). Structures on the margins of clastic injectites can form either during the fracturing and injection of the host rock by the intrusive body (Lutton, 1970; Cosgrove, 1995; Müller and Dahm, 2000), or through later erosion of the fractures by the injecting fluid-sediment mixture (e.g., Martill and Hudson, 1989; Hillier and Cosgrove, 2002; Hubbard *et al.*, 2007; Hurst *et al.*, 2011). If margin structures occur due to fracturing, in the absence of any later reworking by the intruded flows, then the morphology and distribution of structures on injectite margins can be used to infer the properties of the host rock and sediment, and their interaction, at the time of fracture and fluid-sediment emplacement (Woodworth, 1895). The types of structures seen on injectite margins in the Karoo Basin include smooth surfaces, blistered surfaces, plumose ridges, parallel ridges and mudclast surfaces, all of which are observed at the Buffels River section (Fig. 4.6).

4.6.1 Smooth surfaces

Description

Smooth surfaces occur on sills only. No structures or features are present on the sharp top or basal margins, and the sandstone is smooth and flat (Fig. 4.7A).

Interpretation

Sills represent injection along bedding planes within the host strata. Given that smooth, structureless surfaces are only seen on sill margins, they are interpreted here as defining prominent and therefore smooth bedding planes within the host mudstone. During injection of sills, the overlying strata are presumed to be lifted or forced upwards.

4.6.2 Blistered surfaces

Description

A smooth surface with small (<2 cm diameter, <1 cm high) sub-circular bulges or bumps, which are referred to as blisters. The blisters are composed of sandstone, roughly circular with sub-rounded to sub-angular margins and can be concentrated into patches (Fig. 4.7B1) or occur in isolation (Fig. 4.7B2), and are only seen on sills. Occasionally, a lateral transition from smooth to blistered surfaces is observed, albeit associated with a degree of cutting upwards and downwards (Fig. 4.6B insert).

Interpretation

The largest blisters (2 cm diameter) are much smaller than the ellipsoid mudstone clasts (typically up to 10 cm in long-axis length and 4 cm diameter) that are present within the injectites, which indicates that they do not reflect primary plucking and entrainment of clasts by the injecting flow. Since blistered surfaces are only seen on sills, the blistering is related to the nature of horizontal fracturing through the host mudstones. Their presence suggests that the host mudstone is more homogeneous and lacks the prominent bedding planes associated with smooth fracture surfaces. Instead the fracturing of a relatively homogeneous mudstone leads to a fracture surface characterised by greater surface roughness; the blisters reflect the asperities on this surface. It is not clear why there is an abundance of sub-circular blisters instead of a more random shape distribution, though it is likely influenced by the mechanisms by which the bedding planes break apart. Transitions from smooth to blistered surfaces (Fig. 4.6B insert) may represent spatial changes in the relative heterogeneity of the mudstone as the fractures propagate laterally and cut up and down stratigraphy.

4.6.3 Plumose ridges

Description

All plumose features are observed on the margins of dykes and consist of fan-like features that range in scale from 20-100 cm in width with an angle of spread up to 180° and with relief of up to 2 cm (Fig. 4.7C). The main elements of the fan-like features are parallel striae down the centre of the feature, diverging striae that increase in relief away from the central axis, and en échelon segments at the fringes of diverging striae. Commonly, en échelon structures on the fringes of plumose features display superimposed plumose markings on their surfaces. At the outer edge

or fringe of these plumes, ridges form a step-like morphology of higher relief and a rougher texture often perpendicular to, or at an acute angle to, the parallel axial ridges. Restored orientation data collected for the azimuth of plumose ridges indicates a range from 265° to 015° (Fig. 4.6C).

Interpretation

We consider these features as an indication of the initial opening of a fracture during injection. Plumose patterns are a morphology found along fractures formed through mode I opening of homogeneous rock (e.g. Müller and Dahm, 2000; Fossen, 2010), and it has long been recognised that they provide an indication of unidirectional propagation direction (Lutton, 1970) parallel with axial striae and in the direction of plume opening and spreading (Fig. 4.8). As plumose patterns are only observed on the margins of dykes, they are interpreted to form through fracturing and breaking apart of host mudstone itself, and the pattern left is a cast of this fracturing. Restored propagation data indicate injection dominantly ranging between North and West (Fig. 4.6).

4.6.4 Ridged margins

Description

Ridges are parallel, have up to 4 cm relief and nearly always have a secondary set of asymmetric orthogonal ridges or hackle marks superimposed down one side that fan outwards (Fig. 4.7D1). Outcrop exposure allows for a maximum measured length of 1 m with ridges always observed together in sets. They are found on the margins of dykes, and where both margins are exposed the ridges are parallel. Typically, the crestlines of the ridges are oblique, up to 60°, to host strata bedding planes, and restored lineations are orientated 267-303° (Fig. 4.6C).

Interpretation

The ridged texture on dyke margins has previously been attributed to the fracturing of mudstone during forcible injection, supported by the 'jigsaw' like nature of both margins (Kane, 2010). Fracture propagation direction would have been along strike of the ridge crests (Hull, 1996), however this only offers a bidirectional constraint. The superimposed secondary ridges or marks, which are interpreted as hackles, indicate unidirectional propagation in the direction of fanning or towards the steep side of individual hackles (Hodgson, 1961; Lutton, 1970; Pollard *et al.*, 1982) (Fig. 4.8C). Figure 4.6C shows this propagation to be between West and Northwest along the Buffels River outcrop.

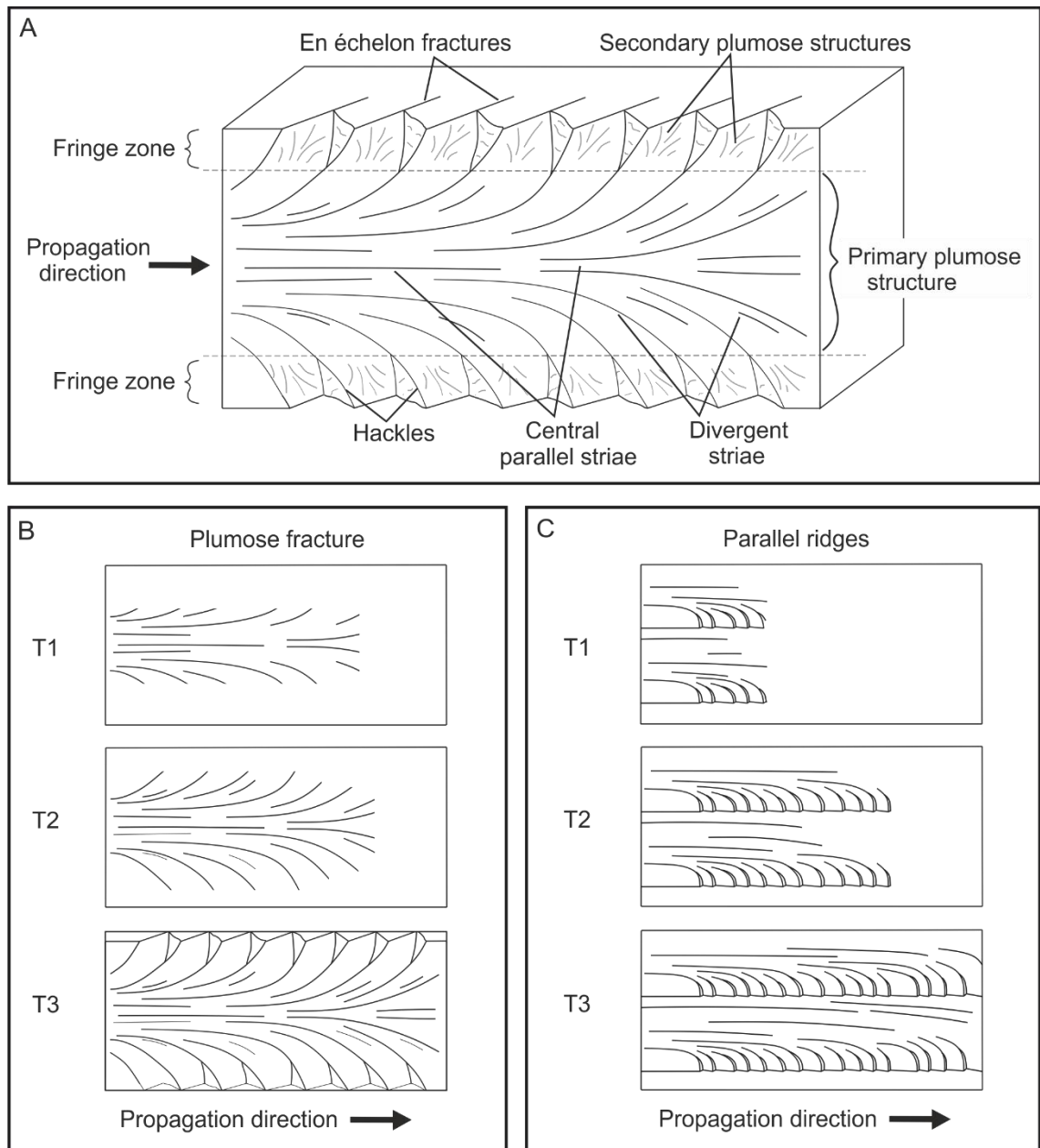


Figure 4.8 A) Schematic block diagram depicting joint faces and features on a plumose fracture (adapted from Fossen, 2010). B) Three time phases depicting formation of a single plumose fracture. C) Three time phases depicting formation of parallel ridges with hackles.

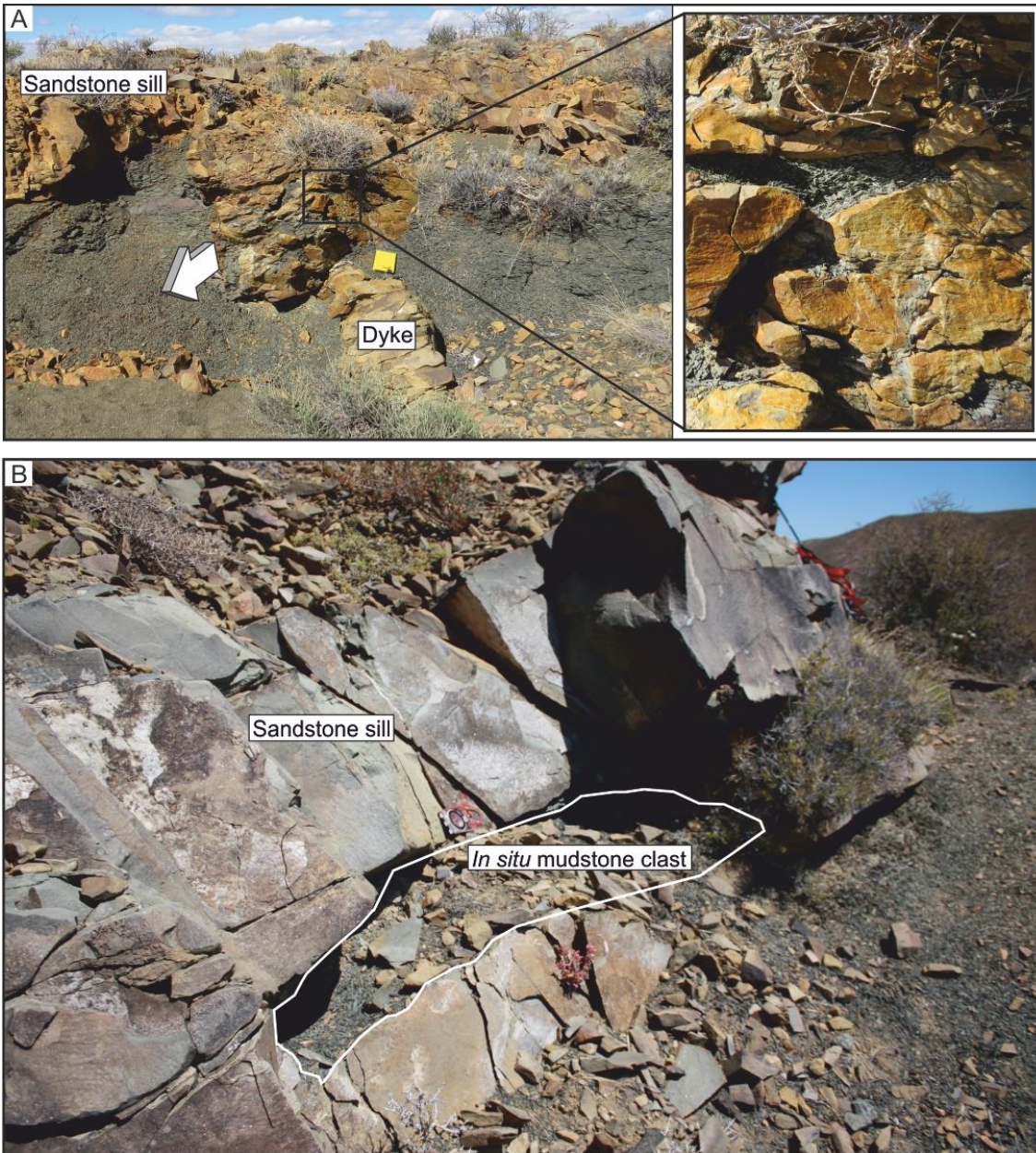


Figure 4.9 A) Sill-to-dyke transition zone, showing an area of *in situ* clasts at the sill/dyke junction. Arrow represents injectite propagation direction. Notebook for scale. B) Sill with an *in situ* mud clast >1 m in length; compass clinometer for scale. Figure 4.2 shows schematic views of the temporal development of these features.

4.6.5 Mudstone clasts

Description

Mudstone clasts are observed associated with clastic injectites in several different ways; i) at sill/dyke intersections, ii) within sills, iii) concentrated at sill margins.

Sill/dyke intersection: Where dykes are fed by sills, angular mudstone clasts, up to 20 cm in diameter are commonly present. Laminations within the mudstone clasts follow the character and orientation of laminations in the host mudstone (Fig. 4.9A). This is seen in injectites >10 cm in thickness.

In sills: Mudstone clasts are also present within the body of sills, in patches up to 2 m across with the biggest clasts reaching 1 m in diameter (Fig. 4.9B). The clasts can themselves host minor sandstone injectites. The thickness of the sand remains continuous around the clasts.

At sill margins: Sill margins show areas up to 5 m² concentrated in mudstone clasts on both the upper and basal surfaces. Individual clasts are up to 10 cm along the long-axis (of an ellipsoid pebble) and range from angular to rounded in cross-sectional shape (Fig. 4.7E). The largest clasts are associated with the thickest sills (>1 m thick) whereas sills <30 cm thick often only exhibit mudstone clasts <6 cm in length. Other than this broad correlation between sill thickness and mudstone clast size, no sorting of clasts by size or shape has been observed, and no imbrication of clasts is apparent (Fig. 4.7E) though the a and b axes are aligned parallel to sill margins.

Interpretation

It is widely assumed that mudstone clasts within clastic injectites are sourced from the host strata, plucked at dyke margins and incorporated into the flow of fluidised sand (Chough and Chun, 1988; Diggs, 2007; Hamberg *et al.*, 2007; Hubbard *et al.*, 2007). Where mudstone clasts are observed in sills, often towards the margins, it has been interpreted that the clasts were ripped-up or ripped-down from the host lithology and incorporated into the flow (e.g. Macdonald and Flecker, 2007). However, the absence of surfaces with evidence for plucking of large clasts suggests that their production was not directly associated with erosion by the sills during injection.

Sill/dyke intersection: An alternative source of mudstone clasts is the complex zone of brecciation and injection immediately adjacent to the connection between sills and dykes (Fig. 4.9A). This *in situ* brecciation of the host rock through hydraulic fracturing (e.g. Duranti and Hurst, 2004) creates clasts that either remain *in situ* where the primary lamination can be followed across clasts (Fig. 4.2: Sill-to-dyke intersection), or are entrained into the flow of fluidized sand.

In sills: As with sill/dyke intersections, it is most likely that these clasts are *in situ* as laminations within clasts are parallel with those of the host stratigraphy (cf. Newsom, 1903). The thickness of the sill itself remains constant where these clasts are present (Fig. 4.9B) suggesting that the injecting flow, was funnelled around or through conduits above and below these clasts, leaving them *in situ* (Fig. 4.2: Clast within sill body).

At sill margins: The occurrence of mudstone clasts predominantly along injectite margins is suggestive of high concentration flow with minimal mixing since flow concentration must have been high enough to support the clasts and enable deposition along the top margins of sills as well as deposition on the base. The sub-angular nature of the clasts implies low erosion and abrasion during transport and deposition. An obvious source for these clasts is the zone of brecciation at sill/dyke intersections. Erosion of injectite walls during injection is ruled out due to the complete lack of any erosive features both on sills and dykes. Blistered surfaces have dimples, bumps and bulges with maximum diameters of 2 cm, whereas the largest clasts are up to 10 cm in long-axis length and 4 cm in diameter (see Appendix 1). The difference in size between blisters and clasts suggest that the blistered surfaces were not the source of the clasts.

4.6.6 Stepped sills

Description

Step-ramp-step geometries are generally up to 1 m in height and crosscut stratigraphy at between 10 and 70°. Structures seen on step margins are either plumose (most common) or parallel ridges. Figure 4.6B shows an example of a sheet sill stepping through stratigraphy multiple times over 500 m of outcrop.

Interpretation

Steps refer to the particular geometry of an injectite, which are also recognised in igneous intrusions (e.g. Schofield *et al.*, 2012a) (Fig. 4.10A). As the intrusion geometry represents the fracture mechanics of the host strata and not the injecting fluid, the same interpretation of step formation can be applied to clastic dykes and sills. Similar step features have previously been identified in clastic injectites (Vétel and Cartwright, 2010). Steps occur when intrusion tips propagating through brittle strata, become slightly offset (Schofield *et al.*, 2012a) resulting in en échelon fracture propagation with individual steps increasing in height or offset in the direction of fracture growth (Pollard *et al.*, 1975; Schofield *et al.*, 2012a). Therefore the exposure of steps at outcrop, as well as at a larger scale in seismic data, could be used to identify initial fracture and therefore propagation direction (Fig. 4.6B and 4.10A).

4.6.7 Summary of spatial distribution of injectite margin structures

These differing margin structures each occur in spatial positions specific to the injectite geometry. The array of margin structures is synthesised in Figure 4.10; mudstone clasts, smooth

and blistered surfaces are found on margins of sills where injection is parallel with host strata, whilst in contrast ridged and plumose margins are associated with dykes and where injection is discordant with host strata (Figs. 4.7F and 4.10B). Figure 4.10 also illustrates the relative positions of mudstone clasts within injectites; those within sill bodies and those at the sill/dyke intersection. In summary, each of the structures described in the previous section only occur in specific localities relating to injectite architecture and can be categorized on this basis.

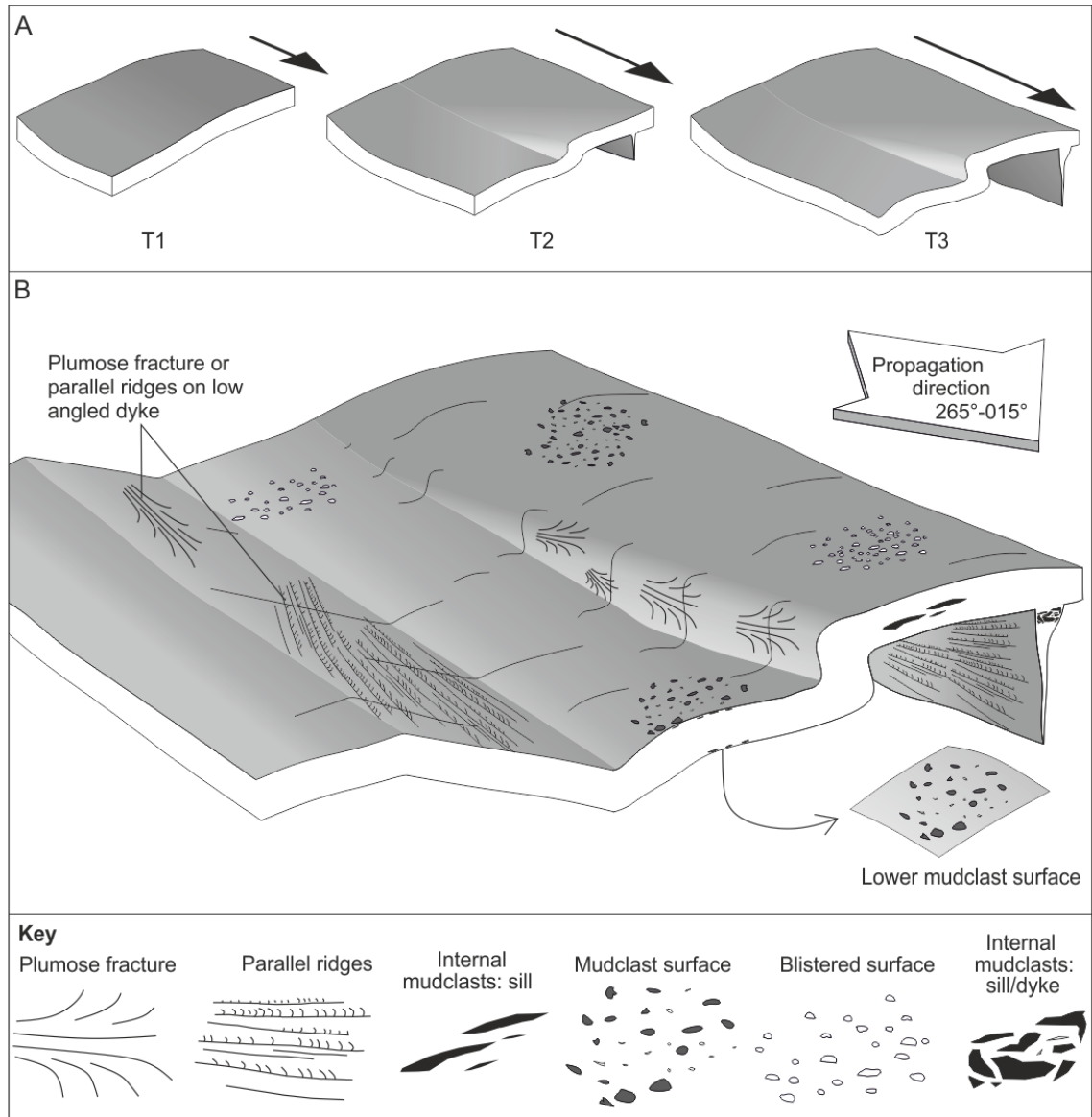


Figure 4.10 A) Three time phases showing the formation of a stepped sill as an injectite propagates. B) Schematic diagram showing spatial distribution of internal and external injectite structures.

4.7 Discussion

Previous work on structures on injectite margins has identified both those of a primary nature associated with initial fracturing, and features related to later erosion by flows associated with the injection process (Peterson, 1968; Taylor, 1982; Surlyk and Noe-Nygaard, 2001; Hillier and Cosgrove, 2002; Hurst *et al.*, 2005; Diggs, 2007; Hubbard *et al.*, 2007; Kane, 2010). In the present study, many of these margin structures show strong similarities with fracture-related features formed in previously documented settings and experimental research (plumose, parallel ridges, steps opening in direction of propagation) (Hodgson, 1961; Lutton, 1970; Müller and Dahm, 2000). In addition, the dykes and sills show no evidence for erosion along their margins, with many sill/dyke intersection regions showing the only evidence for host lithology entrainment. Intricate features such as the plumose structures on dykes and steps are preserved in a pristine state, whilst the sill margins are either smooth or associated with structures that are far smaller than the clasts that are observed within the injectite. Consequently, there is strong evidence that these injectite margin structures are primary features caused directly by the fracturing process, and the injectites essentially serve as casts of the fracture surface. This allows us to use these features to determine propagation direction, depth of emplacement relative to the tensile strength of the host mudstone, and processes of the injecting flows.

4.7.1 Determining injection propagation direction using margin structures

Plumose pattern

Plumose patterns are interpreted to reflect the way in which the host mudrock initially fractured immediately prior to injection of fluids and sand, with the direction of fracture, and therefore injection, parallel with the plume axis (Fossen, 2010). Generally, a fracture in a brittle rock propagates along a plane perpendicular to the axis of minimum compression, and the fracture itself forms under tension (Fig. 4.1: mode I) (Pollard *et al.*, 1982; Lorenz *et al.*, 1991; Fossen, 2010). However, if the principle stress axis rotates as plumose fractures form, causing fracture direction to change, then shear fracturing (mode III) will occur at the newly orientated fracture front in order to adjust to the new stress state (Fig. 4.1; Sommer, 1969). Therefore, if the propagation at the tip of the main fracture is occurring under a tensional regime, then as the ridges that form the plumose fracture diverge, the fracture propagation direction is no longer perpendicular to the axis of minimum compression. To compensate, fracture by shearing takes place, which leads to the formation of en échelon steps at its tip (Pollard *et al.*, 1982), orientated

oblique to the parent fracture plane (Bahat, 1986) (Fig. 4.8). En échelon structures always form in a specific orientation related to the overall stress regime and therefore, at a given outcrop, will likely all have the same orientation. Orientation data from the sheet injection and connected dykes of the Buffels River outcrop indicate a northwest propagation direction (Fig. 4.6B, 4.6C and 4.10B).

Where outcrop allows for injectites to be observed in three-dimensions, multiple sets of plumose fractures are observed along steps. In these cases, multiple plumose fractures are indicative of a broad yet definitive propagation direction; synthesised in Figures 4.8 and 4.10B. Experimental work by Sharon *et al.* (1995) has related velocity of fracture propagation through multiple fractures with a constant overall energy state. From initial fracture, velocity of propagation increases until the critical velocity for the onset of branching (v_c) is reached. It is at this point that the en échelon style fringe of the plumose fracture initiates (Sharon *et al.*, 1995; Bahat, 2001). Fracture propagation velocity decreases as the relief on the fracture plane increases due to the enlargement in fracture area (Müller and Dahm, 2000; Bahat, 2001; Chemenda *et al.*, 2011). In the case of plumose fractures, this would be from the central plumose structure to the en échelon fringes. Energy that was solely being used to propagate the parent fracture is now subdivided between parent and daughter cracks (central axis striae and en échelon respectively). Less energy is available for the fracture to continue propagating and therefore overall propagation velocity slows (Sharon *et al.*, 1995). The daughter en échelon cracks have a restricted lifetime and once they stop all of the energy is then returned to forward propagation and another plumose fracture forms (Sharon *et al.*, 1995). These extensional fractures grow in pulses, with each propagation pulse ending by slowing down or completely stopping until enough energy has built up to initiate the next pulse and plumose fracture (Fossen, 2010). At outcrop, therefore, it is possible to gain an understanding of local stress within the rock at the time of fracture from a small group of plumose patterns and it is feasible to estimate a more widespread stress regime from collecting orientation data over a large area.

Parallel Ridges

Kane (2010) suggested that an observed “ropey” texture on injectite margins is a result of the splitting apart of the host sediment as the feature is often parallel on opposite margins. Second order hackle marks (Fig. 4.8C) indicate unidirectional fracture propagation and therefore injection direction can be determined through observation of this particular structure using similar criteria to plumose fractures (Figs. 4.7D1 and 4.8A). This is supported where injection

direction is constrained from plumose fractures and steps. On outcrop, ridges are continuous as far as observation allows, and therefore unlike pulsed plumose fracture propagation, it is likely that these occur during quasi-constant fracture propagation.

4.7.2 Estimating injection depth

Where injectite complexes reach the seabed and extrude sand it is possible to give a minimum depth of injection from lowermost injectites up to extrusions (Surlyk and Noe-Nygaard, 2001; Thompson *et al.*, 2007; Ross *et al.*, 2013, 2014). For example, the Panoche Giant Injection Complex in California has an estimated thickness of up to 1500 m (Vigorito *et al.*, 2008; Vigorito and Hurst, 2010; Scott *et al.*, 2013). However, where clastic injectites do not reach the surface there has been no methodology proposed for estimating the depth of intrusion. This chapter shows that the mode of fracture can be used for relative depth estimation. This chapter also explores the possibility of extending this to estimation of true depths, and discusses why this is not presently possible.

The state of stress during burial in a tectonically quiescent basin is assumed to be confining and therefore extensional fractures are unusual. However, natural hydraulic fractures are a form of extension in a setting with confining stresses (Phillips, 1972; Cosgrove, 2001). Clastic dykes form in extensional (tensile) fractures, which are usually typical of deformation at low differential stresses ($\sigma_1 - \sigma_3$) or confining pressures. In settings of high fluid pressure, however, low differential stress and mode I (tensile) fractures can occur at several 100s m depth (Secor, 1965; Aydin, 2000; Cosgrove, 2001) with the expression or relief of these features increasing with increasing pressure (Chemenda *et al.*, 2011). Near to the surface mud has low tensile strength despite being cohesive, and therefore will undergo plastic deformation when stress is applied (Lowe, 1975; Nichols *et al.*, 1994). Muds exhibit higher tensile strengths at depth thereby enabling mode I failure in the host sediment (Jolly and Lonergan, 2002). This combination of the depth distribution of tensile strength in muds, and the high fluid pressures associated with injection, suggests that mode I failure will occur at considerable depths (up to 100s of m).

Shear failure occurs at a depth where the applied shear stress, S , is greater than 4 times the tensile strength of the rock, T , changing from extensional fracturing at shallower depths (Fig. 4.1) (Cosgrove, 2001). Plumose fractures with en échelon fringes form from mainly extensional deformation (central and divergent striae), but with a component of shear fracturing. This could

place a depth range on formation of fractures and injection at or near to the bounding zone from extensional to shear stresses.

Extending this estimation of relative depth to true depths is challenging for a number of reasons. Firstly, a depth profile for the tensile strength of the host shale must be calculated. This can be achieved by: i) calculating porosity as a function of depth for shales (e.g., Baldwin and Butler, 1985), ii) calculating the uniaxial compressive strength of shale as a function of porosity:

$$C_0 = 243.6\varphi^{-0.96} \quad \text{Eq. 4.1}$$

where C_0 is the uniaxial compressive strength and φ is porosity (Horsrud, 2001; Lothe *et al.*, 2004), and finally, iii) assuming that the tensile strength is $1/10^{\text{th}}$ that of the uniaxial compressive strength (Lothe *et al.*, 2004). Thus an estimate of the profile of tensile strength, T , with depth can be calculated. Given that shear failure occurs where applied shear stress is $>4T$, then the applied stress needs to be calculated. Estimates of propagation rate in injectites range from $0.1\text{-}10 \text{ ms}^{-1}$ (Bureau *et al.*, 2014) based in part on comparison with igneous intrusions (Rubin, 1995). However, the applied stress at the tip of a palaeofracture is difficult to estimate because knowledge of the processes occurring in the area immediately around the propagating fracture tip is limited, and the rate of fracture propagation is hard to predict (Fineberg and Marder, 1999; Bahat *et al.*, 2005).

Although absolute depths of injection cannot be calculated, relative depth of injection can be estimated. Based on analysis of the fracture patterns occurring at a depth where tensile strength is at least four times that of the host mudstone, it is possible to rule out very shallow injection. Furthermore, injectites with margin structures indicative of this range of fracture modes, are able to form at up to several 100's of metres depth. This approach enables relative injection depth to be inferred for systems that are not connected to the surface.

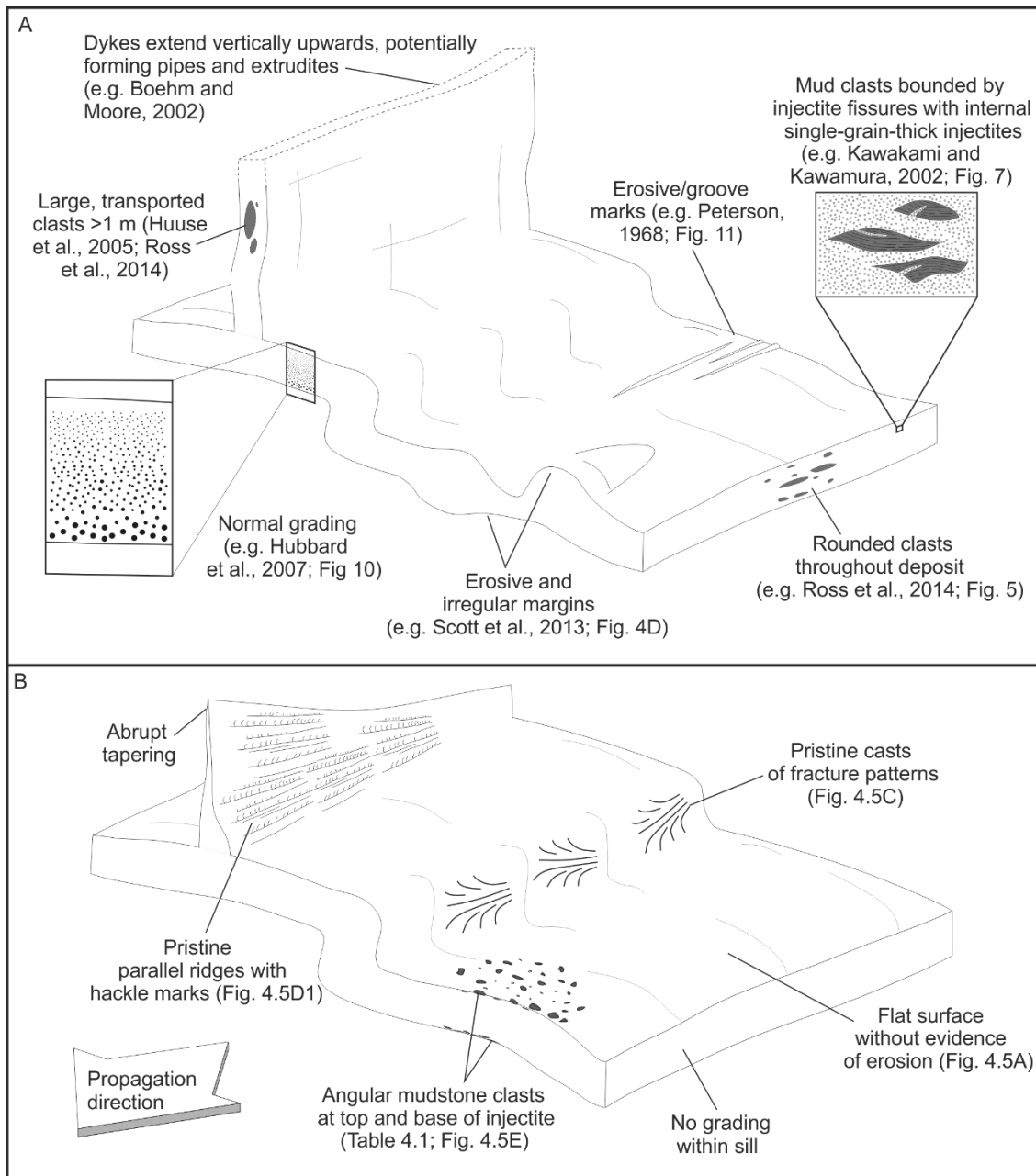


Figure 4.11 Recognition criteria for distinguishing between laminar and turbulent flow in clastic injectites. A) Injectite architecture and features expected as a product of turbulent flow during clastic injection. Grading, both normal and reversed, within injectites is typically related to turbulent flow and is most likely a function of parent sand composition and preferential fluidisation of grain sizes. Erosive or groove marks on the margins of sills or dykes and rounded clasts throughout the deposit also suggest turbulent flow. Mud clasts within the injected sandstone are sometimes bounded by or injected by one-grain thick sand filled fissures. Dykes forming extensive vertical conduits, potentially forming pipes and subsequently extrudites are also an indicator of turbulent flow. B) Schematic diagram of typical injectite architecture and structures associated with laminar flow.

4.7.3 Flow processes during injection

The nature of flow in injectites has been the subject of much debate, with arguments for both laminar flow (Dott, 1966; Peterson, 1968; Taylor, 1982; Sturkell and Ormö, 1997) and turbulent flow (Obermeier, 1996; Duranti, 2007; Hubbard *et al.*, 2007; Scott *et al.*, 2009) being forwarded. Scott *et al.* (2009) suggest that a “spectrum of flow conditions from low-velocity viscous, hydroplastic laminar flow to high-velocity, turbulent flow probably occurs”. In a more recent paper, Hurst *et al.* (2011) have argued that “evidence of a turbulent flow regime during sand injection is prevalent”.

The distribution of transported mud clasts at both the top and base of sills (Figs. 4.7E and 4.10B) suggests that the flow was highly-concentrated, since the particles at the top were unable to settle through the sediment; similar features are also observed in other examples (see Macdonald and Flecker, 2007; Hurst *et al.*, 2011). The mechanism for this observed segregation of mud clasts towards the wall regions of the sills is unclear, but both potential mechanisms: i) incorporation and maintenance of particles near the edge of the flow, and ii) segregation of particles within the flow, suggest high-concentration, slow-moving flows. Particles may have been incorporated near the edge of the flow and given the short transport distances and high-concentration may not have mixed into the flow. Another possible mechanism is inertial induced lateral migration of particles towards the walls which occurs in laminar flows (Segré and Silberberg, 1962a,b). Where density differences in particles are present, less dense particles will preferentially move towards the walls (Hogg, 1994). Densities of shales at the suggested depths of hundreds of metres are likely in the region of 1900-2300 kg m⁻³ (Rieke and Chilingarian, 1974; Castagna *et al.*, 1993) so the mud clasts will be less dense than the quartz-dominated sand grains (~2650 kg m⁻³). Such effects have been observed experimentally for small particles, with correspondingly low particle Reynolds numbers, under laminar flow conditions (Segré and Silberberg, 1962a,b; Hogg *et al.*, 1994). However, it is unclear if this mechanism extends to larger low-density particles in laminar flows. Rounding of many of the mud clasts is in accordance with some transport prior to deposition, although the angularity of some clasts and the absence of evidence for local sourcing, suggests that the flow was not particularly turbulent and abrasive. The preservation of delicate structures such as the pristine plumose structures also indicates that significant abrasion did not take place at fracture margins during injection emplacement. For example, there is no evidence for scratches on these features, or of features indicative of turbulent flow such as flute marks (Allen, 1982; Hurst *et al.*, 2011). In fact, no evidence of erosion has been observed within the sills and dykes, and the main features on injectite margins are all

interpreted to be a primary function of the fracture process. The absence of any evidence of abrasion or erosion, further suggests that the injections were associated with high-concentration, relatively slow moving flows.

The flow processes are further assessed through calculation of flow Reynolds numbers, Re , using the methodology of Ross *et al.* (2014) and the parameter values in Table 4.1:

$$Re = (U \cdot A \cdot \rho_{pf}) / \mu_{pf} \quad \text{Eq. 4.2}$$

where U is velocity of the injection, A is the fracture aperture, and ρ_{pf} and μ_{pf} are the pseudofluid density and viscosity respectively, with the pseudofluid being the mixture of water and fine-grained particles (Di Felice, 2010; Ross *et al.*, 2014). The method estimates the velocity of the injected suspension, U , as being equal to, or greater than, the fall velocity of the largest particle (see Ross *et al.*, 2014 for full details). Previous estimates of velocities in injectites were based on two-dimensional sections and utilised the largest observable length as the grain-diameter (Scott *et al.*, 2009; Ross *et al.*, 2014), leading to potential errors in the calculation of velocities if particles are strongly ellipsoid (Matthews, 2007). In this field example, the way in which the ellipsoidal mud clasts weather out on surfaces enables a more accurate equivalent spherical diameter to be calculated.

Parameter	
g (ms^{-2})	9.81
ρ_s (kg m^{-3})	2650
ρ_L (kg m^{-3})	2100
ρ_f (kg m^{-3})	1000
ϕ	0.54 - 0.4
ϕ_s	0.53 - 0.39
ϕ_L	0.01
$C_{D,o}$	1.4
D_p Large particle (m)	0.071
D_s Large particle (m)	0.044
μ_f (paS)	0.00106
A (m)	0.1 – 1.3
ρ_{pf} (kg m^{-3})	0.0087 – 0.028
μ_{pf} (PaS)	0.0043 – 0.0091
n	2.25

Table 4.1 Parameters used in order to calculate flow velocity and Reynolds number of fluid flow of clastic injections in the Karoo Basin. The methodology of Ross *et al.*, (2014) was implemented here.

The velocity calculations assume that the volumetric particle concentrations are high, since the large particles are unable to settle through the flow. However the exact volumetric flow concentration is unknown and therefore a range of concentrations (solid volume fractions) is considered. Solid volume fractions range from close to the highest possible value for fluidisation (0.54) (Leva, 1959; Scott *et al.*, 2009; Ross *et al.*, 2014), down to a more conservative value of 0.4 that might not be expected to fully support the large particles at the upper margins of sills. These calculations demonstrate that flow Reynolds numbers for many of the dykes and sills are either in the laminar flow regime, $Re < \sim 2300$ (for fractures, injectites and pipes; Singhal and Gupta, 1999; Faisst and Eckhardt, 2004; Scott *et al.*, 2009; Post, 2011), or in the transitional flow regime, $Re > \sim 2300$ $Re < \sim 4000$ (Faules and Boyes, 2009; Munson *et al.*, 2012); see Table 4.2. If as argued here solid volume fractions are close to the highest grain concentration possible for fluidisation (0.54), then almost all the injectites likely formed under laminar conditions (up to 1.1 m thick), with the remainder exhibiting transitional flows (up to the maximum observed thicknesses of 1.3 m) (Table 4.2). If lower solid volume fractions were prevalent then flows were likely laminar or in the transitional regime for the vast majority of sills (up to 0.8 m thick) for solid volume fractions of 0.47, and even at solid volume fractions as low as 0.4, sills and dykes up to 0.35 m thick are predicted to be laminar or transitional (Table 4.2).

Predicting laminar and turbulent injection flow processes and products

Evidence in support of turbulent flows (Fig. 4.11A) in injectites comes from flow Reynolds number calculations based on fall-velocities of large clasts (Duranti and Hurst 2004; Scott *et al.* 2009; Sherry *et al.* 2012; Ross *et al.* 2014), erosional margins and the formation of features such as scours (Hubbard *et al.*, 2007; Vigorito *et al.*, 2008; Vigorito and Hurst 2010; Scott *et al.*, 2013), and normal grading (Obermeier, 1996; Hubbard *et al.*, 2007; Ross *et al.*, 2014). Internal laminations have been interpreted as the product of both laminar (Dott, 1966) and turbulent flows (Hurst *et al.*, 2011 citing Lowe's (1975) work), and their observation in terms of flow process remains equivocal (Hurst *et al.*, 2011). The examples of interpreted turbulent flow described in the references above are either from injectite systems that reached the palaeo-surface, or are of unknown vertical extent (Hubbard *et al.*, 2007). In contrast, systems

interpreted to exhibit laminar flows (Fig. 4.11B) lack evidence for grading or scouring, and contain abruptly tapering sills and dykes, suggesting that they formed at depth, and without a surface connection (Taylor, 1982). The present study exhibits the same structures and geometric relationships as the examples of Taylor (1982) but enables quantification of flow conditions for the first time, demonstrating that small dykes and sills at depth (up to a few 10s of cm in thickness) almost certainly form under laminar conditions, and suggesting that even relatively large sills (order 1 m) may well be formed under laminar conditions.

Aperture (m)	Grain concentration 54%	Grain concentration 47%	Grain concentration 40%
0.1	199.37	490.03	1030.01
0.2	398.74	980.06	2060.02
0.3	598.10	1470.09	3090.03
0.4	797.47	1960.12	4120.04
0.5	996.84	2450.16	5150.05
0.6	1196.21	2940.19	6180.06
0.7	1395.57	3430.22	7210.07
0.8	1594.94	3920.25	8240.08
0.9	1794.31	4410.28	9270.09
1.0	1993.68	4900.31	10300.10
1.1	2193.04	5390.34	11330.10
1.2	2392.41	5880.37	12360.11
1.3	2591.78	6370.41	13390.12

Table 4.2 Flow Reynolds numbers for grain concentrations of 54%, 47% and 40% in sill apertures ranging from 0.1 m to 1.3 m. All calculations are for an ellipsoid mudstone pebble 10 cm along the longest axis.

When fractures occur at depth without an open connection to the surface, then there is a limited capacity for flow dilution, with liquid and particulate components moving together from high to low pressure, thereby encouraging high-concentration flows. Such high-concentration flows are far less likely to exhibit turbulent conditions since flow viscosity varies strongly (by orders of magnitude) with flow concentration (e.g., Krieger and Dougherty, 1959). As a consequence the viscous term in the Reynolds equation (equation 4.2) is likely dominant unless the cross-sectional dimensions (fracture aperture) of injectites become large. In contrast, once connection to the surface occurs a greater fraction of carrier fluid to particles can be accommodated, enabling highly turbulent and lower-concentration flows to form. Essentially, overpressured water is able to escape to the surface and in so doing carry particles with it. Observations of active sand volcanoes in nature and in the laboratory demonstrate that the resulting extrusions are not high-concentration granular flows, but are lower-concentration systems (Ross *et al.*, 2011; Quigley *et al.*, 2013).

Given these parameters it is possible to envisage three broad categories of flow during injection: i) flows that are connected to the surface where flows are relatively low-concentration and highly turbulent; ii) large-scale injectites that do not have a connection to the surface, that will exhibit high-concentration turbulent flows, and iii) flows with no connection to the surface and with relatively small cross-sectional dimensions (10s cm) where flows will be highly concentrated and laminar. Correspondingly, the products of these flows will be different, with structures such as grading and erosional scours prevalent in low-concentration open conduits, whilst such features will be lacking in smaller-scale laminar injectites in closed conduits. The degree to which larger-scale closed systems might exhibit erosive structures and grading is largely unknown.

4.8 Conclusions

The clastic injectites studied herein have provided a classification for common structures seen on the margins of sills and dykes as well as common assemblages of clasts within the injectites. Using plumose marks, parallel ridges and steps within sills it is possible to establish initial fracture propagation directions, and therefore overall injection direction of dykes and sills. The use of these margin structures also makes it possible to estimate relative injection depth where applied stress exceeds four times the tensile strength of the host rock. Furthermore flow estimates for clastic injections suggest that laminar conditions prevail in dykes up to 10's cm thick, and in sills up to a metre thick, if as the evidence suggests, particle concentrations were

close to the limit of fluidisation (solid volume fraction of 0.54). This study provides a new set of criteria for determining flow direction and depth of emplacement within clastic injectites, as well as demonstrating high-concentration laminar flow during injection. The existing debate on the nature of flow, laminar versus turbulent, during injection, is addressed here in terms of whether the injection occurred in an open (linked to surface) or closed system.

5. An integrated model of clastic injectites and basin floor lobe complexes: implications for stratigraphic trap plays

5.1. Introduction

Improvements in subsurface imaging quality in recent years have led to increased recognition and understanding of the impact of injectites on the architecture and fluid flow of sedimentary basin-fills. However, the distribution of subseismic scale injectites and their relationship to those of a seismic-scale are poorly understood (Hurst & Cartwright, 2007). The literature is dominated by examples of clastic injectites that are associated with primary deposits on a slope setting, such as deep marine channel-fills (Hiscott, 1979; Rowe *et al.*, 2002; Parize & Friès, 2003; Duranti & Hurst, 2004; Huuse *et al.*, 2005; Diggs, 2007; Duranti, 2007; Frey-Martínez *et al.*, 2007; Hamberg *et al.*, 2007; Jackson, 2007; Jonk *et al.*, 2007; Surlyk *et al.*, 2007; Vigorito *et al.*, 2008; Kane, 2010; Svendsen *et al.*, 2010; Szarawarska *et al.*, 2010; Jackson *et al.*, 2011; Løseth *et al.*, 2013; Morton *et al.*, 2014; Bain & Hubbard, 2016) and intraslope lobes (Monnier *et al.*, 2014; Yang & Kim, 2014; Sychala *et al.*, 2015). In cases where the parent sand cannot be directly constrained, regional context still suggests that injectites were originally sourced from a submarine slope sandbody (e.g. Panoche complex: Vigorito *et al.*, 2008) or slope channel-fills (e.g. Chile: Hubbard *et al.*, 2007). These depositional environments commonly provide the key conditions for clastic injection, including: i) pore pressure in parent sandbody higher than that within the mud-prone host strata (Lorenz *et al.*, 1991; Cosgrove, 2001; Jolly & Lonergan, 2002), and ii) clean, fine to very fine unconsolidated sand that is most susceptible to fluidisation and grain transport (Richardson, 1971; Jolly & Lonergan, 2002). In contrast, injectites demonstrably sourced from base of slope and basin floor sandbodies have rarely been documented (Cobain *et al.*, 2015).

In sedimentary basins, lithology is the principle control on basin wide fluid migration (Bjørlykke, 1993; Jonk *et al.*, 2005a), and in the absence of clastic injectites fractures and faults form the most efficient conduits for fluid flow (Chapman, 1987; Knipe *et al.*, 1998; Aydin, 2000). However, clastic injectites create additional fluid flow pathways, and their impact depends on their timing and location (e.g. Hurst *et al.*, 2003; Jonk, 2010; Ross *et al.*, 2014). Net migration of fluids, including water and hydrocarbons, into an unconsolidated sandbody can provide the overpressure and trigger mechanism needed for sands to fluidise and inject (Vigorito & Hurst,

2010; Bureau *et al.*, 2014). Post-injection, sandstone dykes and sills can act as fluid flow conduits for hydrocarbon leakage (Jonk, 2010) until cementation, at which point injectites become fluid flow baffles and barriers. Later, reactivation of clastic injectites as fluid flow conduits can occur through preferential brittle deformation of competent sandstones within a low-competence (majority mudstone) host rock (Jonk *et al.*, 2005a).

For the first time, we present examples of injectites at outcrop where the palaeogeographic and stratigraphic context of the basin-floor parent sandstone bodies are well constrained. We address the following objectives: i) to document the architecture and character of injectites in basin-floor settings in terms of thickness and morphology in relation to parent sand, ii) to investigate the association between the architecture and character of the basin-floor parent sandbody as a control on the location and orientation of injectites, iii) to construct an integrated model of clastic injectites in basin-floor settings, iv) to consider the role of basin-wide fluid flow pre-, syn-, and post-injection, and v) to discuss the association and implication for subsurface stratigraphic trap plays and the presence of injectites.

5.2. Geological Setting

The Karoo Basin has long been interpreted as a retro-arc foreland basin that formed on the southern margin of the Gondwana palaeocontinent behind a magmatic arc and fold-and-thrust belt (Johnson, 1991; Visser & Praekelt, 1996; Catuneanu *et al.*, 1998; Johnson *et al.*, 2006). However, more recent studies suggest subsidence during the Permian was driven by mantle flow and foundering of basement blocks coupled to subduction of the palaeo-Pacific Plate to the south, pre-dating the Cape Orogeny (Tankard *et al.*, 2009). The Ecca Group, a siliciclastic succession, was deposited in the southwestern Karoo Basin during the Permian (Flint *et al.*, 2011). This part of the basin is subdivided into the Laingsburg and Tanqua depocentres (Fig. 5.1A), and this study focusses on three outcrop examples of exhumed clastic injectites hosted in deep water strata of the Ecca Group across these depocentres (Figs 5.1C and 5.1D).

The Tanqua depocentre infill comprises 1.3 km of deep-water sediments (Hodgson *et al.*, 2006) of the upper Ecca Group (Tierberg and Skoorsteenberg formations; Wickens, 1994; Wickens & Bouma, 2000) overlain by submarine slope and shelf-edge deltaic deposits (Kookfontein Formation; Wild *et al.*, 2009) (Fig. 5.1B). The 400 m thick Skoorsteenberg Formation comprises four sand-prone basin-floor fans (Fans 1-4) that are separated by laterally extensive fine grained

intervals (Hodgson *et al.*, 2006) and overlain by a 100 m thick channelized slope succession (Unit 5) (Fig. 5.1B). The adjacent Laingsburg depocentre was infilled by a 1.8 km thick shallowing upward succession from distal and proximal basin-floor (Vischkuil and Laingsburg formations respectively; van der Merwe *et al.*, 2010; Flint *et al.*, 2011) through leveed slope-channels (Fort Brown Formation; Kane & Hodgson, 2011; Morris *et al.*, 2014) to shelf-edge and shelf deltas (Waterford Formation; Jones *et al.*, 2015)(Fig. 5.1B). Sand-prone Units C to G, which comprise the Fort Brown Formation (Fig. 5.1B), have been mapped over 2500 km² (van der Merwe *et al.*, 2014), and are separated by regional mudstones interpreted to represent clastic input shutdown due to relative sea level rise (Di Celma *et al.*, 2011; Flint *et al.*, 2011; Fig. 5.1B).

5.3. Methodology and dataset

Three outcrops were studied in detail; Bizansgat (Tanqua depocentre: injectites associated with Fan 3) (Figs 5.1-5.4), Zoutkloof and Slagtersfontein (Laingsburg depocentre: injectites associated with Unit C, Subunits C1 and C2) (Figs 5.1 and 5.5-5.7). Recognition criteria of injectites in the Karoo Basin include cross-cutting relationships, direct connection to overlying sandstones, preserved patterns on fracture surfaces of injectite margins, such as plumose patterns and parallel ridges, and blistered and mudstone clast-rich surfaces (c.f. Cobain *et al.*, 2015). Field-based sedimentological and stratigraphic observations include logged vertical profiles, photo-panels, and dip and strike data of bedding and injectites. Physical correlation of individual beds and injectites between logs enabled the changing position of injectites with respect to host stratigraphy to be constrained from cm to km scale, which can be subtle.

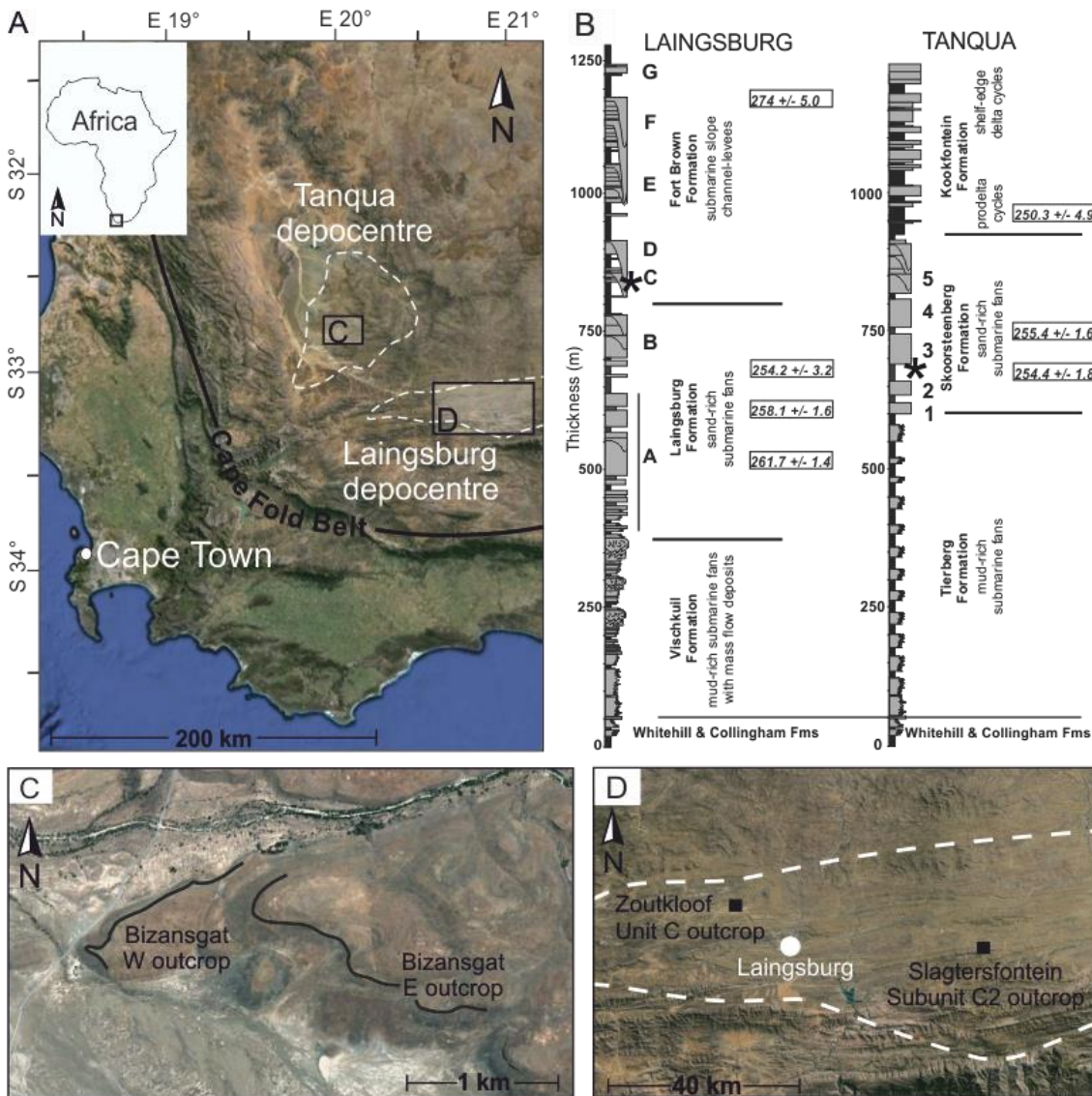


Figure 5.1 A) GoogleEarth image of SW Karoo Basin with Tanqua and Laingsburg depocentres outlined. Insets show outcrop localities in each depocentre respectively. B) Summary stratigraphic logs of Laingsburg depocentre, letters A-G refer to Units A-G (Flint *et al.*, 2011) and Tanqua depocentre, numbers 1-4 refer to Fans 1-4, whilst 5 refers to Unit 5, a 100 m thick channelised slope succession (Hodgson *et al.*, 2011b). Location of injectites, studied in the present paper, denoted by asterisks. Ages from U-Pb zircon analysis of volcanic ashes (see Fildani *et al.*, 2007; McKay *et al.*, 2015) are displayed in boxes as Ma. C) Tanqua depocentre study area. D) Laingsburg depocentre study areas (Appendix A.3 for panels and logs, Appendix B.3 for outcrop measurements).

5.4. Outcrop data

5.4.1. Bizansgat; Tanqua Depocentre

Fan architecture

The depositional architecture of Fan 3 is well constrained due to extensive outcrop study (e.g. Johnson *et al.*, 2001; Prélat *et al.*, 2009; Jobe *et al.*, 2012; Hofstra *et al.*, 2015), and behind-outcrop research boreholes (Hodgson *et al.*, 2006; Luthi *et al.*, 2006). Research borehole NB4 (Fig. 5.2) confirmed that Fans 1 and 2 are not present in this part of the study area (Hodgson *et al.*, 2006; Luthi *et al.*, 2006). Fan 3 pinches out northward (down dip) from 65 m thick over 30 km (~2.2 m/km thinning rate) (Hodgson *et al.*, 2006). Southward (oblique up dip) thinning is more abrupt, and Fan 3 thins to less than 2 m thick over a distance of 3 km (~22 m/km thinning rate) (Hodgson *et al.*, 2006; Oliveira *et al.*, 2009). The beds at the southward pinchout remain sand dominated, between 5 and 30 cm in thickness, and display some planar and ripple lamination. Across the Ongeluk River locality to the pinchout, the upper beds of Fan 3 remain thinner bedded than those below. Fan 4 also thins abruptly southward, although the mudstone between Fan 3 and 4 maintains a constant thickness (Oliveira *et al.*, 2009). At the Ongeluk River locality (Fig. 5.2), Fan 3 is 65 m thick and is composed of clusters of sand-rich channel-fills, interpreted as base-of-slope channel complexes (Sullivan *et al.*, 2000; Luthi *et al.*, 2006; Hofstra *et al.*, 2015). The channels are orientated dominantly towards the NE (Luthi *et al.*, 2006; their Fig. 11) with variations to the N and E (Hodgetts *et al.*, 2004). The palaeoslope feeding Fan 3 was NE-facing (Hodgson *et al.*, 2006). The abrupt southeastward pinchout is interpreted to be due to lateral onlap, forming a sharp-based contact, onto a confining NE-SW-trending and NW-facing slope (Oliveira *et al.*, 2009) in a proximal base-of-slope setting (Hodgson *et al.*, 2006).

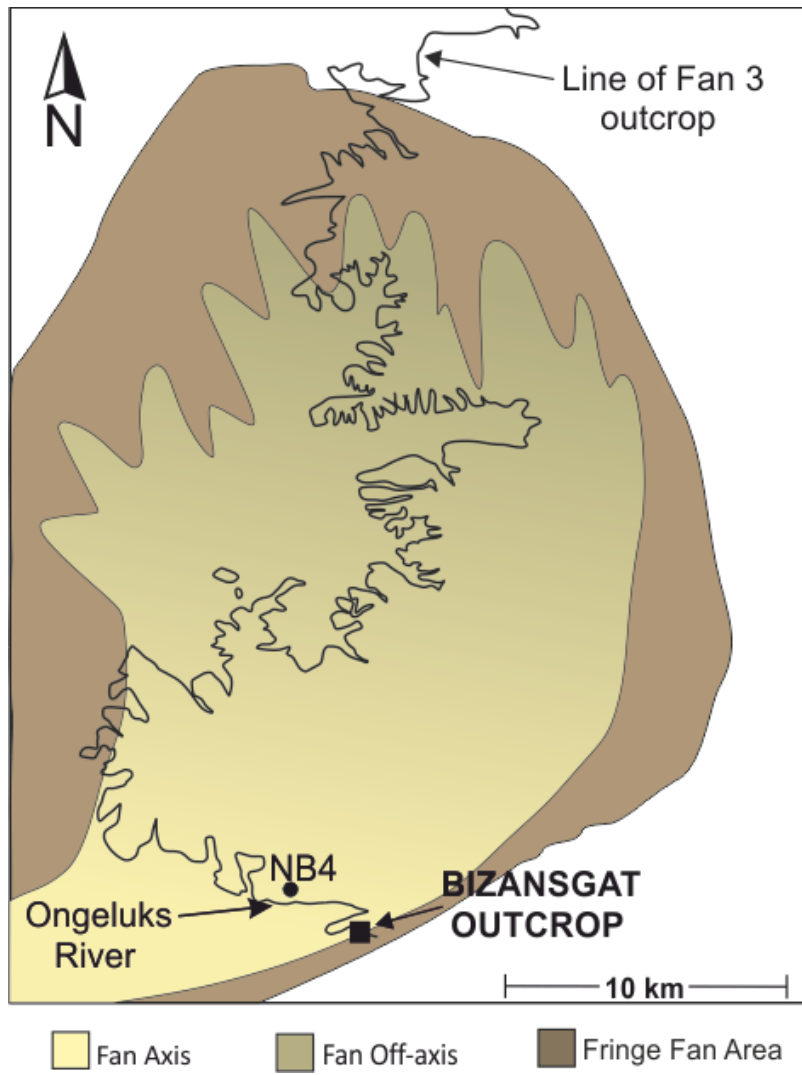


Figure 5.2 Palaeogeography of Fan 3 (adapted from Hofstra *et al.*, 2015) with location of NB4 core and Ongeluks River section.

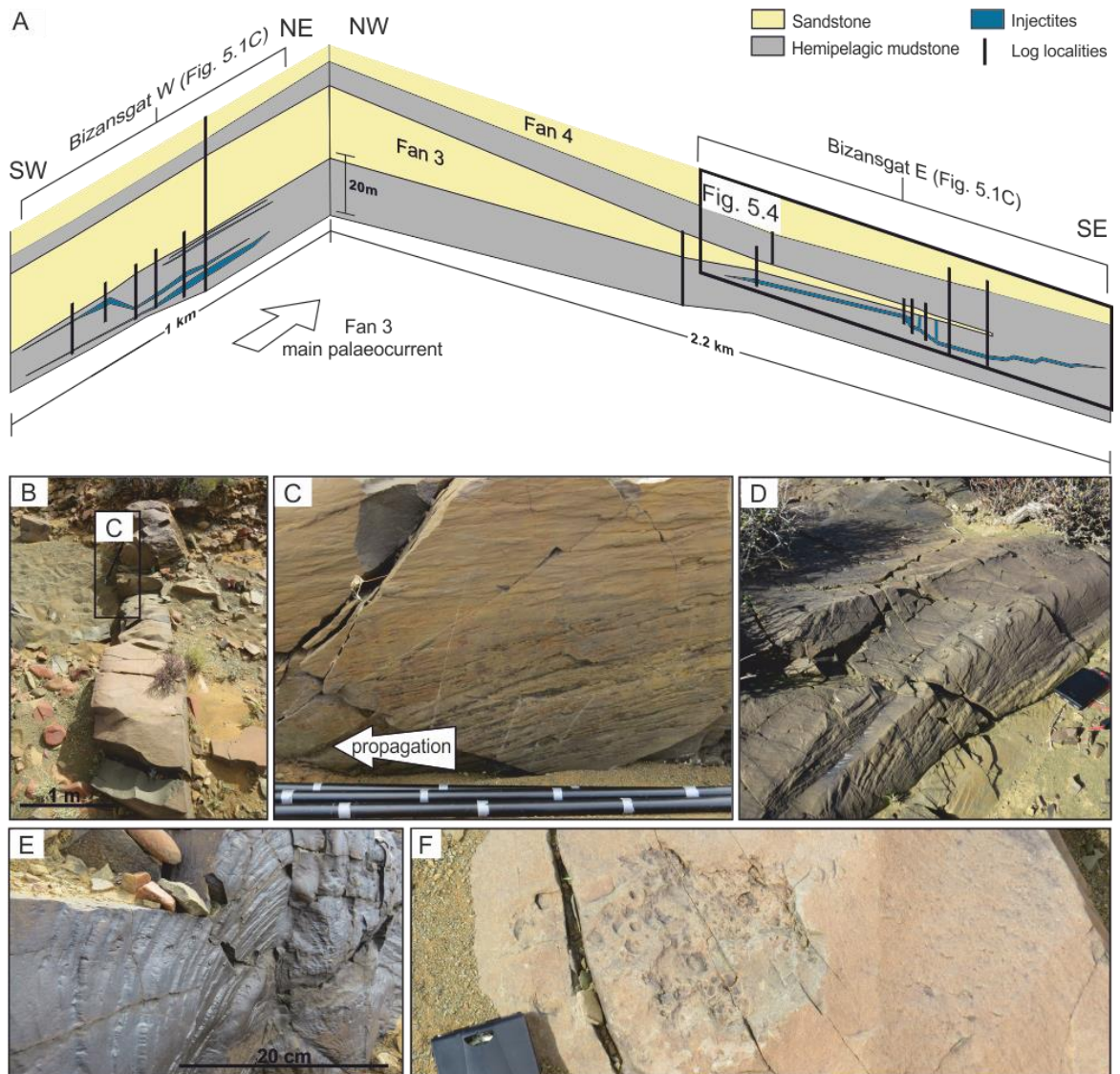


Figure 5.3 Bizansgat outcrop – correlation panels and injectite margin structures. A) Correlation panel of logs taken at Bizansgat through Fan 3 and injectites. B) Typical dyke connecting base of Fan 3 with sheet sill displayed in (Fig. 5.4B). C) Ridges on margin of dyke indicating injectite propagation direction. D) Example of plumose fracture pattern along top margin of small-scale step. E) Plumose fracture pattern along sill step. F) Patch of mudstone clasts on top surface of a sill.

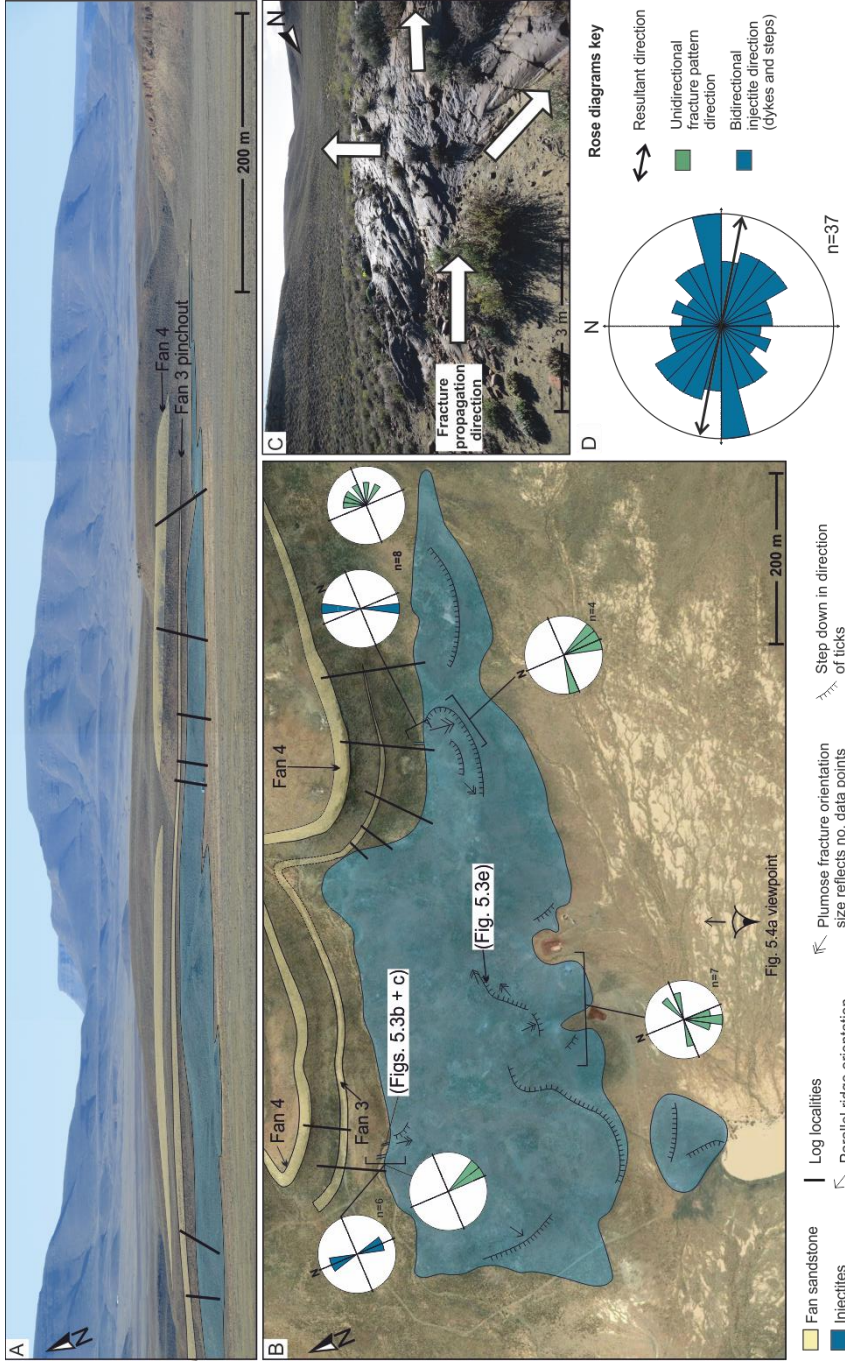


Figure 5.4 Bizansgat outcrop – injectite geometries and orientations. A) Panel view of outcrop showing extent of injected sandstone beyond that of the parent sand. B) Map view of study area, Fan 3 and Fan 4 outcrop shown stratigraphically above injected sands. Rose diagrams display orientation data for dyke orientation and fracture patterns. C) Photograph depicting large plumose fracture, main propagation direction is SE with diverging striae spanning almost 180°. D) Rose diagram of step orientation across entire outcrop, widespread variation in direction due to curvilinear nature of steps but prominent step direction is E-W.

Injectites below Fan 3

Injectites exposed in the Bizansgat area of the Tanqua depocentre reported here occur in mudstones below Fan 3 (Fig. 5.1B) in the most proximal exposures to the south of the outcrop belt (Fig. 5.2). The nature of the outcrop means that the 3D geometry of the larger injectites exposed in the mudstone below Fan 3 can be constrained. Locally, a single main laterally extensive ~1 m thick clastic sill steps up to the south and east to form a discordant relationship with the stratigraphy (Fig. 5.3A). Figure 5.4A and 5.4B shows the outcrop extent of the main stepped sill, which connects to at least three 0.4-0.6 m wide sub-vertical dykes that connect to the base of Fan 3 over a vertical distance of between 3 and 7 m. Steps on this sill are curvilinear along strike (Fig. 5.4), forming crescent-like geometries up to 200 m across and are no more than 1 m in vertical height. Propagating below the main sill are several thinner dykes (<0.2 m) that extend <6 m vertically, and bifurcate and taper out. Ridges that are orientated sub-horizontally with the host strata (Fig. 5.3C) mark the margins of these dykes. Margin structures on both the main stepped sill, and connecting dykes, include plumose patterns on fracture surfaces, parallel ridges, mudstone clast-rich surfaces and planar surfaces (Figs 5.3B–5.3F). The average strike of the steps is WNW-ESE, although there is a wide spread of orientations due to their curvilinear planform geometry (Fig. 5.4). Plumose features, observed on the margins of sills where they step through stratigraphy, form fan-like features with parallel striae down their centre and diverging striae away from the central axis (Fig. 5.4C). The direction of striae divergence is to the S, with a range from SW-SE. The dykes maintain a constant thickness at the scale of the outcrop, and are orientated N-S to NNE-SSW (Figs 5.3B and 5.4B).

Interpretation

All injectites studied in this area are close to the base of Fan 3 (Figs 5.3A and 5.4A), with sub-vertical dykes connecting Fan 3 with the large stepped sill. In the SE part of the outcrop, dykes directly connect the parent sand to the sill (Fig. 5.3), which supports local downward propagation (e.g. Von Brunn & Talbot, 1986; Rowe *et al.*, 2002; Parize & Fries, 2003; Le Heron & Etienne, 2005). The fine sand grain-size of the injectites is the same as Fan 3, and Fans 1 and 2 are not present in the underlying stratigraphy, which comprises several 100's m of mudstone (King *et al.*, 2009). Consequently, Fan 3 is interpreted as the parent sand for all the injectites.

The dykes are orientated approximately perpendicular to the NW-facing palaeoslope that confines Fan 3. Therefore the dyke orientation is hypothesised to relate to a gravitational stress

regime. Although the injectites occur beneath the parent sand, the morphology of the curved steps and the orientation of structures on the injectite surfaces (Fig. 5.4B) (plumose features indicate the propagation direction, Cobain *et al.*, 2015) suggest that the main injectite sill stepped laterally outwards from its centre and cut up stratigraphy towards the south and east. The injectites, therefore, parallel the base of Fan 3 and continue beyond the depositional pinchout (Figs 5.3A and 5.4A). Net injection propagation direction was horizontal rather than vertical from the sharp-based sandbody with an abrupt upslope pinchout configuration in a lower slope to base-of-slope setting.

5.4.2. Zoutkloof; Laingsburg Depocentre

Unit architecture

Unit C of the Fort Brown Formation (Fig. 5.1B) has also been the focus of extensive study, and is subdivided into 3 subunits; C1, C2 and C3, each separated by a laterally extensive mudstone (Di Celma *et al.*, 2011; Flint *et al.*, 2011; Hodgson *et al.*, 2011a; van der Merwe *et al.*, 2014). Extensive dip and strike outcrop control allow the distribution of sedimentary facies and architectural elements, and therefore depositional environments, to be constrained (Di Celma *et al.*, 2011). Subunit C1 forms a 50 m thick lobe complex 8 km to the southeast (Fig. 5.5) where the overlying subunit C2 is thin-bedded and forms part of an external levee to a channel system (Di Celma *et al.*, 2011). At the Zoutkloof locality, subunit C1 is sharp-based, thins from 2 m of amalgamated fine sandstone (Fig. 5.6C) to <12 cm thin bedded very fine sandstone over ~1.5 km at the oblique up dip pinchout of the lobe complex (Fig. 5.6B). The confining palaeoslope at subunit C1 time, based on isopach thickness maps and palaeocurrents, was orientated N-S and E-facing (Di Celma *et al.* 2011; Fig. 5.5). Locally, the base of C1 forms a sharp contact with the underlying mudstone, and the top surface is marked by the lower C mudstone that separates subunits C1 and C2 (Di Celma *et al.*, 2011) at a constant thickness of 0.9 m. This upper mudstone was used as a datum (Fig. 5.6A and 5.6D).

Zoutkloof injectites

At Zoutkloof, injectites crop out over 1.7 km (Fig. 5.6D) below subunit C1, in the upper 13 m of the 40 m thick regional mudstone that separates Units B and C (Brunt *et al.*, 2013), at an abrupt, oblique lateral pinchout (Di Celma *et al.*, 2011) (Figs 5.5 and 5.6D). At this locality, the main form of injection is stepped sills. Curved steps are no more than 2 m in vertical height and continue

laterally for 10's m. Steps are closely spaced so that the sills are discordant with the host stratigraphy for more than 2-3 m. The majority of dyke margins exhibit ridges, both plumose and parallel (Cobain *et al.*, 2015). Several sub-vertical dykes are observed to connect the base of subunit C1 with the stepped sills, the thickest is 1.5 m wide (between logs 7 and 8; Fig. 5.6A). Most other dykes are thinner (<0.3 m-thick) and connect with the base of subunit C1. The steps and parallel ridges are primarily aligned E-W and the orientation of striae divergence of plumose patterns on the fracture surfaces is dominantly WSW (Fig. 5.6D). The dominant trend in dyke orientation measurements is NNW-SSE, approximately perpendicular to the orientation of the steps (Fig. 5.6).

Interpretation

In the Zoutkloof area, all injectites are close to the base of subunit C1, at the NW margin of the sharp-based lobe complex, and vertical dykes connect large stepped sills with the base of subunit C1. Therefore, subunit C1 is interpreted to be the parent sand of the injectites. The main sills, fed by dykes sourced from the overlying parent sand, abruptly step up stratigraphy to parallel the abrupt pinchout of the parent sand. Injection propagation is sub-parallel (WSW) to the unit pinchout direction and occurs where the base of parent sand has a sharp sand-to-mud contact. The orientation of the dykes is close to perpendicular to the slope-facing direction suggesting a causal relationship. The apparent propagation direction of sub-vertical dykes is downward but the ridges on the dyke margins suggest that propagation during injection was dominantly lateral (e.g. Kane, 2010).

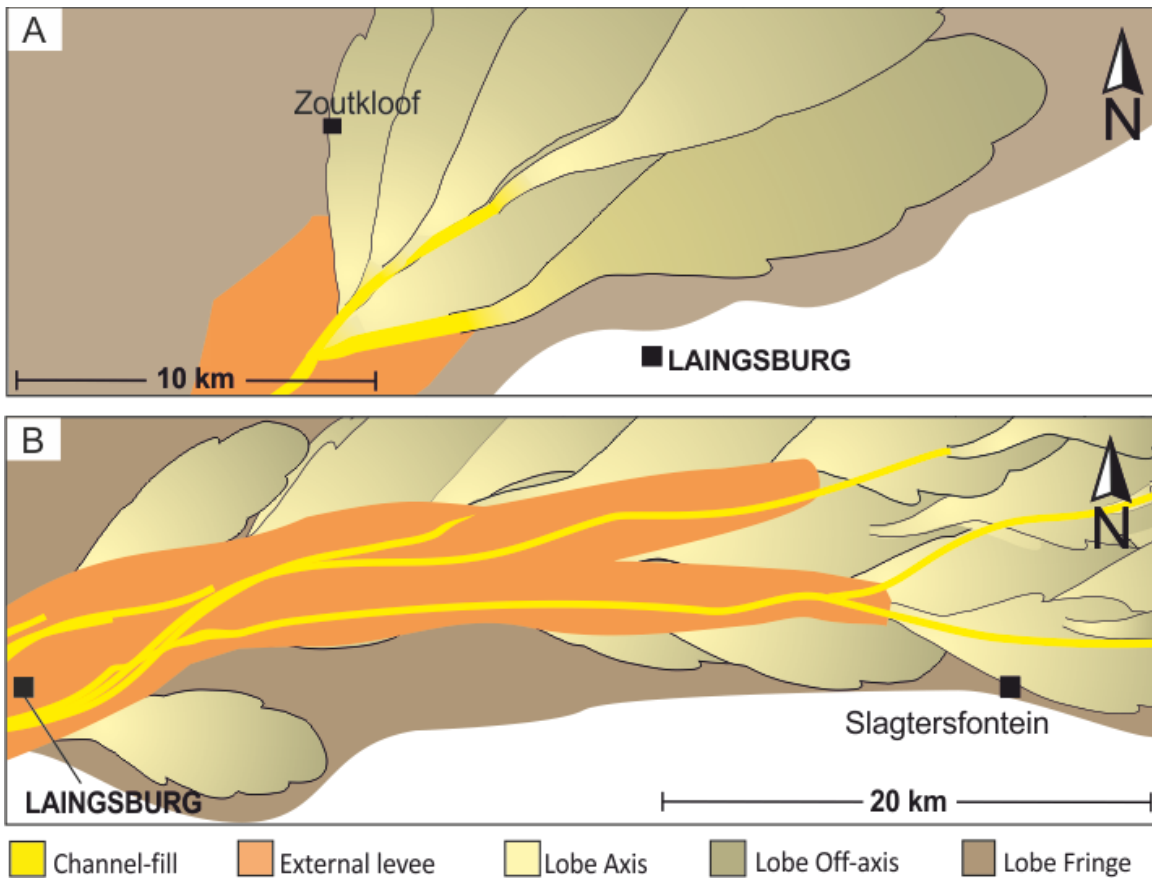


Figure 5.5 A) Palaeogeography of subunit C1, clastic injectites are present at Zoutkloof locality. B) Palaeogeography of subunit C2, injectites are present along outcrop at Slagtersfontein (van der Merwe *et al.*, 2014).

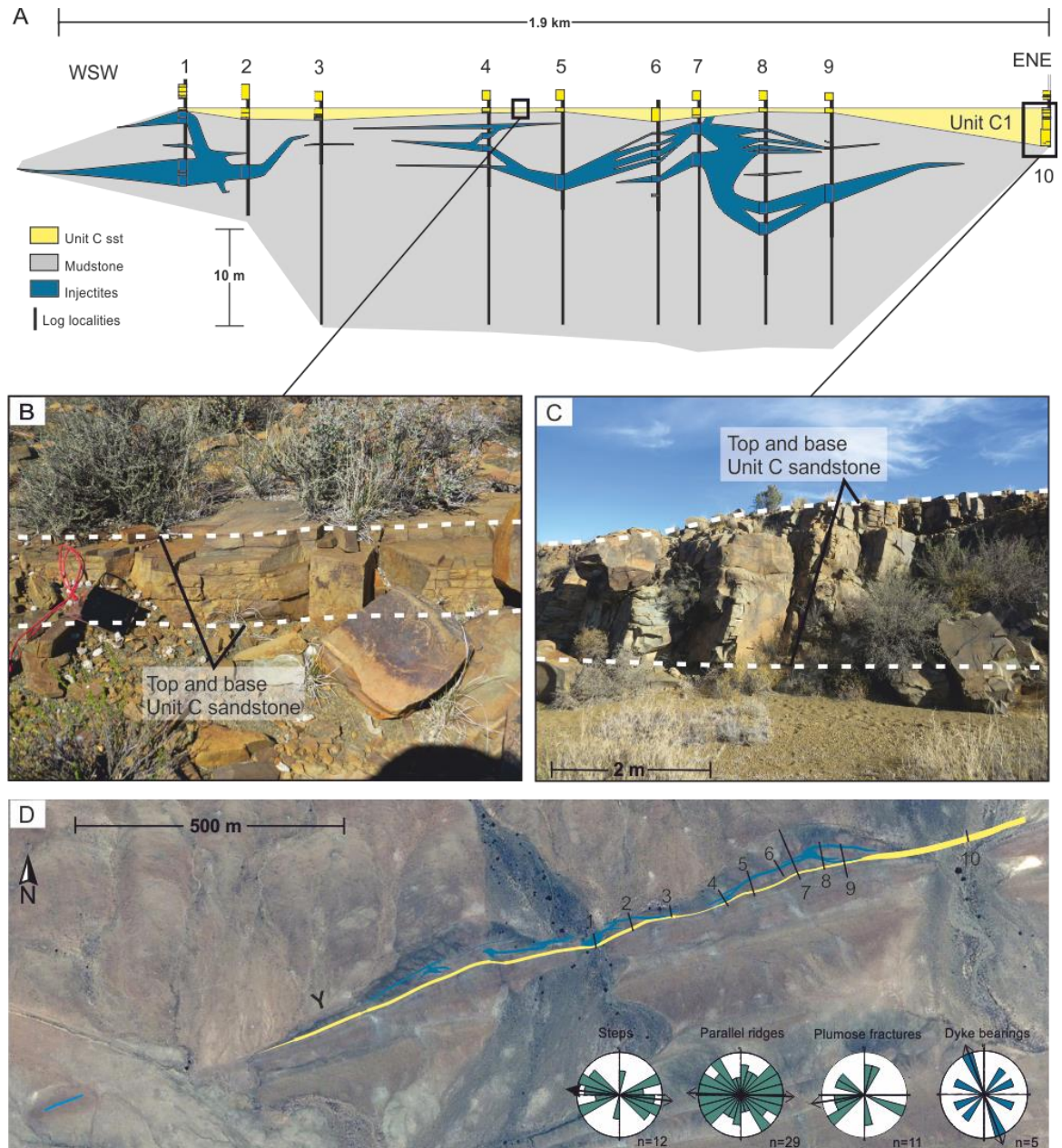


Figure 5.6 Zoutkloof outcrop and injectites. A) Correlation panel of logs taken along length of outcrop. B) Unit C is 10 cm thick, very fine, and bedded sandstone. C) Unit C is >2 m thick, massive, very fine sandstone. D) Map view of outcrop with Unit C, injectites and log locations indicated, rose diagrams depict fracture pattern directional data and step and dyke orientations. Refer to Figure 5.4 for rose diagram colours.

5.4.3. Slagtersfontein; Laingsburg Depocentre

Unit architecture

C2 is the only subunit of Unit C present in the Slagtersfontein region of the depocentre. Here, palaeogeographic and isopach maps indicate the location to be at the edge of a lobe complex that thins abruptly to the south (Fig. 5.5), with palaeoflow towards the east (van de Merwe *et al.*, 2014). These data suggest a WNW-ESE trending and NNE-facing confining palaeoslope during deposition of subunit C2 at Slagtersfontein (van der Merwe *et al.* 2014). The top of the underlying Unit B consists of a widespread thin-bedded siltstone succession. The base of the overlying Unit D comprises tabular structureless sandstones (van de Merwe *et al.*, 2014; Hodgson *et al.*, 2016), therefore this was chosen as a datum from which to hang the panel (Fig. 5.7A). Along the Slagtersfontein outcrop, subunit C2 is sand-prone, sharp-based, and thickens from 0 m at the western extent of the outcrop to >20 m thick downdip to the east over 1.5 km. Lower beds within subunit C2 are structureless and amalgamated sandstones, whereas the upper beds are thin bedded and laminated (Fig. 5.7B). Locally, the base of subunit C2 is erosional, and incises underlying mudstones to the east (e.g. Fig. 5.7B).

Slagtersfontein injectites

Injectites exposed in the Slagtersfontein area are hosted within the regional mudstone separating Units B and C. The majority of injectites at the Slagtersfontein outcrop are 0.1–0.6 m thick sills that extend laterally for up to 500 m. Dykes (0.1–0.5 m thick) are common near the base of subunit C2, and are observed to connect to the base of Unit C (Figs. 5.7B and 5.7C). Injectites crop out over the entire exposure length of Unit C, and for a further kilometre up dip where Unit C is absent in the mudstone separating Units B and D (Fig. 5.7A). Injectites in the mudstone that separates Units B and C are most abundant close to, and directly connect with, Unit C where the base is erosive and has a sharp contact between the Unit C sandstone and the underlying mudstone. Injectite margins are mostly planar, although some parallel ridges are present on dykes. Some smaller injectites, mainly <0.2 m thick sills, occur close to the base of, and are directly connected to, Unit D (Fig. 5.7A). The outcrop character at Slagtersfontein only permitted collection of dyke orientation data, the mean of which is NW-SE (Fig. 5.7).

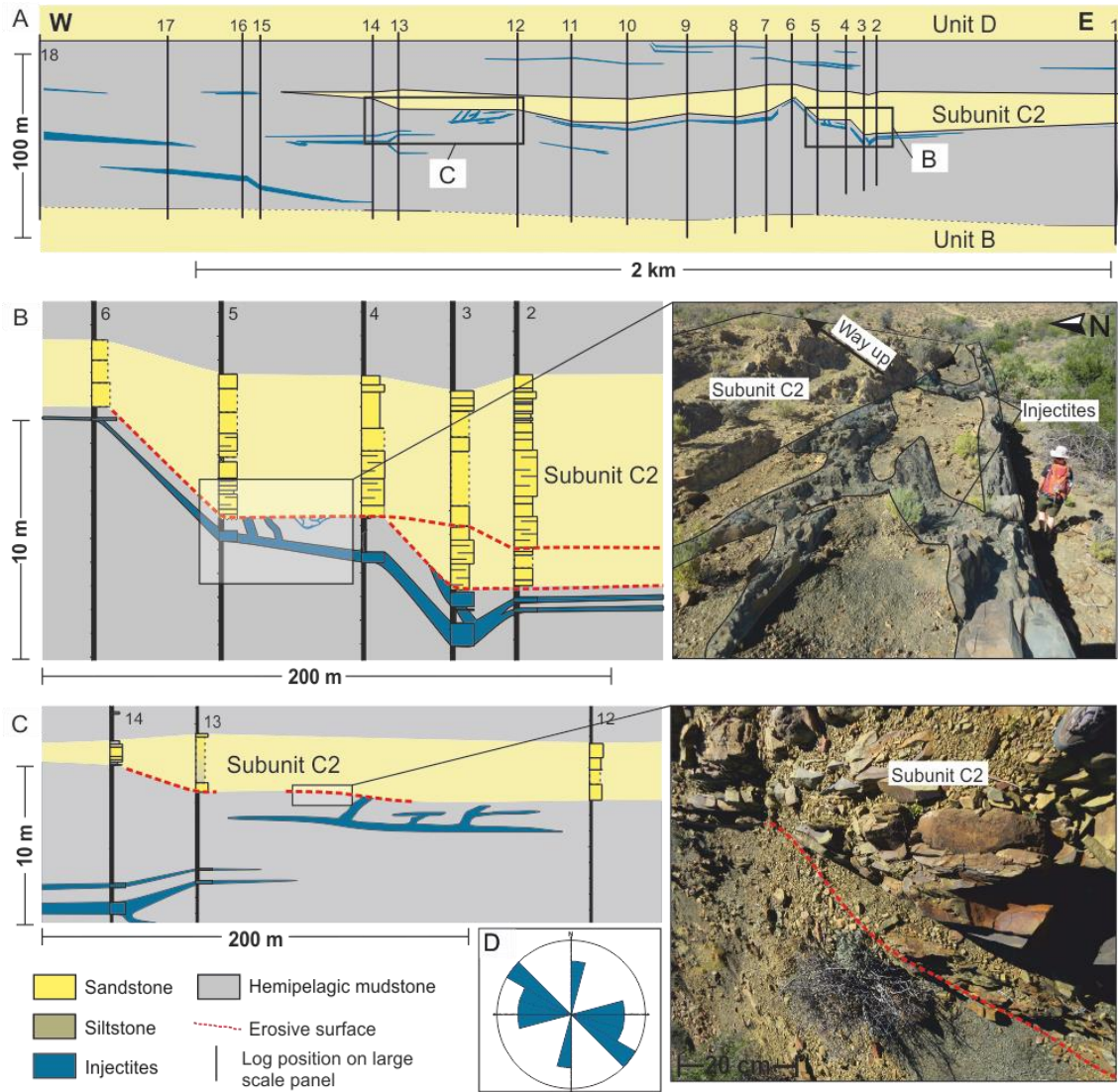


Figure 5.7 Slagtersfontein outcrop and injectites. See Appendix A.3 for individual logs. A) Correlation panel of logs (numbered) through Unit C2, injectites present throughout (C2 is the only subunit of Unit C to be present). B) Section through logs 2-6, where C2 has an erosive base, and dykes directly connect with the base of C2. Inset shows expression of unit and injectites at outcrop. C) Section through logs 12-14, where a single dyke extends from the base of C2 and feeds the sill/dyke network. Inset depicts example of erosive base. D) Rose diagram displaying orientation of dykes below Unit C. these are oblique-strike to the likely palaeoslope, which locally was NNE-facing based on the isopach maps of van der Merwe *et al.* (2014).

Interpretation

Injectites connect directly with subunit C2, therefore this is interpreted to be the parent sandstone for the main injectite network, with Unit D likely acting as a minor source (see Fig. 5.7A; direct connection of 2 small dykes between logs 9 and 10). The underlying Unit B is topped with several metres of thin bedded silty strata, which is consequently less likely to produce sandstone injectites; there is also an absence of any dykes emanating from this unit, in outcrop. The parent sand is at an abrupt sand-prone pinchout of a lobe complex (subunit C2) where locally the base is in erosive contact with underlying mudstones. The majority of clastic injectites are sills that extend laterally beyond the parent sand towards the west in cross-section (Fig. 5.7A). Therefore, the net propagation direction of injected sand was to the west and south, with injectites exploiting pre-existing bedding plane weaknesses (Cobain *et al.*, 2015). The orientation of the dykes are sub-parallel to the local NNE-facing palaeoslope, which suggests a causal relationship, such as a gravity-driven stress regime.

5.4.4. Comparison of study areas

Previous research in the Karoo Basin (Wickens, 1994; Wickens & Bouma, 2000; Hodgson *et al.*, 2006; Oliveira *et al.*, 2009; Pr lat *et al.*, 2009; Di Celma *et al.*, 2011; Flint *et al.*, 2011; Brunt *et al.*, 2013; van der Merwe *et al.*, 2014) means that the palaeogeographic context of the parent sandbodies to the studied injectite networks is extremely well constrained. The style and extent of outcrop means that it has been possible to collect data and geometries of injectite networks to provide 3D constraints over several kilometres. The Fan 3 and Unit C study sites were deposited in basin-floor environments (Hodgson *et al.*, 2006; Di Celma *et al.*, 2011; Brunt *et al.*, 2013). Injectites sourced from Fan 3 in the Tanqua area, and subunits C1 and C2 in the Laingsburg area, coincide with sites of abrupt basin-floor sand-prone pinchout, with mudstone above and below. Additionally, the basal contact of the parent sand with the underlying mud is erosional and/or sharp where injection occurs. The injectites propagated laterally paralleling the base of the parent sandbody, and extend beyond the pinchout, and dykes are sub-parallel to the strike of the palaeoslope in all examples. Furthermore, the extensive previous research in the field area also helps to constrain where injectites are not present, meaning models are not biased towards outcrops that only show injectites. For example, detailed mapping and coring of the fringes of lobe complexes (Johnson *et al.* 2001; van der Werff & Johnson 2003; Hodgson *et al.*, 2006; Pr lat *et al.*, 2009) has identified only rare isolated injectites associated with Fan 1 and Fan 4.

5.5. Discussion

5.5.1. Injectite emplacement in the Karoo Basin: mechanisms and controls

We have presented three examples of basin-floor lobe complex pinchouts that have been subject to post-depositional fluidisation of the parent sandbody and clastic injection into the surrounding mudstone. Discussion on emplacement takes into account the common features observed across all outcrop examples described here, the well-constrained architecture and palaeogeography of each of the units, and the prerequisite conditions needed for clastic injection.

Conditions prior to injection

Typically, the same conditions observed to form overpressured uncemented sand liable to fluidisation in slope channel-fills are also met in these examples from basin-floor lobe complexes: i) proximal deposits within the lobe complexes provide clean, fine to very fine sand (e.g. Marchand *et al.*, 2015) that increases the likelihood of fluidisation, and hence susceptibility for sediment transport (Richardson, 1971; Jolly & Lonergan, 2002); and ii) the deep-marine environment and regional changes in clastic sediment supply allow for alternating sand-rich channel-fed lobe complexes encased by regional hemipelagic mudstone drapes that provide the seal required for overpressure to develop (Lorenz *et al.*, 1991; Cosgrove, 2001; Jolly & Lonergan, 2002). These surrounding mudstones may also provide an additional source of pore fluids during the initial stages of compaction (Magara, 1981).

Geographic location and parent sandstone architecture

Based on the outcrop positions of the observed injectites, and the existing palaeogeographic knowledge of the Karoo Basin (Wickens, 1994; Wickens & Bouma, 2000; Hodgson *et al.*, 2006; Oliveira *et al.*, 2009; Prélat *et al.*, 2009; Di Celma *et al.*, 2011; Flint *et al.*, 2011; Brunt *et al.*, 2013; van der Merwe *et al.*, 2014), the injectites are interpreted to be located at the abrupt pinch-out of sand-rich lobe complexes (Figs 5.3 and 5.5). At their abrupt updip pinchout, such as Bizangat (Fan 3) and Zoutkloof (subunit C1) the parent sand is generally homogenous, well sorted, and has a sharp contact with the underlying strata. The same configuration occurs in the abrupt lateral pinchout at Slagtersfontein (subunit C2). Clastic injectites occur stratigraphically beneath the parent sandstone, with net lateral propagation towards and beyond the margin of the parent sandstone lobe complex. In other examples, where injectites of seismic-scale are known to be

sourced from lobe complexes (as observed in intra-slope lobes), the source point is the proximal lobe (complex) fringe (Yang & Kim, 2014; Sychala *et al.*, 2015), or the lateral lobe margin pinchout (Monnier *et al.*, 2014). In the latter case the lobe reaches its highest point laterally. This suggests that an abrupt and sand-prone pinchout in the most elevated position on the lobe, which will typically occur in the proximal or lateral parts of lobes, is a preferential site for clastic injection processes.

Nature of stratigraphic contact

Considering the geographic and stratigraphic distribution of the required unconsolidated sandstone and the surrounding fine grained sediments, injectites might be expected at all positions within lobe complexes. As long as sand remains unconsolidated, the surrounding hemipelagic mud may form a seal around the entire unit. The observation of preferential hydraulic fracture at a sharp sand-to-mud contact, with clean sands, however, favours the proximal area of lobe complexes at their base. In these situations, erosional relationships and/or steeper slopes promote a more abrupt onlap geometry and the formation of a sharp basal contact from where the injectites are sourced. Commonly, the upper part of lobe complexes are thin-bedded (e.g. Hodgson *et al.*, 2006; Prélat *et al.*, 2009), and in such cases injectites are absent. In the presence of subtle confinement (Sixsmith *et al.*, 2004), or in more distal settings (van der Werff & Johnson, 2003; Hodgson, 2009; Prélat *et al.*, 2009), injectites are not observed. However, in a few cases where there is an abrupt sand-to-mud contact on top of a lobe complex, due to large-scale avulsion or sudden clastic input shutdown, injectites are observed (e.g. Subunit A5; Cobain *et al.*, 2015). Where clastic material is finer and/or less well-sorted, clastic injection is not observed. What mechanism controls this preferential occurrence of injectites at the interface between clean sands and muds? A key attribute of clean sands is a tighter grain-size and shape distribution, and therefore higher permeability relative to less clean sands (Krumbein & Monk, 1942; Beard & Weyl, 1973). Transient changes in pressures related to variations in grain-size, and thus permeability, might be expected to influence the position of hydraulic fracturing. However, cyclic loading of sands in closed systems demonstrates that lower permeability sands exhibit higher transient pressures (e.g., Kelly *et al.*, 2006). Consequently, variations in permeability do not appear to be the controlling mechanism. Furthermore, if aseismic, overpressure builds more gradually over geological time, the pressure at the sand-mud boundary may be similar at all points. In contrast, clean sands are more susceptible to fluidisation (Richardson, 1971; Jolly & Lonergan, 2002), and consequently they may preferentially fill any hydraulic fractures that occur.

5.5.2. Possible trigger mechanisms

In order to develop the overpressure required to fluidise and liquefy parent sand, and subsequently inject it into the surrounding strata, a trigger mechanism is required (Jolly & Lonergan, 2002; Oliveira *et al.*, 2009). Several different trigger mechanisms have been postulated to account for clastic injectites in deep-marine environments: seismicity (e.g. Obermeier 1996; Boehm & Moore, 2002; Huuse & Mickelson, 2004; Obermeier *et al.*, 2005), tectonic stress (e.g. Peterson, 1966; Jolly & Lonergan, 2002), rapid burial (e.g. Truswell, 1972; Allen, 2001), instability of overlying sediments (e.g. Hiscott 1979; Jonk, 2010) or migration of basinal fluids into the sealed sand body (e.g. Vigorito & Hurst, 2010; Jackson *et al.*, 2011; Bureau *et al.*, 2014; Monnier *et al.*, 2014).

A substantial depth of burial prior to sand injection in the Karoo Basin examples examined herein consists of a number of lines of evidence, including the preservation of initial brittle, hydraulic patterns on fracture surfaces on the margins of injectites seen at the Zoutkloof and Bizansgat localities (Figs 5.3D and 5.3E). These suggest that the muds were sufficiently hard to form and maintain these surface patterns; no evidence for later compaction of these surface patterns on dyke margins is observed (Cobain *et al.*, 2015). Furthermore, the observed injectites show features (vertical distribution of particles within sills; lack of erosion) commensurate with high-concentration, laminar flow conditions, suggesting that the units were sufficiently far from the contemporaneous seabed that breakthrough and subsequent extrusion did not occur; such open-conduit conditions are linked to turbulent flow conditions (Cobain *et al.*, 2015). However, the fractures exhibit extensional failure, indicating that the applied shear stress is less than 4 times the tensile strength of the rock (Cosgrove, 2001), suggesting for these high fluid pressure settings, an upper limit on formative depth of several hundreds of metres (Secor, 1965; Aydin, 2000; Cosgrove, 2001). There is a notable absence of overlying slides and slumps, and the absence of growth strata above seabed folds and faults in the basin-fill (e.g. Hodgson *et al.*, 2006; Di Celma *et al.*, 2011; Flint *et al.*, 2011; Jones *et al.* 2015) indicate it was largely tectonically quiescent. Therefore, fluidisation and injection due to localised excess pore fluid pressures generated by depositional processes such as mass flows (Truswell, 1972; Jolly & Lonergan, 2002) and shallow seismicity (Obermeier, 1996; Lunina & Gladkov, 2015), in these outcrop examples, are considered unlikely trigger mechanisms.

Disequilibrium compaction is a major source of overpressure in sedimentary basins (Osborne & Swarbrick, 1997), however within a single body or unit, this overpressure will dissipate over

geologic time, and high overpressures can only be maintained in the shallow subsurface through high rates of sedimentation (Jonk *et al.*, 2010). Therefore, disequilibrium compaction alone may not be an adequate source of overpressure to trigger clastic injectites. Overpressure due to fluid volume increase is associated with aquathermal expansion and clay dehydration, though these alone are considered too insignificant to generate high amounts of overpressure (Osborne & Swarbrick, 1997). Deep or regional seismicity has been commonly cited as a primary cause of sand intrusion, however the energy required to fluidise and inject such quantities of sand in regionally extensive injectites likely exceeds that produced by earthquakes (Huuse *et al.*, 2005; Duranti, 2007; Vigorito & Hurst, 2010). If such regional seismicity were a cause, then hydraulic fracturing, failure of encasing mudstone, and resultant injection would be expected across the entire lobe complex. Additionally, an absence of seismicity for a significant period would be needed in order to bury the sediments to depth and enable overpressure to build; consequently, a large-scale change in tectonic regime would be required. Regional seismicity, therefore, is considered an unlikely trigger of injection for these deeper injectites (Duranti, 2007; Hurst *et al.*, 2011).

Another mechanism for triggering injection in deep-water systems is the migration of fluids caused by lateral pressure transfer: the lateral transfer of fluids from deeper, overpressured parts of the basin along laterally extensive, inclined, porous units (Osborne & Swarbrick, 1997; Yardley & Swarbrick, 2000). The lower parts of the basin-fill are likely to experience enhanced overpressure as a result of compaction, and thus cause movement of fluid upwards towards the highest point. This form of fluid migration is most likely to be concentrated at the up dip margins of a unit (Cartwright, 2010), such as a lobe complex margin, where the abrupt pinchout architecture at the fringe of lobe complexes promotes fluid migration towards the edge (Monnier *et al.*, 2014). The surrounding mud limits further fluid migration. Migration of fluids due to lateral pressure transfer operates in basins such as the Gulf of Mexico, where simple tilting causes a pressure gradient (Flemings *et al.*, 2002; Gay *et al.*, 2011). Lateral pressure transfer is interpreted to be the likely cause of post-Eocene intrusions along the margin of the San Joaquin Basin (Schwartz *et al.*, 2003; Cartwright, 2010). In the San Joaquin Basin, the fluids that produce overpressure and cause lateral pressure transfer are not derived locally. Migrating hydrocarbons may also cause an increased pore pressure in sand units sealed by impermeable strata (Jolly & Lonergan, 2002). Consequently, increased overpressure of an unconsolidated sand body by compaction driven fluid expulsion, and fluid migration through lateral pressure transfer (water, oil, gas), is the preferred trigger mechanism responsible for clastic injection in

the Karoo Basin (see also Cobain *et al.*, 2015). The parent sand architecture in all examples promotes lateral fluid migration to the updip lobe complex margins. Larger-scale injectites have also been attributed to this kind of trigger (Løseth *et al.*, 2013; Huuse *et al.*, 2005; Hurst *et al.*, 2011).

5.5.3. An integrated model of injectites in basin-floor lobes

Synthesising the observations discussed previously enables an integrated model of injectites in basin-floor lobes to be proposed. Injectites are observed to form preferentially at the updip margins of basin-floor lobe complexes (Bizansgat Fan 3 and Zoutkloof subunit C1) and on lateral margins where the pinchout is abrupt and sand-prone (Slagtersfontein subunit C2) (Fig. 5.8). This geographic distribution is linked to the nature of the triggering mechanisms. The presence of patterns on fracture surfaces, the absence of significant compaction of these structures, and the evidence for confined laminar flow, suggest that these injectites formed at substantial depths, but the extensional nature of fracturing indicates a maximum depth of no more than a few hundred metres. Consequently, disequilibrium compaction and lateral pressure transfer are the likely trigger mechanisms, and in the case of a lobe complex deposited above a basinal slope, these mechanisms will lead to updip fluid migration. Furthermore, in a tilted sandbody the confining lithostatic pressure will also decrease updip. Therefore, hydraulic fracturing will predominantly occur at the up-dip margin where fluid migration and the lowest confining pressures combine. Within the proximal lobe complex, injectites are shown to occur at pinchouts (Figs 5.8 and 5.9); these areas both concentrate fluid-flow from lateral transfer and provide sharp boundaries at their basal surfaces between clean sands and the underlying mudstones. We argue that initiation of hydraulic fracturing is favoured at the bases of these pinchouts because these clean sands are the most susceptible to fluidisation (Richardson, 1971; Jolley & Lonergan, 2002) and therefore will preferentially infill any hydraulic fractures that occur. Theoretically, hydraulic fracturing might be expected to occur on the upper surface of the most up-dip point, as shown in some examples (Cobain *et al.*, 2015), but in many cases proximal parts of lobes exhibit a transition towards lower permeability facies (e.g., thinner bedded siltstones and sandstones) at their tops (Fig. 5.8; Pr lat *et al.*, 2009). The distal parts of basin-floor lobes are not favoured sites for injection as a consequence of their down-dip position, and their more heterogeneous, mud-rich, facies including thin-bedded silts and sands, and hybrid beds (Fig. 5.8; Hodgson, 2009; Pr lat *et al.*, 2009; Marchand *et al.*, 2015). Whilst the physical linkage between sills and the parent sands suggests that the initial hydraulic fracturing and injection can be downwards, the increasing lithostatic pressure below the parent sands will encourage lateral

propagation with sands able to step beyond the lobe complex margins (Figs 5.8 and 5.9). This is supported by the direction of injection flow being at a high angle to the orientation of sand pinchout (Fig. 5.9).

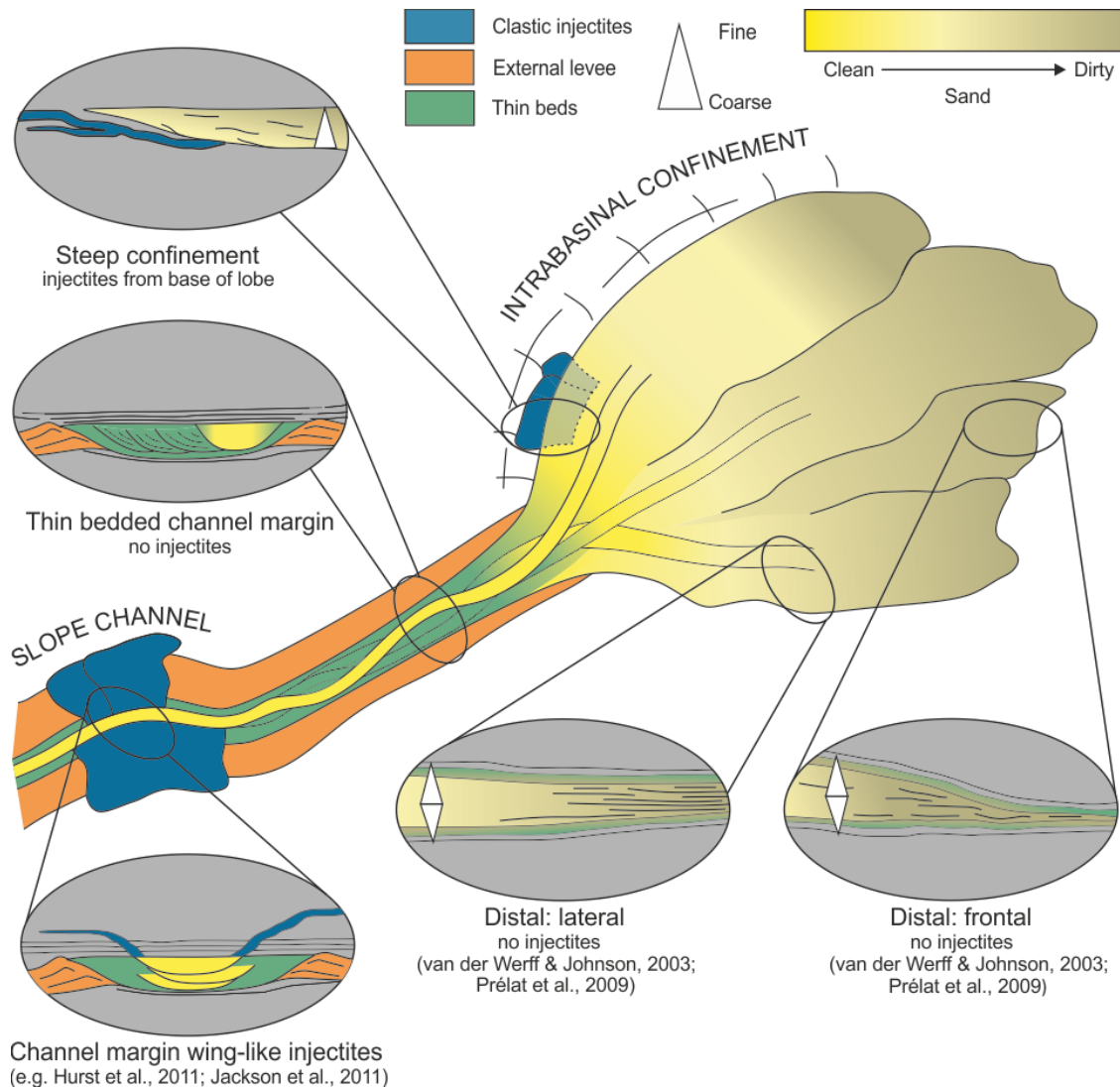


Figure 5.8 Schematic diagram to indicate likely areas of injection in a deep marine system; examples of previously reported clastic injectites occur on the slope (Huuse *et al.*, 2004; Jackson *et al.*, 2011) (note that injectites in this setting may be more broad ranging), whereas this study reports examples from basin-floor lobe complexes. Injectites occur in areas where sand is steeply confined and/or proximal within the lobe complex, while palaeogeographic locations that are downdip exhibit subtle confinement or have less clean-sand for fluidisation and therefore do not produce injectites.

The dykes at all three study sites are aligned sub-parallel to the strike of the palaeoslope (Fig. 5.9), which suggests that a controlling factor in injectite morphology is the orientation of the slope onto which the lobes onlap. Tensile features would preferentially develop perpendicular to slope facing direction in a gravitational stress field, leading to a narrow range of dyke orientations after injection was triggered. This would provide the necessary anisotropy for the documented preferred direction. In contrast, several studies have found limited to no relationship between injectite orientation and palaeoslope (Hiscott, 1979; Rowe *et al.*, 2002; Diggs, 2007; Jackson, 2007; Vétel & Cartwright, 2010; Bain & Hubbard, 2016; Palladino *et al.*, 2016), and ascribe measured orientations to later tectonic controls (e.g. Diggs, 2007; Vétel & Cartwright, 2010; Palladino *et al.*, 2016), or in association with submarine channel orientation (e.g. Jackson, 2007) and/or the emplacement direction of mass transport emplacement (Hiscott, 1979; Rowe *et al.*, 2002). However, here we demonstrate that for injectites sourced from lobe complexes in tectonically quiescent basins, palaeoslope can be a controlling factor on injectite orientations.

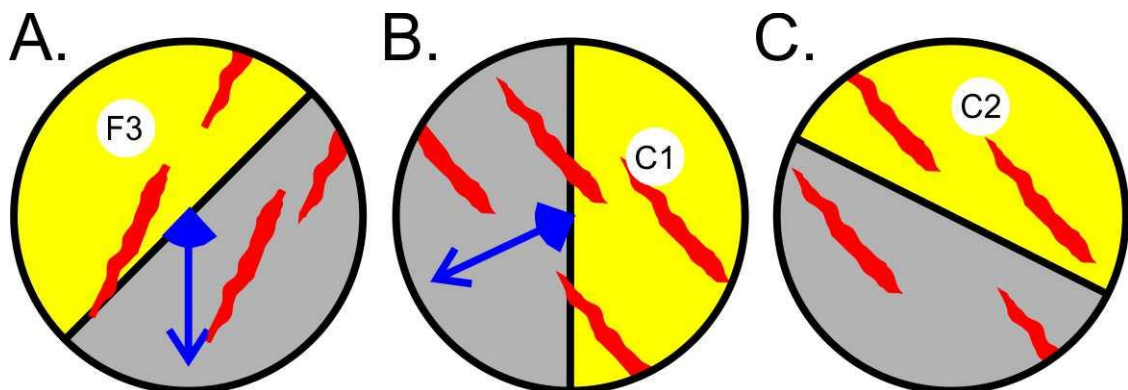


Figure 5.9 Simplified map view illustrations of the orientation of parent sand and injectites at the three study sites, (A) Bizansgat (Fan 3), (B) Zoutkloof (subunit C1), and (C) Slagtersfontein (subunit C2). The yellow marks the parent sand, the grey is the underlying mudstone. The red lines are dykes, using mean orientation. The blue arrows show the mean direction for flow of the intrusions; note that data are not available for part C. Note that the dykes are sub-parallel to the pinchout of the sandbody (approximately perpendicular to the onlap slope) and that the dominant flow direction is at a high angle to the pinchout.

5.5.4. Stages of fluid flow associated with injectites

Understanding fluid flow through time in sedimentary basin-fills is essential when considering aquifers and hydrocarbon reservoirs. In large-scale cases, injectites can promote basin-wide fluid flow and offer vertical and lateral permeable networks through low permeability successions (Huuse *et al.*, 2005; Vigorito *et al.*, 2008; Jonk, 2010; Hurst *et al.*, 2011). Four main elements of basin-wide fluid flow are identified (Jonk *et al.*, 2005a): i) gravity-driven, downward flow of meteoric water (Bjørlykke, 1993), ii) compaction of sediments through burial causes fluids to be expelled and flow upwards (Osborne & Swarbrick, 1997), iii) upward flow of fluids through overpressure (Osborne & Swarbrick, 1997), and iv) upward migration of hydrocarbons due to buoyancy (Bonham, 1980). Clastic injectites are associated with basinal fluid flow at several stages; pre-injection, during the process of clastic injection, post-injection and pre-cementation, and post-cementation (Fig. 5.10).

Pre-clastic injection

The migration of fluids as a trigger for clastic injectites through lateral pressure transfer has already been discussed; a schematic representation of the processes is shown in Figure 5.10B.

During injection

During clastic injection, grains are suspended and transported down a pressure gradient, by fluids moving from the overpressured parent unit towards the tip of the propagating hydraulic fracture, a source of relatively lower pressure (Cosgrove, 2001). The flow regime during injection can be turbulent (Hubbard *et al.*, 2007; Scott *et al.*, 2009; Hurst *et al.*, 2011) or laminar (Duranti, 2007; Cobain *et al.*, 2015) (Fig. 5.10C).

Post-injection, pre-cementation

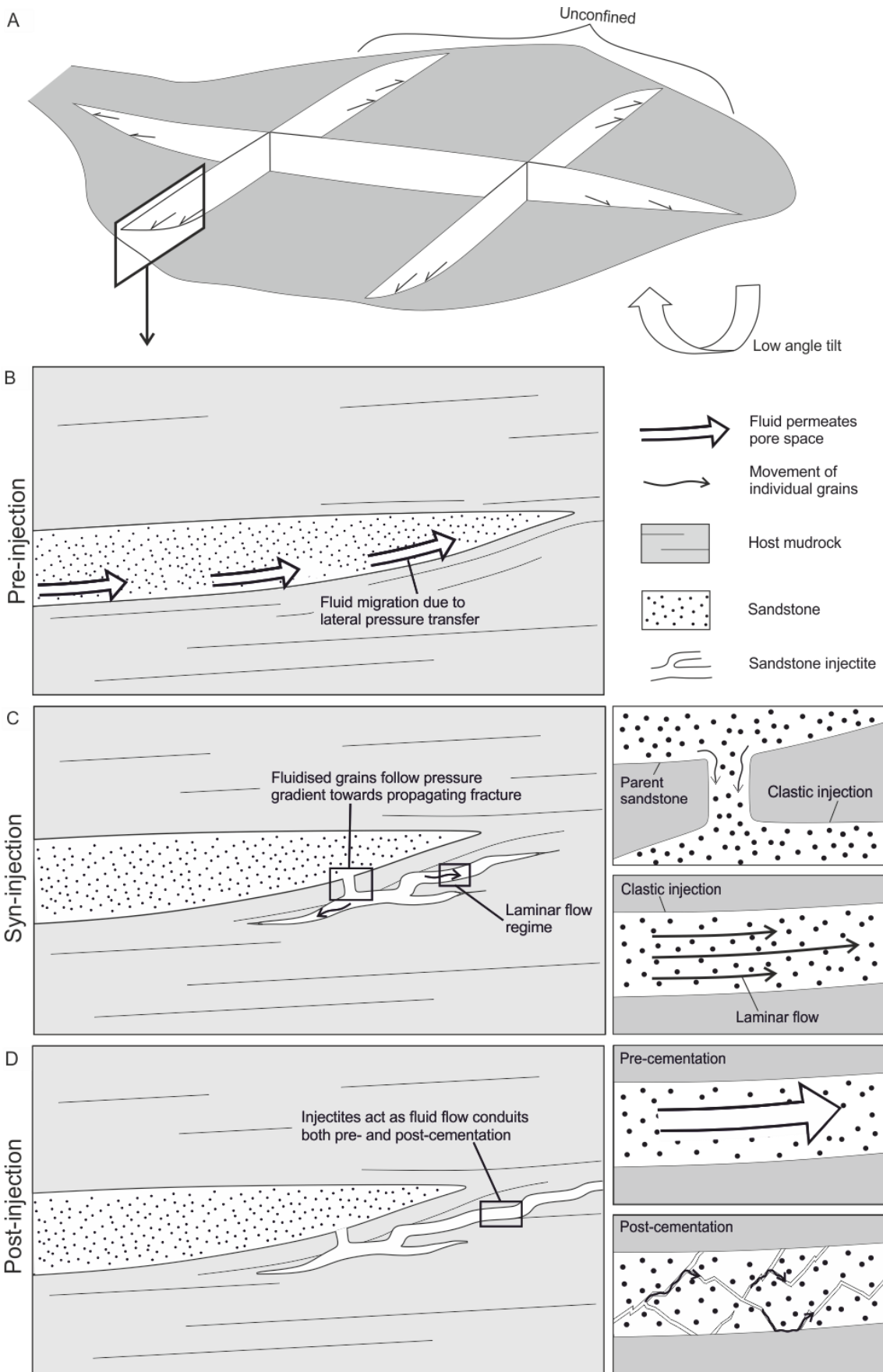
In previous studies, petroleum inclusions in late diagenetic cementation phases, and multiple cementation phases, indicate that injectites can act as long-lived fluid flow conduits (Jonk *et al.*, 2005b, 2005c, 2007; Ross *et al.*, 2014). Injectites can act as fluid flow conduits up to depths of approximately 1 km (Jonk *et al.*, 2005a; Jonk, 2010) prior to cementation. However, thicker sandstones (i.e. 20–30 m) can remain uncemented up to depths of 1.5–2 km burial, for example those within the Tertiary of the Northern North Sea (Lonergan *et al.*, 2000; Duranti *et al.*, 2002). Additionally, many of the large-scale injectite networks in the Tertiary of the North Sea have maintained excellent reservoir properties (Hurst & Cartwright, 2007) and outcrop examples such as the Panoche Giant Injection Complex have been shown through fluid inclusion analysis to have maintained migration of fluid for almost 2 Ma post injection (Minisini & Schwartz, 2007;

Hurst *et al.*, 2011). Besides acting as fluid migration pathways, clastic injectites can connect otherwise separate reservoirs, and form traps when injected solely into—or capped by—impermeable strata (Frey-Martínez *et al.*, 2007; Schwab *et al.*, 2015).

Post-cementation

When cemented, injectites become fluid flow barriers, preventing any further migration of basinal fluids. However, cemented injectites also have the potential to act as conduits, through structural deformation in the form of fractures focussed on the competent sands within low-competence mudrock host lithology (Jonk *et al.*, 2005a) (Fig. 5.10D). Understanding the timing of deformation phases helps to determine if clastic injectites will be reactivated as fluid flow conduits.

Figure 5.10 Fluid flow associated with stages of clastic injection. A) Simple lobe complex architecture, injectites sourced from steeply confined margin. B) Overpressured sandstone: pre-injection overpressure from compaction and expulsion of fluids from surrounding strata followed by fluid flow due to lateral pressure transfer. C) Trigger and fluidisation: syn-injection fluid flow, grains liquefied and fluidised into propagating fracture. D) Diagenesis: post-injection fluid flow, both pre- and post-cementation.



5.5.5. Implications for hydrocarbon extraction

Is there an association of stratigraphic traps and clastic injectites?

Each outcrop locality presented herein is an example of a basin-floor lobe complex that has been subject to clastic injection at its abrupt proximal (Bizansgat, Zoutkloof) or lateral (Slagtersfontein) pinchout. In each case, injectites are fed from the sharp sand-to-mud contact that make the base of a lobe complex, they then parallel the base of the depositional body, stepping upwards and outwards (e.g. Figs 5.3A and 5.7A), ultimately projecting beyond the limit of the lobe complex. The clastic injectites produced are of sub-seismic scale.

Sandy lobe complexes such as those described have been a prime target for hydrocarbon exploration as stratigraphic traps (e.g., Halbouty, 1966; Walker, 1978; Brown *et al.*, 1995; Gardiner, 2006; Stoker *et al.*, 2006; Nagatomo & Archer, 2015). In particular, proximal turbidites on the basin floor as they provide clean sands that pinch out abruptly, providing an optimal trap configuration. We have shown here that these sands are prone to injection, particularly on a sub-seismic scale. In addition, we have shown that dykes can have a strong preferential orientation at abrupt pinchout of lobe complexes against confining slopes, and that injection flow will be towards, and beyond, sand pinchout. This helps to constrain the architecture and prediction of injectite networks at stratigraphic traps on the basin-floor. The presence of clastic injectites at stratigraphic traps can be beneficial; they can provide connection between otherwise separated sand units, allowing flow of hydrocarbons through impermeable shale, and balancing pressure differences across reservoir complexes. However, the complicated geometry of injectites and their potential to connect otherwise separate sand bodies needs to be taken into consideration when building reservoir models and when using outcrops as analogues for geological and petrophysical model development.

Are basin-floor lobe injectites under-reported?

The relative lack of documented examples of injectites associated with lobe complexes compared to submarine slope channel-fills may simply be due to less of these systems being drilled and therefore a data bias. However, this disparity is also likely a reflection of scale. Parent sands of the injectites described here are volumetrically larger than many slope channel-fills, but comprise much thinner lobe complexes. Therefore, as observed in the Karoo Basin outcrops, thinner injectites can be expected as a product of remobilisation in comparison to slope channel-fills, thus being sub-seismic scale and frequently unrecognised or poorly documented on many

seismic data sets (e.g. Shepherd *et al.*, 1990). Another factor contributing to the lack of recognition in subsurface data is the style of injection; Karoo injectites are primarily laterally extensive sills. These would be hard to identify in reflection seismic data, and misinterpretation as primary deposits rather than remobilised units in core is possible.

5.6. Conclusions

The majority of injectites are reported as being sourced from submarine slope settings and have been rarely documented in base-of-slope and basin-floor environments. The three outcrop examples of clastic injectites presented here are associated with basin-floor environments, and specifically occur at the abrupt pinchouts of basin-floor lobe complexes. Architecture and bed-scale similarities across the injectite parent sand have led to the development of a model to help predict likely areas and orientations of clastic injectites in a deep marine system. Injectites occur where sand is: i) confined and pinches out abruptly, ii) proximal within the lobe complex, and iii) exhibits sharp contacts with underlying and/or overlying mudstone. In contrast, palaeogeographic locations that exhibit subtle to no confinement, have less clean-sand for fluidisation, and heterolithic stratigraphic boundaries do not result in injectites. Clastic injectites, even those of a sub-seismic scale, provide the potential to rearrange fluid flow pathways within deep-water successions. Injectites, such as those in the Karoo Basin, can extend laterally for several kilometres, and beyond the stratigraphic pinchout, yet are too thin to be resolved in seismic data, however they may connect otherwise separate bodies of sand or reservoirs, offering highly permeable networks through impermeable successions. The association of clastic injectites and stratigraphic traps can be beneficial in subsurface plays because they provide connection between otherwise separate sand units, allowing flow of hydrocarbons through impermeable mudstones, and balancing pressure differences across reservoirs. In the Karoo Basin, we see clastic injection and therefore the potential for fluid flow in basin floor settings, where, up until now, injectites and associated fluid flow have dominantly been associated with channelised slope environments.

6. Genesis and morphology of clastic injectites in a Palaeocene North Sea case study: constraints on parent sand and formative depth

6.1. Introduction

Clastic injectites are the forceful intrusion of clastic material into a host lithology (Jolly and Lonergan, 2002), the source of the intrusive material therefore, must undergo some form of depletion (Løseth *et al.*, 2012). In core, outcrop, or seismic datasets it is often challenging to associate injectites with their parent sand unit unless the connection is directly observed, and even more challenging if the parent sand is depleted, essentially looking for something that is no longer there.

Being able to define injectites and their parent sand in the subsurface is important in modelling fluid flow pathways between bodies of sand. Presented here, is a North Sea case study example of clastic injectites, mapped using a high resolution broadband dataset, and an assessment made of the associated potential area of depletion of the underlying source unit.

6.2. Geological setting

6.2.1. Case study stratigraphy, North Sea

The North Sea case study is composed of Palaeocene sediments that onlap Devonian basement and Early Palaeocene chalk landward (Fig. 6.1) (Ahmadi *et al.*, 2003). The lowermost sands are interpreted to be a series of massive, stacked, submarine channel and fan deposits (Maureen Formation; Mudge and Copestake, 1992; Mudge, 2014). Sands were delta-fed via channels from the north-west (Galloway *et al.*, 1993). A >600 m thick hemipelagic mudstone succession (Lista Formation; Ahmadi *et al.*, 2003) directly overlies the submarine fan and channel-fill sands, which formed during a period of relative sea-level rise. Located within these mudstones are a series of sand-prone channelised systems (Ahmadi *et al.*, 2003). Injected and remobilised sand has been interpreted in the Lista Formation mudstone in many locations (Cheret and Carrillat, 2004; de Boer *et al.*, 2007; Satur and Hurst, 2007; Kilhams *et al.*, 2012). This study focuses on the

architecture and source of clastic injectites in the Lower Lista Formation that directly overlies the Maureen Formation (Fig. 6.1B).

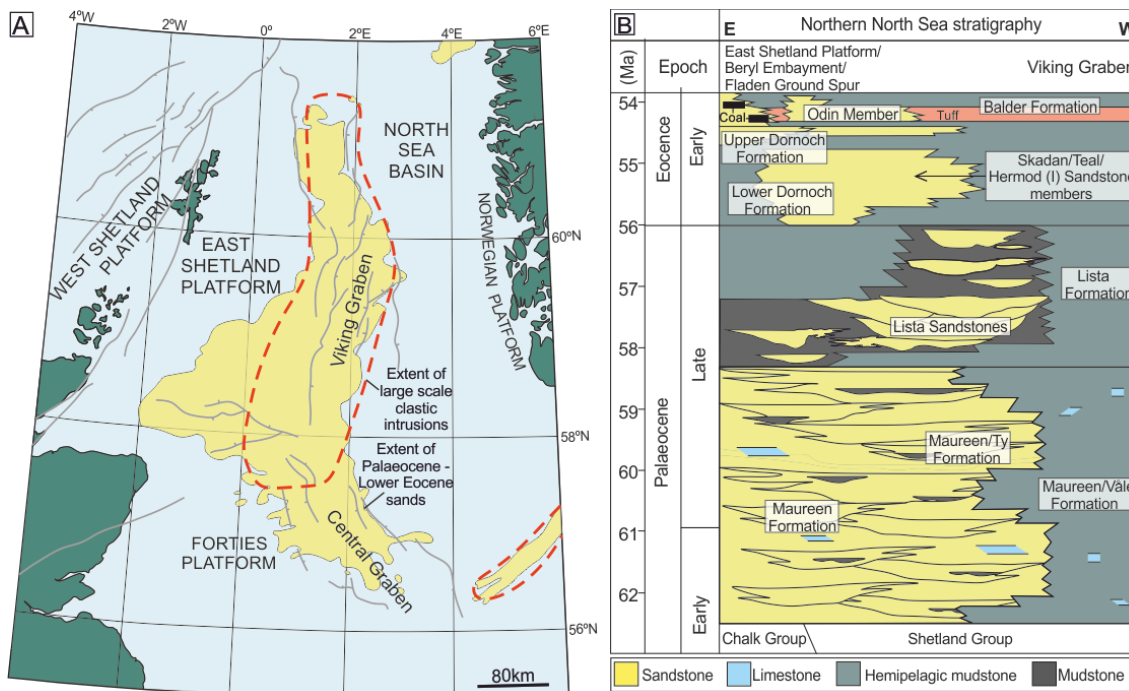


Figure 6.1 A) North Sea Basin showing present day distribution of Palaeocene-Lower Eocene sandstone in yellow (adapted from Mudge, 2014) and locations of large scale sandstone injectites in the Palaeogene of the Northern North Sea outlined in red (after Huuse *et al.*, 2007). B) Stratigraphy of the North Sea case study (adapted from Ahmadi *et al.*, 2003).

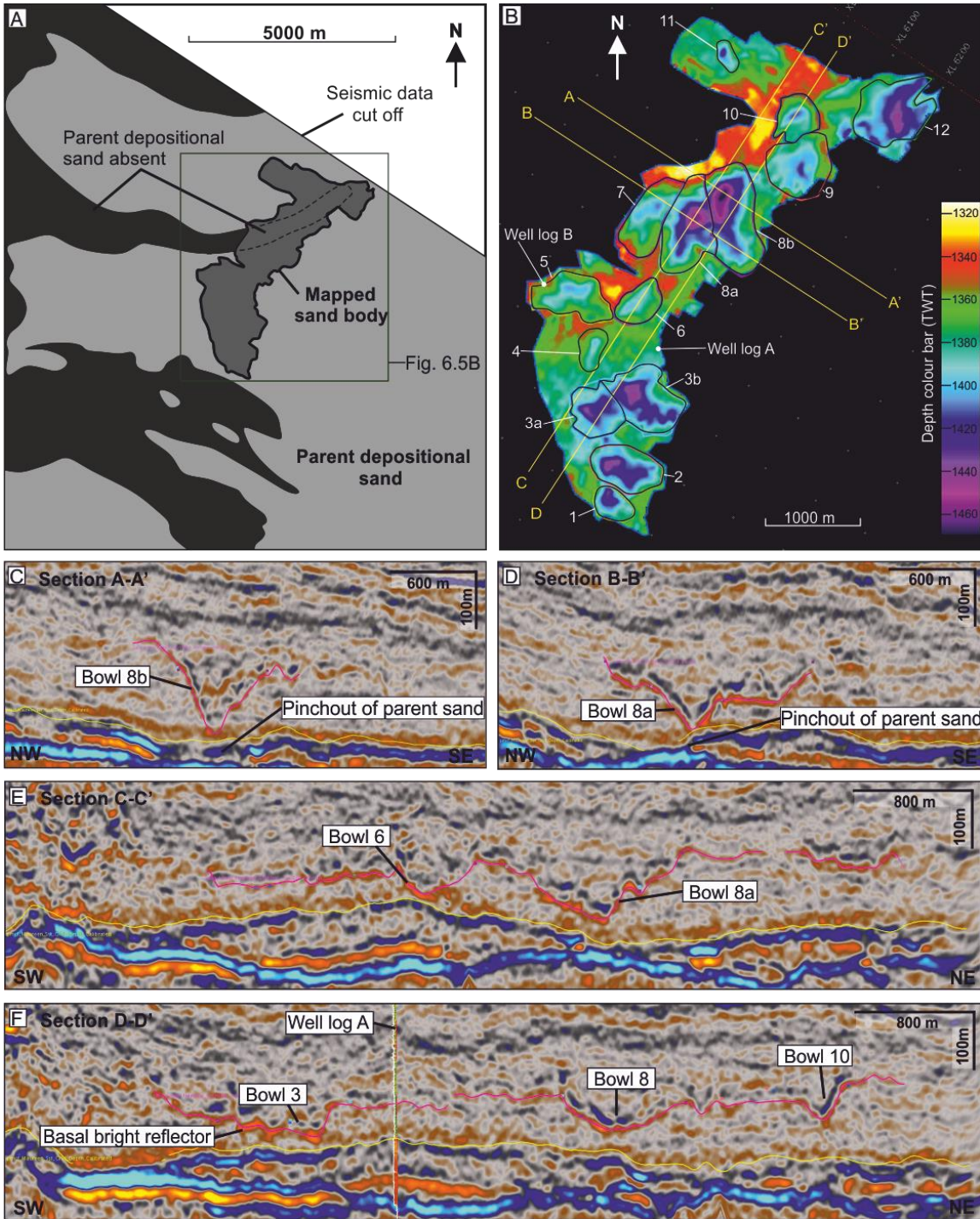
6.3. Methodology

6.3.1. Seismic mapping

The seismic study covers a 5.75 km long, and 2.12 km wide (7.7 km²) area of high quality 3D seismic data within the Lower Lista Formation (Figs. 6.2A and 6.2B). The data used is a broadband survey with an in-line (IL) and cross-line (XL) spacing of 6.25 m at northwest-southeast and northeast-southwest orientation respectively and has been time migrated with a standard anisotropic 3D Kirchhoff migration. A positive peak event (black reflection) represents a downward increase in acoustic impedance whereas a negative trough (orange reflection) represents a downward decrease in acoustic impedance (Figs. 6.2C – 6.2F). In the study area, reflections are brighter imaged on the near angle stack (5°-17.5°), and were chosen for mapping.

Mapped sands are penetrated directly by two vertical wells allowing them to be calibrated with the well logs (Fig. 6.3). Initially, the base of the sand bodies were mapped every 16 IL and XL (100 m) and then from the grid created by this method every IL and XL was mapped. Where correlating between 2 lines was problematic, arbitrary lines were used. Mapped sands crosscut stratigraphy, display both low and high angles of dip (defined as $<20^\circ$ and $>20^\circ$ respectfully (Hurst *et al.*, 2011)), and form bowl shaped structures in 3D. A major uncertainty with mapping injectites is that steeply dipping injectites (usually $>60^\circ$ (Jackson *et al.*, 2011)) are not imaged on seismic data. However because the dataset used in this study is of such high resolution, it is possible to infer where an absence or break of seismic reflection is due to steeply dipping sand units. The complicated nature of injectite geometries, which locally includes the separation of a single mappable sand body into several thinner sand units on different stratigraphic levels, can produce a chaotic seismic response. Where this occurred either the brightest reflector was selected, or where no obviously bright reflector was present the lowermost reflector was selected (e.g. Fig. 6.2F).

Figure 6.2 Mapped area of North Sea case study. A) Plan view of the study area showing extent of the Maureen Formation in pale grey. Black areas and the dashed line denote where Maureen is absent, and darker grey represents mapped sands within the Lista Formation. B) Depth map in plan view of sands within the Lower Lista shale and polygons outlining each individual bowl feature mapped. Yellow lines represent sections shown in Figure 6.2C-F. C-F) Seismic cross-sections through mapped sands; yellow line is the top Maureen Formation pick, pink line picks base sand in Lower Lista shale. C) Section A-A'; steeply dipping, v-shaped bowl with complex internal sand architectures. D) Section B-B'; v-shaped bowl where base of bowl is in contact with the top of the Maureen Formation. E) Section C-C'; 5 km long section cutting through several outlined polygons (Fig. 6.2B). F) Section through several bowl structures and well log A used to correlate sand bodies.



6.4. Results and analysis

6.4.1. Seismic mapping

Fourteen bowl structures were mapped in detail over the 7.7 km² study area, including bright reflections interpreted to be sands that connect to, or sit in-between, bowl-shaped structures. These structures are shown to crosscut stratigraphy at high angles (Fig. 6.2C-F) and internally have chaotic seismic response. After being mapped in 3D, 2D seismic profiles were taken at intervals of 50 m along both ILs and XLs for quantitative analysis (Table 6.1) with some results displayed as crossplots (Fig. 6.4). The key geometric parameters measured for each individual bowl includes: i) plan view area is an aerial parameter (m²) that was defined where the steeply dipping sandstone bodies pass abruptly into sills concordant with host strata; ii) height of bowl, defined as the vertical extent (m) from the base (lowest depth) to the abrupt change between steeply dipping side and shallow dipping sill; and iii) the width of each bowl through both IL and XL sections, defined as the horizontal extent (m) along both IL and XL inside the aerial extent of the bowl (Table 6.1). Internal sand geometries and sand thicknesses are difficult to estimate as well calibrations show these are likely clustered zones of thin sands (Loneragan *et al.*, 2007) as opposed to a single, thick, high net-to-gross body (Huuse *et al.*, 2004; de Boer *et al.*, 2007).

Most of the bowl structures are between 60 and 85 m in height. Maximum measured widths are between 200 and 900 m (Fig. 6.2), with an average width of 574 m. The vertical distance between the top of the Maureen sandstone and the base of the lowermost section of each bowl ranges from 0 m (bowl 8a is in contact with Maureen Formation; Figure 6.2D) to 88.8m (bowl 9). There are 2 distinct stratigraphic horizons above the Maureen Formation along which injectites abruptly change from being steeply dipping to concordant with stratigraphy (Figs. 6.2C and 6.2D). Quantitative data show that the degree of variability between the bowls is low to moderate. There is a strong relationship between the width and height of bowl structures (Fig. 6.4B).

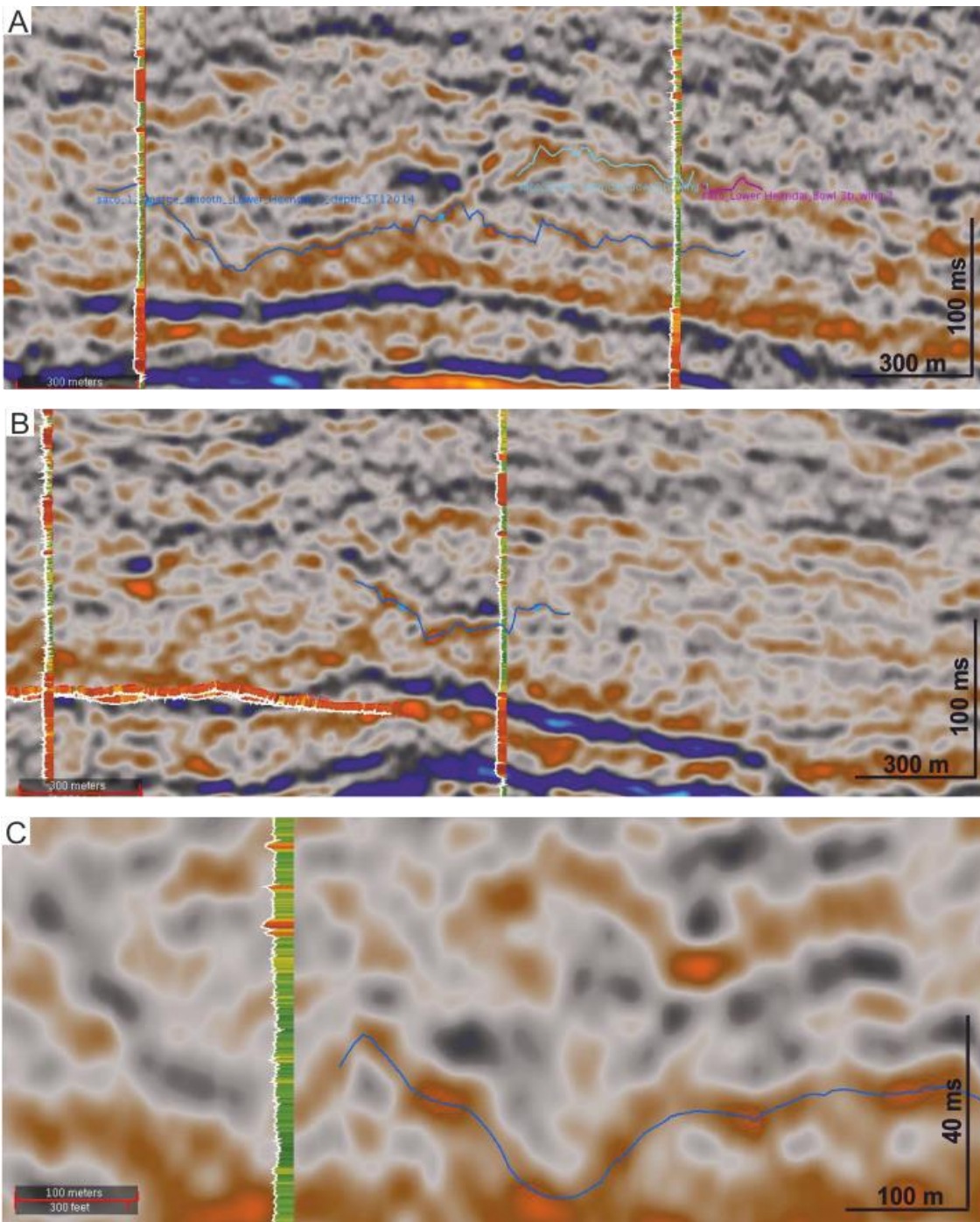


Figure 6.3 Well log ties to seismic interpretation, orange colour denotes higher sand content. A) Profile through Bowl 5 (Fig. 6.2B). The underlying Maureen Formation shows thick sand packages. In contrast sediments overlying the bowl consist of thin sand units interpreted as injectites. B) Western edge of Bowl 5, again, the Maureen Formation picked is out by high sand content; the edge of the bowl shows multiple, thin sands interpreted as injectites. C) Edge of Bowl 5, sand bodies appear to have pinched out. Some sand layers higher up in stratigraphy.

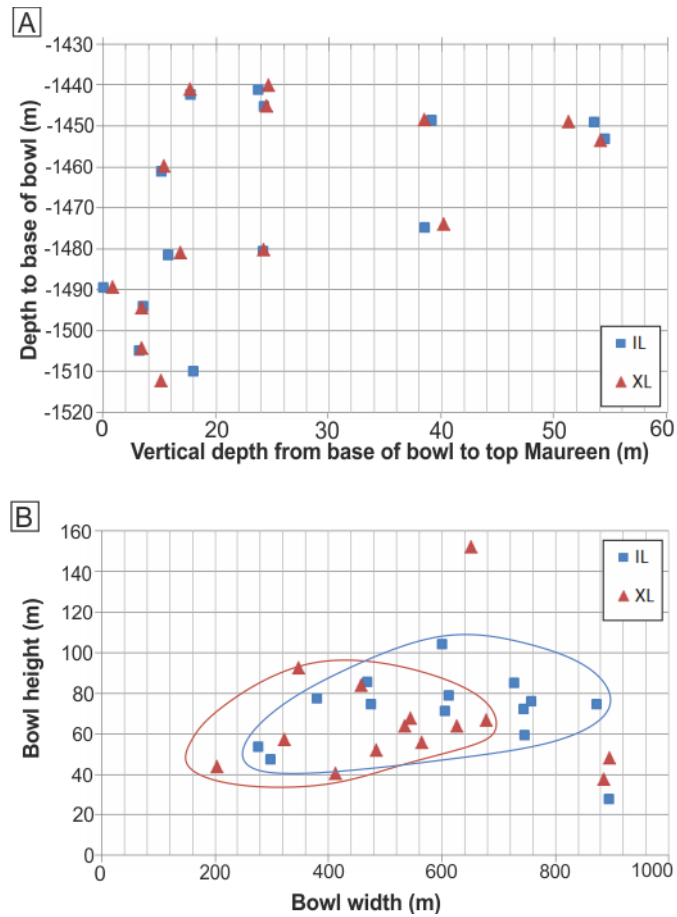


Figure 6.4 Geometric properties and vertical position of the mapped sands. A) Vertical depth to base of each bowl and depth from base of bowl to the top of the Maureen Formation. B) Bowl height versus width, showing low to moderate degree of variability in height through bowls of different widths.

Bowl no.	Plan view area (m ²)	Perimeter (m)	XL transect (m)	IL transect (m)	Depth of top Maureen (IL) (m)	Top Maureen to base bowl (IL) (m)	Base bowl (IL) (m)	Top bowl (IL) (m)	Depth of bowl (m)	Depth to top Maureen (XL) (m)	Top Maureen to base bowl (XL) (m)	Base bowl (XL) (m)	Top bowl (XL) (m)	Depth of bowl (m)
1	114008	1277	323	475	-1509	28	-1481	-1406	75	-1509	28	-1480	-1424	57
2	288197	2086	458	728	-1489	0	-1489	-1404	85	-1491	2	-1490	-1406	84
3a	235329	1982	535	606	-1493	11	-1482	-1410	71	-1495	14	-1481	-1417	64
3b	376346	2720	627	872	-1501	7	-1494	-1419	74	-1501	7	-1495	-1431	64
4	99857	1250	413	277	-1468	27	-1441	-1388	54	-1469	29	-1440	-1400	40
5	309185	2461	485	746	-1474	29	-1445	-1386	60	-1474	29	-1445	-1393	52
6	162283	1577	565	380	-1458	15	-1442	-1365	77	-1457	15	-1441	-1385	56
7	297238	2371	347	893	-1536	87	-1449	-1421	28	-1532	83	-1449	-1357	92
8a	419498	2838	895	613	-1511	6	-1505	-1426	79	-1511	7	-1504	-1457	48
8b	508267	3086	652	600	-1526	16	-1510	-1406	104	-1523	10	-1512	-1360	152
9	364621	2274	679	743	-1542	89	-1453	-1381	72	-1542	88	-1454	-1387	67
10	175801	1810	545	468	-1507	58	-1449	-1363	85	-1505	57	-1449	-1381	68
11	52870	950	204	298	-1471	10	-1461	-1414	47	-1471	11	-1460	-1416	44
12	4539	3140	886	757	-1532	57	-1475	-1398	76	-1535	60	-1474	-1437	38

Table 6.1 2D seismic profiles were taken at intervals of 50 m along both ILs and XLs for quantitative analysis of 14 bowl structures and the underlying Maureen formation: plan view area (m²), perimeter (m), XL transect length (m), IL transect length (m), depth of top Maureen Formation (IL) (m), top Maureen Formation to base bowl vertical distance (IL) (m), depth to base bowl (IL) (m), depth to top bowl (IL) (m), vertical depth of bowl (m), depth of top Maureen Formation (XL) (m), top Maureen Formation to base bowl vertical distance (XL) (m), depth to base bowl (XL) (m), depth to top bowl (XL) (m), vertical depth of bowl (m).

6.5. Discussion

6.5.1. Source of North Sea case study injectites

Overpressure is a key factor required to generate clastic injectites. For the North Sea case study studied here, the overpressure is thought to be generated from: i) depositional sands being encased in low permeability mudstones, and ii) influx of hydrocarbons into sandstone units (Ahmadi *et al.*, 2003). However, the parent sand of these injectites is still under debate; the two possibilities are either the Lista Sandstones, a series of sand-prone channelised deposits within the Lista Formation (Fig. 6.1), or the underlying Maureen Formation, which comprises stacked lobe and channel deposits (Fig. 6.1). The mapped bowl structures presented here show strong spatial affinity with the underlying sandstones from the Maureen Formation, with some bowls showing direct contact at their base with the top of Maureen Formation sands (e.g. Bowl 8a; Fig. 6.2D). Additionally, the location of the mapped bowls within this study shows a spatial relationship with the pinchout or absence of the underlying Maureen Formation (Figs. 6.2A, 6.2C, 6.2D and 6.5). In cross section, the absence of Maureen Formation sand resembles incision and removal by a channel-form (Fig. 6.5).

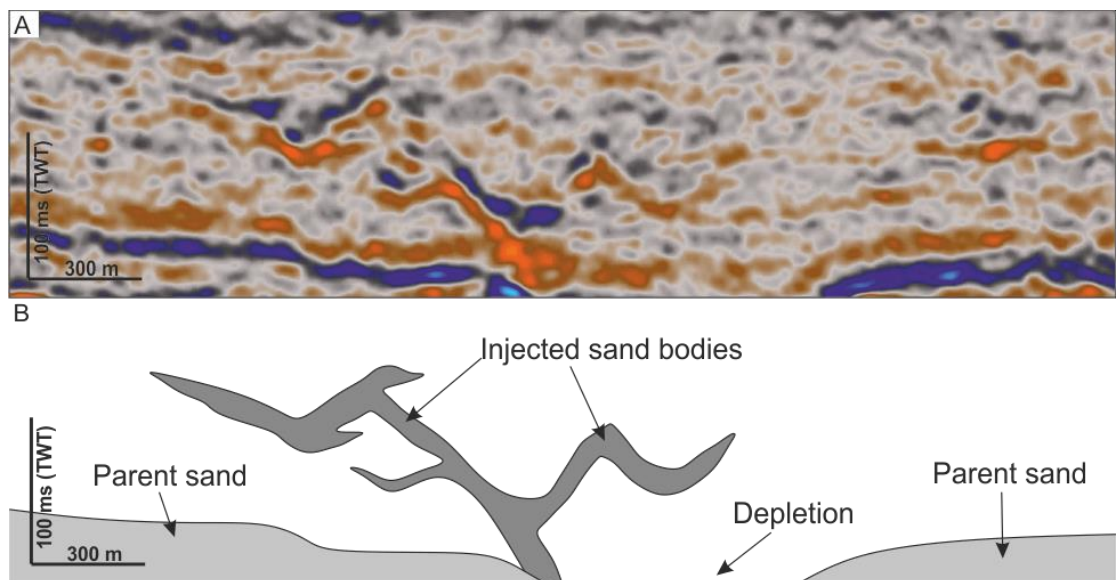


Figure 6.5 A) Section taken through bowls 8a and 8b in the case study area. B) Simplified interpretation of depleted parent sand and resultant injected sand.

One explanation for this pinchout is the presence of a mud-filled channel system. However, removal by a channel would mean a strongly different orientation (WSW-ENE and curving northwards) to other channels along the same palaeoslope, which are orientated west-to-east (Mudge, 2014). A channel would commonly be one of many similar systems, but this is also the only feature of its type in the study area. An alternative explanation is that the lack of Maureen Formation sands in this area is the result of depletion through the remobilisation and injection of sand into the overlying Lista Formation. The spatial relationship between the absence of Maureen Formation and the presence of overlying large bowl structures, the abrupt pinchout of the Maureen Formation, and the connection with the overlying injectites, supports an interpretation that the most likely source for the clastic injectites is the Maureen Formation (Fig. 6.6).

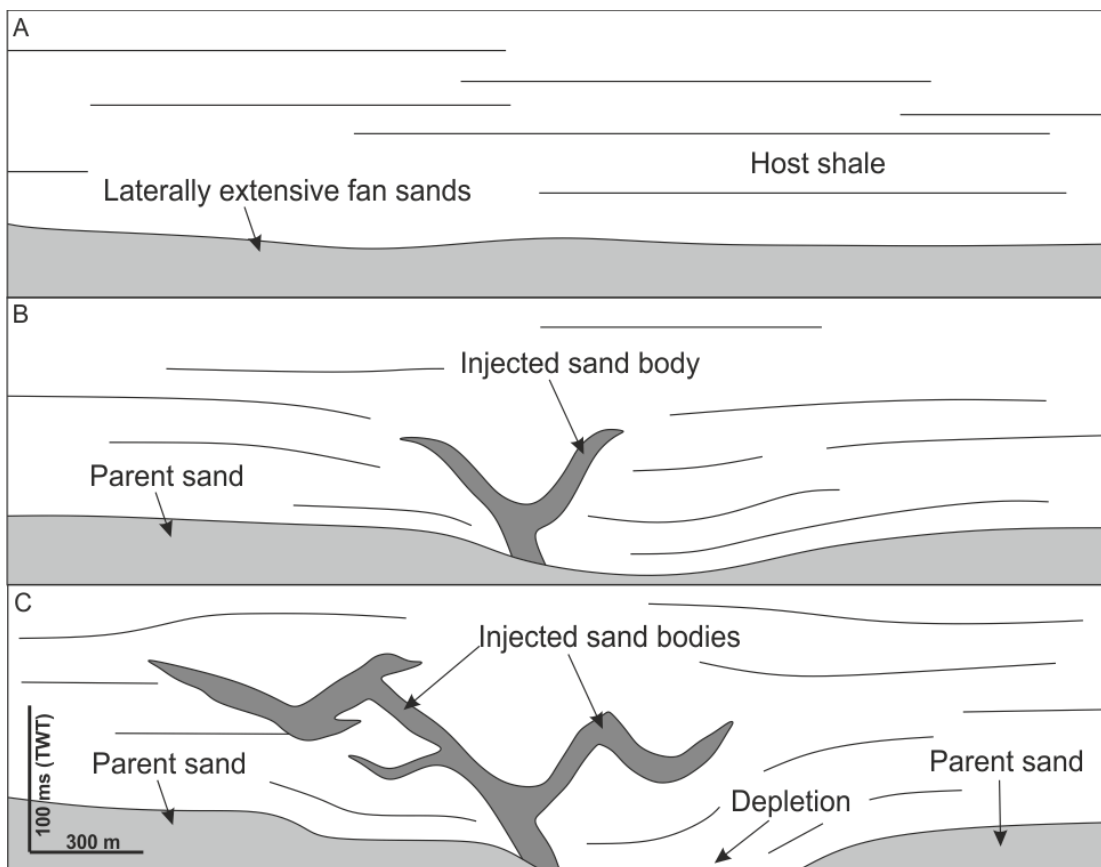


Figure 6.6 Temporal model of parent sand depleting as injectites form. A) T1: pre-injection, fan sands remain unconsolidated and become overpressured as overlying shale deposited. B) T2: parent sand starts to drain and deform as it injects into overlying strata. Overlying shale starts to deform in response to sand draining and injecting. C) T3: injectites cease propagating with development of a sand ‘weld’, resulting in a large area of parent sand depleted and forming a “channel-like” cross-sectional shape.

6.5.2. Timing of Mariner injectites

Hydrocarbon migration from the Beryl Embayment into the up dip Palaeocene sands is constrained to between 55 and 65 Ma and is known to be post calcite cementation (Ahmadi *et al.*, 2003). Fluid pressures within the relatively shallow sandstones at the time of oil migration would have been, and generally still are, hydrostatic (Chiarelli and Richy, 1984). Fluid migration may not only have provided the source for overpressure but could potentially be the trigger mechanism needed for the initiation of clastic intrusion. Constraints on the timing of the process of injection are limited, however the maximum vertical thickness of a single intrusion structure is 152 m, indicating a minimum burial depth of at least this amount prior to intrusion. Although the sands within the Lower Lista are relatively shallow compared to some injectite complexes, they have undergone some burial and compaction since remobilisation and deposition. However, the constraints on the timing of this process are limited and the values presented herein have not been decompacted. Consequently, the measured vertical heights in features represent a minimum burial depth (Huuse *et al.*, 2004; Parize *et al.*, 2007).

6.5.3. Implications for hydrocarbon exploration

Subsurface remobilisation and injection of sand has significant consequences on reservoir architecture, geometry, and porosity and permeability, which impact hydrocarbon recovery. In this North Sea case study, the procedure has been employed to provide unequivocal evidence for the origin of the sand bodies mapped in the Lower Lista Formation shale to be clastic injectites and not of primary deposition. Moreover, there is likely more complexity to those sand bodies than can be observed in reflection seismic data (see Chapter 7). Therefore a larger volume of sub-seismic injectites, and hence greater volume of sand and connectivity, is likely present than would be predicted from seismic data alone (Fig. 6.7).

As more exploration drilling in the North Sea is specifically targeting clastic injectite complexes (de Boer *et al.*, 2007; Schwab *et al.*, 2015), having the ability to map and interpret injected sandstones and predict their sub-seismic distribution accurately is crucial to achieve economic viability of drilling and production from such fields. Increasing our understanding of the architecture of clastic injectites will allow more accurate interpretation during exploration, and more informed placement of production wells, increasing the economic viability of reservoirs (Fig. 6.7).

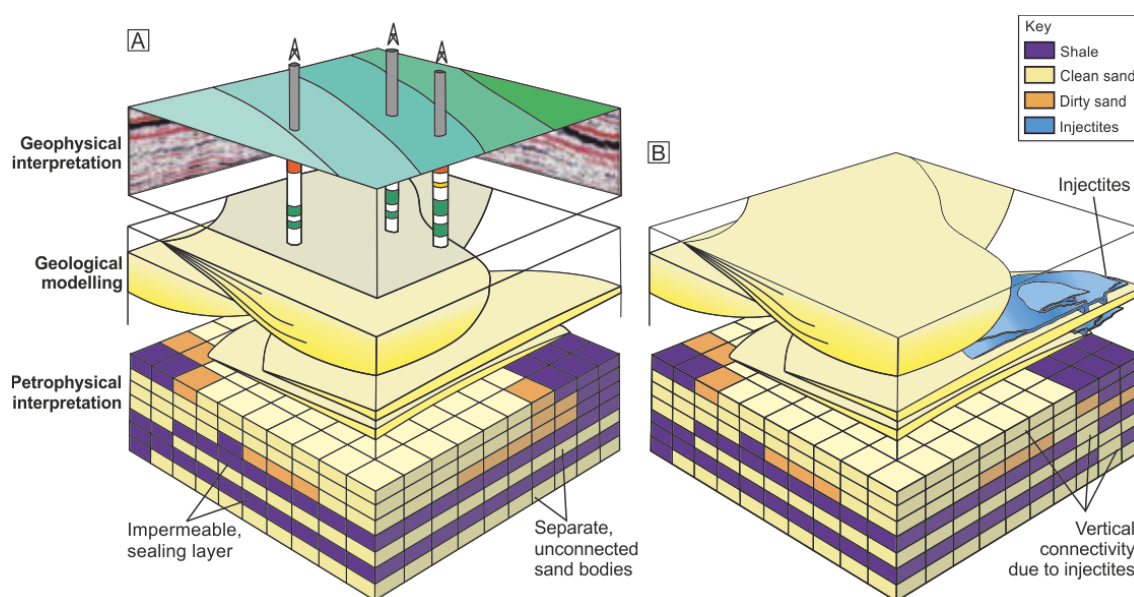


Figure 6.7 A) 3D reservoir modelling process for a single geological model (adapted from Bentley and Smith 2008). B) Same model with sub-seismic injectites providing vertical connectivity between reservoir units.

6.6. Conclusions

The broadband seismic survey data from the North Sea case study, combined with well logs from the area of the discovery, were used to map in detail the 3D geometries of clastic injectites over an area of 7.7 km². Fourteen bowl structures were identified, some of which showed a direct connection with the underlying Maureen Formation. The Maureen Formation is partly absent, suggesting draining or depletion as clastic material is forcibly injected upwards into the Lower Lista Formation forming the sand bodies mapped and interpreted as injectites. These form bowl structures covering up to 900 m laterally and giving a minimum (compacted) burial depth of 152 m prior to injection. This is a rare case where, in the subsurface, the parent unit can be confidently associated with clastic injectites. The impact of injectites on hydrocarbon reservoirs (Fig. 6.7), as well as an increase in the industry targeting unconventional or complex reservoirs, means that the need for this knowledge and understanding has never been so pertinent.

7. Forward seismic modelling of exhumed clastic injectites: the importance of scale invariance

7.1. Introduction

Clastic injection processes alter the architecture, connectivity, volumetrics, and pore-scale properties of deep marine reservoirs (Lonergan and Cartwright, 1999; Duranti *et al.*, 2002), and therefore affect exploration and development programmes. Clastic injectites are recognised from mm to km scale at outcrop and in the subsurface (e.g. Hiscott, 1979; Archer, 1984; Dixon *et al.*, 1995; Hillier and Cosgrove, 2002; Monnier *et al.*, 2013; Ross *et al.*, 2013, 2014; Morton *et al.*, 2014; Ravier *et al.*, 2015). It is, therefore, critical to correctly interpret clastic injectites on reflection seismic data, but also to improve prediction of their sub-seismic occurrence and architecture.

Forward seismic modelling of outcrops is a technique that allows reservoir petrophysical properties to be integrated with outcrop-constrained geometries and depositional architecture (Biddle *et al.*, 1992). The technique helps to bridge the gap between outcrop and seismic data, and enables the full incorporation of outcrop scale detail into the interpretation of seismic data (Campbell and Stafleu, 1992; Schwab *et al.*, 2007; Bakke *et al.*, 2008; Falivene *et al.*, 2010). This technique has been used to improve accuracy in the interpretation of reflection seismic profiles and seismic facies (Armitage and Stright, 2010), to reduce uncertainties in facies distributions and architecture of conventional clastic and carbonate reservoirs (Bakke *et al.*, 2008) and to improve predictability of subsurface connectivity (Falivene *et al.*, 2010). The majority of forward seismic modelling approaches have used primary depositional environments, including shallow-water carbonate systems (e.g. Rudolph *et al.*, 1989; Biddle *et al.*, 1992; Campbell and Stafleu, 1992; Stafleu *et al.*, 1994; Anselmetti *et al.*, 1997), shallow-marine depositional systems (e.g. Helland-Hansen *et al.*, 1994; Hodgetts and Howell, 2000; Holgate *et al.*, 2014) and deep-marine depositional systems (e.g. Sullivan *et al.*, 2004; Schwab *et al.*, 2007; Bakke *et al.*, 2008, 2013; Armitage and Stright, 2010; Pringle *et al.*, 2010; Falivene *et al.*, 2010). In these settings, parameters such as grain-size range, orientation, and tectonic setting should be considered. The successful application of forward seismic modelling is dependent on using suitable analogues. In particular, the scale of the exhumed feature being modelled either needs to be comparable

to the subsurface features, or there is an implicit assumption that similar architectures occur across different vertical and/or horizontal scales.

Secondary features in sedimentary basin-fills, such as clastic injectites, extrudites, and diapirs, have rarely been the focus of forward seismic modelling (Parize *et al.*, 2007, Huuse *et al.*, 2007). Parize *et al.* (2007) is the only published study with a main focus on forward seismic modelling of clastic injectites, although their study focussed on comparison of outcrop data with shallow, high frequency seismic data shot behind the same outcrop. This is despite the recognition that clastic injectites have an important role in production in many hydrocarbon fields (Dixon *et al.*, 1995; Duranti and Hurst, 2004; Huuse *et al.*, 2004; Hurst and Cartwright, 2007; Jackson *et al.*, 2011). Due to their complicated architecture and limited predictability of sub-seismic geometry, clastic injectites pose both imaging and modelling problems. We use geometric data from exhumed injectites, and forward seismic modelling techniques, to assess to what degree injectites are scale invariant and to improve understanding of the complicated, and sometimes chaotic, expression of clastic injectites.

7.2. Geological setting

7.2.1. Karoo Basin, South Africa

Clastic injectites crop out at several localities within the deep-water stratigraphy of the Karoo Basin, South Africa. The SW part of the Karoo Basin is subdivided into the Laingsburg and Tanqua depocentres (Fig. 7.1A). The Laingsburg depocentre comprises a 1.8 km thick shallowing upwards succession. The base comprises distal basin floor stratigraphy (Vischkuil Formation; van der Merwe *et al.*, 2010) that passes up through proximal basin-floor (Laingsburg Formation; Sixsmith *et al.*, 2004) and channelised slope (Fort Brown Formation; Di Celma *et al.*, 2011) to shelf-edge and shelf deltas (Waterford Formation; Jones *et al.*, 2015) (Fig. 7.1C). Injectites are hosted within mudstones that represent regional shutdown of coarse clastic input between subunits A to G of the Laingsburg and Fort Brown formations (Flint *et al.*, 2011; van der Merwe *et al.*, 2014). The Tanqua depocentre comprises 1.3 km of deep-water stratigraphy (Hodgson *et al.*, 2006), the lower most units comprise submarine fan deposits (Skoorsteenbergh Formation; Wickens, 1994; Wickens and Bouma, 2000), shallowing upwards into slope and shelf edge delta deposits (Kookfontein Formation; Wild *et al.*, 2009). The Skoorsteenbergh Formation, which consists of four basin-floor fans (Fans 1-4) and a channelised slope succession (Unit 5) (Hodgson

et al., 2006). Clastic injectites are observed across both depocentres and associated with many of the sand prone units, here, 3 outcrop examples have been selected to forward model, these display a variety of injectite geometries that are typically seen in the Karoo Basin.

Unit C of the Fort Brown Formation is split into 3 subunits; C1, C2 and C3, each separated by a laterally extensive mudstone (Flint *et al.*, 2011; Hodgson *et al.*, 2011a; van der Merwe *et al.*, 2014). Injectites exposed in the Zoutkloof area in the Laingsburg depocentre occur directly below subunit C1 in the upper 13 m of the underlying 40 m thick regional mudstone that separates Units B and C (Brunt *et al.*, 2013). Unit E of the Fort Brown Formation within the Laingsburg depocentre, located at Geelbeck (Fig. 7.1B), is bound by regionally extensive and thick (20-30 m) mudstones separating it from Units D and F. Unit E is further divided into 3 subunits; E1, E2 and E3, each separated by a regionally extensive thin (1-2 m) mudstone (Figueiredo *et al.*, 2010). In the Geelbeck area, subunit E1 is not present and injectites are located in the top 10 m of the ~30 m thick mudstone that separates Units D and E (Spsychala *et al.*, 2015). Injectites exposed in the Bizansgat area of the Tanqua depocentre reported here occur in mudstones below Fan 3 (Fig. 7.1D) in the most proximal exposures to the south of the outcrop belt. The nature of the outcrop means that the 3D geometry of the larger injectites exposed in the mudstone below Fan 3 can be constrained. Locally, a single main laterally extensive ~1 m thick clastic sill steps up to the south and east to form a discordant relationship with the stratigraphy.

7.3. Methodology

Forward seismic modelling of outcrop data is a method used to support the analysis and interpretation of reflection seismic images of geological structures. Modelling uses geological architectures, commonly derived from outcrop data, combined with petrophysical properties from subsurface fields to produce a synthetic seismic profile that can be compared to both subsurface seismic and the source outcrop data. Here, outcrop panels capturing injectite geometries from several localities are forward modelled to produce synthetic seismic sections.

7.3.1. Outcrop

Injectites are exposed in many places in the Karoo Basin (Flint *et al.*, 2007; Brunt *et al.*, 2013; Cobain *et al.*, 2015). The main outcrop study areas were Unit C at Zoutkloof and Unit E at

Geelbeck in the Laingsburg depocentre (Fig. 7.1C), and Fan 3 in the Tanqua depocentre (Fig. 7.1B), which were chosen for the range of injectite geometries exposed. Sedimentary logs and a photographic panel were taken across the well-exposed sections with individual injectites walked out in order to correlate between logs. Laterally extensive mudstones directly above the parent sand were used as the datum (Fig. 7.2). Figure 7.2 shows the outcrop panels that were used in the forward seismic modelling with examples of injectite expression at outcrop.

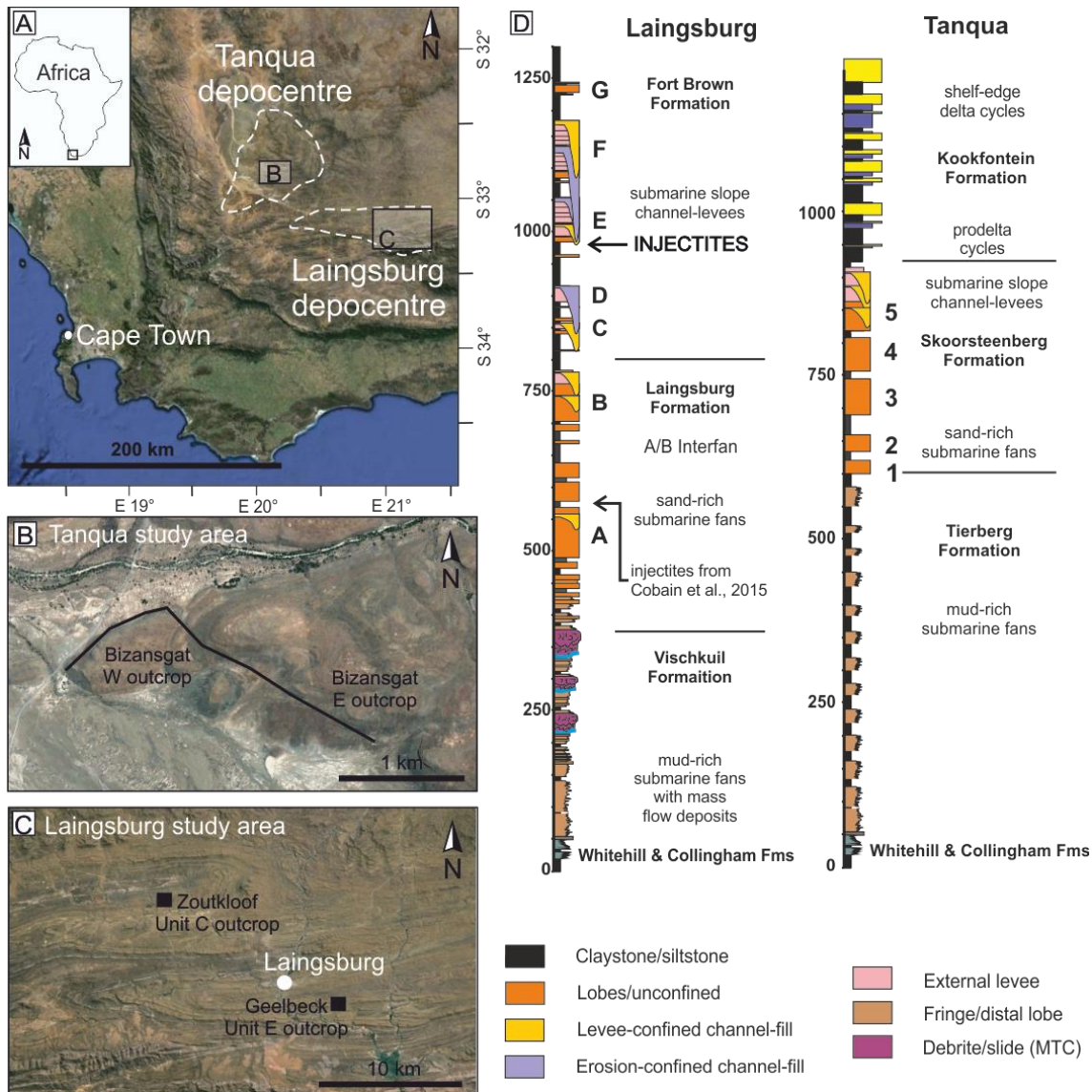


Figure 7.1 A) Locality of Tanqua and Laingsburg depocentres, SW Karoo Basin, South Africa. B) Bizangsat, Tanqua locality, 2 panels are depicted by black line. C) Locality of Zoutkloof and Geelbeck outcrops. D) Simplified stratigraphic log for Laingsburg (Flint *et al.*, 2011) and Tanqua depocentres. See Appendices A.3, A.4, B.3 and B.4 for individual logs and data collected.

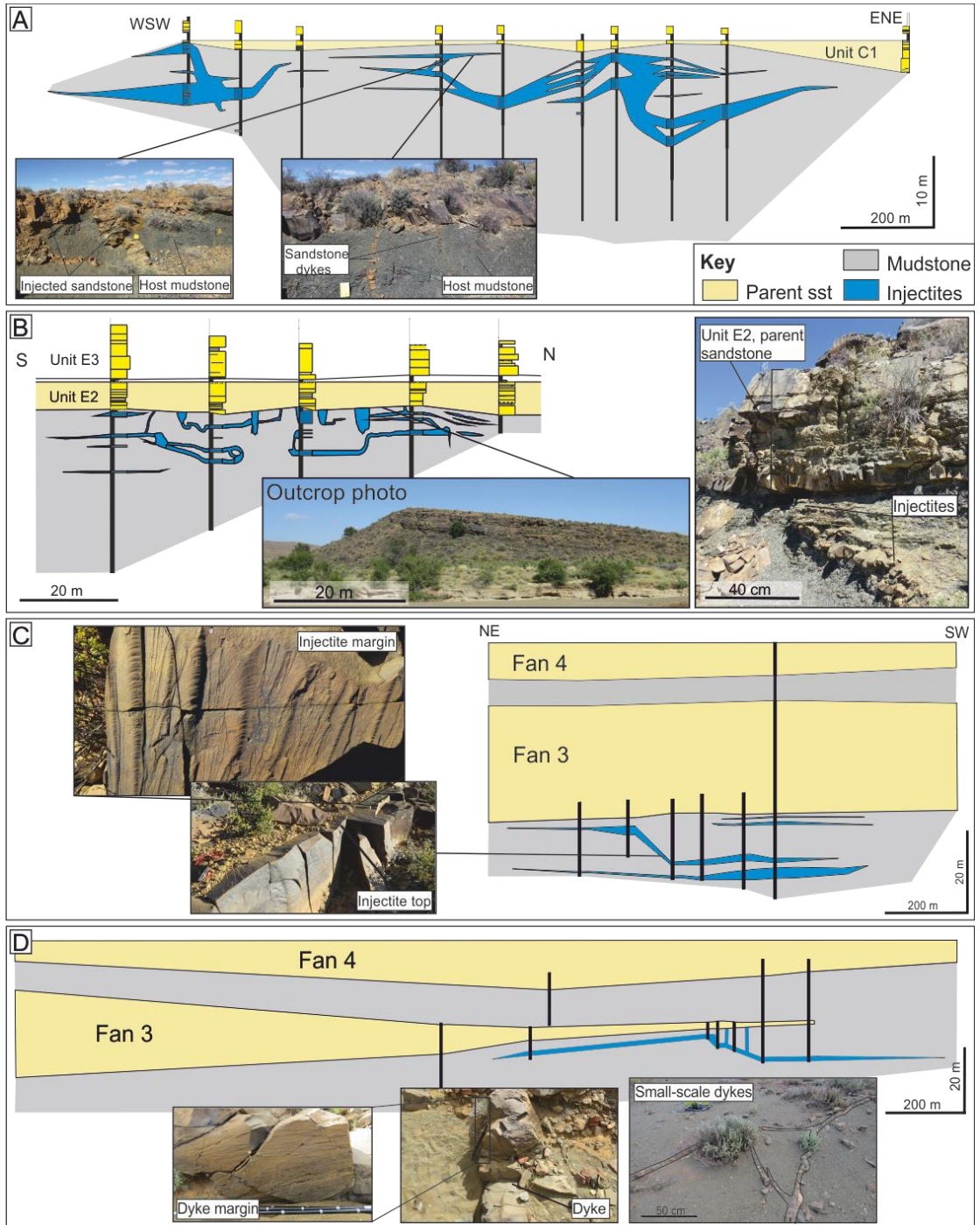


Figure 7.2 Outcrop panels used in forward seismic modelling with examples of outcrop expression of injectites. A) Zoutkloof. B) Geelbeck. C) Bizansgat East. D) Bizansgat West. For detailed sedimentary logs see Appendix B.

7.3.2. Synthetic seismic

Synthetic seismic sections of the outcrop panels and individual injectite geometries were created in the software RokDoc (Ikon Science). Before being entered into the program, architecture outcrop panels were scaled up by a factor of 4. This more closely represents the thicknesses and lateral extent of sands mapped within the Lower Lista Formation in Chapter 6, whilst maintaining the geometries and architectures accurate to the outcrop.

Initial work in RokDoc created “perfect seismic” images of published injectite geometries in order to experiment with the parameters and limitations of the program. Completely homogenous shale and sandstone bodies were used, “typical” subsurface rock properties were used (Chapter 6) and a Ricker wavelet of 50 Hz (Fig. 7.3). Several test forward seismic models were then produced of the outcrop panels, using a range of different physical rock properties and wavelet frequencies. Sand units within the synthetic seismic models were assigned homogeneous rock properties taken from well logs A and B (taken from the case study in Chapter 6) (Fig. 7.4). Test models used completely homogeneous sand and shale with wavelet frequencies between 25 and 50 Hz (Fig. 7.5). In order to i) create realistic layering within the host shales and, ii) attribute identical shale rock properties to the outcrop panels from the subsurface, two wells provided real background layering (stratification), and were selected on the basis that they contained a high proportion of shale. The well logs in Figure 7.4 demonstrate layering applied to the shale units within the model; the distribution of well logs throughout the model are shown as black vertical lines in Figure 7.4. The result of background layering applied to each model is demonstrated in the acoustic impedance log (Fig. 7.4). For each model, well logs were spaced to ensure continuous horizontal layering of the shales around, and between, the complicated geometries of the injectites (e.g. Fig. 7.6). Where sandstone intersects the well logs, the bodies were given homogeneous properties to reflect the typically structureless sandstones observed at outcrop; the well log data in these particular bodies were not used. Acoustic impedance profiles illustrate the stratigraphic variability and layering within the shale in comparison to structureless sandstone bodies (Fig. 7.4C). The advantage of using well logs to provide background shale values is that there is a relatively large amount of data within each model, whereas models using one impedance value per facies or unit would display overly simplified acoustic impedance, and therefore produce unrealistic forward seismic models.

Multiple tests were run in an iterative process to determine the best methodology for the final forward seismic model. Variables such as well trace spacing, well log spacing and near and far

angle offsets were explored during the preliminary model building process (Figs. 7.5 and 7.6). A Ricker wavelet of 25 Hz, and a zero angle offset produced a best match to the seismic data mapped in Chapter 6 and were therefore chosen for this study. The resultant synthetic seismic is displayed with a peak (blue reflection) that represents a downward increase in acoustic impedance and a trough (red reflection) that represents a downward decrease in acoustic impedance (Fig. 7.8).

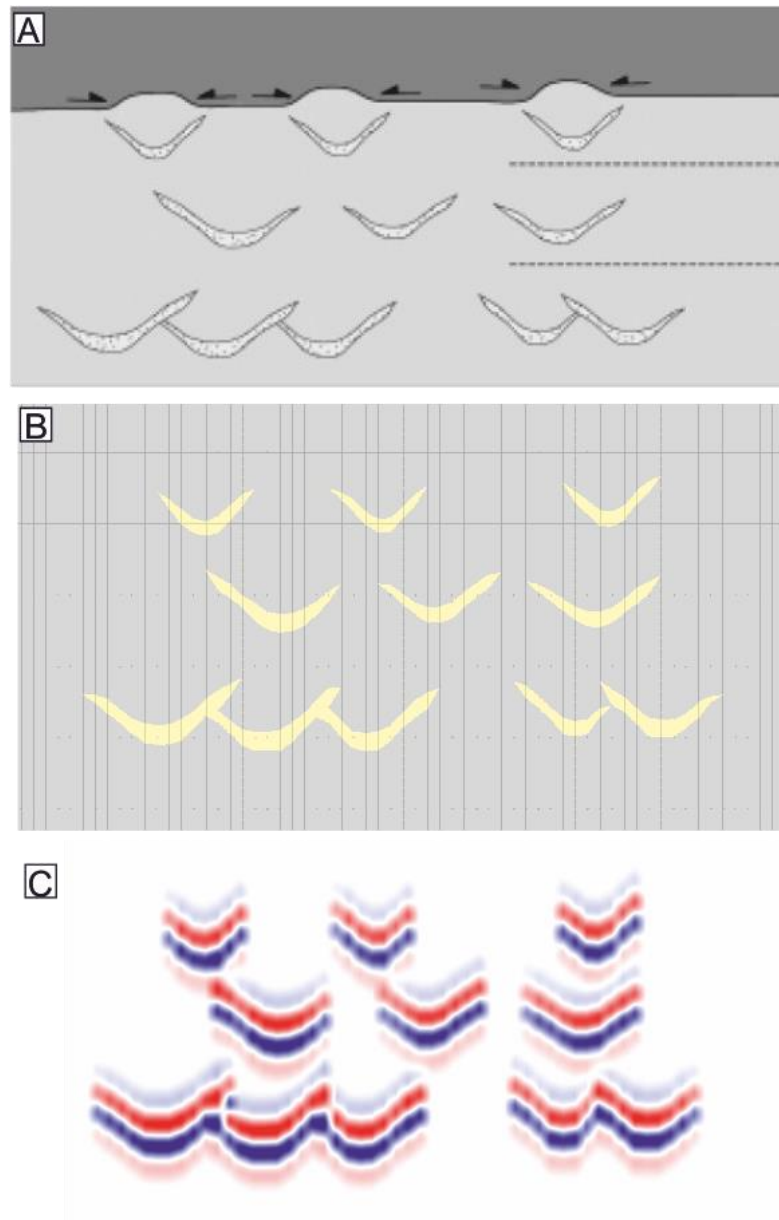


Figure 7.3 Initial test model of simple injectite geometries. A) Several conical sandstone intrusions surrounded by host mudstone (Cartwright *et al.*, 2010). B) Input as bodies in RokDoc. C) Seismic expression at 50Hz Ricker wavelet with homogenous sand and background shale.

Limitations

As with any modelling, there are several limitations that should be considered. Injectite geometries are limited and simplified by the trace separation; a denser population of traces adds resolution. Here, a trace separation of 12.5 m was utilised to best match the resolution of sand bodies mapped in Chapter 6. The thicknesses of sand bodies may also be overestimated due to vertical exaggeration. Additionally, vertical bodies such as dykes cannot be drawn in RokDoc, only high angled surfaces.

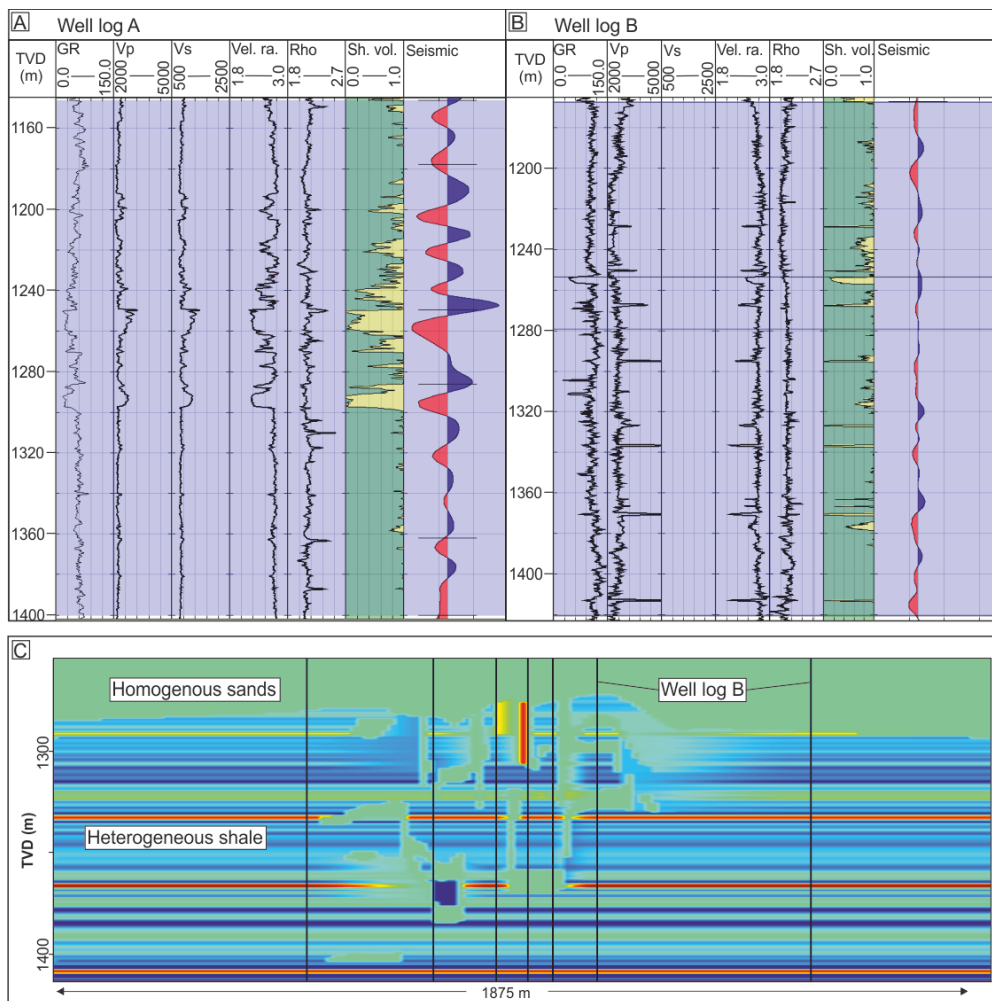


Figure 7.4 A) and B) Well logs A and B used in forward modelling, these are taken from the seismic case study in Chapter 6. True vertical depth (TVD) depth in m. Logs display Gamma Ray (GR), P-wave velocity (Vp), S-wave velocity (Vs), ratio between P- and S-waves (Vel. ra.), density (Rho), shale volume (Sh. vol.) and seismic response (Seismic). Both A and B display the entire Lista Formation at the locality of the well logs. In well log A, the Lower Lista Formation contains minor sand-prone units, whereas well log B has minimal sand throughout. C) Acoustic impedance image of the panel in RokDoc, displaying the complexity of layering within the host shales compared to the homogeneity of both parent and injected sandstone.

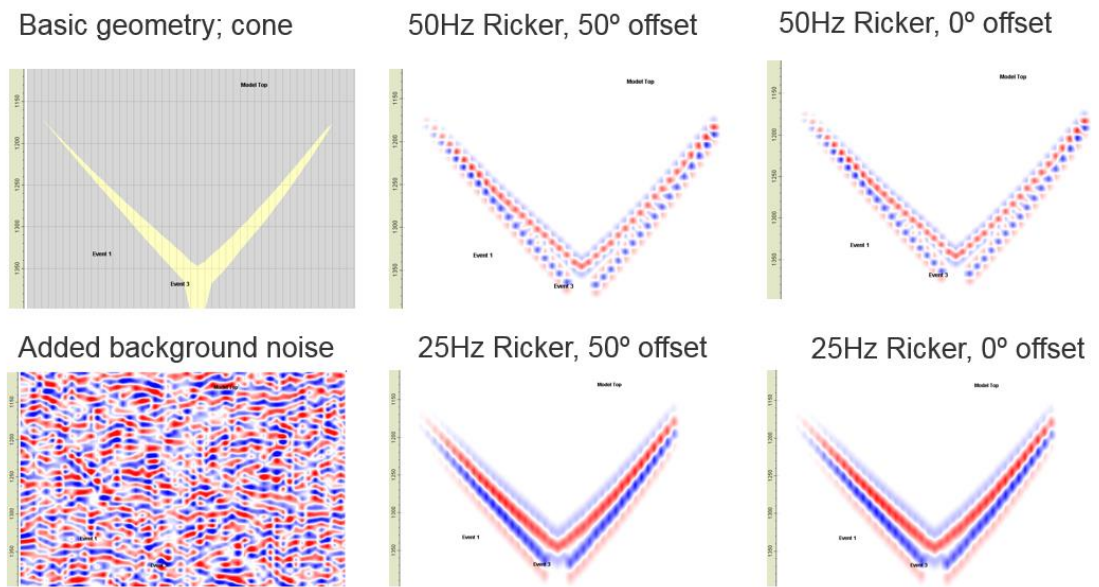


Figure 7.5 Same input: V-shaped cone fed by dyke, but varying the wavelet frequency and angle of offset.

Type	Constant Value
GR	43.5
Vp	2340
Vs	939
Rho	2.1
Por	0.3
Quartz	0.8
Shale	0.2

Table 7.1 Final values used for sandstone when modelling in RokDoc. Values were taken from a brine filled sand in well 9/11A-6.

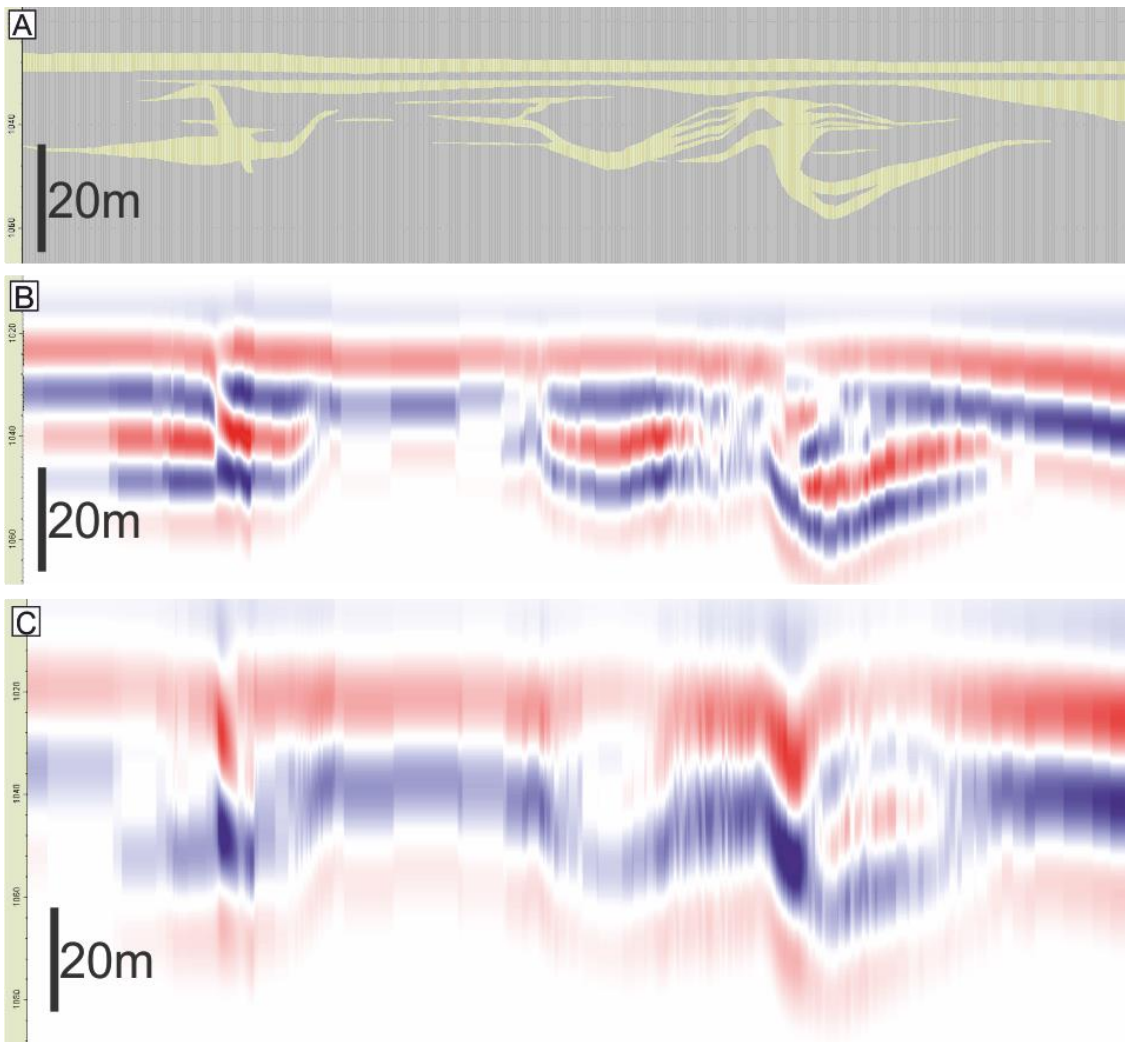


Figure 7.6 Initial models of outcrop panel Zoutkloof in RokDoc. A) Original outcrop panel input at 4 times vertical exaggeration. B) Seismic response at 50 Hz Ricker wavelet with 50° offset. C) Seismic response at 25 Hz Ricker wavelet with 50° offset. Scales refer to outcrop scaling.

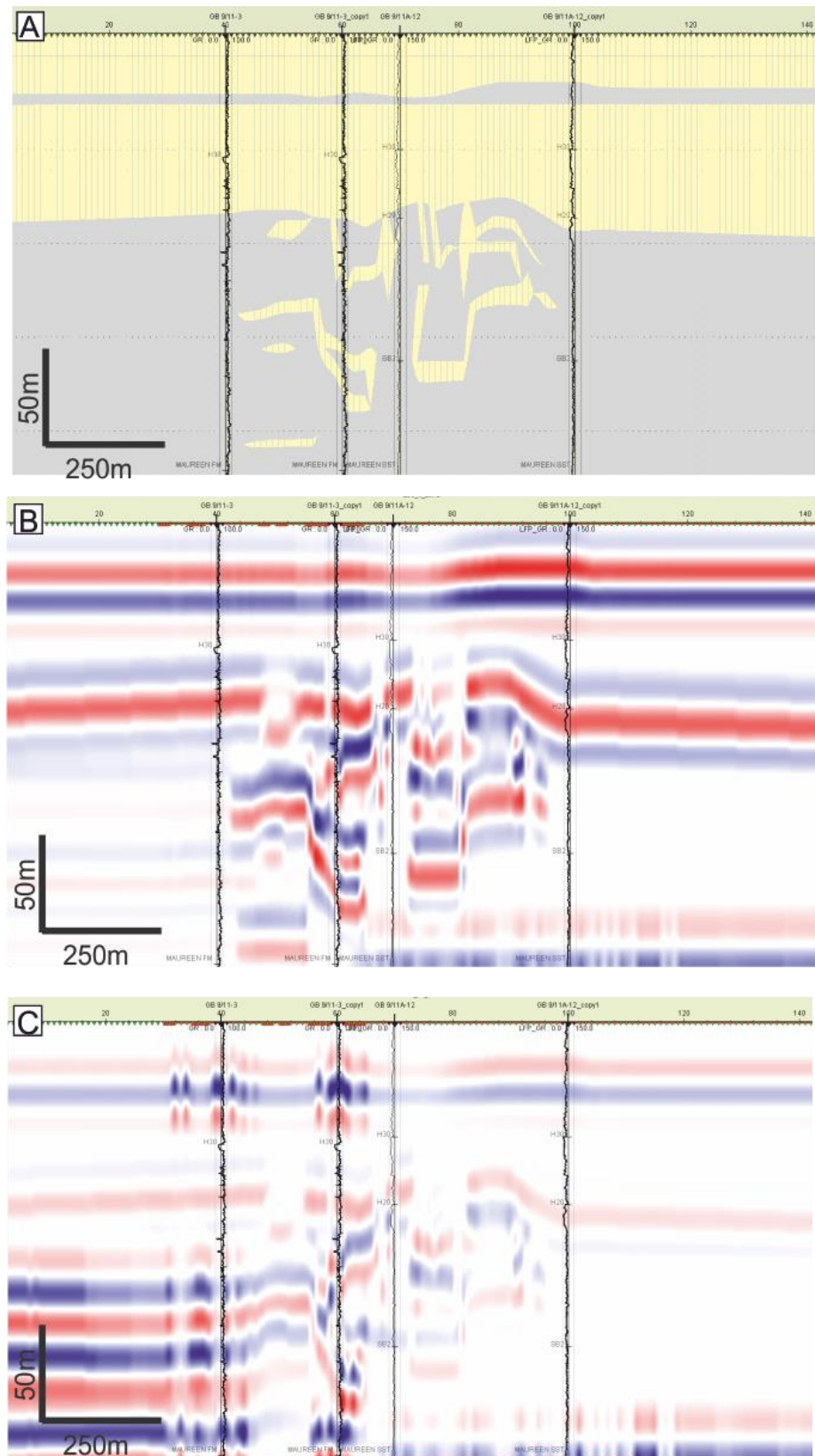


Figure 7.7 Initial models of outcrop panel Geelbeck in RokDoc. A) Original outcrop panel input at 4 times vertical exaggeration. B) Seismic response at 25 Hz Ricker wavelet with 0° offset. C) Seismic response at 25 Hz Ricker wavelet with 50° offset.

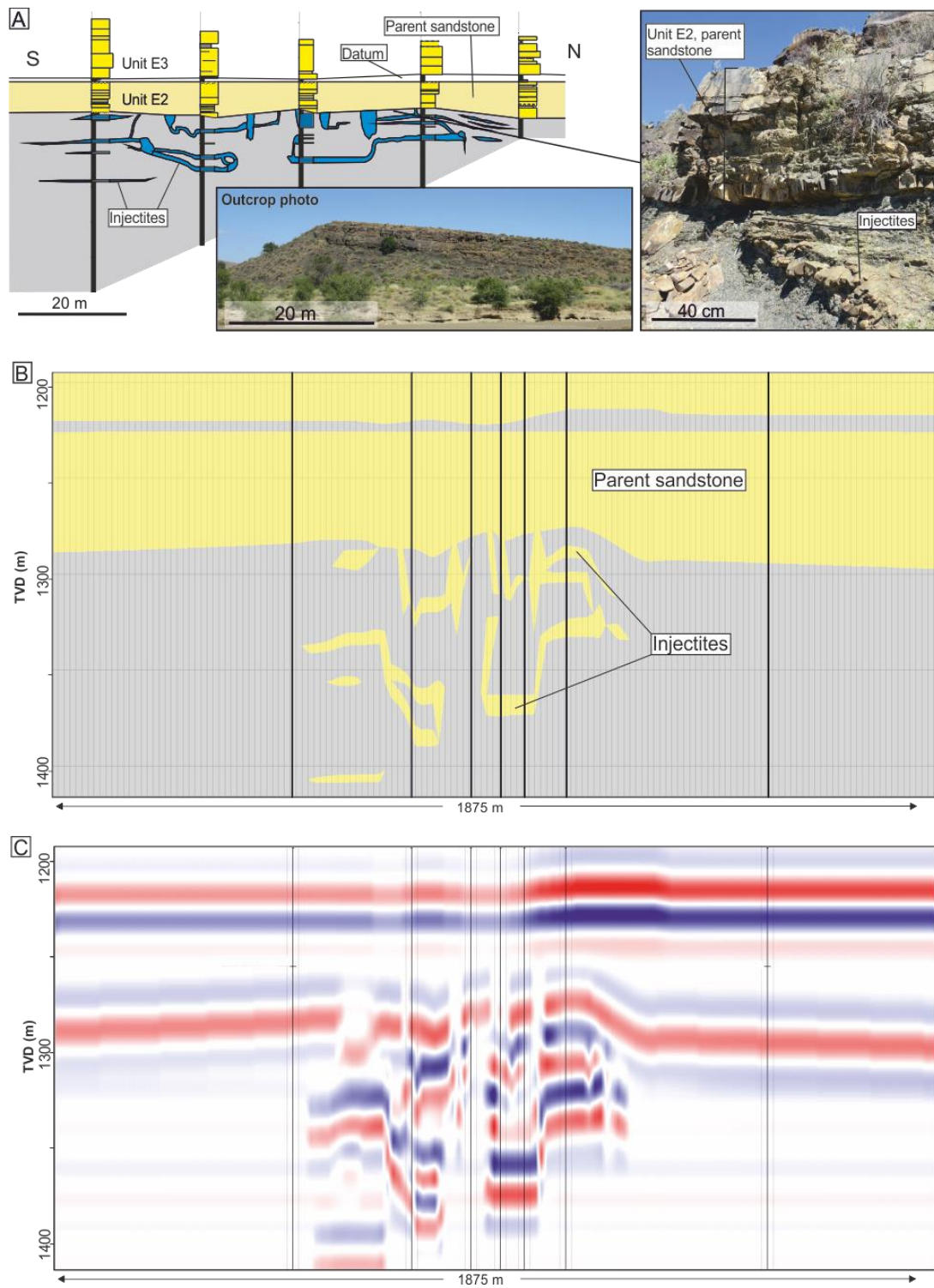


Figure 7.8 Outcrop to RokDoc synthetic seismic workflow. A) Correlation panel of Unit E and associated injectites. (B) Panel in RokDoc at 4 x vertical exaggeration, well logs (vertical black lines), background mudstone (grey) and sandstone (yellow). C) Synthetic seismic section. Seismic is displayed with a peak (blue reflection) representing a downward increase in acoustic impedance and a trough (red reflection) representing a downward decrease in acoustic impedance.

7.4. Results and analysis

7.4.1. Injectite morphologies

Seismic forward modelling captured six different injectite morphotypes identified at outcrop. These are: Morphotype 1: Low-angled bowl, Morphotype 2: Anastomosed injectite, Morphotype 3: Abrupt step, Morphotype 4: Bifurcated injectite, Morphotype 5: Connecting vertical injectites, commonly connecting two sills, and Morphotype 6: Composite intra-bowl injectites. The following descriptions are depicted in Figures 7.9 and 7.10 (equivalent outcrop expression and as forward modelled seismic). All the outcrop examples are displayed at a scaled up factor of 4, and the upscaled outcrop and seismic images are all 4 x vertically exaggerated. Due to the resolution of both the RokDoc inputs and the seismic response, thin, individual injectites were not imaged in the synthetic seismic created. All of the panels show both shallow- and steeply-dipping injectites.

Morphotype 1 – Low-angled bowl

The low-angled bowl morphotype is commonly reported in seismic data, and is widely described as a conical intrusion (Molyneux, 2002; Huuse *et al.*, 2005a; Cartwright *et al.*, 2008; Huuse, 2008) up to several 100's m in height. In planform, these features form circular or elliptical shapes. At outcrop the bowl is formed of a sill or series of sills stepping up stratigraphy laterally outwards (Fig. 7.9).

Morphotype 2 – Anastomosed injectite

In seismic data, the anastomosed injectite morphotype forms an apparent loop or circle of sand in section that encompasses host lithology (Fig. 7.9). At outcrop, a single sill splits, or diverges laterally for some distance, before merging to become a single body of sand again (Fig. 7.9).

Morphotype 3 – Abrupt step

In seismic data, an abrupt step is imaged as a near vertical dyke that abruptly shallows to form a sill. The step may be several metres to 10's m in height (Fig. 7.9). At outcrop, this is a simple step, forming a ramp between two sills (Fig. 7.9).

Morphotype 4 – Bifurcated injectite

In seismic data, bifurcated injectite morphotypes appear as a single, low-angled dyke or sill that splits into 2 or more discrete bodies. Commonly, one body may display a brighter reflection (e.g. Fig. 7.9). At outcrop, a sill splits into two, where the lower body will continue along the same stratigraphic height and the upper body of sand cuts up through stratigraphy before shallowing off to run parallel to the lower sill.

Morphotype 5 – Connecting vertical injectites

In seismic data sets, steep dykes are usually “invisible” (Jackson *et al.*, 2011), this is generally true for dykes $>60^\circ$ in dip (Fig. 7.9; Type 5). At outcrop this can either be a single vertical dyke or a network of variously angled smaller dykes connecting two bodies of sandstone.

Morphotype 6 - Composite intra-bowl injectites

Within a bowl structure up to 600 m in diameter, whether flat based or cone-shaped, seismic often displays chaotic reflections, with the base of the bowl being a single solid reflection. At outcrop this type of geometry is formed where the “base of bowl” is a single sill stepping upwards and outwards (Fig. 7.6), with relatively small steps compared to the lateral extent of the sill. The chaotic centre is likely formed by a network of sub-seismic scale dykes and sills, for instance the outcrop example in Figure 7.7A is formed of a series of sills, all of similar thicknesses (10-20 cm) connected by dykes <5 cm thick.

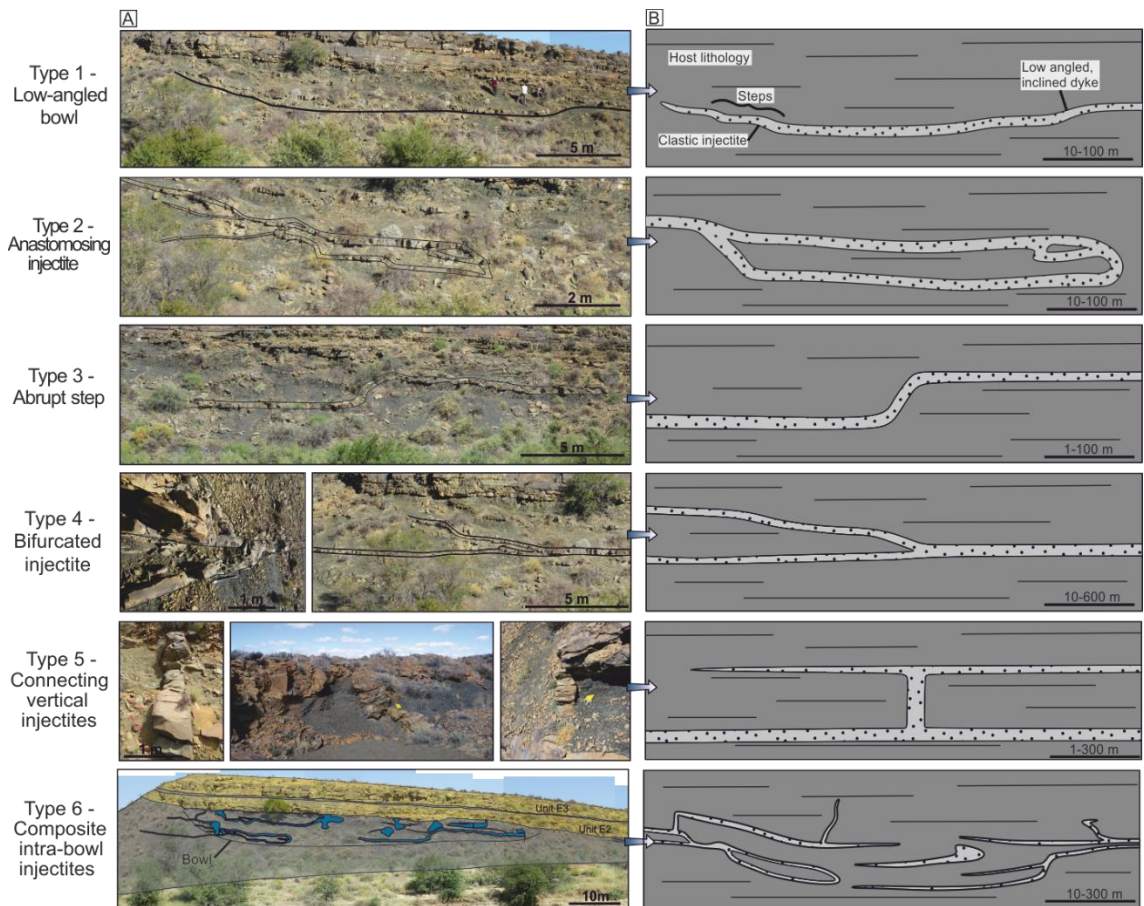


Figure 7.9 Recognised injectite geometry types 1-6. A) Outcrop examples (Morphotype 5 examples not from Unit E). B) Schematic drawing. Morphotype 1: Low-angled bowl, Morphotype 2: Anastomosed injectite, Morphotype 3: Abrupt step, Morphotype 4: Bifurcated injectite, Morphotype 5: Connecting vertical injectites, commonly connecting two sills, and Morphotype 6: Composite intra-bowl injectites.

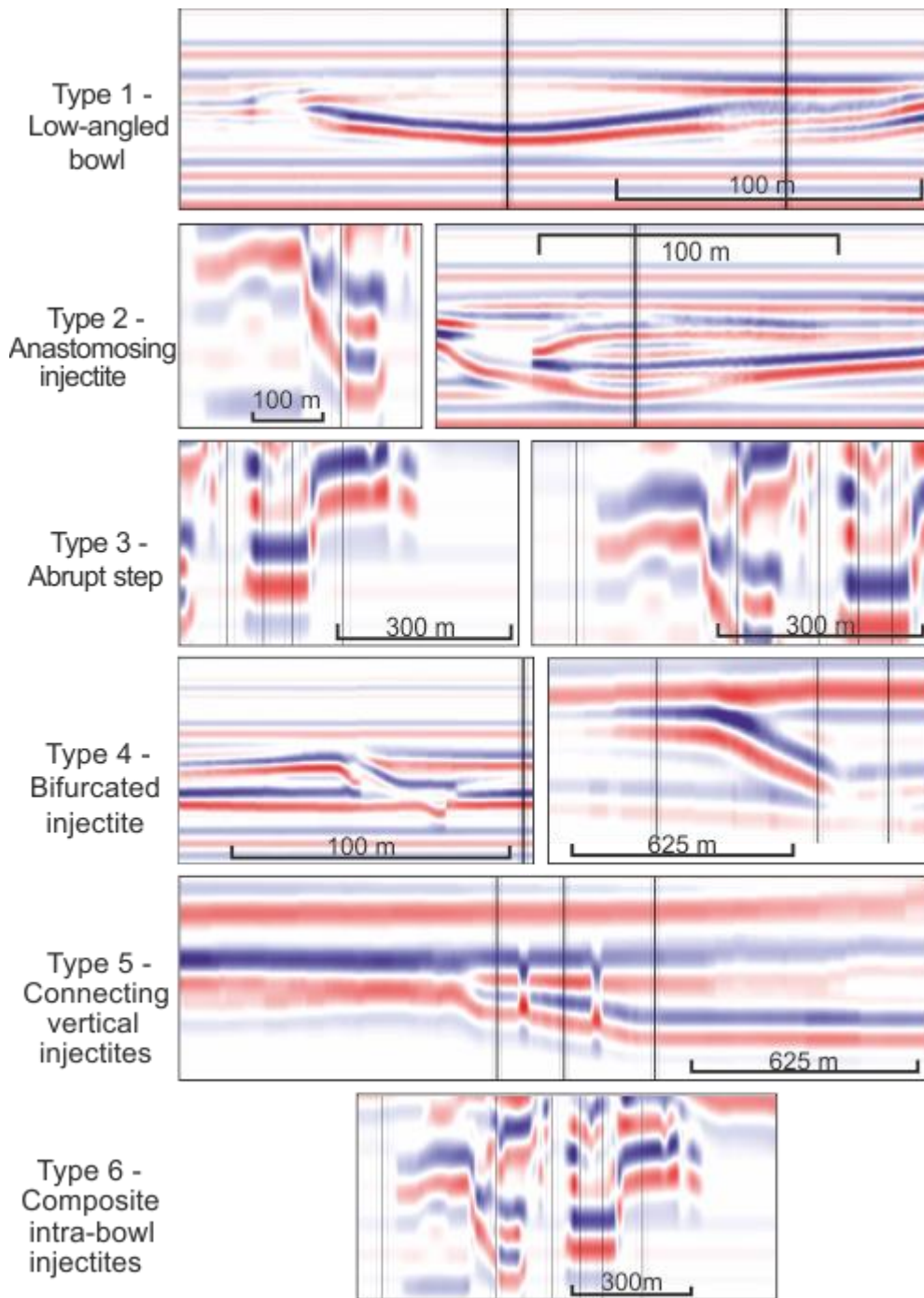


Figure 7.10 Recognised injectite morphotypes 1-6 in synthetic seismic. Seismic is displayed with a peak (blue reflection) representing a downward increase in acoustic impedance and a trough (red reflection) representing a downward decrease in acoustic impedance.

7.5. Discussion

7.5.1. Scale invariance and clastic injectites

Sand(stone) injectites have been reported on scales ranging from mm in length and thickness (Goodall *et al.*, 1999; Duranti *et al.*, 2002; Hurst *et al.*, 2011) to 10s m thick and laterally extensive for kms (Huuse *et al.*, 2004; Hurst *et al.*, 2005, 2011; Hubbard *et al.*, 2007; Cartwright, 2010).

Here the scale invariance of sand(stone) injections in sedimentary basins is assessed. Research on intrusion dynamics has focussed primarily on igneous systems (McCaffrey and Petford, 1997; Thomson, 2007; Thomson and Schofield, 2008; Schofield *et al.*, 2012a; Magee *et al.*, 2015). However, similar geometries observed in both igneous and sedimentary intrusions suggest that emplacement mechanisms are comparable and controlled by the same external parameters (Cartwright *et al.*, 2008; Polteau *et al.*, 2008; Mourgues *et al.*, 2012). Properties of host lithology that affect intrusion morphology during emplacement include the propensity for brittle behaviour versus non-brittle (Schofield *et al.*, 2012a), the homogeneity of the host strata (Jolly and Lonergan, 2002), and the principle stress orientation (Jolly and Lonergan, 2002; Rowe *et al.*, 2002). As it is primarily the host lithology that controls final intrusion architecture, research and literature for scale invariance within igneous intrusions are utilised here.

Scale invariance over several orders of magnitude is recognised in igneous intrusions. One example is 'broken bridges', a distinctive morphology within igneous intrusions that has been well documented from cms up to several metres at outcrops (Nicholson and Pollard, 1985; Bussel, 1989). Schofield *et al.* (2012b) recognised that broken bridges developed between elongate magma lobes in the Faroe-Shetland Basin on a seismic scale of at least 10's of metres in height and laterally extensive over several kms. Field data have also been used to test dimensional scaling and mechanical models, where a range of power-law scaling relationships for different types of intrusive structures can predict geometry for laccoliths and thickness-to-length relationships for mafic sills (Cruden and Bungler, 2010) implying scale invariance.

Experimental modelling also uses the underlying principle of scale invariance, where the use of dimensionless numbers demonstrates geometric and kinematic similarities between model and its natural prototype. This was first recognised by Hubbert (1937), and since then the principles of dimensional analysis of scaling have been used in many experiments replicating natural geological processes (Hubbert, 1951; Hubbert and Willis, 1957; Mourgues and Cobbold, 2003;

Kavanagh *et al.*, 2006; Rodrigues *et al.*, 2009; Gressier *et al.*, 2010). For clastic injectites specifically, Rodrigues *et al.* (2009) and Mourgues *et al.* (2012) both successfully recreated injectite geometries comparable to those in nature that can be up to several kms in size (Vigorito and Hurst, 2010), yet experimentally may only be several cms. These experiments support injectite morphologies being scale invariant where outside factors, such as host rock lithology, fluid pressure, and principle stress orientation, are at a scaled equivalent both geometrically and kinematically (Rodrigues *et al.*, 2009; Mourgues *et al.*, 2012).

The apparent scale invariance of clastic injectites permits outcrop-scale data to be upscaled and applied to seismic-scale interpretation. Therefore, the injectite morphotypes forward modelled from outcrop can be used to aid recognition of injectites in reflection seismic data. Previously, the use of outcrop studies of injectites as analogues for subsurface examples has been limited to cases where the outcrop itself is of seismic scale, an approach that limits the range of usable analogues (Surlyk and Noe-Nygaard, 2001; Vigorito *et al.*, 2008; Scott *et al.*, 2009, 2013; Vigorito and Hurst, 2010). This study suggests that injectite geometries and architectures seen at both outcrop and seismic scale can be highly comparable through applying scale invariance.

7.5.2. Implications for hydrocarbon exploration

Subsurface remobilisation and injection of sand has significant consequences on reservoir architecture, geometry, and porosity and permeability, which impacts hydrocarbon recovery. The types of injectite architecture identified in forward seismic models presented herein can be used to aid identification of injectites for more accurate mapping during seismic interpretation. The simplification of injectite geometries and features in forward seismic modelling has suggested that there is likely more complexity to those sand bodies than can be observed in the reflection seismic data. Therefore a larger volume of sub-seismic injectites, and hence greater volume of sand and connectivity, is likely present than would be predicted from seismic data alone.

7.6. Conclusions

Outcrops from the Karoo Basin, South Africa show 2D geometries of clastic injectites from mm- to metre-scale. Six different injectite morphotypes were identified: Morphotype 1: Low-angled bowl, Morphotype 2: Anastomosed injectite, Morphotype 3: Abrupt step, Morphotype 4:

Bifurcated injectite, Morphotype 5: Connecting vertical injectites, commonly connecting two sills, and Morphotype 6: Composite intra-bowl injectites. The identification of distinct geometries of sandstone injectites seen across experimental modelling, igneous intrusions and seismic suggests scale invariance, which permits the outcrop data to be run through forward seismic modelling software using rock properties from a North Sea case study (Chapter 6). This study helps to bridge the gap between outcrop and seismic data of clastic injectites (Figs. 7.9 and 7.10); the detail acquired at outcrop can be applied to subsurface data and the 3Dimensional injectite geometries mapped in seismic can be applied to inform the 2-dimensional outcrop data. The injectite morphotypes forward modelled from outcrop can be used to aid recognition of injectites in seismic (Fig. 7.9).

8. Injecting life into the deep biosphere: a new macrofaunal limit

8.1. Introduction

The deep-sea infauna is one of the most elusive branches of life on Earth; little is known about the modern deep-sea floor environment, and less about the ancient. The limits of the macrofaunal biosphere in the deep-sea, and factors controlling life at depth below the seabed, are generally unknown. It is technologically challenging to collect undisturbed modern samples even as deep as 20 cm below the subsurface, and ancient examples are limited by preservation factors with poor constraint on the original depth. In the modern, burrowing animals are usually found in marine sediments down to 20 cm (Jumars, 1978), very rarely being documented down as far as 2 m (Weaver and Schultheiss, 1983). The primary way to study these deep zones of macrofaunal life is to examine the ichnological record in rocks. One difficulty that arises when using modern analogues for ancient environments is that one or both may be biased through the data available, ease of sampling etc. Modern deep-sea biological studies target clays and silts as these are simpler to sample. Standard sampling methodologies such as giant piston coring are typically unable to sample sandy sediments due to lack of cohesion of the grains. In contrast, the rock record demonstrates a preference for bioturbation in coarser, sandy sediments.

We have studied exhumed, ancient networks of clastic intrusions (injectites) produced by the injection of overpressured sand into surrounding strata (Jolly and Lonergan, 2002). For injectites to occur, an unconsolidated body of clastic material must be sealed by an impermeable barrier, allowing pore pressure within to increase through burial, becoming higher than that of surrounding strata (Lorenz *et al.*, 1991; Cosgrove, 2001; Jolly and Lonergan 2002). The injected sand dykes (vertical to sub vertical) and sills (horizontal) presented here, show evidence for post injection living traces of macrofauna along their surfaces. Previously, injectites have been described as favourable sites for colonisation of microbial life because they are highly permeable and provide a large sand-to-mud interface allowing for readily available electron donors and nutrients (Parnell *et al.*, 2013). Here, for the first time, we demonstrate that macrofauna lived in injectites deep below the seabed.

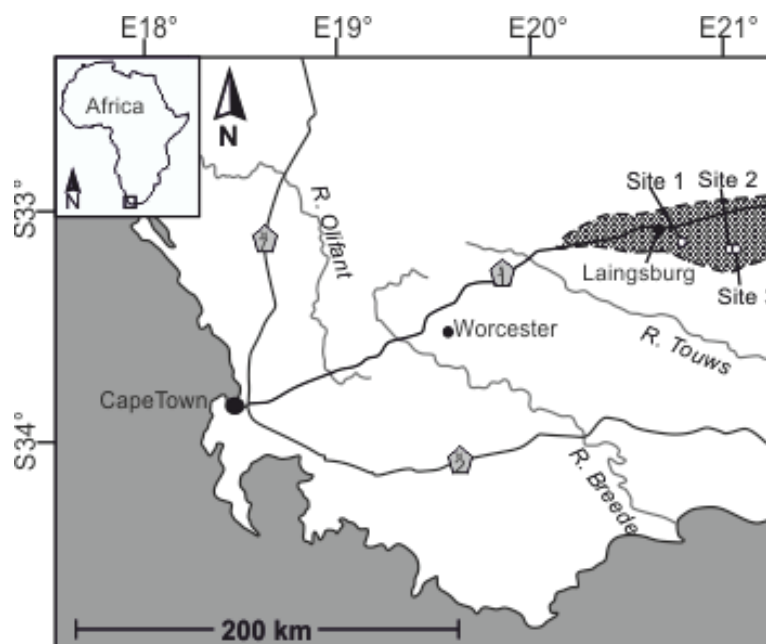


Figure 8.1 Location map of Laingsburg depocentre and outcrop sites 1-3, South Africa. Site 1 = Unit E, Geelbeck, Site 2 = Unit D, Slagtersfontein West, Site 3 = Unit D, Slagtersfontein East.

8.2. Geological setting

The Permian Ecca Group, a succession of siliciclastic material, was deposited within the Tanqua and Laingsburg depocentres of the SW Karoo Basin (Flint *et al.*, 2011). The Laingsburg depocentre (Fig. 8.1) comprises a shallowing upward stratigraphic succession. This study focuses on outcrops of the Fort Brown Formation; a 400 m thick submarine slope succession (Di Celma *et al.*, 2011; Flint *et al.*, 2011) (Fig. 8.2). The Fort Brown Formation comprises sand-prone lithostratigraphic units C to G, which are subdivided into subunits by laterally extensively thin (<2 m thick) fine siltstones consistent with palaeogeographic changes across a unit (Figueiredo *et al.*, 2010; Van der Merwe *et al.*, 2014). Each unit is separated by a thick regionally extensive mudstone (siltstone and claystone) (>10 m thick) interpreted to represent a basin-wide shutdown in sand supply (Di Celma *et al.*, 2011; Flint *et al.*, 2011).

Bioturbation has been documented throughout the Fort Brown Formation (Morris *et al.*, 2014a; Spychala *et al.*, 2015). Small burrows occur within mudstone beds that separate sand beds (Morris *et al.*, 2014a), in thin-bedded siltstones (Spychala *et al.*, 2015) and on the base of structureless and rippled sandstones (Morris *et al.*, 2014b). Ichnofacies assemblages are interpreted to be primarily *Chondrites* and *Planolites* (Morris *et al.*, 2014b).

Individual outcrop sites are indicated by place names and stratal units (Figs. 8.1 and 8.2). At each site, the units are submarine lobe deposits (van der Merwe *et al.*, 2014) and comprise thin, very fine sandstones capped by mudstones (Fig. 8.3A and 8.3C). Clastic injectites are recognised through dykes cross-cutting stratigraphy, sills stepping up and down stratigraphy, and their sharp sided nature on top and base margins (Hurst *et al.*, 2011; Cobain *et al.*, 2015). In the Karoo Basin, injectites are mostly sourced from the base of the very fine sandstone units, they are up to 50 cm thick, sharp sided, and usually subvertical below the source sand. At sites 1, 2 and 3 this is 8 m, 1.5 m and 3 m compacted depths respectively. The same trace fossils present on the base of depositional units (Fig. 8.3) are also observed on the margins of clastic injectites down to their lowermost occurrence.

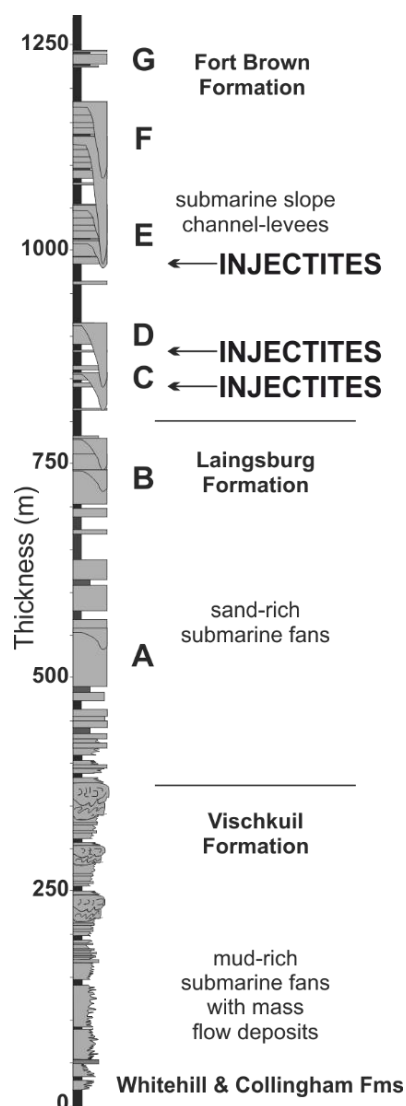


Figure 8.2 Summary stratigraphic log of Laingsburg depocentre, letters A-G refer to Units A-G (Flint *et al.*, 2011).

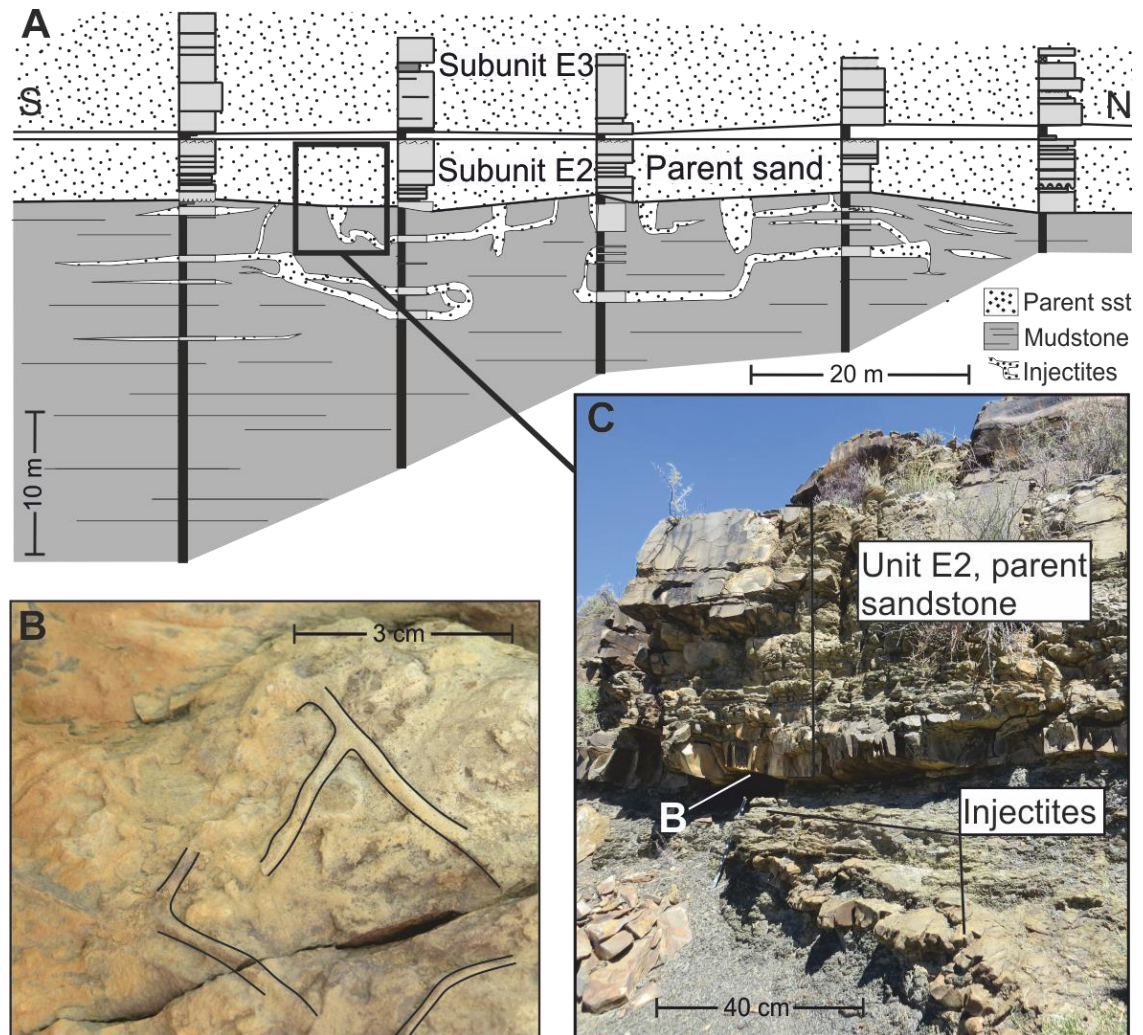


Figure 8.3 A) A representative cross-section panel for outcrop sites with several stratigraphic logs taken from South to North (See Appendix A.4 for detailed panel and logs and B.4 for data collected). Here, Unit E at Geelbeck (Site 1) displays source sand with underlying sand injections. Vertical to subvertical injectites are dykes, horizontal injectites are sills (see arrows). Detailed individual logs are in Appendix A. B) Example of typical bioturbation seen on the base of Unit E2 (see C). C) Outcrop photograph demonstrating how source sand connects to and feeds injectites, intruded into mudstone.

8.3. Outcrop observations

8.3.1. Site 1: Unit E, Geelbeck

At Geelbeck, subunit E1 is absent, subunit E2 is an intraslope lobe complex comprising three stacked lobe deposits, the lowermost of which was deposited in a highly confined environment

(Spychala *et al.*, 2015). The base of Subunit E2 is very well exposed, and therefore so are examples of *Planolites* (Fig 8.3B); individual borrows are up to 10 cm long and < 1 cm in width. The basal bed of Subunit E2 in which they occur is mainly structureless sandstone with ripples present towards the top with a weakly erosive base.

The dykes directly in contact with the base of subunit E2 form an abruptly downward tapering cone ~1 m in width and 1.5 m in depth (Fig. 8.3C). Each cone-like feature comprises multiple dykes passing into a single dyke 5-20 cm wide that feeds multiple sills and dykes below. Sills do not step through stratigraphy and individually do not extend for >20 m. On the margins of the clastic injectites, the same trace fossil, *Planolites*, is present that occurs on the base of Subunit E2 (Fig. 8.4A-7.4D). Additionally, on a subvertical dyke ~2 m below the base of subunit E2 are dewatering structures (*Aristophycus*) (Fig. 8.4A), that are overprinted by *Planolites*. The bioturbation is present on tops and bases of sills and on the margins of dykes and is observed up to 8 m (compacted thickness) stratigraphically below Subunit E2, which is the extent of the injectites.

8.3.2. Site 2: Unit D, Slagtersfontein West

Unit D at Slagtersfontein West is the lowermost sequence, Subunit D1, and is interpreted to be lowstand lobe deposits (Van der Merwe *et al.*, 2014) similar in character to those described by Pr elat and Hodgson (2013) and has been subject to post-depositional remobilisation forming small clastic injectites.

D1 has a sharp, laterally extensive contact with the underlying mudstone unit and comprises structureless sand. Injectites are fed directly from the base of subunit D1 as <40 cm thick dykes, which penetrate up to 2 m into the underlying mudstone (Fig. 8.5B). The margins of these dykes exhibit randomly orientated, and up to 20 cm long, *Planolites* (Fig. 8.5B).

8.3.3. Site 3: Unit C, Slagtersfontein East

Here, C2 is the only subunit of Unit C present and is interpreted to be the proximal edge of a lobe complex (Van der Merwe *et al.*, 2014). Locally, the basal surface of subunit C2 cuts into the underlying B/C mudstone with the lower beds consisting of structureless and amalgamated sandstones. *Planolites* is present along the base of subunit C2. Injectites exposed in the Slagtersfontein area are primarily hosted within the regional mudstone separating Units B and

C (Fig. 8.5A). The majority of injectites at the Slagtersfontein outcrop are 0.1–0.6 m thick sills that extend laterally for up to 500 m. These are fed by subvertical dykes directly in contact with the base of subunit C2. *Planolites* is present on the top and base of sills up to 2 m stratigraphically below C2. The burrows are randomly orientated and fairly common across the injectites.

8.3.4. Outcrop summary

In each of the cases presented here, clastic injectites are stratigraphically below the parent sand from which they are fed. Bioturbation is present on the bases of all parent units as well as on the margins of clastic dykes and sills, which inject though up to 8 m vertical stratigraphy (Fig. 8.4).

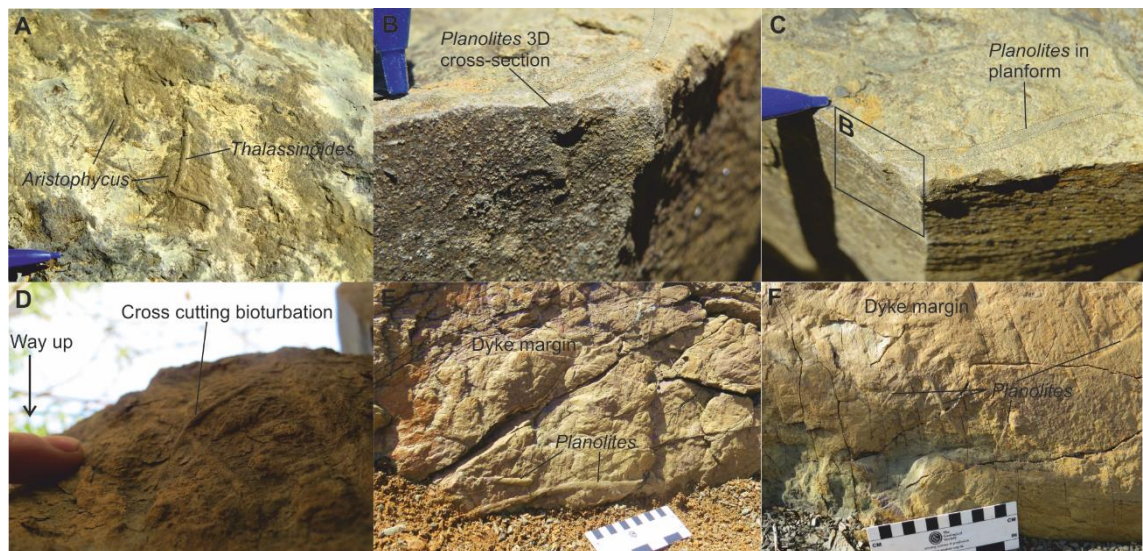


Figure 8.4 Typical examples of bioturbation found on clastic injectite margins. A) Unit E: dewatering structures (*Aristophycus*) on margin of a subvertical injectite, overprinted by *Thalassinoides* bioturbation. B) Unit E: *Planolites* tube protruding in cross-section of sill, planform of tube is outlined on the top margin of the sill. C) view of B) from different perspective. D) Unit E: Cross-cutting *Planolites* on base of sill. E) Unit D: Dyke margin with several examples of bioturbation, largest *Planolites* are indicated. F) Unit C: Dyke margin with several, smaller *Planolites*.

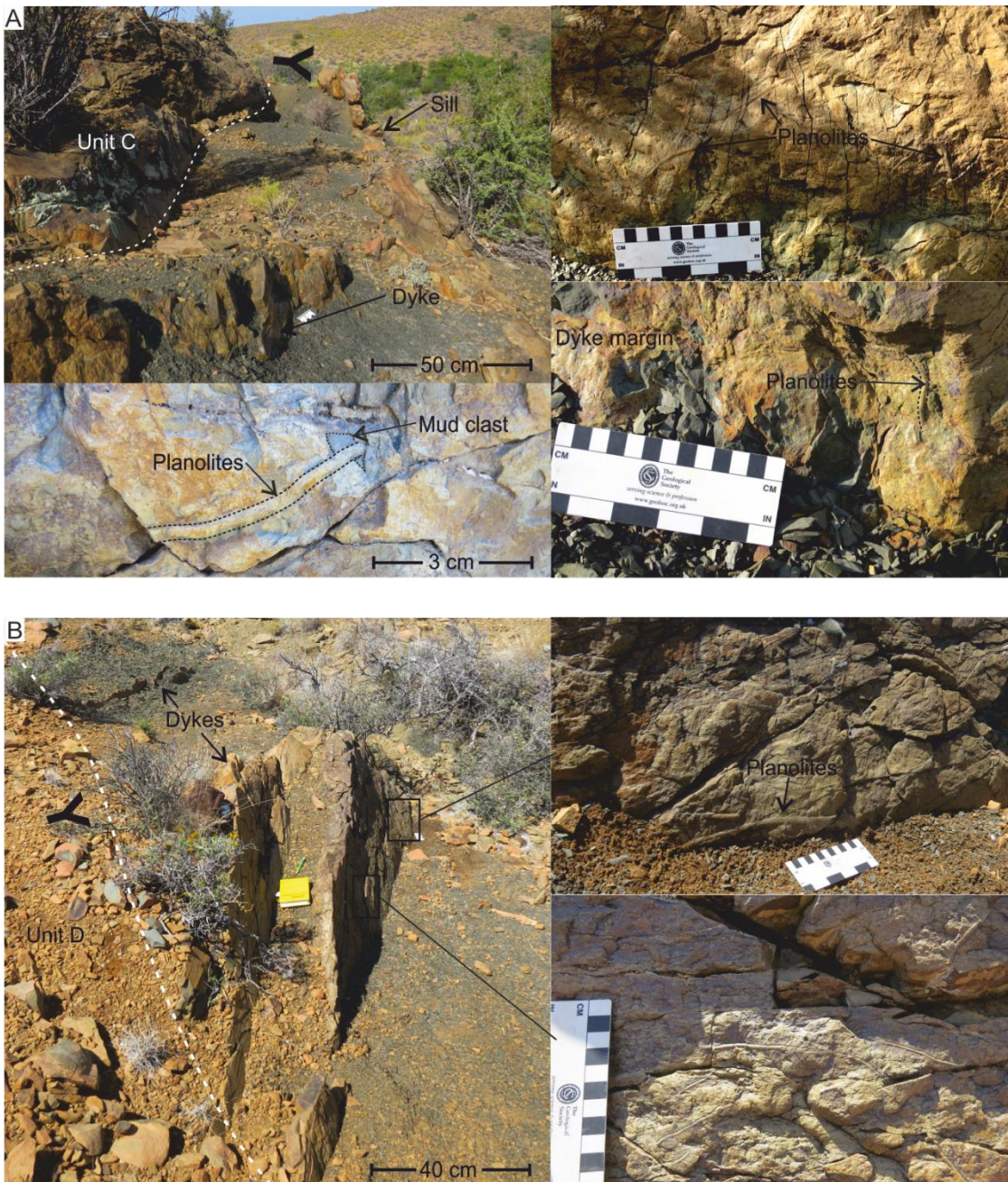


Figure 8.5 Bioturbation examples from injectites related to Units C and D. Detailed, individual logs and panel correlation are in Appendix A.3. A) Unit C, Slagtersfontein East outcrop. “Y” denotes younging direction. Images depict relationship of injectites to base of unit and examples of bioturbation along both dykes and sills. B) Unit D, Slagtersfontein West. Dykes extending from base of Unit and bioturbation examples.

8.4. Interpretation

Up until now, organisms forming *Planolites* and *Thalassinoides* are thought to have mainly lived in the top 20 cm of sediment, rarely attaining maximum depths of 1.5 m (Thomson and Wilson, 1980). Here, we demonstrate the presence of post-injection bioturbation on the margins of clastic injectites up to 8 m below the surface. The structures on injectite margins are interpreted as trace fossils, and not grooves or markings formed through the injection process for several reasons. The branching structure of the *Thalassinoides* traces (Fig. 8.4A) can only be formed through bioturbation processes. Additionally, bioturbation structures show random orientations (Fig. 8.4D and 8.4F), whereas grooves would have a preferential direction caused by flow. It is clear that the bioturbation occurred after the emplacement of clastic injectites as it follows the sand-mud interface on both subvertical and horizontal injectites (Fig 8.4). If bioturbation present on the injectites were simply casts of previously buried burrows then *Planolites* would be expected along sills only, parallel with bed contacts. Traces are also observed on the top and bases of injectites, distinguishing them from seafloor bioturbation, which will only have burrows in full relief on the lower side. In some cases, bioturbation overprints dewatering structures (*Aristophycus*) (Fig. 8.4A), therefore, clastic injection is followed by dewatering and then bioturbation overprinted the dewatering structures. Bioturbation is not observed on injectites elsewhere in the basin-fill that display brittle fracture patterns indicating they occurred after several hundred metres burial (Cobain *et al.*, 2015).

8.5. Discussion

Planolites and *Thalassinoides* formed post-injection emplacement, organisms therefore, exploited this newly deposited sand for the oxygen and the organic matter it provided. In order to produce traces, organisms would need to survive long enough to burrow for hours-to-days. The size of the burrow (4-10 mm in diameter) suggests infaunal invertebrates such as polychaetes. There are 2 possible sources for the injected sand: i) the overlying sand unit that has injected downward, or ii) injectites were sourced from below and hit the palaeosurface. Here, we model the possible survival time of organisms such as polychaetes within an injectite as oxygen and organic matter are depleted through respiration.

8.5.1. Modelling survival times

The concept of doomed pioneers has been examined through laboratory experimentation, this has shown that an organism's biological activity is not severely limited, for up to several days with oxygen being absent. To achieve this, they can switch to an anaerobic mode of metabolism (Thompson and Pritchard, 1969; Swinbanks and Luternauer, 1987). Therefore, at least for a short time, anoxia may not affect the ability of an organism to produce a feeding trace. Using the following equation, we have estimated a conservative lower boundary for the time an organism might survive within an injectite without replenishment of oxygen or POM using:

$$\frac{dO_2}{dt} = -\frac{O_2}{O_{2i}} (SCOC + N \times M_r \times S_x)$$

where: t is time (days), O_2 is the dissolved oxygen at time t (ml / L), O_{2i} is the initial ($t = 0$) dissolved oxygen concentration of the sediment (ml / L), SCOC is the Sediment Community Oxygen Consumption, which accounts for all the bacterial, meiofaunal and macrofaunal metabolic activity (mlO₂/L / day), N is the abundance of polychaetes (number / L), M_r is the metabolic rate of polychaetes (mlO₂ / day), and S_x is the proportion of survival of injected polychaetes (unitless, ratio from 0 - 1). Results show that macrofaunal organisms with a slow metabolism rate would have access to oxygen for up to 270 days post sand body sealing and injection (Fig. 8.6). This is more than sufficient to overpressure the parent sand body, inject, and produce the traces we observe in the Karoo Basin (e.g. traces in Fig. 8.4).

8.5.2. Model assumptions

Several assumptions were made in the building and use of the above equation: i) oxygen will be the main limiting factor for metabolism, as carbon has internal stores. Low levels of oxygen are known to have substantial modifying effects to macrobenthic communities in the deep sea such as in Oxygen Minimum Zones (OMZs) (Levin and Gage, 1998). ii) Pore waters and sediments become homogenised during injection, such that everything is well mixed and any pre-injection structure in fauna or oxygen levels is lost and no re-structuring occurs post injection. iii) There are no external sources of input of oxygen once injection has occurred. The initial oxygen levels, therefore, of the sediment post injection will be the same as those of the ambient overlying waters at the time of turbidity flow deposition. iv) Population dynamics are on too long a time-scale post injection, and so are not considered. v) Rates of oxygen uptake decrease as oxygen concentration decreases due to oxygen losses through the process of diffusion across biological

and chemical surfaces and so oxygen uptake rates are proportional to the current oxygen concentration (scaling term $\frac{O_2}{O_{2i}}$).

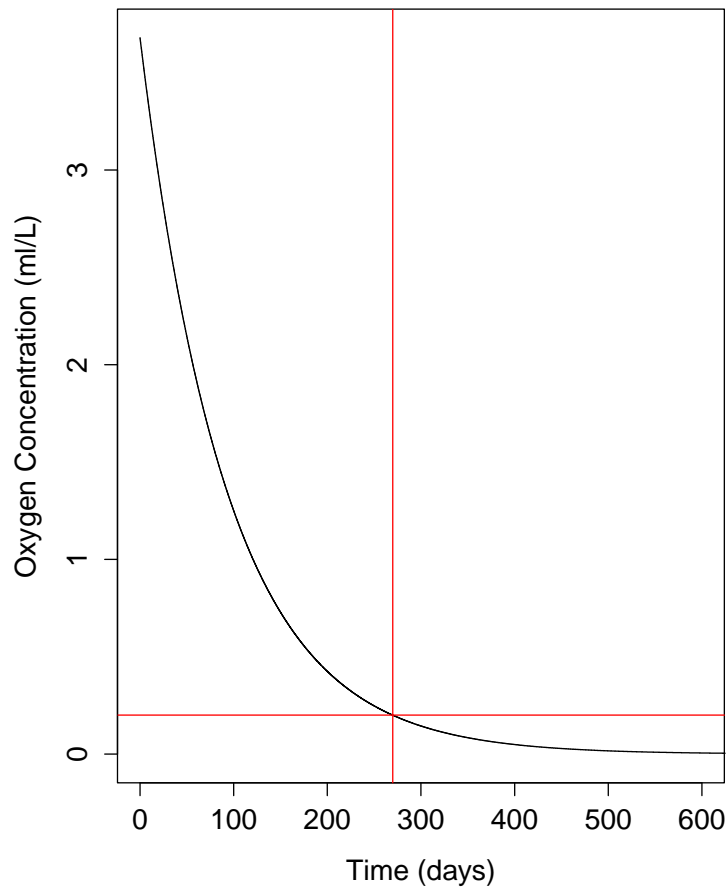


Figure 8.6 Oxygen depletion graph. Rate of oxygen depletion within the sediment starting from the point of burial (and therefore isolation), as calculated from the numerical model. Horizontal red line indicates minimum O_2 needed for survival, vertical red line is the cut off of life in time according to O_2 concentration.

Model Parameterisation

The following section discusses why each of the parameters were chosen in estimating oxygen depletion rates in a newly sealed sand body.

O_{2i}

A review by Levin and Gage (1998) on the effects of oxygen on deep sea sediment communities reports values of 0.2 – 6.21 ml / L from various ocean basins for the concentration of oxygen in waters at the sediment surface in deep sea environments. For a water depth of 740 m, Levin *et al.* (1991) recorded near bottom oxygen concentration values as low as 0.08 ml / L in the eastern Pacific in an oxygen minimum zone (OMZ). Typically, deep water has values near the saturation

value, except for OMZs, with a gradual decrease as they progress further from the site of origin due to metabolic processes, down to 3.6 ml / L in the eastern Pacific (Gage and Tyler, 1991). For the initial oxygen concentration, we used a value of 8 ml / L reflecting relatively well-oxygenated water overlying seafloor sediments. We assume the site is not in an OMZ. To correct for inclusion of sandy sediment in the volumetric space, we assume a porosity (Φ) of 46% such that:

$$O_{2i} = O_{sw} \times \phi$$

This is typical of the sediment injected, fine to very fine sands.

SCOC

All the biologic activity within the sediment is accounted for by the sediment community oxygen consumption (SCOC). This includes macrofauna, however, they typically only account for a small portion of the SCOC, whereas in the model presented, we add in polychaetes. Glud *et al.* (1994) measured values of total oxygen uptake in sediments ranging from 0.0403 – 0.347 mlO₂ / L / day in the south east Atlantic. They suggest these are higher than typical values elsewhere due to high surface productivity. Piepenburg *et al.* (1995) measured median value in sediments east of Svalbard, of 0.0618 mlO₂ / L / day. An average presented by Gage and Tyler (1991) for the north Atlantic and Pacific from depths of between 1 and 2 km is 0.0508 mlO₂ / L / day. Here, we used the median value of 0.0618 mlO₂ / L / day, since this included sampling from sandy sediments, at high latitude, more analogous to the deposits in the Karoo Basin.

N

Gage *et al.* (2002) found an average of 0.39 - 1.724 polychaetes / L depending on the mesh size used to sort sediments from their samples from the Rockall Trough (West of Scotland). Levin *et al.* (1991) found macrofauna abundances of around 1.8 / L. We used a value of 2 worms / L.

M_r

McClain *et al.* (2012) demonstrated that metabolism of deep sea organisms scales in a similar way to shallow water species, where size and temperature account for most of the variability. Mahaut *et al.* (1995) empirically showed that the respiration rates of deep sea organisms (taken from areas of 2 - 4°C) scales with their weight such that:

$$R = 7.4 \times 10^{-3} \times W^{-0.24}$$

where R is the respiration rate (per day) and W is the weight (in mgC) of the organism. We modified this equation to give the respiration rate in units of mlO₂ / day such that:

$$M_r = \frac{1}{0.44} \times 8.4 \times 10^{-3} \times W^{0.76}$$

where $1/0.44$ is the mobilisation of oxygen (in ml) per mg of carbon (taken from Mahaut *et al.* 1995). The weight used was 0.428 mgC, the average size for the deep sea macrofauna used by Mahaut *et al.* (1995) in their study of nematodes, copepods and polychaetes.

S_x

As data were unavailable, a conservative value of 0.5 was used, i.e. only half the population of polychaetes survive the turbidity flow and injection.

S_b

As data were unavailable, a conservative value of 0.5 was used. During the injection event, mechanical shaking of the sediments causes microfauna to be lost as they typically have lower densities than sediments. Further, some proportion of reduced chemicals in the sediment will be oxidised as mixing with overlying waters occurs, reducing oxygen uptake by chemical means post-injection.

Unit conversions and results

Units reported in the literature needed to be converted in many cases prior to being input into the model. In the literature, SCOC and abundances are typically reported as per unit area of sediment surface, therefore these have been converted to volume to provide a depth aspect on oxygen consumption within a community. Molar oxygen concentrations were converted to ml / L using the ratio of $1 \text{ mlO}_2 / \text{L seawater} = 44.661 \mu\text{molO}_2 / \text{L}$ (from ICES oceanography).

Below an oxygen concentration of 0.45 ml / L, the community structure of deep sea macrofauna becomes adversely affected, however, it appears that polychaetes are the most tolerant of macrofaunal taxa (Levin and Gage, 1998). We therefore took the threshold of polychaetes to be 0.2 mlO₂ / L. A length of time can therefore be estimated, before oxygen becomes too low in the sediment. As parameterised above, this occurs at 269.8 days, which provides ample time for burial and injection to occur (Fig. 8.6).

8.5.3. Implications

The injected sand was either sourced from above or from below, both are considered here.

Injectites sourced from above

In order to create the overpressure needed to inject sand/water flows downwards into the substrate, the source sands must have been sealed by overlying muds and sufficient overburden of several metres (a minimum of 8 m of overburden in the case of 8 m downward injection [in

sediments that are now compacted]), therefore macrofauna would have been living at several metres depth prior to injection. Turbidity currents deposit event beds that can be muddy (Talling *et al.*, 2012), occurring over hours to days, providing the necessary seal over the lobe for pressure to build within the sand body during burial. Figure 8.7A shows how a lobe, prone to clastic injection, can be buried to several metres depth and have a steady source of oxygen and nutrients needed for survival brought in by migrating pore fluids. Hence, living organisms were already living at much greater depths than previously thought possible. The volume of sand represented by the injectites indicates a substantial source sandbody, as the sills and dykes themselves are up to 50 cm in width.

Organisms are either synchronous with Injectites, that is, they are transported down with the injecting flow, survive, and inhabit the newly deposited sand. Or, they exploit Injectites post deposition and bury down following fresh oxygen and organic matter gradients. There is ultimately a time limit on how long an organism can survive in injectites. Life in a deep-marine environment means a slow metabolic rate in order to survive cold temperatures and energy deprivation (Mahaut *et al.*, 1995; McClain *et al.*, 2012). Moreover, the fluids that are injected down with the sediment and become pore water will initially be oxygenated to the level that organisms were already inhabiting.

Injectites sourced from below

If Injectites were sourced from below, then the host shale provides the seal required for overpressure and injection. Injectites would have had to reach the palaeoseabed and extrude onto the surface in order to provide a connection for fauna to exploit (Figure 8.7C). Organisms such as polychaetes then buried downwards following the injectite network as it acts as a source of new organic matter. Consequent erosion of the seabed through turbidity flows occurred and deposited sandy lobes overlying the injectite network. (Fig. 8.7D).

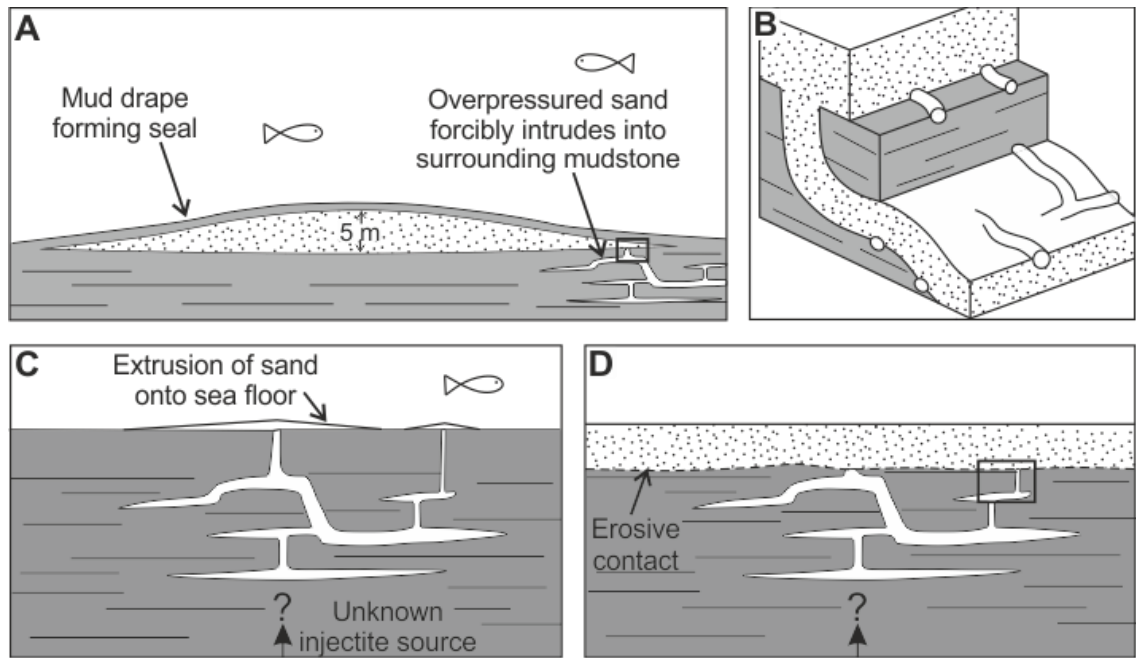


Figure 8.7 Model showing evolution of bioturbation from lobes to injectites over <270 days. Average lobe thickness at axis is 5 m (Prélat *et al.*, 2009). (A) and (B) T1: Sandy lobe unit, with bioturbation along the sand-to-mud interface at the base, several metres below the seabed. Pore water percolates from the top centre of the lobe, where sand is in close contact with seawater. (C) and (D) T2: Overpressure at the edge of the sandy lobes causes unconsolidated sand to forcibly intrude into underlying mudstone, outwards from lobe centre. Macrofauna are transported with the flow and form new living traces on the sand-to-mud contacts that form the margins of the sand intrusions.

Wider implications

Once inhabiting injectites, there is substantial period of time for living organisms to rework sediment and ingest nutrients that would have otherwise been preserved; sediment ingestion and excretion is known to alter the physical characteristics and potentially mineralogy of sediment (Needham *et al.*, 2005). This process of bioturbation contributes as a significant driver during diagenetic evolution of sandstones; organisms, through bioturbation, are capable of degrading primary mineral assemblages and producing newly formed clay minerals in their place (Needham *et al.*, 2005).

Submarine lobes contribute to submarine fans: the largest sedimentary depositional systems worldwide (Curry *et al.*, 2002). The example discussed here is a sandy fan system, however even in muddy systems such as the Amazon Fan, 70% of the lower fan (and therefore lobes)

comprise sand (Piper and Normark, 2001). In addition, forcible intrusion of sand into mud occurs in deep sea deposits in basins across the planet (Huuse *et al.*, 2010). Therefore, this represents a major unexplored macrofauna environment.

8.6. Conclusions

Our findings have several biological and geological implications, i) unusually, we can quantify a minimum depth below the seabed that organisms inhabited in ancient sediments to several metres, ii) less organics are preserved due to carbon consumption during metabolic activity, which then also changes the sediment fabric at depth, with grains being processed and sorted into burrow structures, and iii) most importantly, we have shown that macrofaunal life survives for periods living at depths of up to 8 m below the seabed, giving an entirely new limit to the macro faunal biosphere.

9. Mechanisms, distribution, and subsurface implications of clastic injectites: A synthesis

The four research questions proposed in Chapter 1 are addressed here, with reference to the results presented in Chapters 4-7:

1. What are the physical differences in clastic injectites formed at shallow and deep burial depths, and at what depth does this transition occur? (Section 9.2)
2. What factors control injectite architecture? (Section 9.3)
3. Are clastic injectites (palaeo-)geographically predictable in deep-marine settings? (Section 9.4)
4. What clastic injectite characteristics affect reservoir quality? (Section 9.5)

This Chapter is a review of recent advances regarding the formation and architecture of clastic injectites, highlights the gaps in current understanding, integrates the advances made in the present work, and concludes with suggestions for future work that would address these gaps in understanding.

9.1. Introduction

Understanding the pre-requisite conditions, processes, and products of sand injection is important as they are increasingly recognised as significant components of sedimentary basin-fills (see Hurst *et al.*, 2011; Ross *et al.*, 2011, and references therein) and can impact and form hydrocarbon reservoirs (Lonergan and Cartwright, 1999; Duranti *et al.*, 2002; Huuse *et al.*, 2010; Schwab *et al.*, 2015). Previous studies have demonstrated common injectite architectures in the subsurface (Duranti *et al.*, 2002; Huuse *et al.*, 2007; Cartwright, 2010) and identified potential trigger mechanisms for injection including seismicity (Obermeier 1996; Boehm and Moore, 2002; Huuse and Mickelson, 2004; Obermeier *et al.*, 2005), tectonic stress (Peterson, 1966; Jolly and Lonergan, 2002), rapid burial (Truswell, 1972; Allen, 2001), instability of overlying sediments (Jonk, 2010) or migration of basinal fluids into a sealed sand body (Vigorito and Hurst, 2010; Jackson *et al.*, 2011; Bureau *et al.*, 2014). Physical modelling of clastic injectites (Rodrigues *et al.*, 2009; Ross *et al.*, 2011; Bureau *et al.*, 2014) and outcrop studies have categorised zones of intrusion (Vigorito and Hurst, 2010) and documented how intrusion geometry can change further away from the source sand (Parize and Fries, 2003). Of these and other studies, only a modest number have attempted to analyse specific intrusion mechanisms and internal flow processes.

9.2. What are the physical differences in clastic injectites formed at shallow and deep burial depths, and at what depth does this transition occur?

Injectites have been categorized simply into shallow and deep emplacement depending on depth of burial prior to injection. The range applied to these terms varies substantially. Duranti and Hurst (2004) define shallow as <100 m below the surface, however Jonk *et al.* (2005b) define shallow as <400 m. Yet it has been observed that near surface injectites (<10 m) display vastly different geometries to those defined at 100s or even 10s metres depth (Archer, 1984; Jolly and Lonergan, 2002). Deep burial is generally placed at between 500-1500 m below the surface (Vigorito and Hurst, 2010). Therefore, 3 categories of injectite are recognised according to depth: i) near surface injectites (<10 m), ii) shallow injectites (10 – 500 m), and iii) deep injectites (>500 m). Since injectites can crosscut up to several hundreds of metres of stratigraphy, it is possible that their architecture will vary depending on depth for a single injectite complex (Vigorito *et al.*, 2008).

Where injectite complexes reach the seabed and extrude, it is possible to give a minimum depth of injection from lowermost intrusions up to extrusions (Surlyk and Noe-Nygaard, 2001; Thompson *et al.*, 2007; Ross *et al.*, 2013, 2014). Similarly, minimum depth of injection can be given as the vertical extent of single intrusions. For example, the Panoche Giant Injection Complex in California covers 1500 m of stratigraphy (Vigorito *et al.*, 2008; Vigorito and Hurst, 2010; Scott *et al.*, 2013), yet the largest single dykes are 600 m long, which provides a minimum constraint of depth.

9.2.1. Near surface injectite architecture

Near surface injection (<10 m) produces smaller, thinner injectites (Archer, 1984; Hurst *et al.*, 2003) than deeper injection due to the restricted volumes and minimal stratigraphy that is cross-cut. For examples that are stratigraphically deeper, there is a greater volume of sand and more stratigraphy to cross cut before reaching the surface.

Bioturbation

Until recently, ichnological studies have not been associated with clastic injectites, as bioturbation itself is typically confined to the top few 10's cm of the subsurface. However,

Chapter 7 demonstrates deep marine macrofauna trace fossils on the margins of clastic dykes and sills that were formed by biological activity in the substrate post injectite emplacement (Fig. 9.1A-D). Clastic injection occurred soon after parent sands were sealed by mud, injecting polychaetes down from several to at least 8 metres where they survived for enough time to form *Planolites* and *Thalassinoides*. The presence of bioturbation indicates very shallow injection depths, less than a few metres, at several localities across the Karoo Basin.

Injectite morphology

Where bioturbation is present, clastic injectites have a specific and distinct style of injection (Fig. 9.1A-B). Where injectites are directly in contact with the base of the parent sand, they form abruptly downward tapered cones ~1 m in width and 1.5 m in depth (Fig. 9.1A). Each cone-like feature is made up of multiple dykes that pass into a single dyke 5-20 cm wide, which feeds multiple sills and dykes below. Immediately below the cone-like structures are vertical and subvertical dykes <20 cm wide that extend for no more than 2 m before feeding sills or splitting into multiple dykes. This complicated network of net downward injection terminates no more than 8 m below the parent sand and feeds laterally extensive < 20 cm thick sills up to 100's m.

Sills

The Rosroe Formation, western Ireland is thought to comprise a shallowly injected sill complex (Jolly and Lonergan, 2002). Source bed to sill distances are up to 50 cm, and the limited dykes make up a very small volume of intruded sand. The injectites themselves have abrupt thickness changes, with irregularities on upper surface, changes in stratigraphic level (Archer, 1984) and are thought to have been injected in the top 10 m sediment (Jolly and Lonergan, 2002) (Fig. 9.1F).

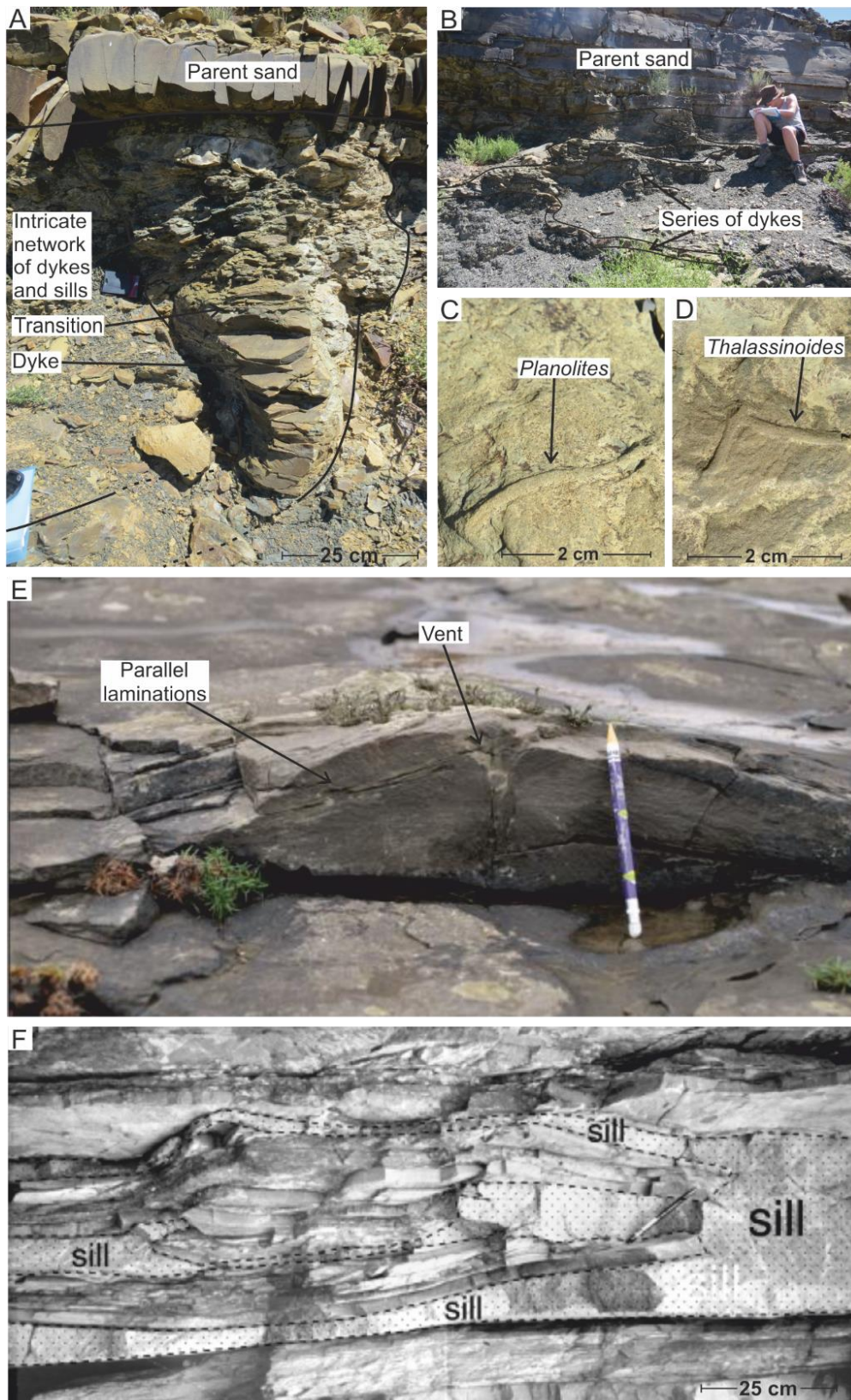


Figure 9.1 Near surface injectites. A) Abruptly tapering down cone. B) Series of sills and dykes fed directly from parent sand above. C) Planolites on sill margin. D) Thalassinoides on dyke margin. E) Sand volcano, Shannon Basin, Co. Clare, Ireland (Ross et al., 2013). F) Sill dominated intrusion, Rosroe Peninsula, western Ireland (Jolly and Lonergan, 2002).

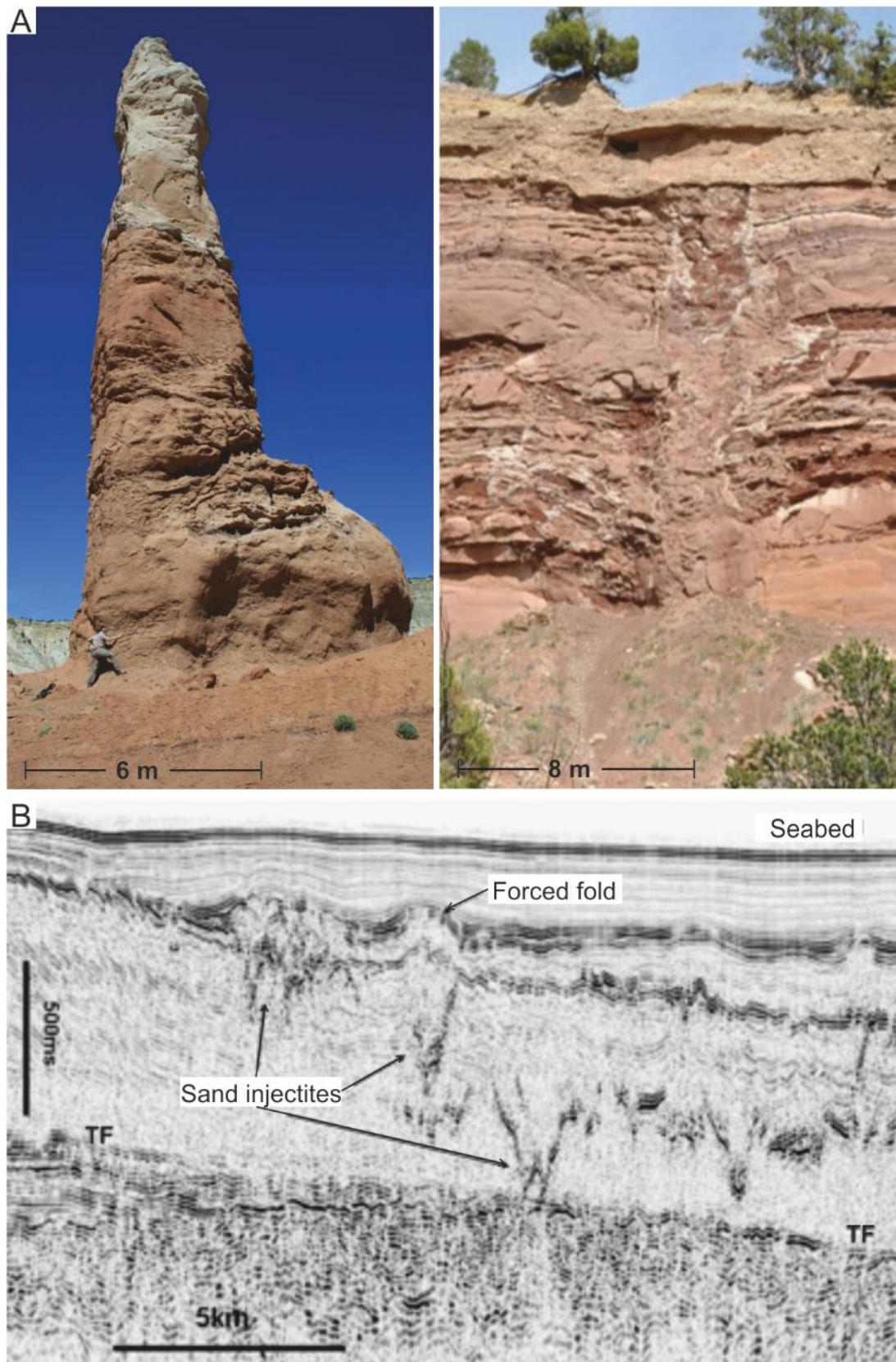


Figure 9.2 Shallow injectites. A) Columnar intrusions, Carmel Formation, Utah. B) Seismic profile from Faeroe-Shetland Basin. Injectites emanate from large submarine fan body (TF) = topfan (Cartwright, 2010).

9.2.2. Shallow injectite architecture

Shallow injectites are defined here as those occurring between >10 m and <500 m palaeodepth.

Extrudites

Extrudites form where clastic injection reaches the surface. Accurate depth of burial at the time of injection can be demonstrated both in outcrop (Obermeier, 1998; Jonk *et al.*, 2007; Vigorito *et al.*, 2008; Ross *et al.*, 2013) and in the subsurface (Huuse *et al.*, 2005a; Hurst *et al.*, 2006) where injectites extend from the parent sand to the palaeosurface. Extrudites take the form of either volcanoes or more laterally extensive sheets (Ross *et al.*, 2013), with many systems exhibiting both (Jonk *et al.*, 2007; Løseth *et al.*, 2012). Volcanoes are subcircular in planform and convex-up cone shaped in cross-section (Hurst *et al.*, 2011 and references therein). They occur on a range of scales and have been reported up to 1000 m in diameter (Løseth *et al.*, 2012). Sheet sands are laterally extensive and gradually thin away from the point of extrusion, like volcanoes, though generally widespread and not subcircular (Løseth *et al.*, 2012). Extruded sheets have been reported as >1 km (Andreson *et al.*, 2009) and potentially up to 20 km across (Løseth *et al.*, 2012).

These types of remobilized sediments are fed from below by columnar intrusions (Chan *et al.*, 2007; Ross *et al.*, 2014), and feeder-dykes (Hurst *et al.*, 2006; Vigorito *et al.*, 2008). Columnar intrusions can be just a few cm in diameter (e.g. Ross Formation, Co. Clare, Ireland, Ross *et al.*, 2013) or several m in diameter (e.g. Kodachrome Basin, Middle Jurassic, SE Utah; Huuse *et al.*, 2005b) (Fig. 9.2A-B).

Forced folding

Folding above clastic intrusions occurs in the top few 100 m of stratigraphy, often forming 4-way folds. This style of feature associated with injectites may form in one of 2 ways: i) by differential compaction of the intrusion relative to the surrounding mud or claystone (Hillier and Cosgrove, 2002), or ii) where forceful intrusion 'jacks-up' the overburden (Stearns, 1978; Shoulders and Cartwright, 2004). Both of these formative methods form at shallow palaeodepths, where rock overburden is low and can accommodate uplift (Johnson and Pollard, 1973; Galland *et al.*, 2009; Muirhead *et al.*, 2012). In cases where overburden is 'jacked up' due to injectite emplacement (Shoulders and Cartwright, 2004; Cartwright *et al.*, 2008; Løseth *et al.*, 2013), the overburden depth can also contribute to estimation of the minimum depth of injection (Fig. 9.2C).

Preserved fracture patterns

Chapter 4 described the process by which preserved fracture patterns on the margins of clastic injectites can be used to estimate relative depth of injection. Here, plumose arrays and hackle marks (Fig. 9.3) give a depth of several hundred metres burial prior to injection, putting these features at the deeper end, stratigraphically, of shallow injectite architecture.

During injectite formation, a hydraulic fracture propagates through the host lithology, and where the intruding flow is not erosive, initial fracture patterns will be preserved on the margins of clastic injectites (Chapter 4). The combination of the depth distribution of tensile strength in muds, and the high fluid pressures associated with injection, suggests that mode I failure will occur at considerable depths (up to 100s of m). Shear failure occurs at a depth where the applied shear stress, S , is greater than 4 times the tensile strength of the rock, T , changing from extensional fracturing at shallower depths (Fig. 4.1; Cobain *et al.*, 2015: their Fig. 1). Plumose fractures with en échelon fringes (Fig. 9.3B) form from mainly extensional deformation (central and divergent striae), but with a component of shear fracturing. This could place a depth range on formation of fractures and injection at or near to the bounding zone from extensional to shear stresses. Plumose fractures have been observed in several clastic injectites systems: Fort Brown formation, Karoo Basin, South Africa (Fig. 9.3A and 9.3B), Los Molles formation, Neuquén Basin, Argentina (Fig. 9.3C), and Tabarka Injectite Complex (TIC), Tunisia (Fig. 9.3D). Based on this analysis of the fracture patterns occurring at a depth where tensile strength is at least four times that of the host mudstone, it is possible to rule out very shallow injection. This approach enables relative injection depth to be inferred for systems that are not connected to the surface.

9.2.3. Deep injectite architecture

Deep injectites are defined here as intruding in >500 m palaeodepths.

Outcrop scale

Injectites that comprise large volumes, are laterally extensive with widths of at least several m, are often associated with deep burial prior to injection. To inject such large volumes of material, significant overpressure, and therefore burial, of large parent units is necessary. One of the few outcrop examples of this style of injection is the Panoche Giant Injection Complex, California. Here, injectites intrude 1500 m of stratigraphy, sourced from multiple parent units (Vigorito *et al.*, 2008). Dykes are up to 18 m in width and up to 600 m in vertical extent (Vigorito *et al.*, 2008;

Vigorito and Hurst, 2010). Parent sands are focused in the lower units of the injectite complex. Locally, sills dominate close to parent sands, with dykes forming the dominant style of intrusion higher up stratigraphy (Vigorito *et al.*, 2008). Injectite numbers and volume decreases away from parent sand units.



Figure 9.3 Plumose fracture patterns preserved on injectite margins. A and B) Examples from Unit A, Karoo Basin, South Africa. C) Los Molles formation, Neuquén Basin, Argentina. D) Tabarka Injectite Complex (TIC), Tunisia (modified from Scott, 2009 thesis).

Seismic scale

Reflection seismic datasets can provide more constraint on depth of injection. Clastic dykes are most readily identified in seismic as they cross-cut stratigraphy whereas sills can only be interpreted through association with dykes. Typically, however, clastic injectites are below the resolution of seismic; being too thin, too steep, or both, to be imaged (Huuse *et al.*, 2007). The vertical extent of dykes gives a minimum depth of injection. There are several, well established geometries assigned to clastic injectites in the subsurface, these are: conical, forming V-shaped bowls in cross-section (Fig. 9.4B) (Huuse *et al.*, 2004, 2007; Shoulders and Cartwright, 2004; Løseth *et al.*, 2013; Monnier *et al.*, 2014), saucer shaped, forming flat-based bowls in cross section (Fig. 9.4C) (Hurst *et al.*, 2003; Monnier *et al.*, 2014), stepped or wing-like (Duranti *et al.*, 2002; Huuse *et al.*, 2004, 2007; Lonergan *et al.*, 2007; Jackson *et al.*, 2011), or polygonal where pre-existing faults were exploited (Lonergan and Cartwright, 1999; Molyneux *et al.*, 2002; Huuse *et al.*, 2004, 2007; Lonergan *et al.*, 2007).

9.2.4. Comparison of injectites as a function of depth

Clastic injectites can be categorised according to depth of emplacement into: near surface, shallow, and deep. Generally, injectites formed at near surface burial depths are only identified in outcrop, such as clastic volcanoes and sheets, bioturbated dykes and sills, and low-volume, abruptly swelling and pinching sills. However, this is a factor of scale, as such injectite architectures and features are unidentifiable in the subsurface. Injectites formed after substantial burial are identifiable at both outcrop and in seismic datasets. Outcrop analysis means minimum depths of burial can be constrained (e.g. Panoche Giant Injection Complex). Small-scale features are not resolvable in seismic data, however, large-scale datasets mean that at least minimum depths of burial prior to injection can be estimated, which can be several 100's m. The 3D architectures mapped in the subsurface are commonly bowl- or wing-like; both stepping upwards and outwards from a point source. This is an aspect that is difficult to observe in outcrop due the scale of exposure. Being able to bridge the gap between outcrop and subsurface datasets is important in understanding formative processes and simply being able to identify styles and architecture of injectites in seismic data.

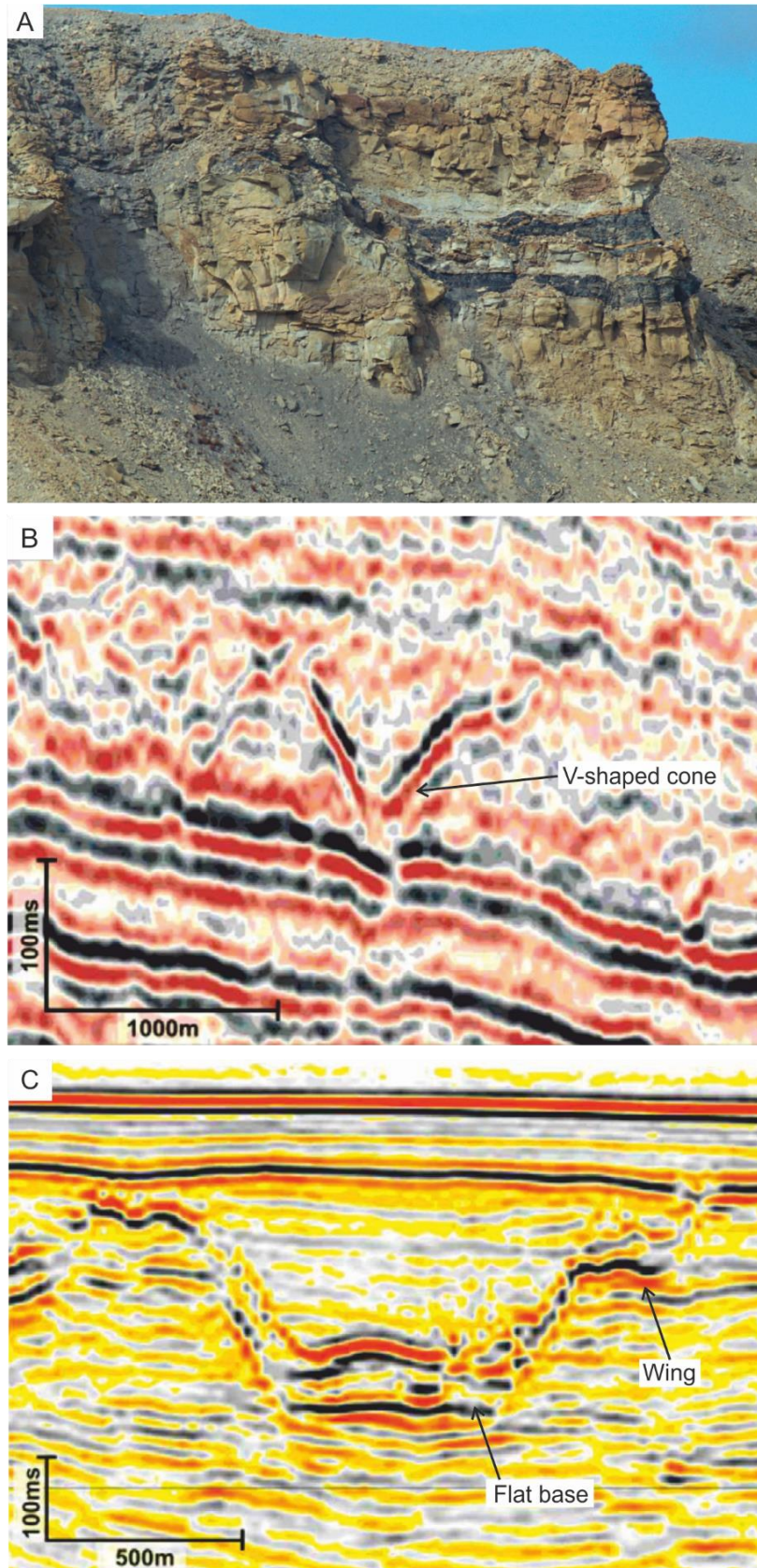


Figure 9.4 Deep injectites. A) Structureless injected sandstone with subhorizontal mudclasts, largest mudclast is 7 m long. Cliff 12 m high. Katedralen Member, Katedralen, Jameson Land, Greenland (Surlyk *et al.*, 2007). B) Apical Cones. C) Flat based bowl (B+C Cartwright *et al.*, 2008).

9.3. What factors control injectite architecture?

Previously, clastic injectites have been categorised according to their morphology in relation to depth of emplacement. For example, the established tripartite division of networks of clastic sills and dykes into zones depending on abundance and angle of dykes and sills, identified in the Panoche Giant Injection Complex (Vigorito *et al.*, 2008; Vigorito and Hurst, 2010). However, this system covers over 1500 m vertical stratigraphy of clastic injectite networks, sourced from multiple parent units, where injection was unlikely to be simultaneous (Friedmann *et al.*, 2002). Though extensively well exposed, this is a general model based on a single example, and therefore, conforming to this depth-based, tripartite division, model of injectite architecture may be inappropriate. An alternative approach is to identify external controls on injectite architecture and formation, taking into account relative depth, but also tectonic environment, parent sand extent and geometry and host lithology when analysing injectite architecture.

Currently, theoretical, numerical and physical models of injection are simplistic and do not incorporate a tectonic stress as can occur in sedimentary basins, consequently the maximum principal stress is vertical (Jolly and Lonergan, 2002; Rodrigues *et al.*, 2009; Mourgues *et al.*, 2012). However, clastic injectites are often associated with tectonically-active environments (Newsom, 1903; Dzulynski and Radomski, 1957; Thompson *et al.*, 1999; Jolly and Lonergan, 2002; Diggs, 2007; Frey-Martínez *et al.*, 2007). Therefore, these idealised models are flawed as they assume tectonic quiescence. Here, we do not attempt to resolve this issue, but examine other controls on injectite architecture.

9.3.1. Large-scale controls

The specific mechanisms controlling the large-scale architecture of clastic injectites remains enigmatic. There are several factors that need to be considered when describing intrusion processes: i) how injectites are fed, ii) the aspects that dictate common saucer-shape geometry, iii) how the overburden is affected regarding failure through faulting, or through being jacked up into a dome shape, and iv) the role in which pre-existing faults have affected the injection process.

Parent sand architecture

Clastic injectites are continually analysed for their geometry, size, and connectivity, but often only considered as single intrusive bodies or injectite complexes. Here, these factors are described in relation to the parent sand in deep marine environments. Two main parent sand architecture types are considered here, laterally extensive lobes, and slope channel-fills. Both can comprise significant volumes of sand, having the potential to source volumetrically large injectite networks.

Chapter 5 describes the geometry of injectites sourced from basin floor lobe complexes. The parent sands of injectites are volumetrically larger than many slope channel-fills, but comprise much thinner, sheet-like sand units forming lobe complexes. Therefore, as observed in the Karoo Basin outcrops, thinner injectites can be expected as a product of subsurface remobilisation in comparison to slope channel-fills, thus being sub-seismic scale and frequently unrecognised or poorly documented on many seismic data sets (e.g. Shepherd *et al.*, 1990). The resulting injectites are rarely above 1 m in thickness, and extend laterally for up to several km. Sills are the dominant injectite type, and step gradually upwards and outwards from lobe complex margins. A factor contributing to the lack of recognition in subsurface data is the style of injection. Primarily, Karoo Basin injectites are laterally extensive sills, which are hard to identify in reflection seismic data, and in core could be misinterpreted as primary deposits rather than remobilised units. Chapter 7 forward seismic models outcrop injectite detail, and shows how this can aid in injectite identification in the subsurface. The style of clastic injectite associated with lobe deposits (Chapter 5) is also observed at outcrop in the Upper Jurassic Hareelv Formation of East Greenland. The lower part of the formation, the Katedralen Member comprises base-of-slope lobe sands, from which sills are the dominant style of injection. It is in these lower lobe deposits that thinner dykes and sills are found (Surlyk *et al.*, 2007).

In contrast, slope channel-fills are sources of significantly different injectites in terms of architecture. Wing-like injectites are often reported where dykes and sills can be observed directly connected to the parent channel sand (Lonergan and Cartwright, 1999; Parize and Friès, 2003; Duranti and Hurst, 2004; Huuse, 2004; Jackson, 2007). In three dimensions, they form long dykes along channel margins, giving the appearance of 'wings' in two dimension (Fig. 9.4C). Wings forming at channel margins can be explained in terms of differential compaction adjacent to the main body of sand; maximum extensional strain is at the channel margins causing small-scale fractures to form parallel along to the main body of sand. These fractures or zones of

weakness are then exploited by the overpressured, unconsolidated sand to form wing-like dykes flanking the channel margins (Cosgrove and Hillier, 1999; Hillier and Cosgrove, 2002; Jackson, 2007). Therefore, where prerequisite conditions for clastic injectite are met on slope channel-fills, wing like intrusions can be expected to occur along the channel margins, at an abrupt pinchout, where differential compaction has caused extensional deformation at the edges of the parent sand body.

Conical geometry

Bowl- or conical-shaped injectites exhibit the same geometric shape as igneous saucer intrusions and comprise 3 main elements (Chevallier and Woodford, 1999; Polteau *et al.*, 2008): i) an inner sill, mostly concordant with bedding, ii) an inclined sheet, discordant with stratigraphy, and iii) an outer sill (Fig. 9.4C). Both are formed in sedimentary basins, in the top few 100 m of strata. These similar geometries observed in both igneous and sedimentary intrusions suggest that emplacement mechanisms can be compared and controlled by the same external parameters (Cartwright *et al.*, 2008; Polteau *et al.*, 2008; Mourgues *et al.*, 2012). The fact that conical shaped intrusions commonly reoccur in sedimentary basins across the world suggests that the controlling mechanisms behind the saucer-like shape is controlled by similar physical processes (Polteau *et al.*, 2008). Properties of host lithology that affect intrusion morphology during emplacement include the propensity for brittle behaviour versus non-brittle (Schofield *et al.*, 2012a), the homogeneity of the host strata (Jolly and Lonergan, 2002), and the principle stress orientation (Jolly and Lonergan, 2002; Rowe *et al.*, 2002). Therefore, research on intrusion dynamics of igneous systems (McCaffrey and Petford, 1997; Thomson, 2007; Thomson and Schofield, 2008; Schofield *et al.*, 2012a; Magee *et al.*, 2015) can be applied here to clastic intrusions.

Analysis by Polteau *et al.* (2008) using anisotropy of magnetic susceptibility measurements (AMS) on magmatic sill intrusions in Golden Valley, South Africa has shown direction of magma propagation during intrusion, and therefore led to a model of how the saucer shapes develop. Magma initially propagates radially outwards from a point source and develops a saucer-shaped geometry, causing new fractures to occur higher up in stratigraphy due to pressure build up caused by the intrusion. The low pressure within this fracture creates a pressure differential drawing in more magma from the first emplaced sill, in turn creating a new sill, forming into a saucer shape (Fig. 9.5). However, not all processes of magma intrusion are applicable to clastic injectite emplacement mechanisms. For example, Polteau *et al.* (2008) also describe the process

of active magma channels within a lower saucer feeding intrusions into stratigraphically higher positions, while other parts of the same sheet intrusion are abandoned and freeze and crystallise. Additionally, once injecting magma has ceased, backflow will occur causing overburden to sag, and in some cases, deflation of sills.

The “V-shape” that is often used to describe clastic injectites in seismic profiles is misleading, it implies a very steep-sided feature with a distinct and sharp source point, which may be representative, but only in vertically exaggerated profiles. Scaling without vertical exaggeration would give much more shallow features. It should be noted however that it is this “V-shape” that is so often reproduced in physical modelling (e.g. Mathieu *et al.*, 2008; Mourgues *et al.*, 2012; Bureau *et al.*, 2014).

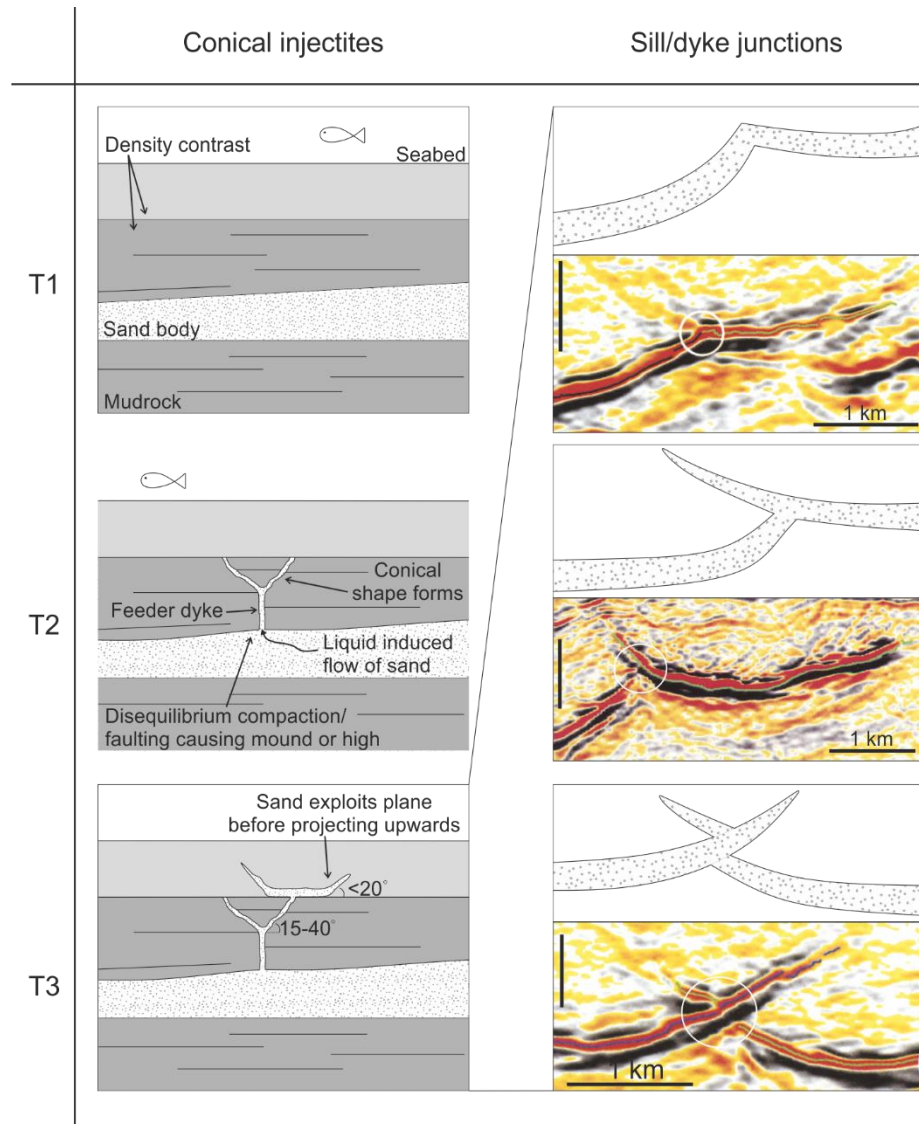


Figure 9.5 Formation of conical injectites through time phases T1-3 (adapted from Huuse *et al.*, 2005a). Varying sill-to-dyke junctions and their expression in seismic profile (adapted from Hansen *et al.*, 2004).

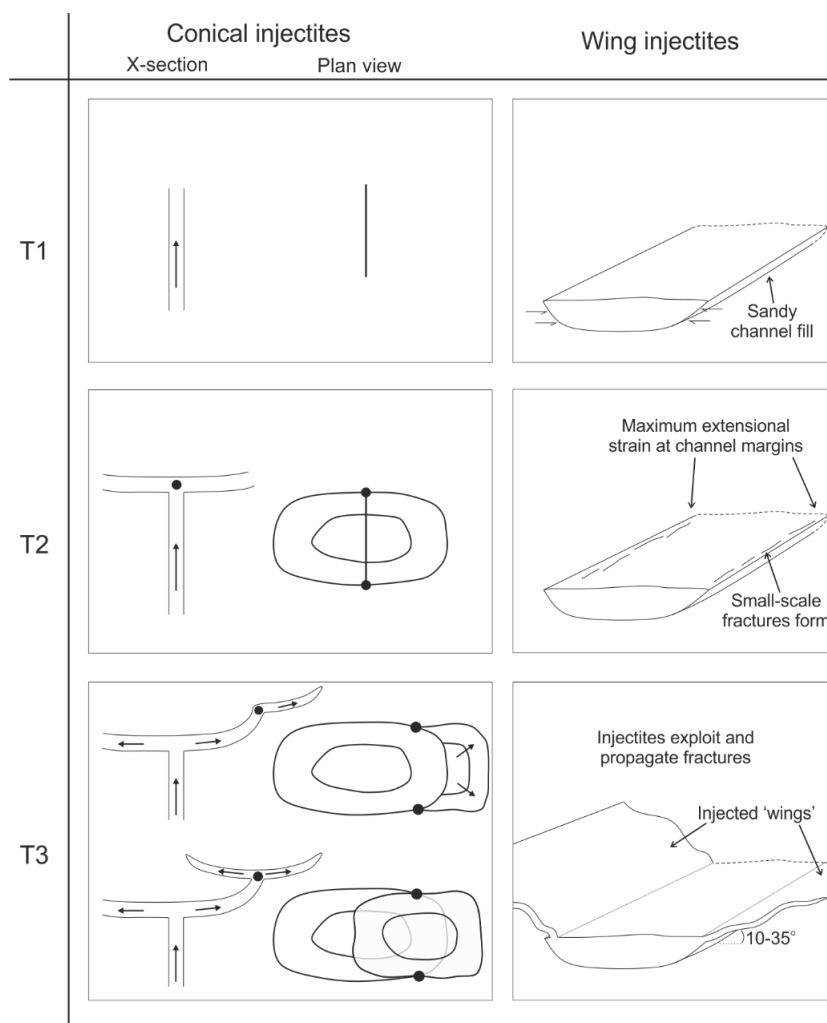


Figure 9.6 Injectite feeder evolution for conical (adapted from Hansen *et al.*, 2004) and wing-like injectites.

Injectite feeders

Feeders of bowl shaped intrusions have been the source of much debate, with the main discrepancy being whether they are fed from the base (Thomson and Hutton, 2004; Hansen and Cartwright, 2006a; Cartwright *et al.*, 2008) or along the rim (Chevallier and Woodford, 1999). With igneous intrusions, where the feeder dykes or sill can be observed, either at outcrop (Chevallier and Woodson, 1999; Polteau *et al.*, 2008), or in seismic (Hansen *et al.*, 2004; Trude *et al.*, 2004; Hansen and Cartwright, 2006a), it is seen that multiple dykes and sills, sourced from below, feed into a complex of saucer shaped intrusions where each sheet is connected to a source, or sources, at its deepest point in the intruded lithology (Figs. 9.5 and 9.6) (Leaman, 1975). Hansen and Cartwright (2006a) using 3D seismic data from the NE Atlantic to show that an igneous saucer sill complex was fed by multiple, low-angled dykes (Hansen and Cartwright,

2006a; their Fig. 2), with lateral amalgamation of several intrusive bodies emplaced within a limited stratigraphic interval (Fig. 9.6). However, Huuse *et al.*, (2005a) speculate that multiple feeder pipes, such as those described from outcrops in Utah (Netoff, 2002; Ross *et al.*, 2014) are the source for conical intrusions in the subsurface.

These models of multiple sill and dyke feeders are very different to the current injectite emplacement model (Cartwright *et al.*, 2008), where a single feeder, often a pipe (Monnier *et al.*, 2014) delivers a sand flux to a seed point in the centre of the saucer or bowl. This model has two end members of saucer geometry, a cone shape where the feeder forms a cone at a minor competence contrast, and a flat based bowl, where a sill propagates along a larger competence contrast before the sill turns upwards towards the surface (Cartwright *et al.*, 2008; their Fig. 12). The single pipe feeder model is not applicable where injectites emanate directly from source to form wings or where there are multiple saucer sills in a sill complex.

The difficulty in determining a style of feeder system for conical intrusions comes from the inability to distinguish high angled structures in seismic data (Jackson *et al.*, 2011), alongside not being able to differentiate between anomalous fluids or cements within intrusions, and seismic imaging artefacts caused by stratal disruptions (Huuse *et al.*, 2005a). It is unlikely that composite sills and saucers have a single feeder, but multiple feeders resulting in lateral amalgamation of intrusive bodies (e.g. Hansen and Cartwright, 2006a), where saucer shapes are fed from their deepest, not necessarily central point, subsequently stepping upwards and outwards. We speculate that the point of origin of conical injectite geometries can be related to high points or ridges in parent sand bodies, as observed on the Top Balder Formation (Huuse *et al.*, 2005a) where ridges may be caused by faulting or differential compaction. A point of weakness or preferential mechanical failure of the overburden would favour the origin of injectites at high points on parent units. At this point dykes then intrude upwards, either along pre-existing fault networks or by creating new fractures through host lithology until a point at which the rheological properties of the host strata causes dykes to feed sills, and therefore conical intrusions.

Overburden

Where overburden can be displaced above shallow-level injectites, the intruding body may preferentially extend laterally rather than form vertical dykes. Seismic profiles through saucer-shaped clastic injectites show that local doming of overlying sediments is common (Lonergan *et al.*, 2000; Molyneux *et al.*, 2002; Huuse and Mickelson 2004; Magee *et al.*, 2014). When large

volumes of sediment are intruded, forced folding of the overlying strata can occur. During this process, overburden may fracture forming new conduits through which injecting fluid and sand can exploit.

During initial intrusion, minimal deformation occurs in overlying strata (Fig. 9.7 T1), however as the thickness of the sill increases, a fold of equal thickness forms above (Fig. 9.7 T2) (Hansen and Cartwright, 2006b). As the sill exploits newly formed, upward propagating fractures at the tip of the intrusion, upward displacement occurs above the margins of the injectite (Fig. 9.7 T3) (Hansen and Cartwright, 2006b). Timing of injectite related forced folds can be constrained when sediments onlap the fold structure (Fig. 9.7 T3) (Hansen and Cartwright, 2006b). The onlap horizon marks the timing of the fold, and therefore, intrusion.

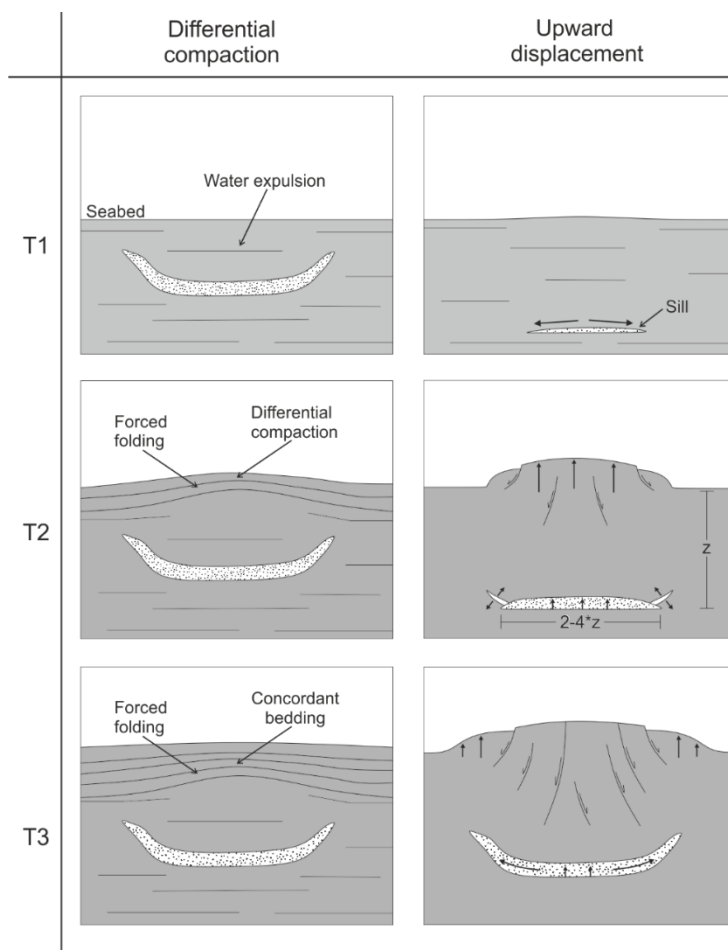


Figure 9.7 Two ways in which forced folding occurs due to injectite emplacement. Differential compaction results in concordance between seabed at time of intrusion and overburden. Upward displacement causes onlap of overburden after intrusion. (After Hansen and Cartwright, 2006b).

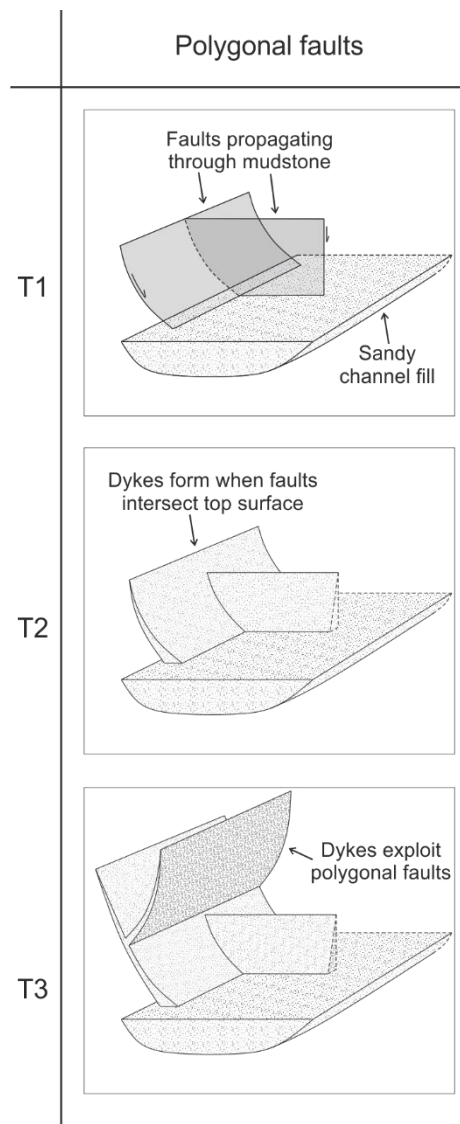


Figure 9.8 Remobilisation and injection due to propagating polygonal faults. Top seal failure occurs as faults intercept channel body fill. Sand fluidises and exploits fault planes (after Jackson, 2007).

Pre-existing faults

Polygonal faults have previously been ascribed as a key control in injectite development and architecture (e.g. Fig. 9.8) (Lonergan and Cartwright, 1999; Lonergan *et al.*, 2000; Molyneux *et al.*, 2002). However, more recently the relationship between polygonal faulting and clastic intrusion development has been shown to be more coincidental or a minor factor in injectite propagation (Huuse *et al.*, 2004; Shoulders *et al.*, 2007). Polygonal faults, in plan view, may form subcircular geometries, but in 3D do not produce cone-shaped structures (Cartwright and

Loneragan, 1996). Therefore it is likely that the association between polygonal faulting and clastic intrusions has been made in the past because injectites occasionally exploit the path of faults, but are not controlled by them. Polteau *et al.*, (2008) note that the idea that conical morphologies developed following pre-existing fractures has been ruled out based on the observation that saucer injectites and polygonal faults have mostly non-overlapping dip populations (Huuse and Mickelson, 2004; Huuse *et al.*, 2005a; Shoulders *et al.*, 2007). However, in the Cretaceous to Lower Tertiary succession of the North Sea, the depositional system and associated clastic intrusions are spatially related to a polygonal fault system that is developed (Fig. 9.8) (Bugge *et al.*, 2001; Jackson, 2007).

9.3.2. Small-scale controls

Even if stresses across bodies or whole beds of rock are uniform, small scale stresses due to flaws or impurities at the tip of a propagating fracture may be uneven causing irregularities in fracture direction and geometries (Lorenz *et al.*, 1991; Aubertin and Simon, 1997) (Fig. 9.9: heterogeneous mudstone). Ben-Zion and Morrissey (1995) have shown that a fracture propagating through a heterogeneous medium (Fig. 9.9) continually interacts with random asperities and diverges as heterogeneities in the fracture energy are incorporated.

The step-like nature attributed to conical intrusions can be explained by a shear component in addition to tensile displacement of host rocks (Mathieu *et al.*, 2015), i.e. a mix of mode I-II fracturing. Therefore, sheets can propagate at an angle to the main principal compressive stress orientation. Sedimentary bedding provides strongly anisotropic host lithology in which propagating injectites may exploit weak bedding planes, however, physical modelling of conical intrusions into homogeneous mediums does reproduce the conical shape (Galland *et al.*, 2014). The stepped geometry can be explained by the small-scale stress field at the tip of propagating fracture (Fig. 9.9).

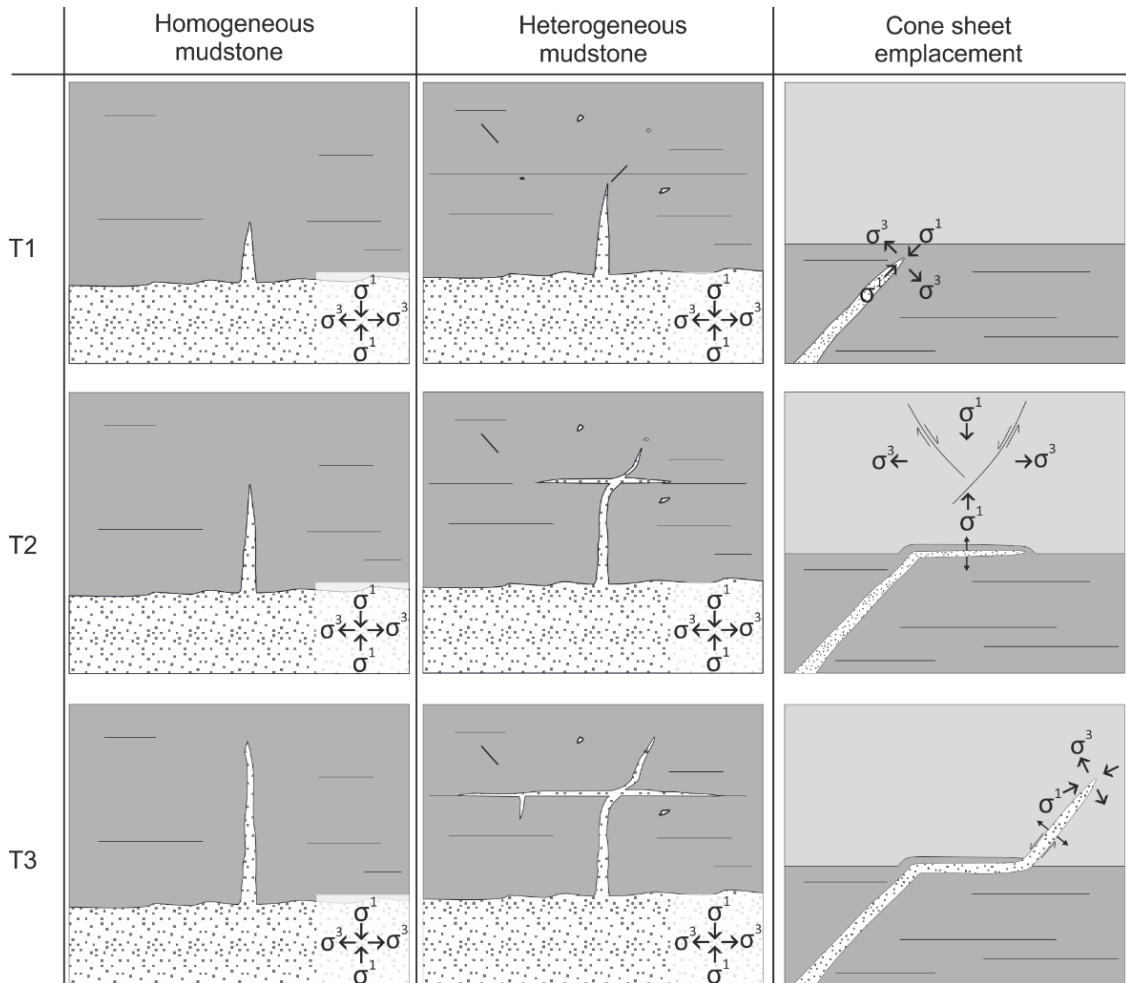


Figure 9.9 Small-scale controls on injectite propagation. Temporal development of injectite fractures showing simple fracture propagation in homogeneous and heterogeneous mudstones. Cone sheet development, occurs initially through mode I fracturing, at planar host rock discontinuities. Variations in rock strength may cause sills to form until differential stresses at fracture tip produce shear failure producing mixed-mode fracturing (after Mathieu *et al.*, 2015).

9.3.3. Fluid flow

The nature of flow in injectites has been the subject of much debate, with arguments for both laminar flow (Dott, 1966; Peterson, 1968; Taylor, 1982; Sturkell and Ormö, 1997) and turbulent flow (Obermeier, 1996; Duranti, 2007; Hubbard *et al.*, 2007; Scott *et al.*, 2009) being postulated. Chapter 4 describes three broad categories of flow during injection: i) flows that are connected to the surface and relatively low-concentration and highly turbulent; ii) large-scale injections that do not have a connection to the surface with high-concentration turbulent flows, and iii) flows with no connection to the surface and with relatively small cross-sectional dimensions (10s cm) that will be highly concentrated and laminar. Correspondingly, the products of these flows

will be different, with structures such as grading and erosional scours prevalent in low-concentration open conduits, whilst such features will be lacking in smaller-scale laminar injectites in closed conduits. The degree to which larger-scale closed systems might exhibit erosive structures and grading is largely unknown, most commonly reported are scallops, eroding into host strata from the top surfaces of sills (Surlyk and Noe-Nygaard, 2003; Hurst *et al.*, 2011) and banding parallel with injectite margins (Surlyk *et al.*, 2007). The different styles of injectite that are produced from laminar and turbulent flows are summarised in Figure 5.9. Turbulent flows cause erosion of the host lithology along the margins of clastic injectites, consequently producing features such as flutes, grooves, tool marks, and other sole structures (Obermeier, 1996; Diggs, 2007; Scott *et al.*, 2009; Kane *et al.*, 2010). Whereas laminar flow will preserve structures created on the margins of clastic injectites during initial fracture (Chapter 4).

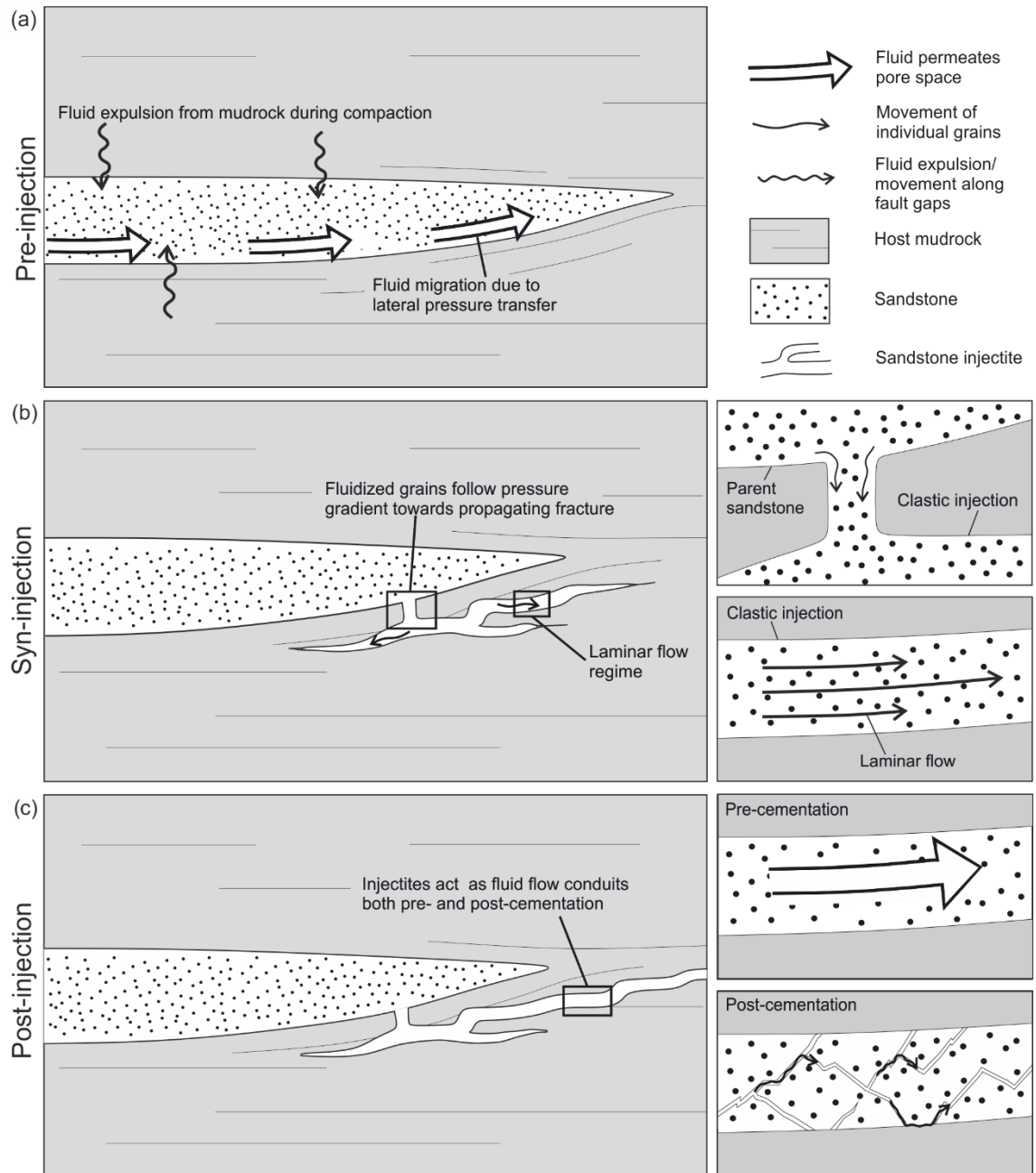


Figure 9.10 Fluid flow associated with stages of clastic injection. a) Pre-injection overpressure from compaction of surrounding strata and lateral pressure transfer. b) Syn-injection fluid flow, grains are liquefied and fluidised into propagating fracture. c) Post-injection fluid flow both pre- and post-cementation.

9.3.4. Depth as a control

Vertical stress is larger than the minimum horizontal stress in most sedimentary basins (Jolly and Lonergan, 2002). Therefore, the mode of fracture opening, and orientation of clastic intrusion, will be vertical. Where the differential between the most and least compressive stress is greatest, i.e. deeper burial, dykes are formed preferentially. This model assumes solely upward propagation sourced from parent sand below. However, at greater depths in a sedimentary basin the pressure gradients upwards *versus* downwards are similar, and therefore the potential for downwards propagating injectites is higher. Sills also form in the top few metres of sediment where there is a low differential stress so bedding planes favour the formation of horizontal intrusions. However, there are not set categories or depths for the preferential formation of dykes or sills; at any depth bedding or layering within the host lithology lowers the tensile and shear strength, enabling fluids and sediment to intrude along the discontinuity (Pollard, 1973, Jolly and Lonergan, 2002). Chapter 5 shows that, even at burial depths of several hundred metres, net propagation direction can be lateral.

At depths greater than a few hundred metres, where the vertical component of the confining stress is greater than the vertical tensile strength of the host strata, sills will preferentially form (Jolly and Lonergan, 2002). However, outcrop studies have shown that sills, sourced from a single parent unit, can form at different stratigraphic levels (Dixon *et al.*, 1995; Surlyk *et al.*, 2007). Therefore, there are limitations in applying theoretical equations to real life data. The ‘tiered’ model of Hurst *et al.* (2011) has multiple different parent sands that feed the different styles of intrusion that have been categorised into ‘injectite zones’ related to depth. These may in fact be related to the nature of the parent sand and surrounding strata (see section 9.3.1.1).

Depth may also have a control on fluid flow, if injectites do not reach the seabed, they remain a closed network and more likely to be emplaced under a laminar flow regime (Cobain *et al.*, 2015).

Analysis of the depth of emplacement of conical intrusions, based on data from outcrop, seismic, and numerical modelling for both igneous and clastic intrusions, has shown that there is a linear relationship between the diameter of the inner sill, and emplacement depth (Goultly and Schofield, 2008; Polteau *et al.*, 2008) (Fig. 9.7). Whereas Shoulders and Cartwright, (2004) attribute conical geometries to reduced overpressure within the flow at 2-300 m below the seabed.

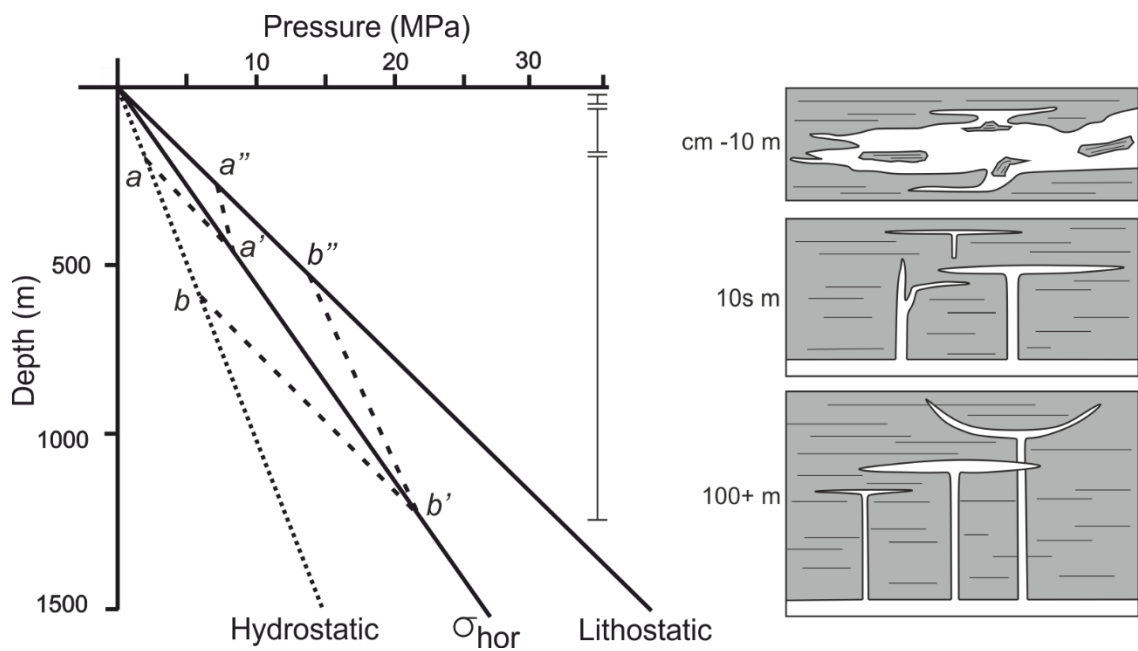


Figure 9.11 Simple model for how depth of injection impacts scale and geometry of injectites where principal stress is vertical. At shallow depths, differential stresses are minimal, bedding anisotropy favours sill formation. At 10's m depth, when fluid pressure reaches minimal horizontal stress, seal failure occurs and dykes form at point a' that propagates until fluid pressure exceeds lithostatic pressure (point a'') and sills will form. If parent body is sealed at deeper depths, then distance to seal failure and sill formation is greater (points b' and b'') creating longer dykes. (Adapted from Jolly and Lonergan, 2002).

9.4. Are clastic injectites (palaeo-)geographically predictable in deep-marine settings?

The prerequisite conditions required for overpressure and clastic injectite formation are universal across injectites in sedimentary systems. In order to predict where clastic injectites may occur, the occurrence of the combination of prerequisite conditions needs to be identified. This chapter focusses on injectites formed on the slope and basin floor, and how their geographic location may be predictable on this basis.

9.4.1. Slope injectites

The majority of clastic injectites described in deep-water settings are on slope settings, associated with deep-marine channel- and gully-fills (Parize and Friès, 2003; Duranti and Hurst, 2004; Huuse *et al.*, 2005a; Diggs, 2007; Duranti, 2007; Frey-Martínez *et al.*, 2007; Hamberg *et*

al., 2007; Jackson, 2007; Jonk *et al.*, 2007; Surlyk *et al.*, 2007; Vigorito *et al.*, 2008; Kane, 2010; Svendsen *et al.*, 2010; Szarawarska *et al.*, 2010; Jackson *et al.*, 2011; Løseth *et al.*, 2013). Injectites in these settings can be divided into those with direct observable connection to parent sand, and those emplaced stratigraphically higher. Stratigraphically higher injectites are discussed in previous sections (9.3.1.2 and 9.3.1.3). Where injectites are observed to emanate directly from the channel- or gully-fill, wing-like architectures dominate. Wing-like intrusions are typically fed from channel margins, dip between 10-35° away from the parent sand, often cross-cut ~100 m, and extend laterally 1- 2 km (Figs. 9.6 and 9.12) (Duranti *et al.*, 2002; Parize and Friès, 2003; Duranti and Hurst, 2004; Jackson, 2007; Szarawarska *et al.*, 2010; Jackson *et al.*, 2011). Wings can comprise solely dykes (Duranti and Hurst, 2004; Jackson, 2007; Jackson *et al.*, 2011) or a combination of dykes and sills forming steps (Kane, 2010; Szarawarska *et al.*, 2010; Jackson *et al.*, 2011).

Where direct contact is observed in outcrop between channel and injectite network, the parent sand contains an erosive body. It is this contact between the sharp, erosive channel and surrounding lithology from which injectites emanate (Parize and Friès, 2003).

9.4.2. Lobe injectites

Injectites are observed to emanate from proximal lobe complex settings (Chapter 5). At their abrupt updip pinchout, the parent sand is generally homogeneous, well sorted, and has a sharp contact with the underlying strata. Clastic injectites occur stratigraphically beneath the parent sandstone, with net propagation being lateral, towards and beyond the margin of the parent sandstone lobe complex. In other examples, where injectites of seismic-scale are known to be sourced from lobe complexes (as observed in intra-slope lobes), the source point is the proximal lobe (complex) fringe (Monnier *et al.*, 2014; Yang and Kim, 2014; Hurst *et al.*, 2016). This suggests that an abrupt and sand-prone pinchout in a proximal lobe complex setting could be a site of injectites.

The relative lack of documented examples of injectites associated within lobe complexes compared to submarine slopes may simply be due to less of these systems being drilled and therefore a data bias. However this disparity is also likely a reflection of scale and injectite orientation. In lobe deposits, the parent sands of injectites are volumetrically larger than many slope channel-fills, but comprise much thinner, sheet-like sand units forming lobe complexes (Surlyk *et al.*, 2007). Therefore, as observed in the Karoo Basin outcrops, thinner injectites can

be expected as a product of remobilisation in comparison to slope channel-fills, thus being sub-seismic scale and frequently unrecognised or poorly documented on many seismic data sets (e.g. Shepherd *et al.*, 1990). Another factor contributing to the lack of recognition in subsurface data is the style of injection; Karoo injectites are primarily laterally extensive sills. These would be hard to identify in reflection seismic data, and in core could be misinterpreted as primary deposits rather than remobilised units.

9.4.3. Model

Synthesising the observations discussed previously enables a general model of injectites in slope channel-fills and basin-floor lobe deposits to be proposed. Injectites are observed to form preferentially at the updip margins of sandy units where the pinchout is abrupt and sand-prone (Fig. 9.12). This geographic distribution is likely linked to the nature of the triggering mechanisms. In lobes, the presence of fractured margin structures demonstrates that these injectites formed at depths where tensile stresses were significant (Chapter 4); consequently disequilibrium compaction and lateral pressure transfer are the likely triggers. In deep marine deposits, disequilibrium compaction and lateral pressure transfer will lead to updip/marginal fluid migration, and in a tilted sand body the confining lithostatic pressure will also decrease updip. Therefore, hydraulic fracturing will predominantly occur at the up-dip margin where fluid migration and the lowest confining pressures combine. Within a proximal lobe complex, injectites are shown to occur at pinchouts (Fig. 9.12) and in sandy channel fills, along the margins; these areas both concentrate fluid-flow from lateral transfer and provide sharp boundaries at their basal surfaces between clean sands and the underlying mudstones. Initiation of hydraulic fracturing is favoured at the bases of these pinchouts because the high permeability of the clean sands will lead to higher transient overpressures during a triggering event. Theoretically, hydraulic fracturing might be expected to occur on the upper surface of the most up-dip point, as shown in some examples (Chapter 4). However, in many cases sand bodies exhibit a transition towards lower permeability facies (e.g., thinner bedded silts and sands) at their tops (Fig. 9.12; Pr  lat *et al.*, 2009). Whilst initial hydraulic fracturing and injection may be downwards, the increasing lithostatic pressure below the parent sands encourages lateral propagation, with sands able to step beyond the parent body (Fig. 9.12).

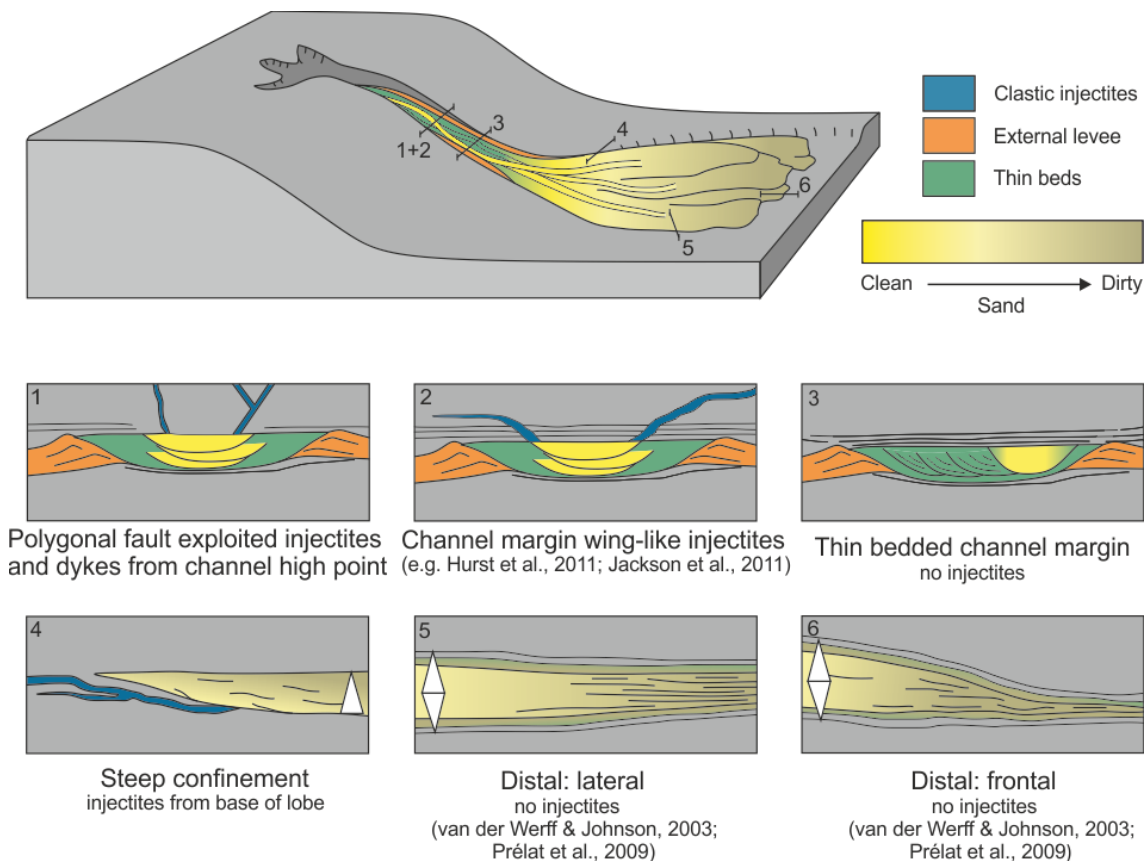


Figure 9.12 Schematic diagram to indicate likely sites of injection in a deep marine system; examples of previously reported clastic injectites occur on the slope, with addition of examples from basin-floor lobe complexes discussed in Chapter 5. Injectites on channel margins occur where clean sand abruptly pinches and form steep dykes and wings. In basin floor lobes, injectites occur in areas where sand is steeply confined and/or proximal within the lobe complex, while palaeogeographic locations that are downdip exhibit subtle confinement or have less clean-sand for fluidisation and therefore do not produce injectites.

9.5. What clastic injectite characteristics affect reservoir quality?

9.5.1. Fluid flow pre-, syn-, and post-injection

Clastic injectites can provide highly permeable migration pathways through otherwise impermeable formations (Huse *et al.*, 2005a). Therefore, it is essential that all stages of fluid flow associated with clastic injectites are considered when evaluating aquifers and hydrocarbon reservoirs. On a large-scale, injectites have the potential to enhance basin-wide fluid flow through otherwise impermeable strata (Huse *et al.*, 2005a; Vigorito *et al.*, 2008; Jonk, 2010; Hurst *et al.*, 2011). Clastic injectites are associated with basinal fluid flow at several stages; pre-

injection, during the process of clastic injection, post-injection and pre-cementation, and post-cementation (Jonk *et al.*, 2005a) (Fig. 9.10).

Pre-clastic injection, the migration of fluids through lateral pressure transfer and compaction can act as a trigger for injectite formation (Schwartz *et al.*, 2003; Cartwright, 2010). This movement of fluids can completely rework sediments of a primary deposition and destroy sedimentary structures and bedding (Surlyk *et al.*, 2007).

During clastic injection, flow types may have a significant impact of the style and heterogeneity of the injectites once formed. Flow regime during injection can be turbulent (Hubbard *et al.*, 2007; Scott *et al.*, 2009; Hurst *et al.*, 2011) or laminar (Duranti, 2007; Cobain *et al.* 2015), resulting in varying injectite morphologies in addition to effecting grain size distribution and packing. Laminar flows are not erosive, preserving initial fracture patterns on the margins of clastic injectites and resulting in sills and dykes that vary little in thickness laterally (Chapter 4). Whereas turbulent flows are erosive, sometimes cutting several metres into host strata (Surlyk *et al.*, 2003; Hurst *et al.*, 2011). The two flow types can result in highly different injectite geometry types (Chapter 4), yet both can entrain clasts and therefore reduce reservoir quality of the injectite. Regarding internal structures, laminar flows lack grading or scouring and produce abruptly tapering dykes and sills and high concentration. These laminar flows can result in the distribution of transported mud clasts at both the top and base of sills (Chapter 4; Macdonald and Flecker, 2007; Hurst *et al.*, 2011). Turbulent flows, in contrast, produce injectites that contain large clasts, normal grading and internal lamination (Obermeier, 1996; Duranti and Hurst, 2004; Hubbard *et al.*, 2007; Scott *et al.*, 2009; Hurst *et al.*, 2011; Sherry *et al.*, 2012; Ross *et al.*, 2014).

Post injection, injectites can act as long-lived fluid flow conduits (Jonk *et al.*, 2005b, 2005c, 2007; Ross *et al.*, 2014) up to depths of approximately 1 km (Jonk *et al.*, 2005a; Jonk, 2010) prior to cementation. Many of the large-scale injectite networks in the Tertiary of the North Sea have maintained excellent reservoir properties (Hurst and Cartwright, 2007) and can themselves form hydrocarbon reservoirs (Schwab *et al.*, 2015; Hurst *et al.* 2016). However, when cemented, injectites become fluid flow barriers, yet fluid flow may still occur along the contact between injected material and host lithology, or at the point where structural deformation occurs, fracturing the injectite. This fracturing may offer a fluid migration pathway (Jonk *et al.*, 2005a).

9.5.2. Four-way traps

Forced folding above clastic injectites creates a 4-way fold, a potential hydrocarbon trap configuration. An understanding of the timing of events and folded lithology is necessary in order to predict whether and when this trap type may be hydrocarbon charged (Hansen and Cartwright, 2006b). Underlying clastic injectites form part or complete migration pathway for hydrocarbons from a deeper source.

9.5.3. Sub-seismic predictability

Clastic injection has a major impact on hydrocarbon exploration and development in deep-marine deposits. Deep-water stratigraphic traps have been a prime target for hydrocarbon exploration (Halbouty, 1966; Walker, 1978; Brown *et al.*, 1995; Gardiner, 2006; Stoker *et al.*, 2006; Nagatomo and Archer, 2015), in particular, proximal turbidites on the basin floor. Typically, they comprise clean sands that pinch out abruptly, providing an optimal trap configuration. However it is this configuration of sand-prone strata that is prone to injection, particularly on a sub-seismic scale. The presence of clastic injectites at stratigraphic traps can be beneficial, they can provide connection between otherwise separated sand units, allowing flow of hydrocarbons through impermeable shale, and balancing pressure differences across reservoir complexes. However, the complicated geometry of injectites and their potential to connect otherwise separate sand bodies needs to be taken into consideration when building reservoir models and when using outcrops as analogues for geological and petrophysical model development. In Chapter 6, six injectite morphotypes are identified across seismic and at outcrop, the link between these datasets aids in identification of injectites in the subsurface, and applying sub-seismic-scale detail to the interpretation of injectite complexes.

9.5.4. Sediment reworking and carbon reduction

Chapter 7 demonstrates that injectites, and potentially surrounding sediments, may be reworked in the form of bioturbation post injectite deposition. Sediment ingestion and excretion is known to alter the physical characteristics and potentially mineralogy of sediment through, for example, development of clay rims on sand grains (Needham *et al.*, 2005) reducing porosity. This process of bioturbation contributes as a significant driver during diagenetic evolution of sandstones; organisms, through bioturbation, are capable of degrading primary mineral assemblages and producing newly formed clay minerals in their place (Needham *et al.*, 2005).

Though small-scale, this still impacts grain alignment and carbon preservation, and should be taken into consideration when modelling shallow-emplaced injectites. Results in Chapter 7 show that macrofaunal organisms with a slow metabolism rate would have access to oxygen for up to 270 days post injection (Fig. 7.2), which is more than sufficient to produce the traces observed and for macrofauna to rework sediment and ingest nutrients that would have otherwise been preserved.

9.6. Conclusions

The emplacement of clastic injectites is a complicated process with multiple pre-, syn- and post-event factors controlling resultant distribution architecture and character. Previously, individual examples, case studies, or specific injectite morphologies have been analysed and explained. Here, studies and data from worldwide have been synthesised in order to review injectites on all scales, at all depths, and how this affects predictability and reservoir quality.

Injectites can be categorised by depth of emplacement into near surface (< 10 m), shallow (10-500 m) and deep (>500 m). However, a wide range of factors need to be taken into consideration when discussing injectite emplacement mechanisms, depth alone does not control final injectite architecture. Large-scale controls include parent sand architecture, how the injectites are fed, whether direct from the parent sand or via dykes cross-cutting large amounts of stratigraphy, the overburden and how this reacts to underlying intrusion, and pre-existing faults in host strata. Small-scale heterogeneities within host sediment and the flow regime during injection also play a part in the final injectite morphology. From these controlling factors, it is possible to build a model for the geographic prediction and style on injectites in deep-marine environments. Injectites formed on the slope, mostly sourced from channel- and gully-fills produce wing-like and high angled injectites of considerable thickness. Whereas injectites sourced from base-of-slope lobes will be thinner and often more laterally extensive.

The models presented here are of value in assessing and predicting mechanisms by which injectites have formed and the subsurface and the impacts that different styles may have on hydrocarbon reservoirs.

9.7. Suggestions for future research

This thesis has provided a greater understanding of the emplacement mechanisms and architecture and clastic injectites on a variety of scales. However, new questions now remain to be answered:

This study provides a methodology, developed from outcrop analysis, for determining flow regime during injection, and resultant injectite features and morphologies (see Chapters 4 and 9.3). The integration of outcrop data with experimental modelling would allow for more accurate inferences of flow velocity, regime, and duration of injection for fluidised flow in open conduits versus closed networks.

Analysis of fracture morphologies on injectite margins is based on experimental modelling of fractures in fine grained mediums (Chapter 4). This study could be taken further through physical modelling of fractures formed from with an injected fluidised flow. This would provide insights to fracture propagation, and therefore injectite propagation velocity, whereas previously this has been achieved through theoretical modelling (Duranti, 2007).

In Chapter 5, a holistic model for the palaeogeographic setting of injectites in base-of-slope lobes is presented. This used detailed outcrop data of both parent sand architecture and injectite geometries. To extend this approach for clastic injectites in other deep marine settings would be key in improving the predictive nature of injectites relating to, for example, slope channels, where spatial distribution of sub-seismic injectite geometries could then be incorporated into geological modelling in known marine settings in hydrocarbon exploration.

It is clear from Chapter 7 that forward modelling of clastic injectites at outcrop can aid in identification and interpretation of injectites in the subsurface. To expand on this by forward modelling more injectite geometries from outcrop examples across various depositional environments would give a more thorough record of types of injectite architectures to be expected over multiple depositional settings.

Reference list

- Allen, J.R.L. (1982) *Sedimentary Structures: Their Character and Physical Basis*. Volume 1. *Developments in Sedimentology 30A*, Elsevier, Amsterdam, 663.
- Allen, J.R.L. (2001) *Principles of Physical Sedimentology: Reprint of first edition (1985), with corrections*. Blackburn Press, Caldwell, 272.
- Ahmadi, Z.M., Sawyers, M., Kenyon-Roberts, S., Stanworth, C.W., Kugler, K.A., Kristensen, J. and Fugelli, E.M.G. (2003) Palaeocene. In: *The Millennium Atlas: Petroleum Geology of the Central and Northern North Sea*. (Eds. Evans, D., Graham, C., Armour A. and Bathurst, P.), Geological Society, London, 552-561.
- Andresen, K.J., Clausen, O.R., and Huuse, M. (2009) A giant (5.3× 10⁷ m³) middle Miocene (c. 15Ma) sediment mound (M1) above the Siri Canyon, Norwegian–Danish Basin: Origin and significance. *Marine and Petroleum Geology*, 26, 1640-1655.
- Anselmetti, F.S., Eberli, G.P. and Bernoulli, D. (1997) Seismic modelling of a carbonate platform margin (Montagna della Maiella, Italy): variations in seismic facies and implications for sequence stratigraphy. In: *Carbonate Seismology*. (Eds. Palaz, I. and Marfurt, K.J.), *SEG Geophysical Development Series*, 6, 373-406.
- Aubertin, M. and Simon, R. (1997) A damage initiation criterion for low porosity rocks. *International Journal of Rock Mechanics and Mining Sciences*, 34, Paper no. 017.
- Archer, J.B. (1984). Clastic intrusions in deep-sea fan deposits of the Rosroe Formation, Lower Ordovician, western Ireland. *Journal of Sedimentary Research*, 54, 1197-1205.
- Armitage, D.A. and Stright, L. (2010) Modeling and interpreting the seismic-reflection expression of sandstone in an ancient mass-transport deposit dominated deep-water slope environment. *Marine and Petroleum Geology*, 27, 1-12.
- Aydin, A. (2000) Fractures, faults, and hydrocarbon entrapment, migration and flow. *Marine and Petroleum Geology*, 17, 797-814.
- Bahat, D. (1986) Criteria for the differentiation of en échelons and hackles in fractured rocks. *Tectonophysics*, 121, 197-206.
- Bahat, D. (2001) Changes of crack velocities at the transition from the parent joint through the en échelon fringe to a secondary mirror plane. *Journal of Structural Geology*, 23, 1215-1221.
- Bahat, D., Rabinovitch, A. and Frid, V. (2005) *Tensile Fracturing in Rocks*: Springer-Verlag, Berlin, 365 – 367.

- Bain, H.A. and Hubbard, S.M. (2016) Stratigraphic evolution of a long-lived submarine channel system in the Late Cretaceous Nanaimo Group, British Columbia, Canada. *Sedimentary Geology*, 337, 113-132.
- Bakke, K., Gjelberg, J. and Petersen, S.A. (2008) Compound modelling of the Ainsa II turbidite system, Spain: Application to deep-water channel systems offshore Angola. *Marine and Petroleum Geology*, 25, 1058-1073.
- Bakke, K., Kane, I.A., Martinsen, O.J., Petersen, S.A., Johansen, T.A, Hustoft, Jacobsen, F.H. and Groth, A. (2013) Seismic modelling in the analysis of deep-water sandstone termination styles. *AAPG Bulletin*, 97, 1395-1419.
- Baldwin, B. and Butler, C.O. (1985) Compaction curves. *AAPG Bulletin*, 69, 622-626.
- Beard, D.C. and Weyl, P.K. (1973) Influence of texture on porosity and permeability of unconsolidated sand. *AAPG Bulletin*, 57, 349-369.
- Ben-Zion, Y. and Morrisey, J. (1995) A simple re-derivation of logarithmic disordering of a dynamic planar crack due to small random heterogeneities. *Journal of the Mechanics and Physics of Solids*, 43, 1363-1368.
- Bentley, M. and Smith, S. (2008) Scenario-based reservoir modelling: the need for more determinism and less anchoring. In: *The Future of Geological Modelling in Hydrocarbon Development*. (Eds. Robinson, A., Griffiths, P., Price, S., Hegre, J. and Muggeridge, A.), *Geological Society of London Special Publication*, 309, 145-159.
- Bezerra, F.H.R., da Fonseca, V.P., Vita-Finzi, C., Lima-Filho, F.P. and Saadi, A. (2005) Liquefaction-induced structures in Quaternary alluvial gravels and gravelly sediments, NE Brazil. *Engineering Geology*, 76, 191-208.
- Biddle, K.T., Schlager, W., Rudolph, K.W. and Bush, T.L. (1992) Seismic model of a progradational carbonate platform, Picco di Vallandro, the Dolomites, Northern Italy. *AAPG Bulletin*, 76, 14-30.
- Bjørlykke, K. (1993) Fluid flow in sedimentary basins. *Sedimentary Geology*, 86, 137-158.
- Boehm, A. and Moore, J.C. (2002) Fluidized sandstone intrusions as an indicator of paleostress orientation, Santa Cruz, California. *Geofluids*, 2, 147-161.
- Bonham, L.C. (1980) Migration of hydrocarbons in compacting basins. *AAPG Bulletin*, 64, 549-567.
- Bugge, T., Tveiten, B. and Bäckström, S. (2001) The depositional history of the Cretaceous in the northeastern North Sea. *Norwegian Petroleum Society Special Publications*, 10, 279-291.
- Brown, L.F., Benson, J.M., Brink, G.J., Doherty, S., Jollands, A., Jungslager, E.H.A., Keenan, J.H.G, Muntingh, A. and van Wyk, N.J.S. (1995) Sequence Stratigraphy in Offshore South African

- Divergent Basins: An Atlas on Exploration for Cretaceous Lowstand Traps by Soekor (Pty) Ltd, *AAPG Studies in Geology*, 41, AAPG, Tulsa, Oklahoma.
- Brunt, R.L., Hodgson, D.M., Flint, S.S., Pringle, J.K., Di Celma, C., Pr lat, A. and Grecula, M. (2013) Confined to unconfined: anatomy of a base of slope succession, Karoo Basin, South Africa. *Marine and Petroleum Geology*, 41, 206-221.
- Bureau, D., Mourges, R. and Cartwright, J. (2014) Use of a new artificial cohesive material for physical modelling: application to sandstone intrusions and associated fracture networks. *Journal of structural geology*, 66, 223-236.
- Bussel, M.A. (1989) A simple method for the determination of the dilation direction of intrusive sheets. *Journal of Structural Geology*, 11, 679-687.
- Campbell, A.E. and Stafleu, J. (1992) Seismic modeling of an Early Jurassic, drowned carbonate platform: Djebel Bou Dahar, High Atlas, Morocco. *AAPG Bulletin*, 76, 1760-1777.
- Cartwright, J.A. (1994) Episodic basin-wide fluid expulsion from geopressed shale sequences in the North Sea basin. *Geology*, 22, 447-450.
- Cartwright, J.A. and Lonergan, L. (1996) Volumetric contraction during the compaction of mudrocks: A mechanism for the development of regional-scale polygonal fault systems. *Basin Research*, 8, 183-193.
- Cartwright, J., James, D., Huuse, M., Vetel, W. and Hurst, A. (2008) The geometry and emplacement of conical sandstone intrusions. *Journal of Structural Geology*, 30, 854-867.
- Cartwright, J. (2010) Regionally extensive emplacement of sandstone intrusions: a brief review. *Basin Research*, 22, 502-516.
- Castagna, J.P., Batzle, M.L. and Kan, T.K. (1993) Rock physics—the link between rock properties and AVO response. In: *Offset-Dependent Reflectivity—Theory and Practice of AVO Analysis*. (Eds. Castagna, P. and Backus, M.M.), *Investigations in Geophysics Series, Society of Exploration Geophysicists*, 8, 124–157.
- Catuneanu, O., Hancox, P.J. and Rubidge, B.S. (1998) Reciprocal flexural behaviour and contrasting stratigraphies: a new basin development model for the Karoo retroarc foreland system, South Africa. *Basin Research*, 10, 417-439.
- Chapman, R.E. (1972) Primary migration of petroleum from clay source rocks. *AAPG Bulletin*, 56, 2185-2191.
- Chapman, R.E. (1987) Fluid flow in sedimentary basins: a geologist's perspective. In: *Fluid flow in Sedimentary Basins and Aquifers*. (Eds. Goff, J.C. and Williams, B.P.J.), *Geological Society of London Special Publications*, 34, 3-18.

- Chan, M., Netoff, D., Blakey, R., Kocurek, G. and Alvarez, W. (2007) Clastic-injection pipes and syndepositional deformation structures in Jurassic eolian deposits: Examples from the Colorado Plateau. In: *Sand Injectites: Implications for Hydrocarbon Exploration and Production*. (Eds. Hurst, A. and Cartwright, J.), *AAPG Memoir*, 87, 233-244.
- Charlez, P.A. (1991) *Rock Mechanics, Volume 1, Theoretical Fundamentals*. Technip.
- Chemenda, A.I., Nguyen, S.H., Petit, J.P. and Ambre, J. (2011) Experimental evidences of transition from mode I cracking to dilatancy banding. *Comptes Rendus Mecanique*, 339, 219-225.
- Cheret, T. and Carrillat, A. (2004) Seismic Scale Sand Injectites in the North Sea. *SPE Annual Technical Conference and Exhibition*. Houston, Texas, 26-29 September. *Society of Petroleum Engineers*.
- Chevallier, L. and Woodford, A. (1999) Morpho-tectonics and mechanism of emplacement of the dolerite rings and sills of the western Karoo, South Africa. *South African Journal of Geology*, 102, 43-54.
- Chough, S.K. and Chun, S.S. (1988) Intrastratal rip-downclasts, Late Cretaceous Uhangri Formation, southwest Korea. *Journal of Sedimentary Petrology*, 58, 530-533.
- Cobain, S.L., Peakall, J. and Hodgson, D.M. (2015) Indicators of propagation direction and relative depth in clastic injectites: Implications for laminar versus turbulent flow processes. *Geological Society of America Bulletin*, 127, 1816-1830.
- Cobbold, P. and Castro, L. (1999) Fluid pressure and effective stress in sandbox models. *Tectonophysics*, 301, 1-19.
- Cosgrove, J.W. (1995) The expression of hydraulic fracturing in rocks and sediments. In: *Fractography: Fracture Topography as a Tool in Fracture Mechanics and Stress Analysis*. (Ed. M.S. Ameen), *Geological Society of London Special Publications*, 92, 187-196.
- Cosgrove, J.W. (2001) Hydraulic fracturing during the formation and deformation of a basin: a factor in the dewatering of low-permeability sediments: *AAPG Bulletin*, 85, 737-748.
- Cosgrove, J.W. and Hillier, R.D. (1999) Forced-fold development within Tertiary sediments of the Alba Field, UKCS: evidence of differential compaction and post-depositional sandstone remobilization. In: *Forced folds and fractures*. (Eds. Cosgrove, J.W. and Ameen, M.S.). *Geological Society, London, Special Publications*, 169, 61-71.
- Cruden, A. and Bungler, A. (2010) Emplacement dynamics of laccoliths, sills and dykes from dimensional scaling and mechanical models. In: *Physical Geology of Subvolcanic Systems - LASI 4 Conference: Laccoliths, Sills and Dykes*. (Eds. Morgan, S., Horsman, E., de Saint Blanquat, M. and Tikoff, M.), Central Michigan University, 15-16.

- Curray, J.R., Emmel, F.J. and Moore, D.G. (2002) The Bengal Fan: morphology, geometry, stratigraphy, history and processes. *Marine and Petroleum Geology*, 19, 1191-1223.
- Curtis, M.L. and Riley, T.R. (2003) Mobilization of fluidized sediment during sill emplacement, western Dronning Maud Land, East Antarctica. *Antarctic Science*, 15, 393-398.
- Davies, R.J., Huuse, M., Hirst, P., Cartwright, J. and Yang, Y. (2006) Giant clastic intrusions primed by silica diagenesis. *Geology*, 34, 917-920.
- de Boer, W., Hurst, A. and Rawlinson, P.B. (2007) Successful exploration of a sand injectites complex: Hamsun Prospect, Norway Block 24/9. In: *Sand Injectites: Implications for Hydrocarbon Exploration and Production*. (Eds. Hurst, A. and Cartwright, J.), AAPG Memoir, 87, 65-78.
- de Vallejo, L.I.G., Tsigé, M. and Cabrera, L. (2005) Paleoliquefaction features on Tenerife (Canary Islands) in Holocene sand deposits. *Engineering geology*, 76, 179-190.
- Delaney, P.T., Pollard, D.D., Ziony, Joseph.I. and Mckee, E.H. (1986) Field relations between dikes and joints: Emplacement processes and paleostress analysis. *Journal of Geophysical Research*, 91, 4920-4938.
- Di Celma, C.N., Brunt, R.L., Hodgson, D.M., Flint, S.S. and Kavanagh, J.P. (2011) Spatial and temporal evolution of a Permian submarine slope channel–levee system, Karoo Basin, South Africa. *Journal of Sedimentary Research*, 81, 579-599.
- Di Felice, R. (2010) Liquid–solid suspension theory with reference to possible applications in geology. *Basin Research*, 22, 591–602.
- Diggs, T.N. (2007) An outcrop study of clastic injection structures in the Carboniferous Tesnus Formation, Marathon basin, Trans-Pecos Texas. In: *Sand Injectites: Implications for Hydrocarbon Exploration and Production*. (Eds. Hurst, A. and Cartwright, J.), AAPG Memoir, 87, 209-219.
- Diller, J.S. (1890) Sandstone dikes. *Bulletin of the Geological Society of America*, 1, 411-442.
- Dixon, R.J., Schofield, K., Anderton, R., Reynolds, A.D., Alexander, R.W.S., Williams, M.C. and Davies, K.G. (1995) Sandstone diapirism and clastic intrusion in the Tertiary submarine fans of the Bruce-Beryl Embayment, Quadrant 9, UKCS. *Geological Society of London Special Publications*, 94, 77-94.
- Dott, R.H. (1966) Cohesion and flow phenomena in clastic intrusions. *AAPG Bulletin*, 50, 610-611.
- Duranti, D., Hurst, A., Bell, C., Groves, S., and Hanson, R. (2002) Injected and remobilized Eocene sandstones from the Alba Field, UKCS: core and wireline log characteristics. *Petroleum Geoscience*, 8, 99-107.

- Duranti, D. and Hurst, A. (2004) Fluidization and injection in the deep-water sandstones of the Eocene Alba Formation (UK North Sea). *Sedimentology*, 51, 503-529.
- Duranti, D. and Mazzini, A. (2005) Large-scale hydrocarbon-driven sand injection in the Paleogene of the North Sea. *Earth and Planetary Science Letters*, 239, 327-335.
- Duranti, D. (2007) Large-scale sand injection in the Paleogene of the North Sea: Modeling of energy and flow velocities. In: *Sand Injectites: Implications for Hydrocarbon Exploration and Production*, (Eds. Hurst, A. and Cartwright, J.), *AAPG Memoir*, 87, 129-139.
- Dzulynski, S. and Radomski, A. (1956) Clastic dikes in the Carpathian Flysch. *Annales de la Socié'te' Ge'ologique de Pologne*, 26, 225-264.
- Faisst, H. and Eckhardt, B. (2004) Sensitive dependence on initial conditions in transition to turbulence in pipe flow. *Journal of Fluid Mechanics*, 504, 343-352.
- Falivene, O., Arbués, P., Ledo, J., Benjumea, B., Muñoz, J.A., Fernández, O. and Martinez, S. (2010) Synthetic seismic models from outcrop-derived reservoir-scale three-dimensional facies models: The Eocene Ainsa turbidite system (southern Pyrenees). *AAPG Bulletin*, 94, 317-343.
- Faules, G. and Boyes, W.H. (2009) Measurement of flow. In: *Instrumentation Reference Book*, (Ed. Boyes, W.H.), *Butterworth-Heinemann*, 31-68.
- Faure, K. and Cole, D. (1999) Geochemical evidence for lacustrine microbial blooms in the vast Permian Main Karoo, Paraná, Falkland Islands and Huab basins of southwestern Gondwana. *Palaeogeography, Palaeoclimatology, Palaeoecology*, 152, 189-213.
- Figueiredo J.J.P., Hodgson, D.M., Flint, S.S. and Kavanagh, J.P. (2010) Depositional environments and sequence stratigraphy of an exhumed Permian mudstone-dominated submarine slope succession, Karoo Basin, South Africa. *Journal of Sedimentary Research*, 80, 97-118.
- Fildani, A., Drinkwater, N.J., Weislogel, A., McHargue, T., Hodgson, D.M. and Flint, S.S. (2007) Age controls on the Tanqua and Laingsburg deep-water systems: New insights on the evolution and sedimentary fill of the Karoo basin, South Africa. *Journal of Sedimentary Research*, 77, 901-908.
- Fineberg, J. and Marder, M. (1999) Instability in dynamic fracture. *Physics Reports*, 313, 1-108.
- Flemings, P.B., Stump, B.B., Finkbeiner, T. and Zoback, M. (2002) Flow focusing in overpressured sandstones: Theory, observations, and applications. *American Journal of Science*, 302, 827-855.
- Flint, S.S., Hodgson, D.M., Sprague, A.R., Brunt, R.L., Van der Merwe, W.C., Figueiredo, J., Prélat, A., Box, D., Di Celma, C. and Kavanagh, J.P. (2011) Depositional architecture and sequence

- stratigraphy of the Karoo basin floor to shelf edge succession, Laingsburg depocentre, South Africa. *Marine and Petroleum Geology*, 28, 658-674.
- Föllmi, K.B. and Grimm, K.A. (1990) Doomed pioneers: Gravity-flow deposition and bioturbation in marine oxygen-deficient environments. *Geology*, 18, 1069-1072.
- Fossen, H. (2010) *Structural Geology*. Cambridge University Press, Cambridge, 123-125.
- Frey-Martínez, J., Cartwright, J., Hall, B. and Huuse, M. (2007) Sand Injectites: Implications for Hydrocarbon Exploration and Production. In: *Sand Injectites: Implications for Hydrocarbon Exploration and Production*. (Eds. Hurst, A. and Cartwright, J.), *AAPG Memoir*, 87, 49-63.
- Friedmann, S.J., Vrolijk, P.J., Ying, X., Desphande, A., Moir, G. and Mohrig, D.C. (2002) Quantitative analysis of sandstone intrusion networks, Panoche Hills, California (abs.). *AAPG Annual Meeting Program*, 11, A59.
- Gage, J.D. and Tyler, P.A. (1991) *Deep-sea biology: A natural history of organisms at the deep-sea floor*. Cambridge University Press, Cambridge.
- Galland, O., Planke, S., Neumann, E.R. and Malthe-Sørensen, A. (2009) Experimental modelling of shallow magma emplacement: application to saucer-shaped intrusions. *Earth and Planetary Science Letters*, 277, 373-383.
- Galland, O., Burchardt, S., Hallot, E., Mourgues, R. and Bulois, C. (2014) Dynamics of dikes versus cone sheets in volcanic systems. *Journal of Geophysical Research: Solid Earth*, 119, 6178-6192.
- Gallo, F., and Woods, A.W. (2004) On steady homogeneous sand-water flows in a vertical conduit. *Sedimentology*, 51, 195-210.
- Galloway, W.E., Garber, J.L., Liu, X. and Sloan, B.J. (1993) Sequence stratigraphic and depositional framework of the Cenozoic fill, Central and Northern North Sea Basin. In: *Petroleum Geology Conference series: Proceedings of the 4th Conference*, (Ed. J.R. Parker), *The Geological Society of London*, 33-44.
- Gardiner, A.R. (2006) The variability of turbidite sandbody pinchout and its impact on hydrocarbon recovery in stratigraphically trapped fields. In: *The Deliberate Search for the Stratigraphic Trap*. (Ed. Allen, M. R.), *Geological Society of London Special Publications*, 254, 267-287.
- Gay, A., Takano, Y., Gilhooly Iii, W.P., Berndt, C., Heeschen, K., Suzuki, N., Saegusa, S., Nakagawa, F., Tsunogai, U., Jiang, S.Y. and Lopez, M. (2010) Geophysical and geochemical evidence of large scale fluid flow within shallow sediments in the eastern Gulf of Mexico, offshore Louisiana. *Geofluids*, 11, 34-47.

- Glud, R.N., Gundersen, J.K., Jørgensen B.B., Revsbech, N.P. and Schulz, H.D. (1994) Diffusive and total oxygen uptake of deep-sea sediments in the eastern South Atlantic Ocean: *in situ* and laboratory measurements. *Deep Sea Research Part I: Oceanographic Research Papers*, 41, 1767-1788.
- González de Vallejo, L.I., Tsigé, M. and Cabrera, L. (2005) Paleoliquefaction features on Tenerife (Canary Islands) in Holocene sand deposits. *Engineering geology*, 76, 179-190.
- Goodall, I., Lofts, J., Mulcahy, M., Ashton, M. and Johnson, S. (1999) A sedimentological application of ultrasonic borehole images in complex lithologies: the Lower Kimmeridge Clay Formation, Magnus Field, UKCS. In: *Borehole Imaging: applications and case histories*. (Eds. Lovell, M.A., Williamson, G. and Harvey, P.K.), *Geological Society London Special Publications*, 159, 203-225.
- Gouly, N.R. and Schofield, N. (2008) Implications of simple flexure theory for the formation of saucer-shaped sills. *Journal of Structural Geology*, 30, 812-817.
- Gressier, J.B., Mourgues, R., Bodet, L., Mathieu, J.Y., Galland, O. and Cobbold, P.R. (2010) Control of pore fluid pressure on depth of emplacement of magmatic sills: an experimental approach. *Tectonophysics*, 489, 1-13.
- Groenenberg, R.M., Hodgson, D.M., Prélat, A., Luthi, S.M. and Flint, S.S. (2010) Flow–deposit interaction in submarine lobes: insights from outcrop observations and realizations of a process-based numerical model. *Journal of Sedimentary Research*, 3, 252-267.
- Guhman, A.I. and Pederson, D.T. (1992) Boiling sand springs, Dismal River, Nebraska: Agents for formation of vertical cylindrical structures and geomorphic change. *Geology*, 1, 8-10.
- Halbouty, M.T. (1966) Stratigraphic-trap possibilities in Upper Jurassic rocks, San Marcos Arch, Texas. *AAPG Bulletin*, 50, 3-24.
- Hamberg, L., Jepsen, A.M., Borch, N.T., Dam, G., Engkilde, M.K. and Svendsen, J.B. (2007) Mounded structures of injected sandstones in deep-marine Paleocene reservoirs, Cecile Field, Denmark. In: *Sand Injectites: Implications for Hydrocarbon Exploration and Production*. (Eds. Hurst, A. and Cartwright, J.), *AAPG Memoir*, 87, 69–79.
- Hansen, D.M., Cartwright, J.A. and Thomas, D. (2004) 3D seismic analysis of the geometry of igneous sills and sill junction relationships. *Geological Society of London Memoirs*, 29, 199-208.
- Hansen, D.M. and Cartwright, J. (2006a) Saucer-shaped sill with lobate morphology revealed by 3D seismic data: implications for resolving a shallow-level sill emplacement mechanism. *Journal of the Geological Society*, 163, 509-523.

- Hansen, D.M. and Cartwright, J. (2006b) The three-dimensional geometry and growth of forced folds above saucer-shaped igneous sills. *Journal of Structural Geology*, 28, 1520-1535.
- Hellend-Hansen, W., Helle, H.B. and Sunde, K. (1994) Seismic modelling of Tertiary sandstone clinothems, Spitsbergen. *Basin Research*, 6, 181-191.
- Hillier, R.D. and Cosgrove, J.W. (2002) Core and seismic observations of overpressure-related deformation within Eocene sediments of the Outer Moray Firth, UKCS. *Petroleum Geoscience*, 28, 149-170.
- Hiscott, R. (1979) Clastic sills and dikes associated with deep-water sandstones, Tourelle Formation, Ordovician, Quebec. *Journal of Sedimentary Petrology*, 49, 1-10.
- Hodgetts, D. and Howell, J.A. (2000) Synthetic seismic modelling of a large-scale geological cross-section from the Book Cliffs, Utah, USA. *Petroleum Geoscience*, 6, 221-229.
- Hodgetts, D., Drinkwater, N.J., Hodgson, D.M., Kavanagh, J., Flint, S.S., Keogh, K.J. and Howell, J.A. (2004) Three-dimensional geological models from outcrop data using digital data collection techniques: an example from the Tanqua Karoo depocentre, South Africa. In: *Geological Prior Information Science and Engineering*. (Eds. Curtis, A. and Wood, R.), *Geological Society of London Special Publications*, 239, 57-75.
- Hodgson, R.A. (1961) Classification of structures on joint surfaces. *American Journal of Science*, 259, 493-502.
- Hodgson, D.M. (2009) Distribution and origin of hybrid bEds.in sand-rich submarine fans of the Tanqua depocentre, Karoo Basin, South Africa. *Marine and Petroleum Geology*, 26, 1940-1956.
- Hodgson, D.M., Flint, S.S., Hodgetts, D., Drinkwater, N.J., Johannessen, E.P. and Luthi, S.M. (2006) Stratigraphic evolution of fine-grained submarine fan systems, Tanqua Depocenter, Karoo Basin, South Africa. *Journal of Sedimentary Research*, 76, 20-40.
- Hodgson, D.M., Di Celma, C.N., Brunt, R.L. and Flint, S.S. (2011a) Submarine slope degradation and aggradation and the stratigraphic evolution of channel–levee systems. *Journal of the Geological Society*, 168, 625-628.
- Hodgson, D.M., van der Merwe, W.C. and Flint, S.S. (2011b) Distribution of submarine mass movement deposits: an exhumed basin perspective. In: *Advances in Natural and Technological Hazards Research - Submarine Mass Movements and Their Consequences* (Eds. Yamada, Y., Kawamura, K., Ikehara, K. Ogawa, Y., Ureles, R., Mosher, D., Chaytor J. and Strasser, M.) *4th Edition*, 619-628.
- Hodgson, D.M., Kane, I.A., Flint, S.S., Brunt, R.L. and Ortiz-Karpf, A. (2016). Time-transgressive confinement on the slope and the progradation of basin-floor fans: Implications for the

- sequence stratigraphy of deep-water deposits. *Journal of Sedimentary Research*, 86, 73-86.
- Hofstra, M., Hodgson, D.M., Peakall, J. and Flint, S.S. (2015) Giant scour-fills in ancient channel-lobe transition zones: Formative processes and depositional architecture. *Sedimentary Geology*, 329, 98-114.
- Hogg, A.J. (1994) The inertial migration of non-neutrally buoyant spherical particles in two-dimensional shear flows. *Journal of Fluid Mechanics*, 272, 285-318.
- Holgate, N.E., Hampson, G.J., Jackson, C.A.-L. and Petersen, S.A. (2014) Constraining uncertainty in interpretation of seismically imaged clinofolds in deltaic reservoirs, Troll Field, Norwegian North Sea: Insights from forward seismic models of outcrop analogs. *AAPG Bulletin*, 98, 2629-2663.
- Horsrud, P. (2001) Estimating mechanical properties of shale from empirical correlations. *SPE Drilling and Completion*, 16, 68-73.
- Hubbard, S.M., Romans, B.W. and Graham, S.A. (2007) An outcrop example of large-scale conglomeratic intrusions sourced from deep-water channel deposits, Cerro Toro Formation, Magallanes basin, southern Chile. In: *Sand Injectites: Implications for Hydrocarbon Exploration and Production*. (Eds. Hurst, A. and Cartwright, J.), *AAPG Memoir*, 87, 199-207.
- Hubbert, M.K. (1937) Theory of scale models as applied to the study of geologic structures. *Geological Society of America Bulletin*, 48, 1459-1520.
- Hubbert, M.K. (1951) Mechanical basis for certain familiar geologic structures. *Geological Society of America Bulletin*, 62, 355-372.
- Hubbert, M.K. and Willis, D.G. (1957) Mechanics of hydraulic fracturing. *Petroleum Transactions of the American Institute of Mining Engineers*, 210, 153-168.
- Hull, D. (1996) Interpretation of river line patterns on indentation generated fracture surfaces with comments on fractal characteristics described by Djordjevic et al. *Journal of Materials Science Letters*, 15, 651-653.
- Hurst, A., Cartwright, J.A. and Duranti, D. (2003) Fluidization structures produced by upward injection of sand through a sealing lithology. In: *Subsurface Sediment Mobilization: Special Publication*. (Eds. P. Van Rensbergen, R.R. Hillis, A.J. Maltman, C.K. Morley, C.K.), *Geological Society of London*, 216, 123-137.
- Hurst, A., Cartwright, J., Huuse, M., Jonk, R., Schwab, A., Duranti, D. and Cronin, B. (2003) Significance of large-scale sand injectites as long-term fluid conduits: evidence from seismic data. *Geofluids*, 3, 263-274.

- Hurst, A., Cartwright, J.A., Duranti, D., Huuse, M. and Nelson, M. (2005) Sand injectites: an emerging global play in deep-water clastic environments. In: *Petroleum Geology: North-West Europe and Global Perspectives—Proceedings of the 6th Petroleum Geology Conference*. (Eds. Doré, A.G. and Vining, B.A.), *Geological Society of London*, 6, 133-144.
- Hurst, A., Cartwright, J.A., Huuse, M. and Duranti, D. (2006) Extrusive sandstones (extrudites): a new class of stratigraphic trap?. *Geological Society of London Special Publications*, 254, 289-300.
- Hurst, A. and Cartwright, J.A. (2007) Relevance of sand injectites to hydrocarbon exploration and production. In: *Sand Injectites: Implications for Hydrocarbon Exploration and Production*. (Eds. Hurst, A. and Cartwright, J.), *AAPG Memoir*, 87, 1-20.
- Hurst, A., Scott, A. and Vigorito, M. (2011) Physical characteristics of sand injectites. *Earth-Science Reviews*, 106, 215-246.
- Hurst, A., Huuse, M., Duranti, D., Vigorito, M., Jameson, E. and Schwab, A. (2016) Application of outcrop analogues in successful exploration of a sand injection complex, Volund Field, Norwegian North Sea. In: *The Value of Outcrop Studies in Reducing Subsurface Uncertainty and Risk in Hydrocarbon Exploration and Production*. (Eds. Bowman M., Smyth R.R., Good T.R., Passey S.R., Hirst J.P.P and Jordan C.J.), *Geological Society of London Special Publications*, 436.
- Huuse, M. (2008) Sandstone intrusions: implications for exploration and production. *World Oil*, 229, 87-91.
- Huuse, M. and Mickelson, M. (2004) Eocene sandstone intrusions in the Tampen Spur area (Norwegian North Sea Quad 34) imaged by 3D seismic data. *Marine and Petroleum Geology*, 21, 141-155.
- Huuse, M., Duranti, D., Steinsland, N., Guargena, C.G., Prat, P., Holm, K., Cartwright, J.A. and Hurst, A., (2004) Seismic characteristics of large-scale sandstone intrusions in the Paleogene of the South Viking Graben, UK and Norwegian North Sea. In: *3D Seismic Technology: Application to the Exploration of Sedimentary Basins*. (Eds. Davies, R.J., Cartwright, J., Stewart, S.A., Underhill, J.R. and Lappin, M.), *Geological Society Memoir*, 29, 263–277.
- Huuse, M., Cartwright, J.A., Gras, R. and Hurst, A. (2005a) Kilometre-scale sandstone intrusions in the Eocene of the Outer Moray Firth (UK North Sea): migration paths, reservoirs and potential drilling hazards. In: *Petroleum Geology: North-West Europe and Global Perspectives—Proceedings of the 6th Petroleum Geology Conference* (Eds. Doré, A.G. and Vining, B.A.), *Geological Society of London*, 1577–1594.

- Huuse, M., Shoulders, S., Netoff, D. and Cartwright, J. (2005b) Giant sandstone pipes record basin-scale liquefaction of buried dune sands in the Middle Jurassic of SE Utah. *Terra Nova*, 17, 80-85.
- Huuse, M., Cartwright, J., Hurst, A. and Steinsland, N. (2007) Seismic characterization of large-scale sandstone intrusions. In: *Sand Injectites: Implications for Hydrocarbon Exploration and Production*. (Eds. Hurst, A. and Cartwright, J.), *AAPG Memoir*, 87, 21-36.
- Huuse, M., Jackson, C. A. L., Van Rensbergen, P., Davies, R. J., Flemings, P. B. and Dixon, R. J. (2010) Subsurface sediment remobilization and fluid flow in sedimentary basins: an overview. *Basin Research*, 4, 342-360.
- Ito, M., Ishimoto, S., Ito, K., and Kotake, N. (2016) Geometry and lithofacies of coarse-grained injectites and extrudites in a late Pliocene trench-slope basin on the southern Boso Peninsula, Japan. *Sedimentary Geology*. *In press*.
- Jackson, C.A.L. (2007) The geometry, distribution, and development of clastic injections in slope systems: seismic examples from the upper cretaceous Kyrre Formation, Måløy Slope, Norwegian Margin. In: *Sand Injectites: Implications for Hydrocarbon Exploration and Production*. (Eds. Hurst, A. and Cartwright, J.), *AAPG Memoir*, 87, 37-48.
- Jackson, C.A.L., Huuse, M. and Barber, G. (2011) Geometry of winglike clastic intrusions adjacent to a deep-water channel complex: Implications for hydrocarbon exploration and production. *AAPG Bulletin*, 95, 559-584.
- Jenkins, O. P. (1930) Sandstone dikes as conduits for oil migration through shales. *AAPG bulletin*, 14, 411-421.
- Jobe, Z.R., Lowe, D.R. and Morris, W.R. (2012) Climbing-ripple successions in turbidite systems: depositional environments, sedimentation rates and accumulation times. *Sedimentology*, 59, 867-898.
- Johnson, M.R. (1991) Sandstone petrography, provenance and plate tectonic setting in Gondwana context of the southeastern Cape-Karoo Basin. *South African Journal of Geology*, 94, 137-154.
- Johnson, M.R., Van Vuuren, C.J., Visser, J.N.J., Cole, D.I., Wickens, H.D.V., Christie, A.D.M., Roberts, D.L. and Brandl, G. (2006) Sedimentary rocks of the Karoo Supergroup. In: *The Geology of South Africa*. (Eds. Johnson, M.R., Anhaeusser, C.R. and Thomas, R.J.), *Geological Society of South Africa and Council for Geoscience*, 461-499.
- Johnson, A. M. and Pollard, D. D. (1973) Mechanics of growth of some laccolithic intrusions in the Henry mountains, Utah, I: field observations, Gilbert's model, physical properties and flow of the magma. *Tectonophysics*, 18, 261-309.

- Johnson, S.D., Flint, S.S., Hinds, D. and Wickens, H. Dev. (2001) Anatomy of basin floor to slope turbidite systems, Tanqua Karoo, South Africa: Sedimentology, sequence stratigraphy and implications for subsurface prediction. *Sedimentology*, 48, 987–1023.
- Jolly, R. J. and Lonergan, L. (2002) Mechanisms and controls on the formation of sand intrusions. *Journal of the Geological Society*, 159, 605-617.
- Jones, G., Fisher, Q.F. and Knipe, R.J. (1998) Faulting, fault sealing and fluid flow in hydrocarbon reservoirs. *Geological Society of London Special Publications*, 147, 319.
- Jones, G.E.D., Hodgson, D.M. and Flint, S.S. (2013) Contrast in the process response of stacked clinothems to the shelf-slope rollover. *Geosphere*, 9, 299-316.
- Jones, G.E.D., Hodgson, D.M. and Flint, S.S. (2015) Lateral variability in clinoform trajectory, process regime, and sediment dispersal patterns beyond the shelf-edge rollover in exhumed basin margin-scale clinothems. *Basin Research*, 27, 657-680.
- Jonk, R., Duranti, D., Parnell, J., Hurst, A. and Fallick, A. E. (2003) The structural and diagenetic evolution of injected sandstones: examples from the Kimmeridgian of NE Scotland. *Journal of the Geological Society*, 160, 881-894.
- Jonk, R., Parnell, J. and Hurst, A. (2005a) Aqueous and petroleum fluid flow associated with sand injectites. *Basin Research*, 17, 241-257.
- Jonk, R., Hurst, A., Duranti, D., Parnell, J., Mazzini, A. and Fallick, A.E. (2005b) Origin and timing of sand injection, petroleum migration, and diagenesis in Tertiary reservoirs, south Viking Graben, North Sea. *AAPG Bulletin*, 89, 329-357.
- Jonk, R., Parnell, J. and Whitham, A. (2005c) Fluid inclusion evidence for a Cretaceous–Palaeogene petroleum system, Kangerlussuaq Basin, East Greenland. *Marine and Petroleum Geology*, 22, 319-330.
- Jonk, R., Cronin, B.T. and Hurst, A. (2007) Variations in sediment extrusion in basin-floor, slope, and delta-front settings: Sand volcanoes and extruded sand sheets from the Namurian of County Clare, Ireland. In: *Sand Injectites: Implications for Hydrocarbon Exploration and Production*. (Eds. Hurst, A. and Cartwright, J.), *AAPG Memoir*, 87, 221-226.
- Jonk, R., Duranti, D., Hurst, A., Parnell, J. and Fallick, A.E. (2007) Aqueous and petroleum fluids associated with sand injectites hosted by lacustrine shales from the oil-shale group (Dinantian), Midland Valley, Scotland. In: *Sand Injectites: Implications for Hydrocarbon Exploration and Production* (Ed. By A. Hurst and J Cartwright) *AAPG Memoir*, 87, 265-274.
- Jonk, R. (2010) Sand-rich injectites in the context of short-lived and long-lived fluid flow. *Basin Research*, 22, 603-621.

- Jumars, P.A. (1978) Spatial autocorrelation with RUM (Remote Underwater Manipulator): vertical and horizontal structure of a bathyal benthic community. *Deep-Sea Research*, 25, 589-604.
- Kane, I. A. (2010) Development and flow structures of sand injectites: The Hind Sandstone Member injectite complex, Carboniferous, UK. *Marine and Petroleum Geology*, 27, 1200-1215.
- Kane, I.A. and Hodgson, D.M. (2011) Sedimentological criteria to differentiate submarine channel levee subenvironments: Exhumed examples from the Rosario Fm. (Upper Cretaceous) of Baja California, Mexico, and the Fort Brown Fm. (Permian), Karoo Basin, S. Africa. *Marine and Petroleum Geology*, 28, 807-823.
- Karig, D.E., and Hou, G. (1992) High-stress consolidation experiments and their geologic implications. *Journal of Geophysical Research: Solid Earth*, 97, 289-300.
- Kavanagh, J.L., Menand, T. and Sparks, R.S.J. (2006) An experimental investigation of sill formation and propagation in layered elastic media. *Earth and Planetary Science Letters*, 245, 799-813.
- Kawakami, G. and Kawamura, M. (2002) Sediment flow and deformation (SFD) layers: evidence for intrastratal flow in laminated muddy sediments of the Triassic Osawa Formation, northeast Japan. *Journal of Sedimentary Research*, 79, 171-181.
- Keighley, D.G. and Pickerill, R.K. (1994) Flute-like marks and associated structures from the Carboniferous Port Hood Formation of eastern Canada: evidence of secondary origin in association with sediment intrusion. *Journal of Sedimentary Research*, 64, 253-263.
- Keighley, D.G. and Pickerill, R.K. (1994) Flute-like marks and associated structures from the Carboniferous Port Hood Formation of eastern Canada: evidence of secondary origin in association with sediment intrusion. *Journal of Sedimentary Research*, 64.
- Kelly, R.B., Houlsby, G.T. and Byrne, B.W. (2006) Transient vertical loading of model suction caissons in a pressure chamber. *Géotechnique*, 56, 665-675.
- Kilhams, B., Hartley, A., Huuse, M. and Davis, C. (2012) Characterizing the Paleocene turbidites of the North Sea: the Mey Sandstone Member, Lista Formation, UK central graben. *Petroleum Geoscience*, 18, 337-354.
- King, R.C., Hodgson, D.M., Flint, S.S., Potts, G.J. and van Lente, B. (2009) Development of subaqueous fold belts as a control on the timing and distribution of deepwater sedimentation: an example from the southwest Karoo Basin, South Africa. In: *External Controls on Deep-water Depositional Systems*. (Eds. Kneller, B.C., Martinsen O.J. and Mccaffrey, W.), *SEPM Special Publications*, 92, 261-278.

- Knipe, R.J., Jones, G. and Fisher, Q.J. (1998) Faulting, Fault Sealing and Fluid Flow in Hydrocarbon Reservoirs: an introduction In: *Faulting, Fault Sealing and Fluid Flow in Hydrocarbon Reservoirs* (Ed. by G. Jones, Q.J. Fisher & R.J. Knipe). *Geological Society, London Special Publications*, 147, vii-xxi.
- Krieger, I.M. and Dougherty, T.J. (1959) A mechanism for non-Newtonian flow in suspension of rigid spheres. *Transactions of the Society of Rheology*, 3, 137-152.
- Krumbein, W.C. and Monk, G.D. (1942) Permeability as a function of the size parameters of unconsolidated sand. *American Institute of Mining, Metallurgy and Petroleum Engineers, Technical Publication*, 1492, 1-11.
- Le Heron, D.P. and Etienne, J.L. (2005) A complex subglacial clastic dyke swarm, Sólheimajökull, southern Iceland. *Sedimentary Geology*, 181, 25-37.
- Leaman, D.E. (1975) Form, mechanism, and control of dolerite intrusion near Hobart, Tasmania. *Journal of the Geological Society of Australia*, 22, 175-186.
- Leva, M. (1959) *Fluidization*. New York, McGraw-Hill, 327.
- Levin, L.A., Huggett, C.L. and Wishner, K.F. (1991) Control of deep-sea benthic community structure by oxygen and organic-matter gradients in the eastern Pacific Ocean. *Journal of Marine Research*, 49, 763-800.
- Levin, L.A. and Gage, J. D. (1998) Relationships between oxygen, organic matter and the diversity of bathyal macrofauna. *Deep Sea Research Part II: Topical Studies in Oceanography*, 45, 129-163.
- Lonergan, L. and Cartwright, J. A. (1999) Polygonal faults and their influence on deep-water sandstone reservoir geometries, Alba Field, United Kingdom Central North Sea. *AAPG Bulletin*, 83, 410-432.
- Lonergan, L., Lee, N., Johnson, H.D., Cartwright, J.A. and Jolly, R.J. (2000) Remobilization and injection in deepwater depositional systems: Implications for reservoir architecture and prediction. In: *Deep-water Reservoirs of the World*. (Eds. Weimer, P., Slatt, R.M., Coleman, J., Rosen, N.C., Nelson, H., Bouma, A.H., Styzen, M.J. and Lawrence, D.T.), *GCSSEPM Foundation, 20th Annual Conference, Houston*, 515-532.
- Lonergan, L., Borlandelli, C., Taylor, A., Quine, M. and Flanagan, K. (2007) The three-dimensional geometry of sandstone injection complexes in the Gryphon field, United Kingdom North Sea. In: *Sand Injectites: Implications for Hydrocarbon Exploration and Production*. (Eds. Hurst, A. and Cartwright, J.), *AAPG Memoir*, 87, 103-112.

- Lorenz, J.C., Tuefel, L.W. and Warpinski, N.R. (1991) Regional Fractures I: A mechanism for the formation of regional fractures at depth in flat-lying reservoirs. *AAPG Bulletin*, 75, 1714-1737.
- Løseth, H., Rodrigues, N. and Cobbold, P.R. (2012) World's largest extrusive body of sand?. *Geology*, 40, 467-470.
- Løseth, H., Raulline, B. and Nygård, A. (2013) Late Cenozoic geological evolution of the northern North Sea: development of a Miocene unconformity reshaped by large-scale Pleistocene sand intrusion. *Journal of the Geological Society*, 170, 133-145.
- Lothe, A.E., Borge, H. and Gabrielsen, R.H. (2004) Modelling of hydraulic leakage by pressure and stress simulations and implications for Biot's constant: an example from the Halten Terrace, offshore Mid-Norway. *Petroleum Geoscience*, 10, 199-213.
- Lowe, D. (1975) Water escape structures in coarse-grained sediments. *Sedimentology*, 22, 157-204.
- Lunina, O.V. and Gladkov, A.S. (2015) Seismically induced clastic dikes as a potential approach for the estimation of the lower-bound magnitude/intensity of paleoearthquakes. *Engineering Geology*, 195, 206-213.
- Luthi, S.M., Hodgson, D.M., Gell, C.R., Flint, S.S., Goedbloed, J.W., Drinkwater, N.J. and Johannessen, E.P. (2006) Contribution of research borehole data to modelling fine-grained turbidite reservoir analogues, Permian Tanqua-Karoo basin-floor fans (South Africa). *Petroleum Geoscience*, 12, 175-190.
- Lutton, R.J. (1970) Tensile fracture mechanics from fracture surface morphology. In: *Dynamic rock mechanics*. (Eds. Clark, G.B.), *U.S. Symposium on Rock Mechanics*, 12th, 561-571.
- Macdonald, D. and Flecker, R. (2007) Injected sand sills in a strike-slip fault zone: A case study from the Pil'sk Suite (Miocene), Southeast Schmidt Peninsula, Sakhalin. In: *Sand Injectites: Implications for Hydrocarbon Exploration and Production*. (Eds. Hurst, A. and Cartwright, J.), *AAPG Memoir*, 87, 253-263.
- Magara, K. (1981) Mechanisms of natural fracturing in a sedimentary basin. *AAPG Bulletin*, 65, 123-132.
- Magee, C., Jackson, C.L. and Schofield, N. (2014) Diachronous sub-volcanic intrusion along deep-water margins: insights from the Irish Rockall Basin. *Basin Research*, 26, 85-105.
- Magee, C., Maharaj, S.M., Wrona, T. and Jackson, C.A-L. (2015) Controls on the expression of igneous intrusions in seismic reflection data. *Geosphere*, 11, 1024-1041.
- Mahaut, M. L., Sibuet, M. and Shirayama, Y. (1995) Weight-dependent respiration rates in deep-sea organisms. *Deep Sea Research Part I: Oceanographic Research Papers*, 42, 1575-1582.

- Maltman, A. (1994) Deformation structures preserved in rocks. In *The geological deformation of sediments*. Springer Netherlands. 261-307
- Marchand, A.M.E., Apps, G., Li, W. and Rotzien, J.R. (2015) Depositional processes and impact on reservoir quality in deepwater Palaeogene reservoirs, US Gulf of Mexico. *AAPG Bulletin*, 99, 1635-1648.
- Martill, D.M. and Hudson, J.D. (1989) Injection clastic dykes in the Lower Oxford Clay (Jurassic) of central England: relationship to compaction and concretion formation. *Sedimentology*, 36, 1127–1133.
- Mathieu, L., De Vries, B.V.W., Holohan, E.P. and Troll, V.R. (2008) Dykes, cups, saucers and sills: Analogue experiments on magma intrusion into brittle rocks. *Earth and Planetary Science Letters*, 271, 1-13.
- Mathieu, L., Burchardt, S., Troll, V. R., Krumbholz, M. and Delcamp, A. (2015) Geological constraints on the dynamic emplacement of cone-sheets–The Ardnamurchan cone-sheet swarm, NW Scotland. *Journal of Structural Geology*, 80, 133-141.
- Matthews, M.D. (2007) The effect of grain shape and density on size measurement: In: *Principles, Methods and Application of Particle Size Analysis*. (Ed. Syvitski, J.P.M.) Cambridge University Press, 22-33.
- McCaffrey, K.J.W. and Petford, N. (1997) Are granitic intrusions scale invariant? *Journal of the Geological Society*, 154, 1-4.
- McClain, C.R., Allen, A.P., Tittensor, D.P. and Rex, M.A. (2012) Energetics of life on the deep seafloor. *Proceedings of the National Academy of Sciences*, 109, 15366-15371.
- McKay, M.P., Weislogel, A.L., Fildani, A., Brunt, R.L., Hodgson, D.M. and Flint, S.S. (2015) U-PB zircon tuff geochronology from the Karoo Basin, South Africa: Implications of zircon recycling on stratigraphic age controls. *International Geology Review*, 57, 393-410.
- Minisini, D. and Schwartz, H. (2007) An early Paleocene cold seep system in the Panoche and Tumey Hills, central California (United States). In: *Sand Injectites: Implications for Hydrocarbon Exploration and Production*. (Eds. Hurst, A. and Cartwright, J.), AAPG Memoir, 87, 185-197.
- Molyneux, S., Cartwright, J.A. and Lonergan, L. (2002) Conical amplitude anomalies as evidence for large scale sediment intrusions. *First Break*, 20, 123-129.
- Monnier, D., Imbert, P., Gay, A., Mourgues, R. and Lopez, M. (2014) Pliocene sand injectites from a submarine lobe fringe during hydrocarbon migration and salt diapirism: a seismic example from the Lower Congo Basin. *Geofluids*, 14, 1-19.

- Moretti, M. and Sabato, L. (2007) Recognition of trigger mechanisms for soft-sediment deformation in the Pleistocene lacustrine deposits of the Sant'Arcangelo Basin (Southern Italy): Seismic shock vs. Overloading. *Sedimentary Geology*, 196, 31-45.
- Moretti, M., Alfaro, P., Caselles, O., and Canas, J.A. (1999) Modelling seismites with a digital shaking table. *Tectonophysics*, 304, 369-383.
- Morris, E.A., Hodgson, D.M., Brunt, R.L. and Flint, S.S. (2014a) Origin, evolution and anatomy of silt-prone submarine external levées. *Sedimentology*, 61, 1734-1763.
- Morris, E.A., Hodgson, D.M., Flint, S.S., Brunt, R.L., Butterworth, P.J. and Verhaeghe, J. (2014b) Sedimentology, stratigraphic architecture, and depositional context of submarine frontal-lobe complexes. *Journal of Sedimentary Research*, 84, 763-780.
- Morton, A., McFadyen, S., Hurst, A., Pyle, J. and Rose, P. (2014) Constraining the origin of reservoirs formed by sandstone intrusions: Insights from heavy mineral studies of the Eocene in the Forties area, United Kingdom central North Sea. *AAPG Bulletin*, 98, 545-561.
- Mourgues, R. and Cobbold, P.R. (2003) Some tectonic consequences of fluid overpressures and seepage forces as demonstrated by sandbox modeling. *Tectonophysics*, 376, 75-97.
- Mourgues, R., Bureau, D., Bodet, L., Gay, A. and Gressier, J.B. (2012) Formation of conical fractures in sedimentary basins: Experiments involving fluids and implications for sandstone intrusion mechanisms. *Earth and Planetary Science Letters*, 313, 67-78.
- Mudge, D.C. (2014) Regional controls on Lower Tertiary sandstone distribution in the North Sea and NE Atlantic margin basins. In: *Tertiary Deep-Marine Reservoirs of the North Sea Region*. (Eds. Mckie, T., Rose, P.T.S, Hartley, A.J., Jones, D.W. and Armstrong, T.L.), *Geological Society of London Special Publications*, 403.
- Mudge, D.C. and Copestake, P. (1992) Lower Palaeogene stratigraphy of the northern North Sea. *Marine and Petroleum Geology*, 9, 287-301.
- Muirhead, J.D., Airoidi, G., Rowland, J.V. and White, J.D. (2012) Interconnected sills and inclined sheet intrusions control shallow magma transport in the Ferrar large igneous province, Antarctica. *Geological Society of America Bulletin*, 124, 162-180.
- Müller, G. and Dahm, T. (2000) Fracture morphology of tensile cracks and rupture velocity. *Journal of Geophysical Research*, 105, 723-738.
- Munson, B.R., Rothmayer, A.P., Okiishi, T.H. and Huebsch, W.W. (2012) *Fundamentals of Fluid Mechanics* (7th edition), *John Wiley and Sons*, 796.
- Murchison, R. (1827) Supplementary remarks on the oolitic series in the counties of Sutherland and Ross, and in the Hebrides. *Transactions of the Geological Society*, 2, 353.

- Murdoch, L.C., and Slack, W.W. (2002) Forms of hydraulic fractures in shallow fine-grained formations. *Journal of Geotechnical and Geoenvironmental Engineering*, 128, 479-487.
- Nagatomo, A. and Archer, S. (2015) Termination geometries and reservoir properties of the Forties Sandstone pinch-out, East Central Graben, UK North Sea. *Geological Society of London Special Publications*, 403, 133-155.
- Needham, S.J., Worden, R.H. and McIlroy, D. (2005) Experimental production of clay rims by macrobiotic sediment ingestion and excretion processes. *Journal of Sedimentary Research*, 75, 1028-1037.
- Netoff, D. (2002) Seismogenically induced fluidization of Jurassic erg sands, south-central Utah. *Sedimentology*, 49(1), 65-80.
- Newsom, J.F. (1903) Clastic dikes. *Bulletin of the Geological Society of America*, 14, 227-268.
- Nichols, R.J. (1995) The liquefaction and remobilization of sandy sediments. *Geological Society, London, Special Publications*, 94, 63-76.
- Nichols, R.J., Sparks, R.S.J. and Wilson, C.J.N. (1994) Experimental studies of the fluidization of layered sediments and the formation of fluid escape structures. *Sedimentology*, 41, 233-253.
- Nichols, R., Sparks, R. and Wilson, C. (2006) Experimental studies of the fluidization of layered sediments and the formation of fluid escape structures. *Sedimentology*, 41, 233-253.
- Nicholson, R. and Pollard, D.D. (1985) Dilation and linkage of en-echelon cracks. *Journal of Structural Geology*, 7, 583-590.
- Obermeier, S.F. (1996) Use of liquefaction-induced features for paleoseismic analysis—an overview of how seismic liquefaction features can be distinguished from other features and how their regional distribution and properties of source sediment can be used to infer the location and strength of Holocene paleo-earthquakes. *Engineering Geology*, 44, 1-76.
- Obermeier, S.F. (1998) Liquefaction evidence for strong earthquakes of Holocene and latest Pleistocene ages in the states of Indiana and Illinois, USA. *Engineering Geology*, 50, 227-254.
- Obermeier, S.F., Olson, S.M. and Green, R.A. (2005) Field occurrences of liquefaction-induced features: a primer for engineering geologic analysis of paleoseismic shaking. *Engineering Geology*, 76, 209-234.
- Oliveira, C.M., Hodgson, D.M. and Flint, S.S. (2009) Aseismic controls on in situ soft-sediment deformation processes and products in submarine slope deposits of the Karoo Basin, South Africa. *Sedimentology*, 56, 1201-1225.

- Osborne, M.J. and Swarbrick, R.E. (1997) Mechanisms for generating overpressure in sedimentary basins: a reevaluation. *AAPG Bulletin*, 81, 1023-1041.
- Palladino, G., Grippa, A., Bureau, D., Alsop, G.I. and Hurst, A. (2016) Emplacement of sandstone intrusions during contractional tectonics. *Journal of Structural Geology*, 89, 230-249.
- Parize, O. and Friès, G. (2003) The Vocontian clastic dykes and sills: a geometric model. In: *Subsurface Sediment Mobilization*. (Eds. P. Van Rensberge, R.R. Hillis, A.J. Maltman, C.K. Morley), *Geological Society of London Special Publications*, 216, 51-72.
- Parize, O., Beaudoin, B., Champenhet, J-M., Friès, G., Imbert, P., Labourdette, R., Paternoster, B., Rubino, J-L. and Schneider, F. (2007). A methodological approach to clastic injectites: from field analysis to seismic modelling – examples of the Vocontian Aptian and Albian injectites (Southeast France). In: *Sand Injectites: Implications for Hydrocarbon Exploration and Production*. (Eds. Hurst, A. and Cartwright, J.), AAPG Memoir, 87, 173-183.
- Parnell, J., Boyce, A.J., Hurst, A., Davidheiser-Kroll, B. and Ponicka, J. (2013) Long term geological record of a global deep subsurface microbial habitat in sand injection complexes. *Scientific reports*, 3.
- Peterson, G.L. (1966) Structural interpretation of sandstone dikes, northwest Sacramento Valley, California. *Geological Society of America Bulletin*, 77, 833-842.
- Peterson, G.L. (1968) Flow structures in sandstone dikes. *Sedimentary Geology*, 62, 177-190.
- Phillips, W.J. (1972) Hydraulic fracturing and mineralization. *Journal of the Geological Society*, 128, 337-359.
- Piepenburg, D., Blackburn, T.H., von Dorrien, C.F., Gutt, J., Hall, P.O.J., Hulth, S., Kendall, M.A., Opalinski, K.W., Rachor, E. and Schmid, M.K. (1995) Partitioning of benthic community respiration in the Arctic (northwestern Barents Sea). *Marine Ecology Progress Series*, 118, 199-213.
- Piper, D. J. and Normark, W. R. (2001) Sandy fans--from Amazon to Hueneme and beyond. *AAPG Bulletin*, 85, 1407-1438.
- Pollard, D.D. (1973) Derivation and evaluation of a mechanical model for sheet intrusions. *Tectonophysics*, 19, 233-269.
- Pollard, W.J., Muller, O.H. and Dockstader, D.R. (1975) The form and growth of fingered sheet intrusions. *Geological Society of America Bulletin*, 86, 351-363.
- Pollard, D.D, Segall, P. and Delaney, P.T. (1982) Formation and interpretation of dilatant échelon cracks. *Geological Society of America Bulletin*, 93, 1291-1301.

- Polteau, S., Mazzini, A., Galland, O., Planke, S. and Malthe-Sørensen, A. (2008) Saucer-shaped intrusions: Occurrences, emplacement and implications. *Earth and Planetary Science Letters*, 266, 195-204.
- Post, S. (2011) *Applied and Computational Fluid Mechanics*, Jones and Bartlett Publishers, Sudbury, MA, USA, 600.
- Prélat, A. and Hodgson, D.M. (2013) The full range of turbidite bed thickness patterns in submarine lobes: controls and implications. *Journal of the Geological Society*, 170, 209-214.
- Prélat, A., Hodgson, D.M. and Flint, S.S. (2009) Evolution, architecture and hierarchy of distributary deep-water deposits: a high-resolution outcrop investigation from the Permian Karoo Basin, South Africa. *Sedimentology*, 56, 2132-2154.
- Pringle, J.K., Brunt, D.M., Hodgson, D.M. and Flint, S.S. (2010) Capturing stratigraphic and sedimentological complexity from submarine channel complex outcrops to digital 3D models, Karoo Basin, South Africa. *Petroleum Geoscience*, 16, 307-330.
- Quigley, M.C., Bastin, S. and Bradley, B.A. (2013) Recurrent liquefaction in Christchurch, New Zealand, during the Canterbury earthquake sequence. *Geology*, 41, 419-422.
- Ravier, E., Guiraud, M., Guillien, A., Vennin, E., Buoncristiani, J.F. and Portier, E. (2015) Micro-to macro-scale internal structures, diagenesis and petrophysical evolution of injectite networks in the Vocontian Basin (France): Implications for fluid flow. *Marine and Petroleum Geology*, 64, 125-151.
- Richardson, J.F. (1971) Incipient fluidization and particulate systems. In: *Fluidization* (Eds. Davidson, J.F. and Harrison, D.), *Academic Press, London*, 25-64.
- Rieke, H.H. and Chilingarian, G.V. (1974) *Compaction of Argillaceous Sediments*. Elsevier Scientific Publishing Company, Amsterdam, The Netherlands.
- Rodrigues, N., Cobbold, P.R. and Løseth, H. (2009) Physical modelling of sand injectites. *Tectonophysics*, 474, 610-632.
- Ross, J. A., Peakall, J. and Keevil, G. M. (2011) An integrated model of extrusive sand injectites in cohesionless sediments. *Sedimentology*, 58, 1693-1715.
- Ross, J. A., Peakall, J. and Keevil, G. M. (2013) Sub-aqueous sand extrusion dynamics. *Journal of the Geological Society*, 170, 593-602.
- Ross, J.A., Peakall, J. and Keevil, G.M. (2014) Facies and flow regimes of sandstone-hosted columnar intrusions: Insights from the pipes of Kodachrome Basin State Park. *Sedimentology*, 61, 1764-1792.

- Rowe, C.A., Mustard, P.S., Mahoney, J.B. and Katnick, D.C. (2002) Oriented clastic dike swarms as indicators of paleoslope? An example from the upper Cretaceous Nanaimo Group, Canada. *Journal of Sedimentary Research*, 72, 192-200.
- Rubin, A.M. (1995) Propagation of magma-filled cracks. *Annual Review of Earth and Planetary Sciences*, 23, 287-336.
- Rudolph, K.W., Schlager, W. and Biddle, K.T. (1989) Seismic models of a carbonate foreslope-to-basin transition, Picco di Vallandro, Dolomite Alps, northern Italy. *Geology*, 17, 453-456.
- Satur, N. and Hurst, A. (2007) Sand-injection Structures in Deep-water Sandstones from the Ty Formation (Paleocene), Sleipner Øst Field, Norwegian North Sea. In: *Sand Injectites: Implications for Hydrocarbon Exploration and Production*. (Eds. Hurst, A. and Cartwright, J.), AAPG Memoir, 87, 113-117.
- Schofield, N.J., Brown, D.J., Magee, C. and Stevenson, C.T. (2012a) Sill morphology and comparison of brittle and non-brittle emplacement mechanisms. *Journal of the Geological Society*, 169, 127-141.
- Schofield, N.J., Heaton, L., Holford, S.P., Archer, S.G., Jackson, C.A-L. and Jolley, D.W. (2012b) Seismic imaging of 'broken bridges': linking seismic to outcrop-scale investigations of intrusive magma lobes. *Journal of the Geological Society*, 169, 421-426.
- Schwab, A.M., Cronin, B.T. and Ferreira, H. (2007) Seismic expression of channel outcrops: Offset stacked versus amalgamated channel systems. *Marine and Petroleum Geology*, 24, 504-514.
- Schwab, A.M., Jameson, E.W. and Townsley, A. (2015) Volund Field: development of an Eocene sandstone injection complex, offshore Norway: In: *Tertiary Deep-Marine Reservoirs of the North Sea Region*, (Eds. Mckie, T., Rose, P.T.S., Hartley, A.J., Jones, D.W. and Armstrong, T.L.). *Geological Society of London Special Publication*, 403, 1-16.
- Schwartz, H., Sample, J., Weberling, K.D., Minisini, D. and Moore, J.C. (2003) An ancient linked fluid migration system: cold-seep deposits and sandstone intrusions in the Panoche Hills, California, USA. *Geo-Marine Letters*, 23, 340-350.
- Scott, A. (2009) Processes of sand injection: Relationships with host strata, internal structures, and permeability implications. Unpublished PhD thesis. University of Aberdeen.
- Scott, A., Vigorito, M. and Hurst, A. (2009) The process of sand injection: internal structures and relationships with host strata (Yellowbank Creek Injectite Complex, California, USA). *Journal of Sedimentary Research*, 79, 568-583.
- Scott, A., Hurst, A. and Vigorito, M. (2013) Outcrop-based reservoir characterization of a kilometer-scale sand-injectite complex. *AAPG bulletin*, 97, 309-343.

- Secor, D.T. (1965) Role of fluid pressure in jointing. *American Journal of Science*, 263, 633-646.
- Segré, G. and Silberberg, A. (1962a) Behaviour of macroscopic rigid spheres in Poiseuille flow. Part 1. Determination of local concentration by statistical analysis of particle passages through crossed light beams. *Journal of Fluid Mechanics*, 14, 115-135.
- Segré, G. and Silberberg, A. (1962b) Behaviour of macroscopic rigid spheres in Poiseuille flow. Part 2. Experimental results and interpretation. *Journal of Fluid Mechanics*, 14, 136-157.
- Sharon, E., Gross, S.T. and Fineberg, J. (1995) Local crack branching as a mechanism for instability in dynamic fracture. *Physical Review Letters*, 74, 5096-5099.
- Shepherd, M., Kearney, C.J. and Milne, J.H. (1990) Magnus field. In: *Structural Traps II. Traps Associated with Tectonic Faulting* (Eds. Beaumont, E.A. and Foster, N.H.). *American Association of Petroleum Geologists, Treatise of Petroleum Geology Atlas of Oil and Gas Fields*, 95-125.
- Sherry, T.J., Rowe, C.D., Kirkpatrick, J.D. and Brodsky, E.E. (2012) Emplacement and dewatering of the world's largest exposed sand injectite complex. *Geochemistry, Geophysics, Geosystems*, 13, 1-17.
- Shoulders, S.J. and Cartwright, J. (2004) Constraining the depth and timing of large-scale conical sandstone intrusions. *Geology*, 32, 661-664.
- Shoulders, S.J., Cartwright, J. and Huuse, M. (2007) Large-scale conical sandstone intrusions and polygonal fault systems in Tranche 6, Faroe-Shetland Basin. *Marine and Petroleum Geology*, 24, 173-188.
- Singhal, B.B.S. and Gupta, R.P. (1999) *Applied Hydrogeology of Fractured Rocks*. Kluwer Academic Publishers, Dordrecht, The Netherlands, 400.
- Sixsmith, P.J., Flint, S.S., Wickens, H.dev. and Johnson, S.D. (2004) Anatomy and stratigraphic development of a basin floor turbidite system in the Laingsburg Formation, Main Karoo Basin, South Africa. *Journal of Sedimentary Research*, 74, 239-254.
- Sommer, E. (1969) Formation of fracture 'lances' in glass. *Engineering Fracture Mechanics*, 1, 539-546.
- Spychala, Y.T., Hodgson, D.M., Flint, S.S. and Mountney, N.P. (2015) Constraining the sedimentology and stratigraphy of submarine intraslope lobe deposits using exhumed examples from the Karoo Basin, South Africa. *Sedimentary Geology*. 322, 67-81.
- Stafleu, J., Everts, A.J.W. and Kenter, J.A.M. (1994) Seismic models of a prograding carbonate platform: Vercors, south-east France. *Marine and Petroleum Geology*, 11, 514-527.
- Stearns, D.W. (1978) Faulting and forced folding in the Rocky Mountains foreland. *Geological Society of America Memoirs*, 151, 1-38.

- Stewart, S. A. (2011) Vertical exaggeration of reflection seismic data in geoscience publications 2006-2010. *Marine and Petroleum Geology*, 28, 959-965.
- Stewart, S. A. (2012) Interpretation validation on vertically exaggerated reflection seismic sections. *Journal of structural geology*, 41, 38-46.
- Stoker, S.J., Gray, J.C., Haile, P., Andrews, I.J. and Cameron, T.D.J. (2006) The importance of stratigraphic plays in the undiscovered resources of the UK Continental Shelf. In: *The Deliberate Search for the Stratigraphic Trap*. (Ed. Allen, M. R.), *Geological Society of London Special Publications*, 254, 153–167.
- Sturkell, E.F.F. and Ormö, J. (1997) Impact-related injections in the marine Ordovician Lockne impact structure, Central Sweden. *Sedimentology*, 44, 793–804.
- Sullivan, M., Jensen, G., Goulding, F., Jennette, D., Foreman, L. and Stern, D. (2000) Architectural analysis of deep-water outcrops: Implications for exploration and development of the Diana sub-basin, western Gulf of Mexico. In: *Deep-water Reservoirs of the World*. (Ed. By P. Weimer, R.M. Slatt, A.H. Bouma and D.T. Lawrence), *Gulf Coast Section SEPM Foundation 20th Annual Research Conference*, 1010-1032.
- Sullivan, M.D., Lincoln Foreman, J., Jennette, D.C., Stern, D., Jensen, G.N. and Goulding, F.J. (2004) An integrated approach to characterization and modeling of deep-water reservoirs, Diana Field, Western Gulf of Mexico. In: *Integration of Outcrop and Modern Analogs in Reservoir Modelling* (Eds. Grammer, G.M., Harris, P.M. and Eberli, G.P.), *AAPG Memoir*, 80, 215-234.
- Surlyk, F. and Noe-Nygaard, N. (2001) Sand remobilisation and intrusion in the Upper Jurassic Hareelv Formation of East Greenland. *Bulletin of the Geological Society of Denmark*, 48, 169-188.
- Surlyk, F. and Noe-Nygaard, N. (2003) A giant sand injection complex: the Upper Jurassic Hareelv Formation of East Greenland. *Geologia Croatica*, 56, 69-81.
- Surlyk, F., Gjelberg, J. and Noe-Nygaard, N. (2007) The Upper Jurassic Hareelv Formation of east Greenland: a giant sedimentary injection complex. In: *Sand Injectites: Implications for Hydrocarbon Exploration and Production*. (Eds. Hurst, A. and Cartwright, J.), *AAPG Memoir*, 87, 141-149.
- Svendsen, J.B., Hansen, H.J., Stærmose, T. and Engkilde, M.K. (2010) Sand remobilization and injection above an active salt diapir: the Tyr sand of the Nini Field, Eastern North Sea. *Basin Research*, 22, 548-561.
- Swinbanks, D.D. and Luternauer, J.L. (1987) Burrow distribution of thalassinidean shrimp on a Fraser Delta tidal flat, British Columbia. *Journal of Paleontology*, 61, 315-332.

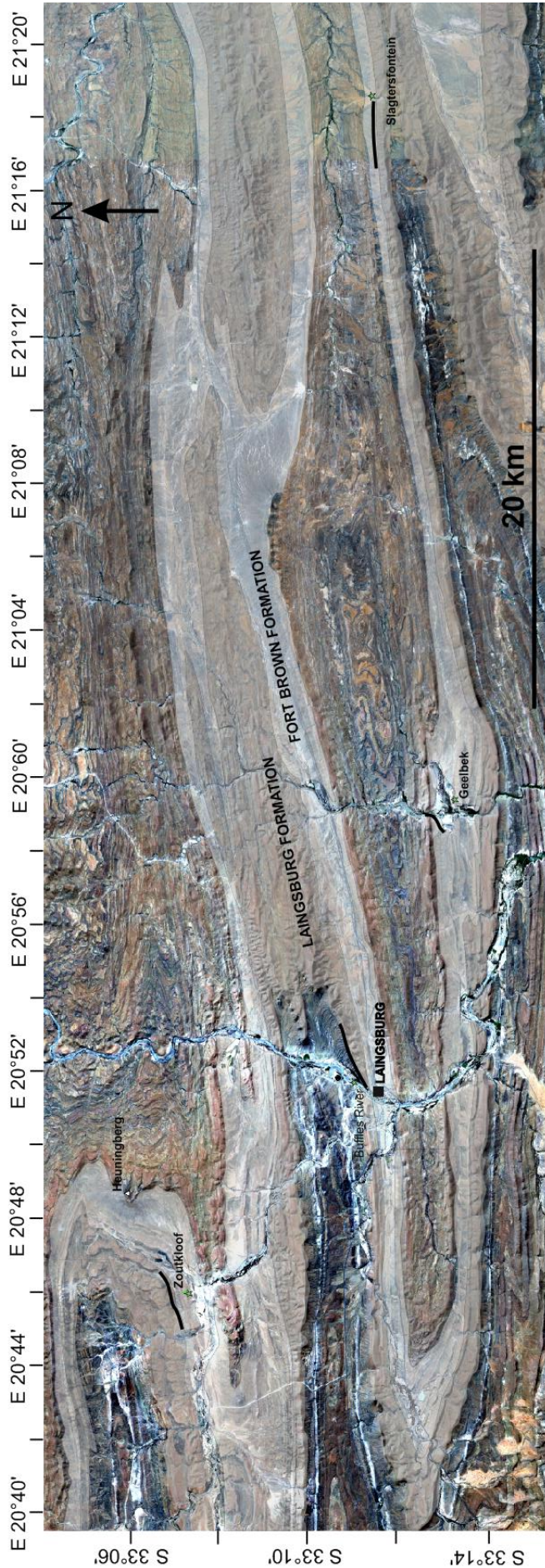
- Szarawarska, E., Huuse, M., Hurst, A., De Boer, W., Lu, L., Molyneux, S. and Rawlinson, P. (2010) Three-dimensional seismic characterisation of large-scale sandstone intrusions in the lower Palaeogene of the North Sea: completely injected vs. In situ remobilised sandbodies. *Basin Research*, 22, 517-532.
- Talling, P.J., Masson, D.G., Sumner, E.J., and Malgesini, G. (2012) Subaqueous sediment density flows: depositional processes and deposit types. *Sedimentology*, 59, 1937-2003.
- Tankard, A., Welsink, H., Aukes, P., Newton, R. and Stettler, E. (2009) Tectonic evolution of the Cape and Karoo basins of South Africa. *Marine and Petroleum Geology*, 26, 1379-1412.
- Taylor, B.J. (1982) Sedimentary dykes, pipes and related structures in the Mesozoic sediments of south-eastern Alexander Island. *British Antarctic Survey Bulletin*, 51, 1-42.
- Thompson, R.K. and Pritchard, A.W. (1969) Respiratory adaptations of two burrowing crustaceans, *Callinassa californiensis* and *Upogebia pugettensis* (Decapoda, Thalassinidea). *Biological Bulletin*, 136, 274-287.
- Thompson, B.J., Garrison, R.E. and Moore, J.C. (1999) A late Cenozoic sandstone intrusion west of Santa Cruz, California: Fluidized flow of water-and hydrocarbon-saturated sediments. In: *Late Cenozoic Fluid Seeps and Tectonics along the San Gregorio Fault Zone in the Monterey Bay Region, California*. (Eds. Garrison, R.E., Aiello, I.W. and Moore, J.C.), AAPG, Pacific Section, Volume and Guide Book, GB-76, 53–74.
- Thompson, B.J., Garrison, R.E. and Moore, J.C. (2007) A reservoir-scale Miocene injectite near Santa Cruz, California. In: *Sand Injectites: Implications for Hydrocarbon Exploration and Production*. (Eds. Hurst, A. and Cartwright, J.), AAPG Memoir, 87, 151-162.
- Thomson, J. and Wilson, T.R.S. (1980) Burrow-like structures at depth in a Cape Basin red clay core. *Deep Sea Research Part A. Oceanographic Research Papers*, 27, 197-202.
- Thomson, K. (2007) Determining magma flow in sills, dykes, and laccoliths and their implications for sill emplacement mechanisms. *Bulletin of Volcanology*, 70, 183-201.
- Thomson, K. and Hutton, D. (2004) Geometry and growth of sill complexes: insights using 3D seismic from the North Rockall Trough. *Bulletin of Volcanology*, 66, 364-375.
- Thomson, K. and Schofield, N. (2008) Lithological and structural controls on the emplacement and morphology of sills in sedimentary basins. In: *Structure and emplacement of high-level magmatic systems*. (Eds. Thomson, K., Petford, N.), Geological Society of London Special Publications, 302, 31-44.
- Trude, K.J. (2004) Kinematic indicators for shallow level igneous intrusions from 3D seismic data: Evidence of flow direction and feeder location. *Geological Society, London, Memoirs*, 29, 209-218.

- Truswell, J.F. (1972) Sandstone sheets and related intrusions from Coffee bay, Transkei, South Africa. *Journal of Sedimentological Research*, 42, 578-583.
- Van der Merwe, W.C., Flint, S.S. and Hodgson, D.M. (2010) Sequence stratigraphy of an argillaceous, deepwater basin-plain succession: Vischkuil Formation (Permian), Karoo Basin, South Africa. *Marine and Petroleum Geology*, 27, 321-333.
- Van der Merwe, W.C., Hodgson, D.M., Brunt, R.L. and Flint, S.S. (2014) Depositional architecture of sand-attached and sand-detached channel-lobe transition zones on an exhumed stepped slope mapped over a 2500 km² area. *Geosphere* 10, 1076-1093.
- Van der Werff, W. and Johnson, S. (2003) High resolution stratigraphic analysis of a turbidite system, Tanqua Karoo Basin, South Africa. *Marine and Petroleum Geology*, 20, 45-69.
- Varga, R. J., Gee, J. S., Staudigel, H. and Tauxe, L. (1998) Dike surface lineations as magma flow indicators within the sheeted dike complex of the Troodos Ophiolite, Cyprus. *Journal of Geophysical Research*, 103, 5241-5256.
- Vétel, W. and Cartwright, J. (2010) Emplacement mechanics of sandstone intrusions: insights from the Panoche Giant Injection Complex, California. *Basin Research*, 22, 783-807.
- Vigorito, M. and Hurst, A. (2010) Regional sand injectite architecture as a record of pore-pressure evolution and sand redistribution in the shallow crust: insights from the Panoche Giant Injection Complex, California. *Journal of the Geological Society*, 167, 889-904.
- Vigorito, M., Hurst, A., Cartwright, J. and Scott, A. (2008) Regional-scale subsurface sand remobilization: geometry and architecture. *Journal of the Geological Society*, 165, 609-612.
- Visser, J.N. and Praekelt, H.E. (1996) Subduction, mega-shear systems and Late Palaeozoic basin development in the African segment of Gondwana. *Geologische Rundschau*, 85, 632-646.
- Von Brunn, V. and Talbot, C. (1986) Formation and deformation of subglacial intrusive clastic sheets in the Dwyka Formation of northern Natal, South Africa. *Journal of Sedimentary Research*, 56.
- Walker, R.G. (1978) Deep-water sandstone facies and ancient submarine fans: models for exploration for stratigraphic traps. *AAPG Bulletin*, 62, 932-966.
- Weaver, P.P.E. and Schultheiss, P.J. (1983) Vertical open burrows in deep-sea sediments 2 m in length. *Nature*, 301, 329-331.
- Wheatley, D.F., Chan, M.A., and Sprinkel, D.A. (2016) Clastic pipe characteristics and distributions throughout the Colorado Plateau: Implications for paleoenvironment and paleoseismic controls. *Sedimentary Geology*. *In press*. doi:10.1016/j.sedgeo.2016.03.027

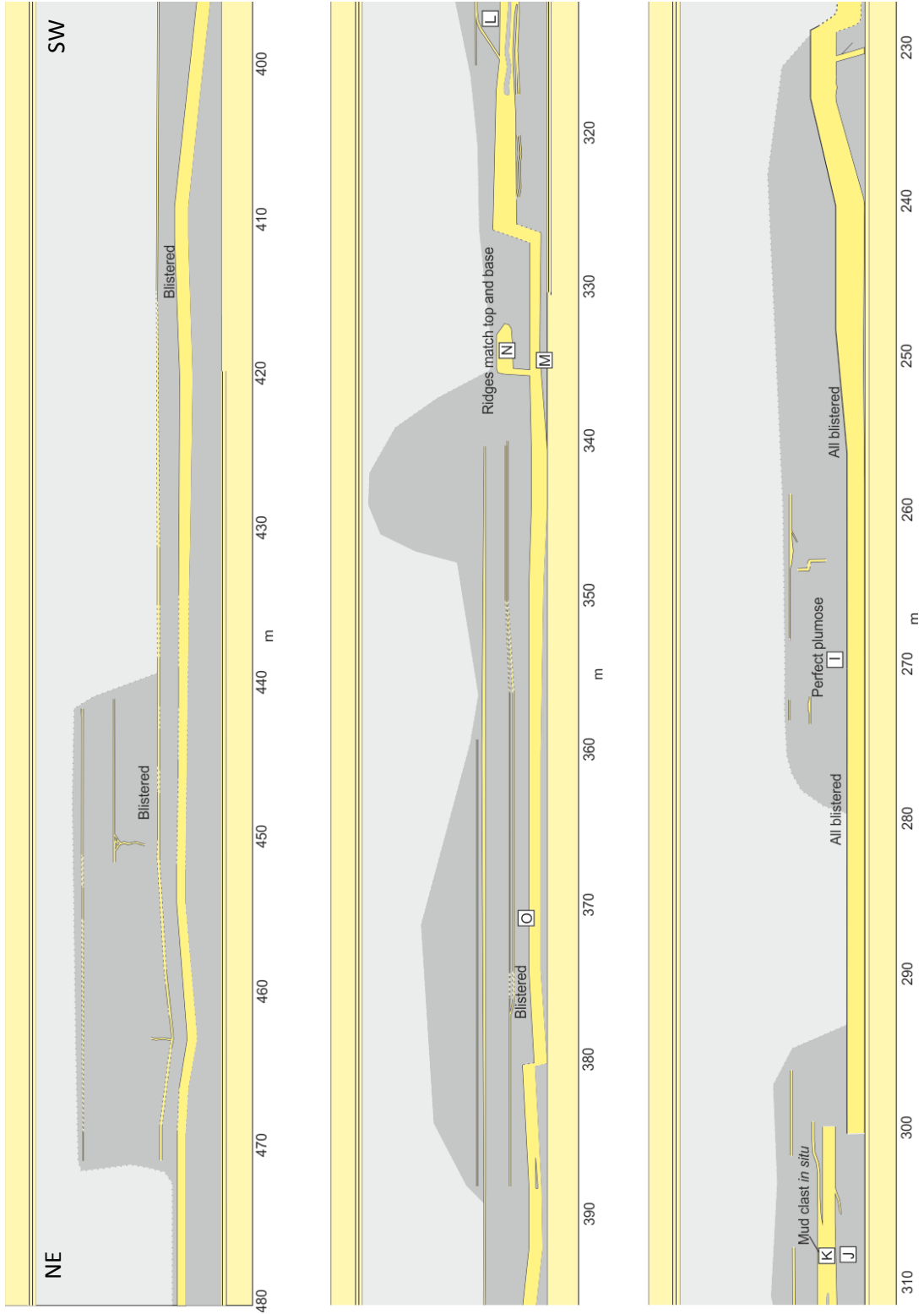
- Wickens, H.Dev. (1994) Basin floor fan building turbidites of the southwestern Karoo Basin, Permian Ecca Group, South Afrika. Phd thesis, University of Port Elizabeth, 233.
- Wickens, H.Dev. and Bouma, A.H. (2000) The Tanqua Fan Complex, Karoo Basin, South Africa— Outcrop analog for fine-grained, deepwater deposits, In: *Fine-Grained Turbidite Systems: American Association of Petroleum Geologists* (Eds. Bouma A.H. and Stone, C.G.) *Memoir 72 and SEPM, Special Publication*, 68, 153–165.
- Wild, R., Flint, S.S. and Hodgson, D.M. (2009) Stratigraphic evolution of the upper slope and shelf edge in the Karoo Basin, South Africa. *Basin Research*, 21, 502-527.
- Woodworth, J.B. (1895) Some features on joints. *Science*, 2, 903-904.
- Yang, S.Y. and Kim, J.W. (2014) Pliocene basin-floor fan sedimentation in the Bay of Bengal (offshore northwest Myanmar). *Marine and Petroleum Geology*, 49, 45-58.
- Yardley, G.S. and Swarbrick, R.E. (2000) Lateral transfer: a source of additional overpressure? *Marine and Petroleum Geology*, 17, 523-537.

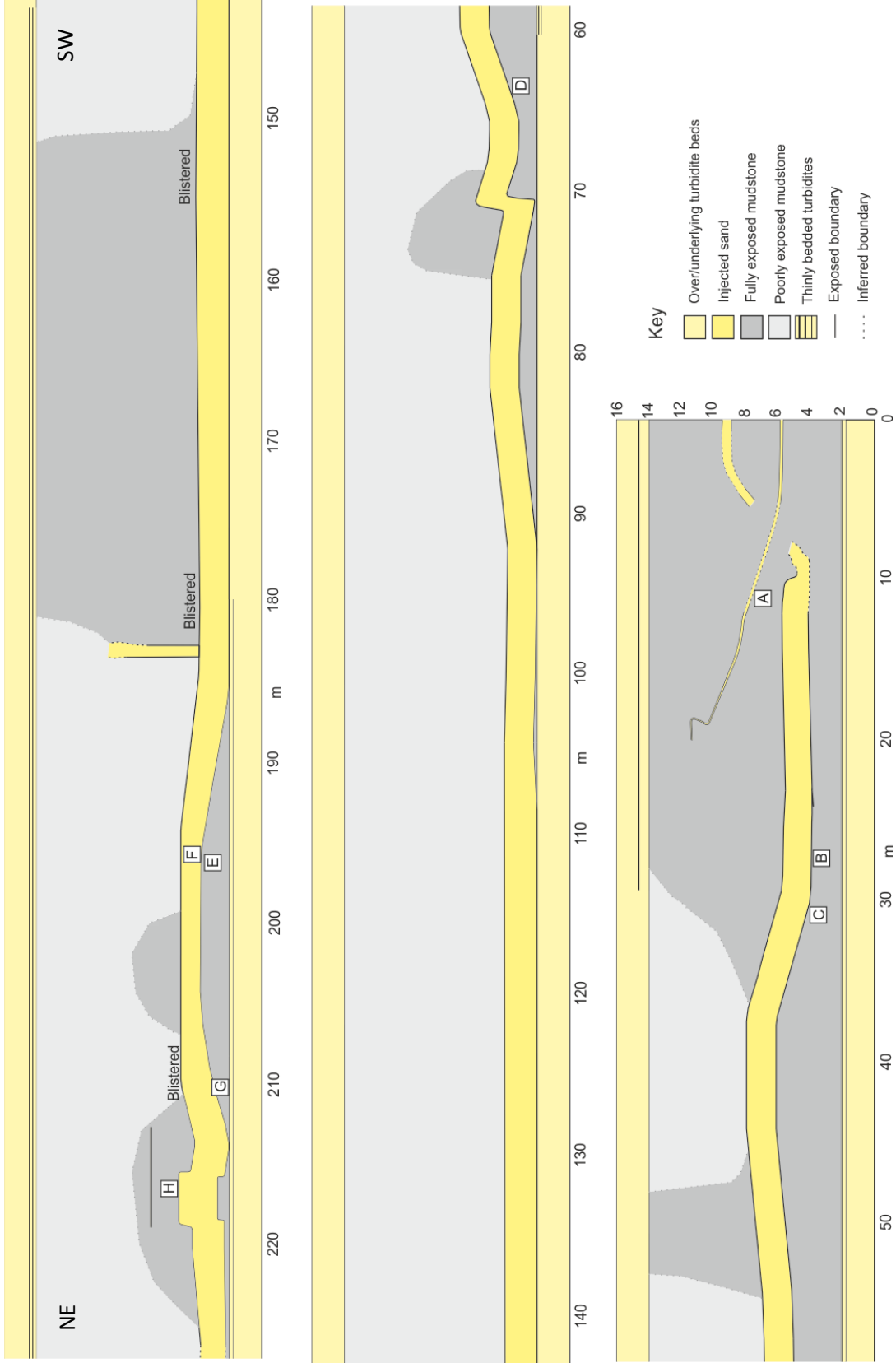
Appendix A

Locality map of outcrops Zoutkloof, Geelbeck, Buffels River and Slagterfontein. Light grey areas highlight outcrop exposure in the Laingsburg depocentre. Black lines are drawn along individual outcrop units where logs were taken. Detailed panels and logs for each outcrop are shown in Appendix A.

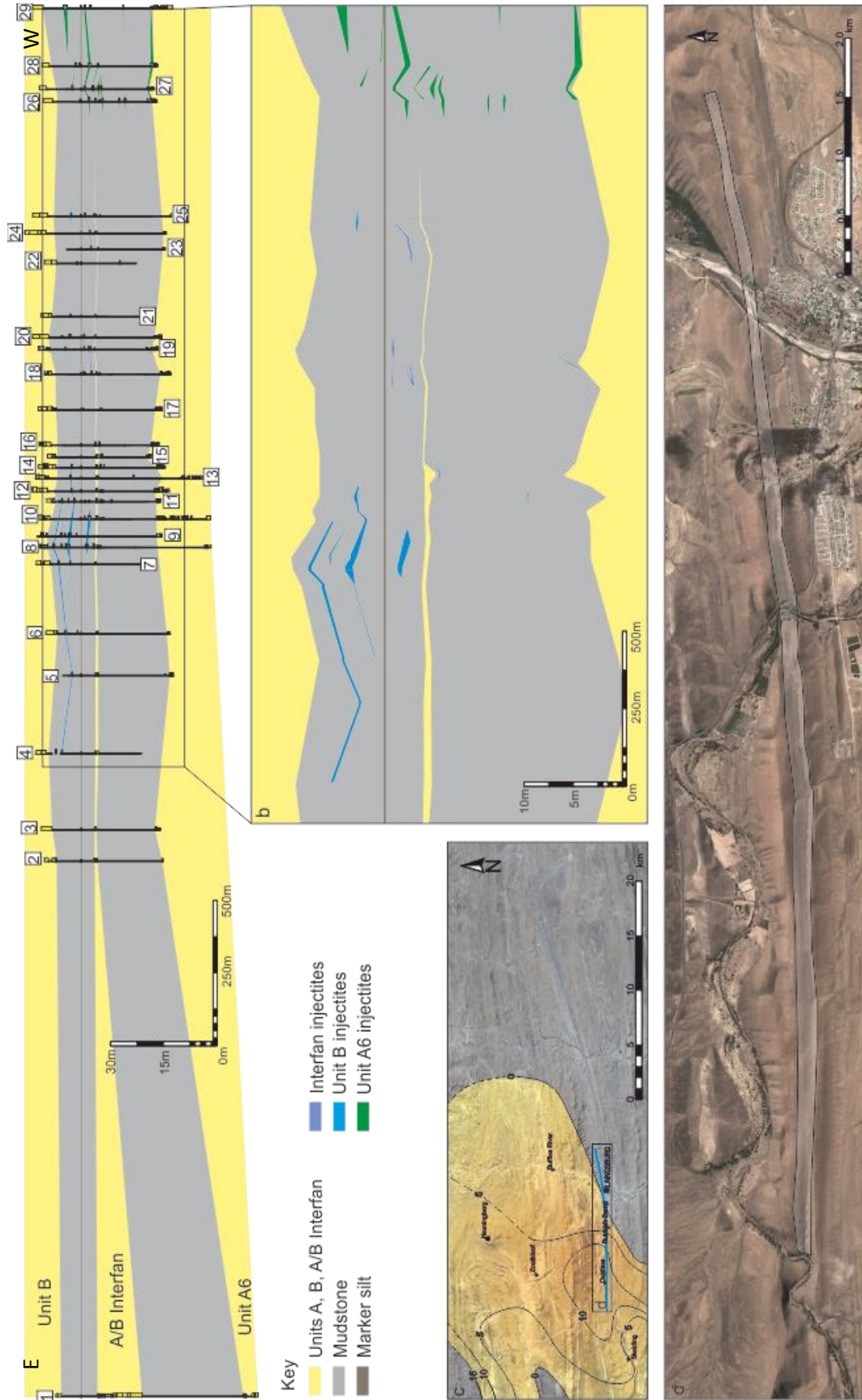


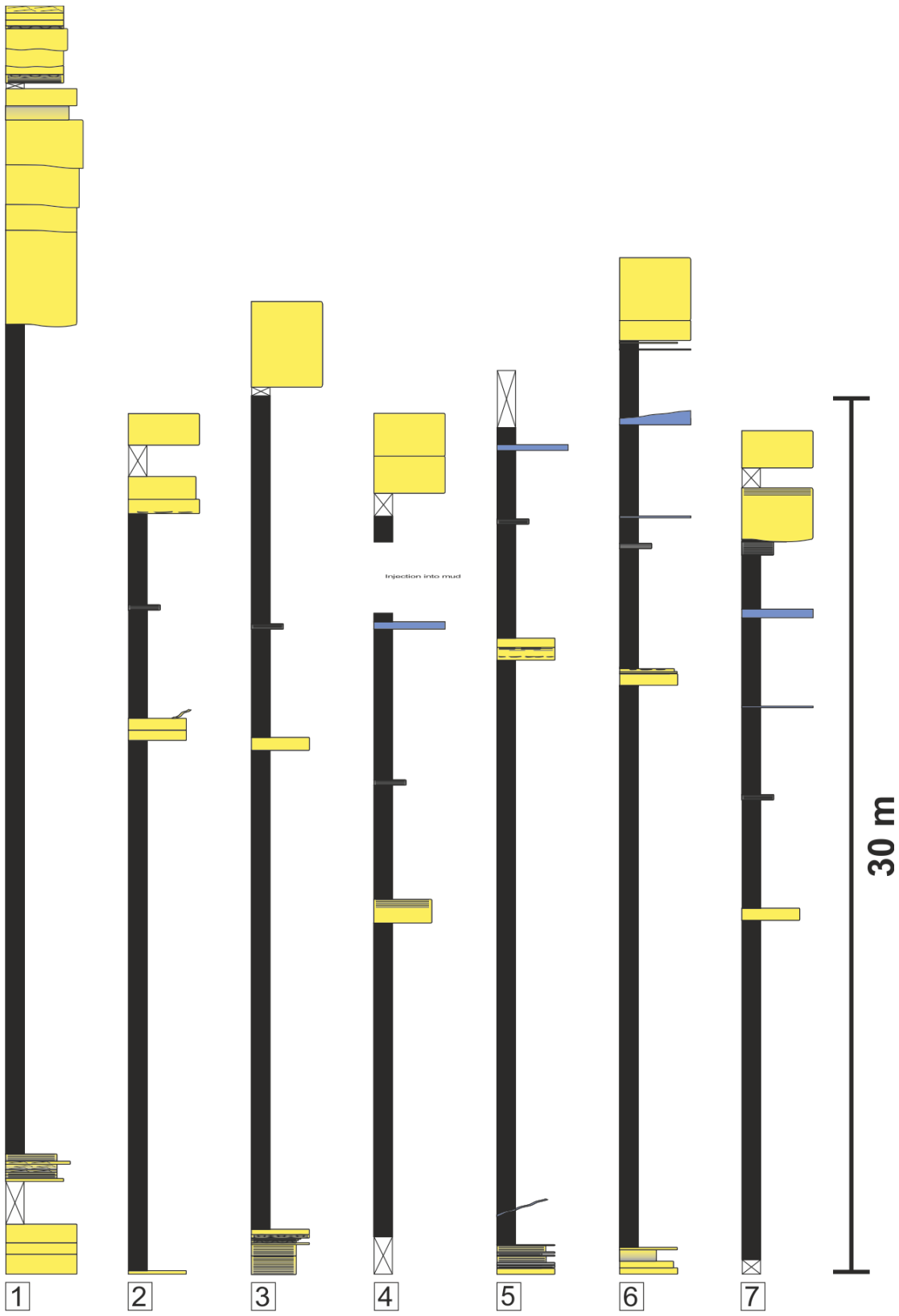
A.1 Buffels River panel with localities

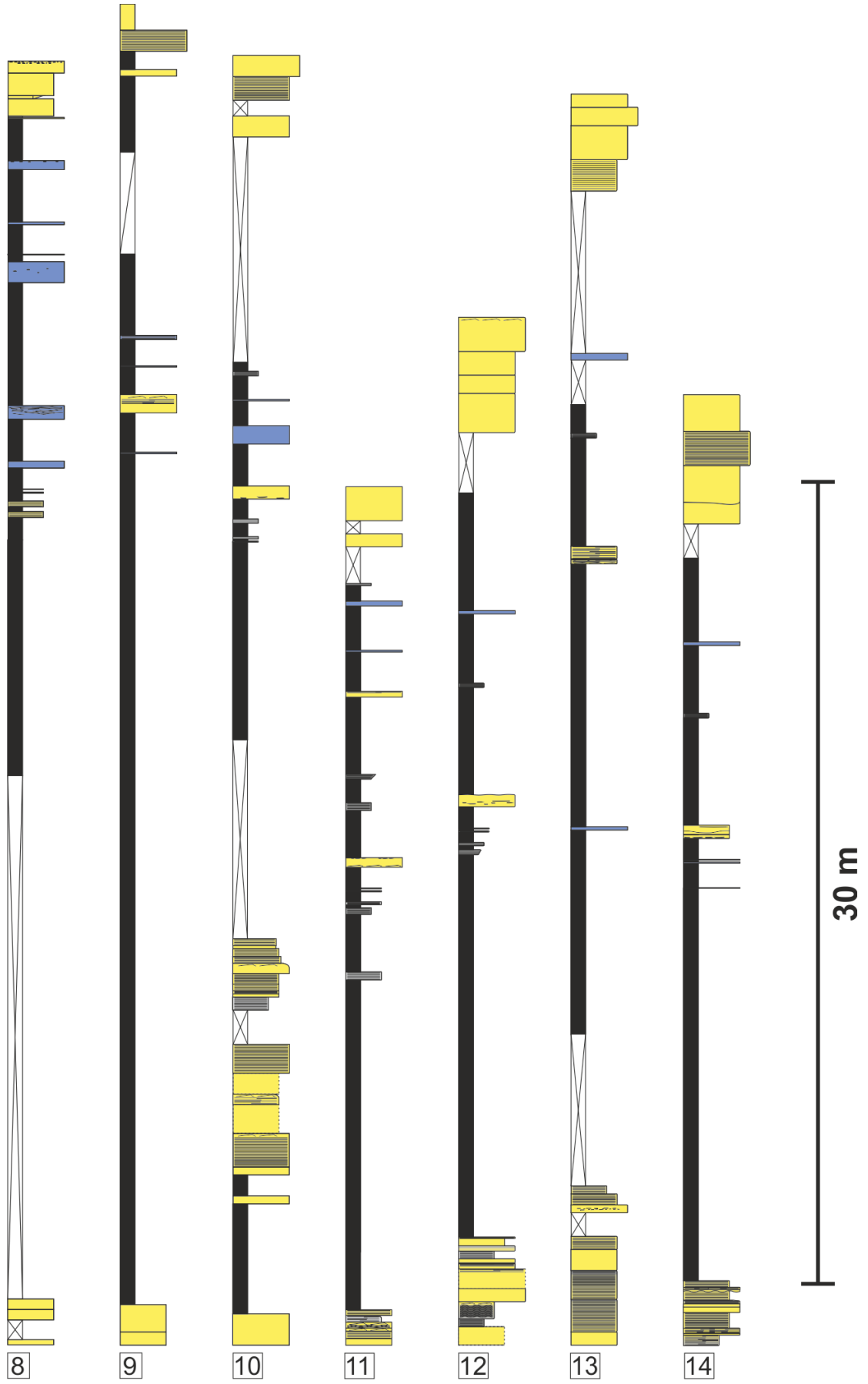


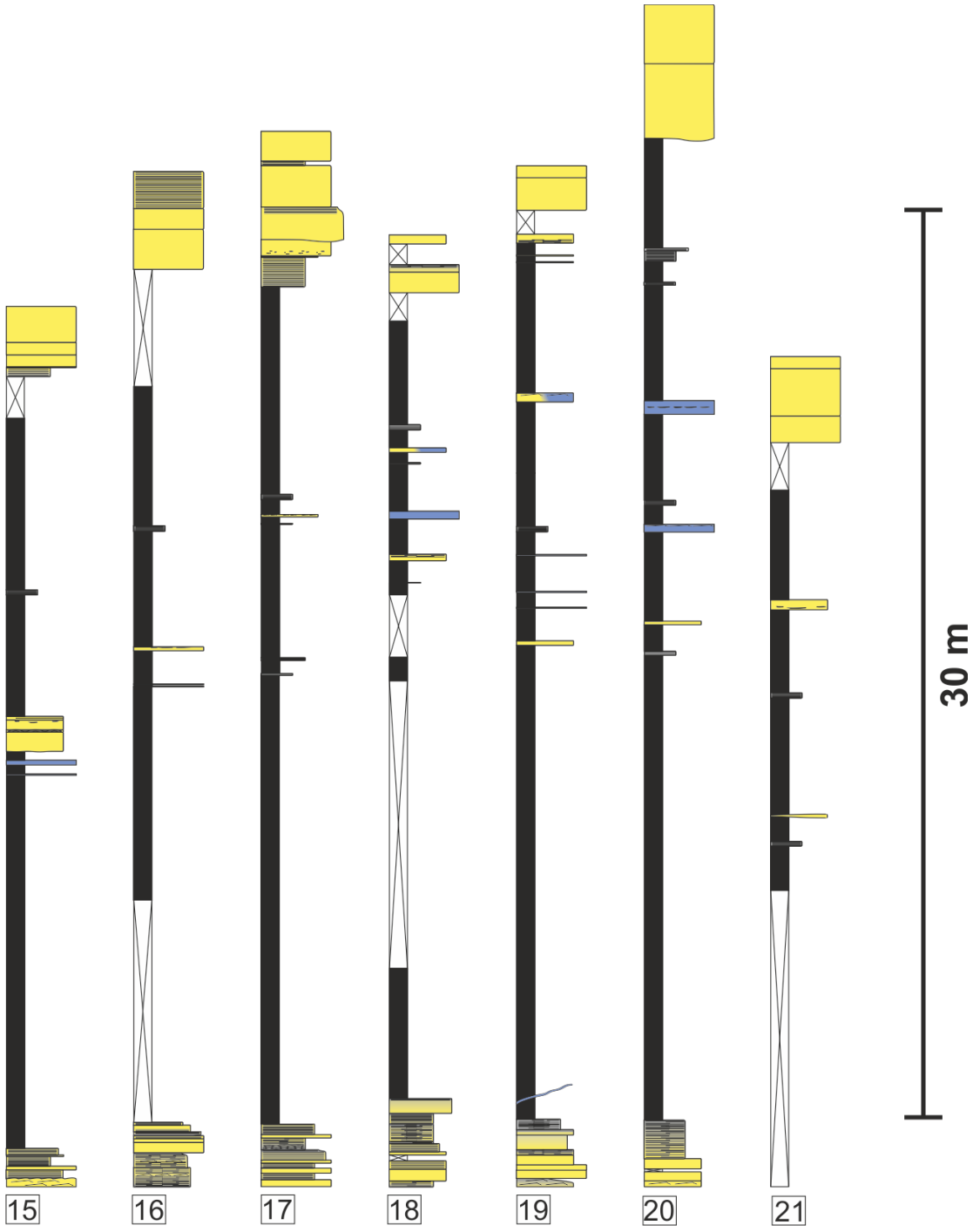


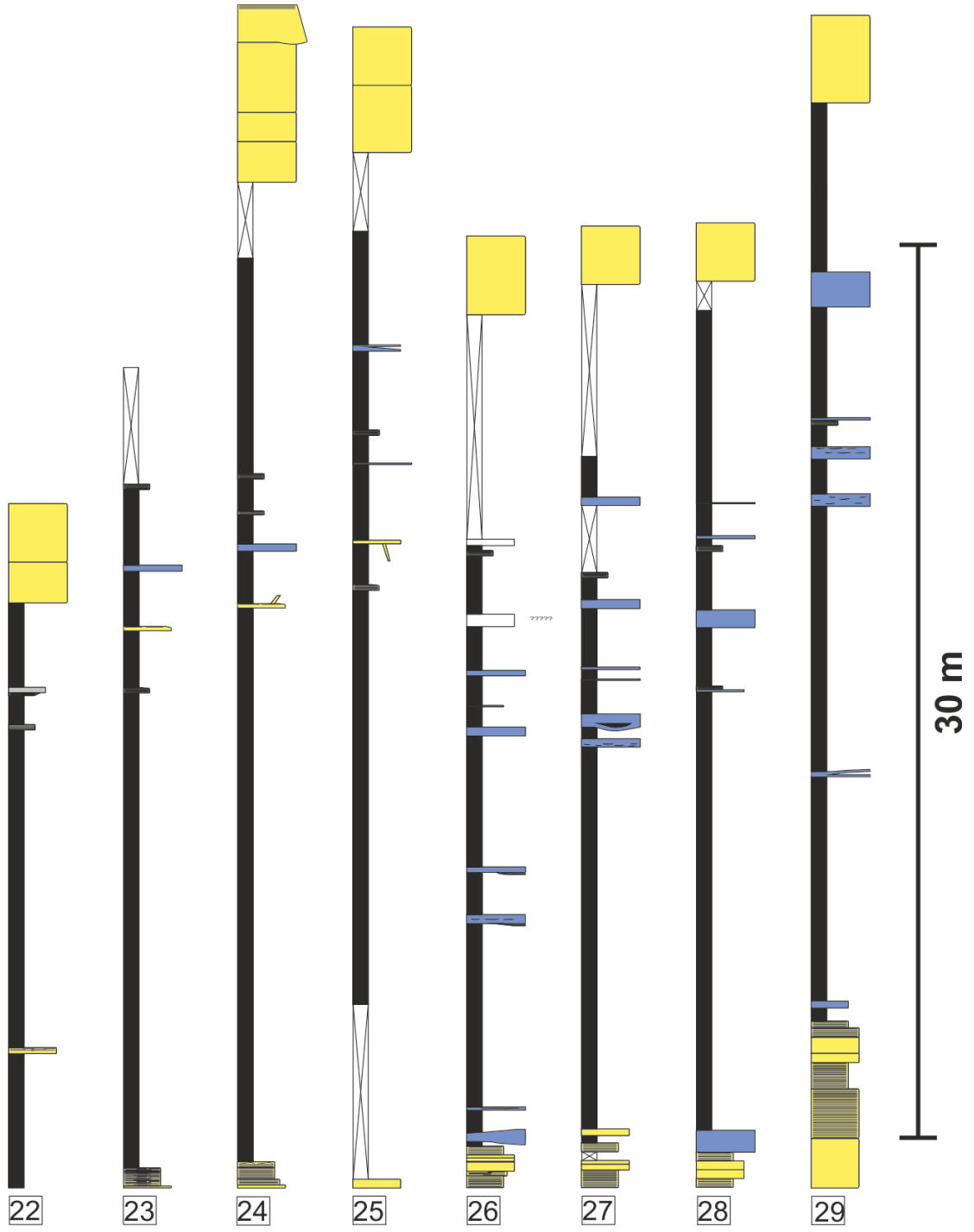
A.2 A/B shale and interfan, Laingsburg



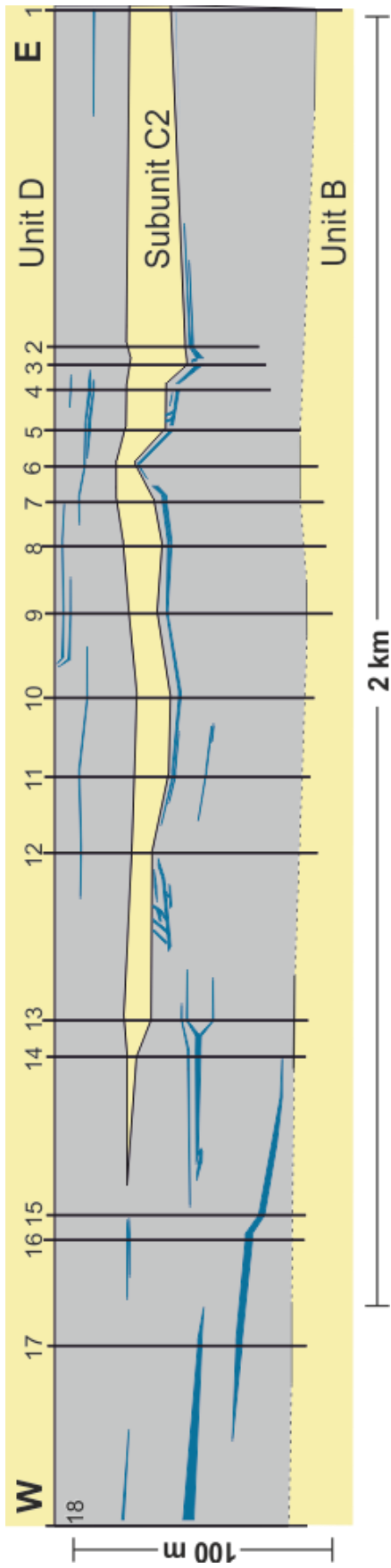


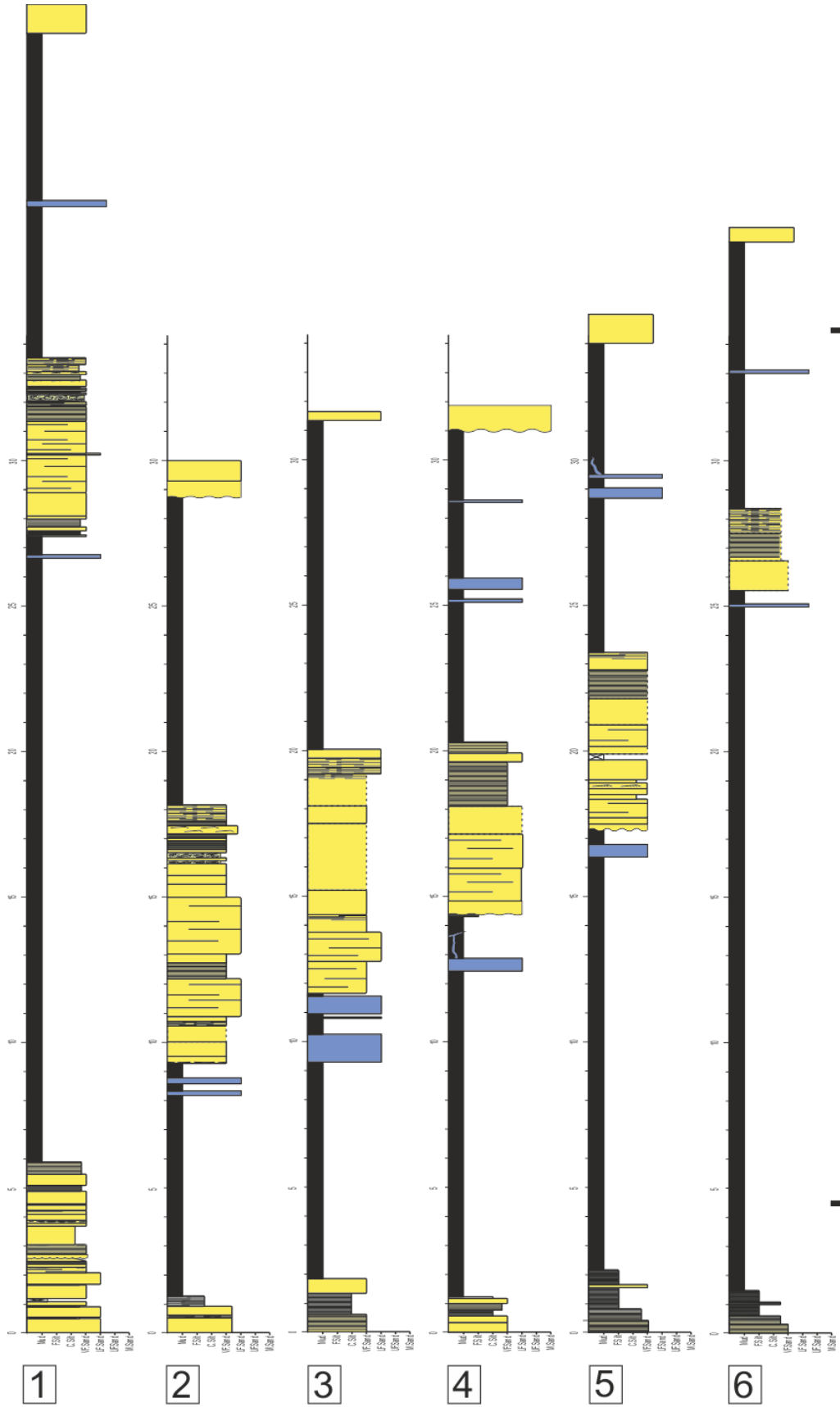


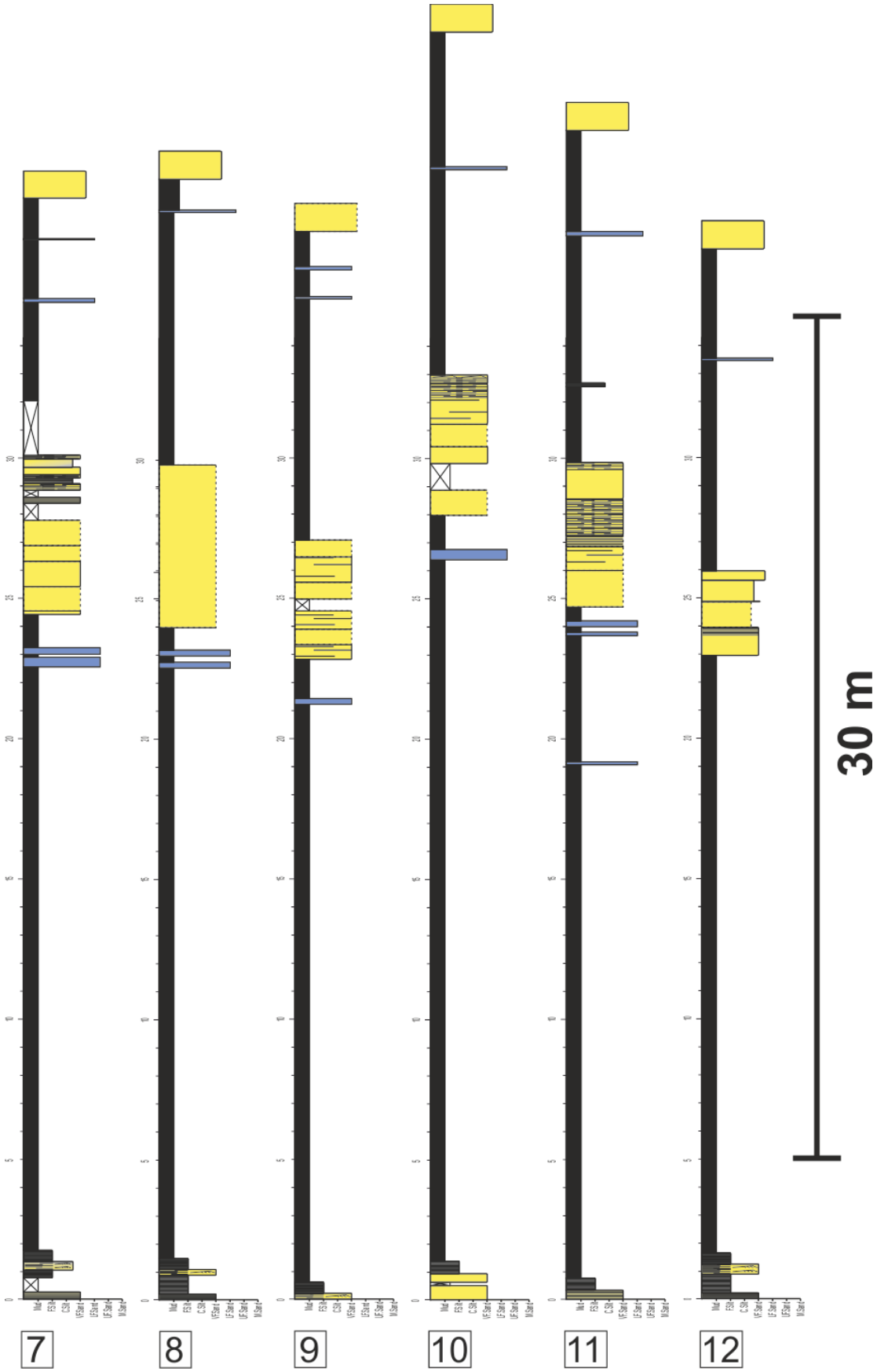


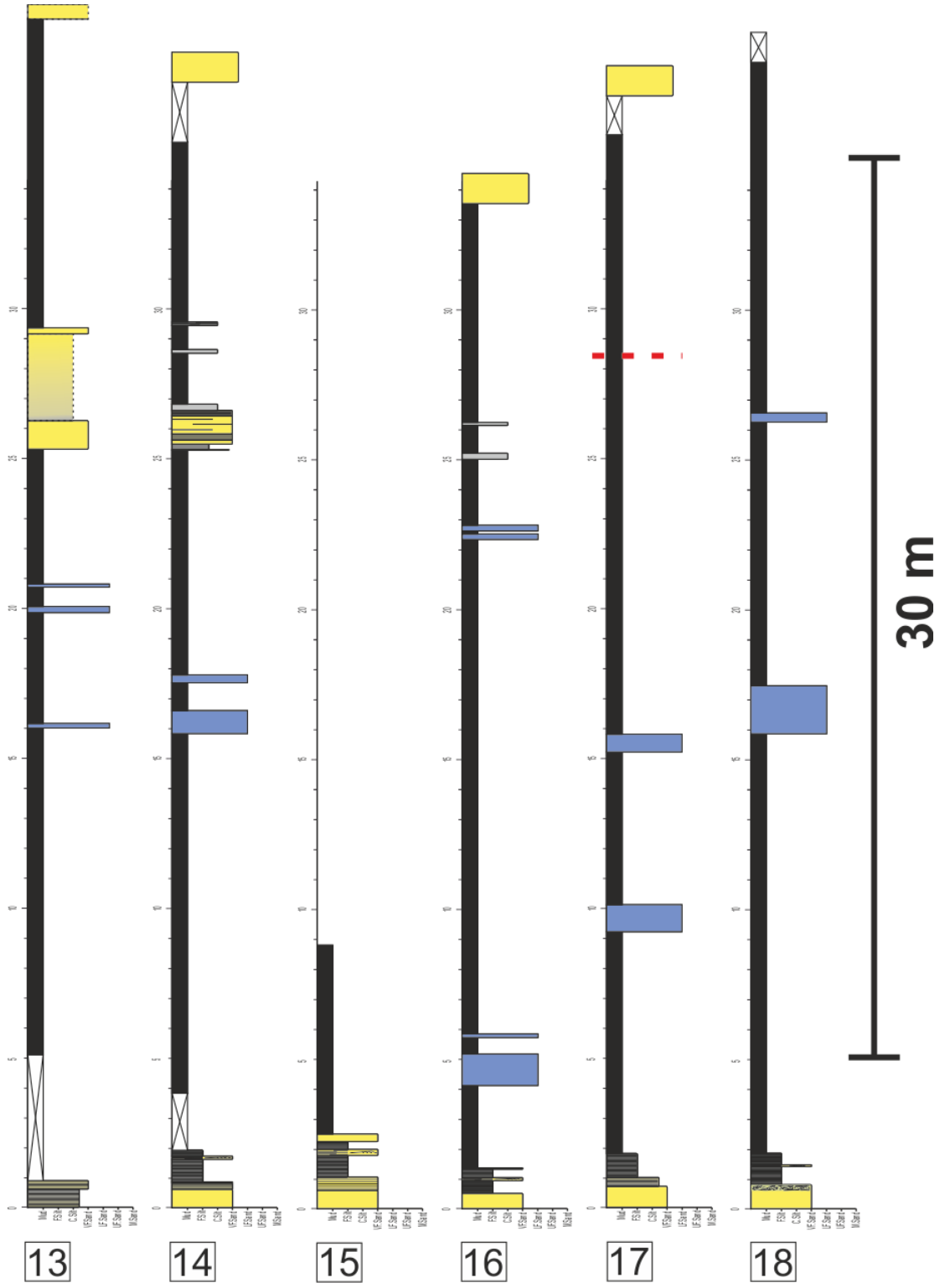


A.3 Slagtersfontein panel with logs

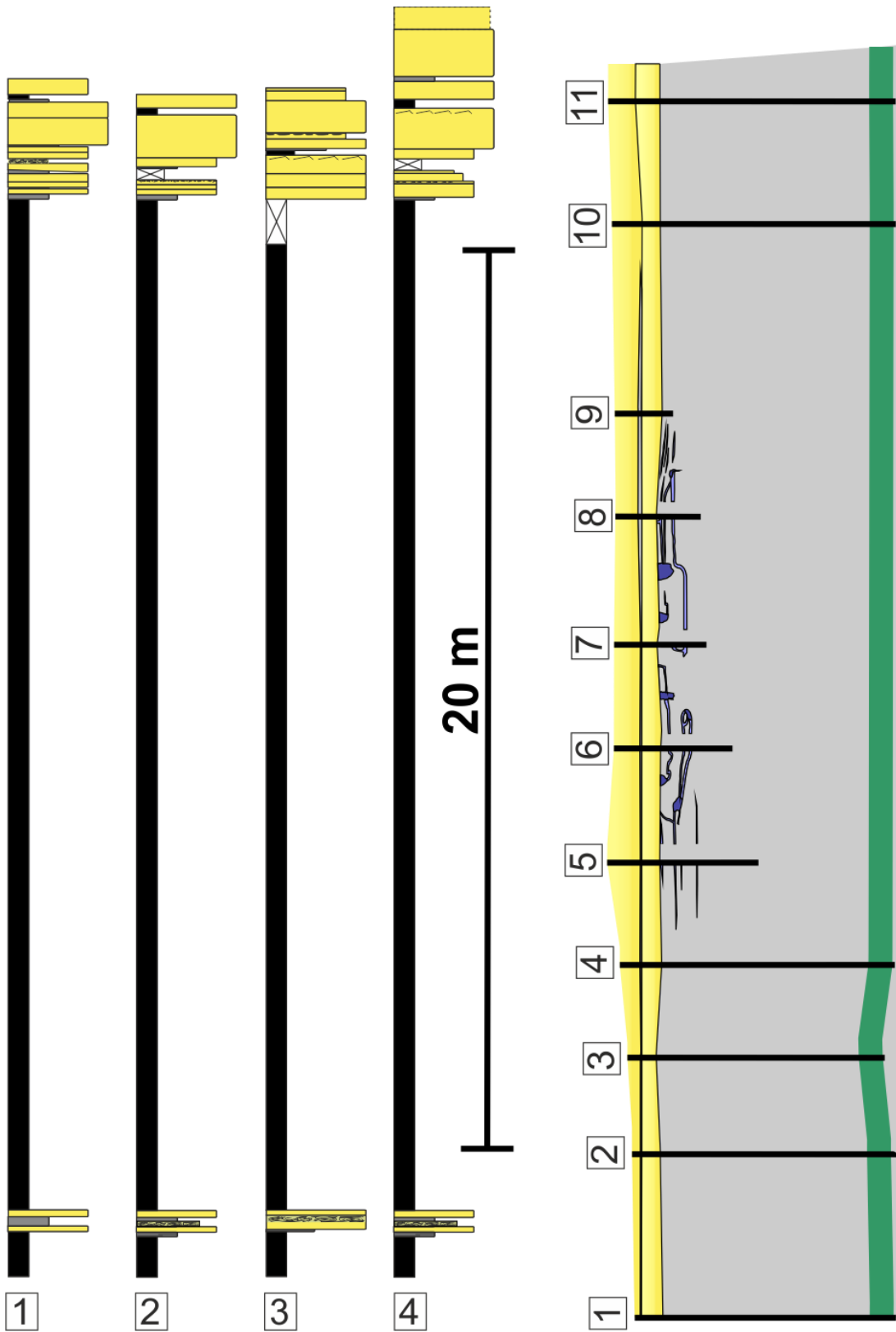


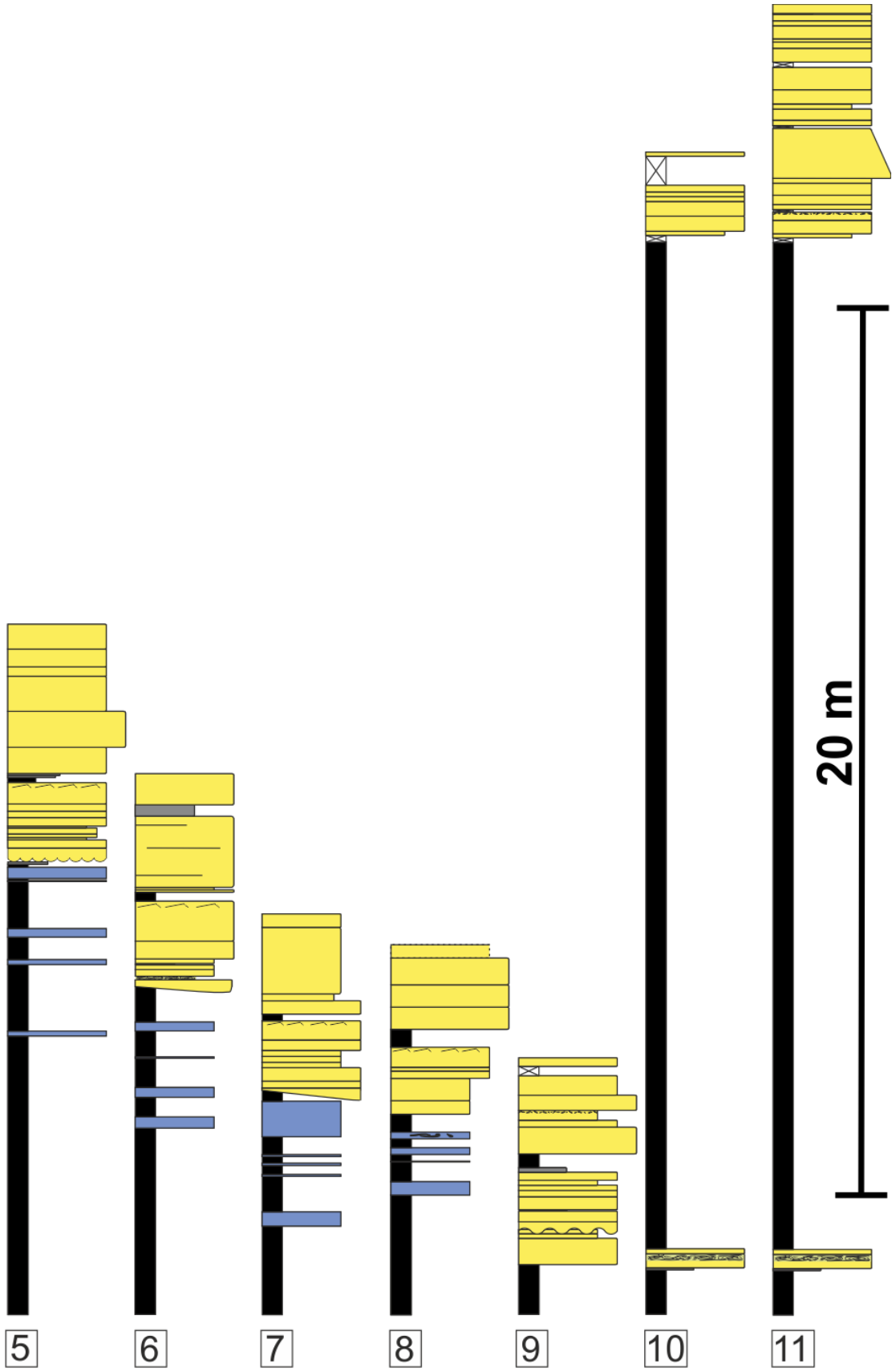






A.4 Geelbeck panel with logs





Appendix B

B.1 Reynolds number calculation

Values used			
A	0.1	m	Aperture of sill
D1	0.000125		
D2	0.044098168	Mudclast	Diameter of mud clast
g	9.81		
Ps(s)	2650	Kgm ⁻³	Small particles
Ps(L)	2100	Kgm ⁻³	Large particles
Pf	1000	Kgm ⁻³	
φ	0.54	0.3	0.15
φ1	0.53		Small particles
φ2	0.01		Large particles
CD0	1.4		
Dp	0.0125	cm	Small particles
Ds	0.0125	cm	Small particles
Dp2	3.6	cm	Large particles
Ds2	8	cm	Large particles
Pi	3.141592654		
μf	0.00106		

Calculations		
Dcross-section (m ²)	0.004	
radius of equivalent circle	0.035682482	$A = \pi r^2$ therefore $r = \sqrt{A/\pi}$
Dp	0.071364965	
Dvolume (m ³)	0.00004	
r ³ of equivalent sphere	9.5493E-06	$V = \frac{4}{3} \pi r^3$ therefore $r^3 = \frac{V}{(\frac{4}{3}) * \pi}$
r of equivalent sphere	0.022049084	

Ds of equivalent sphere	0.044098168	
Ks2 $(\pi/6)*(ds^2^3/dp^2^3)$	= 0.323544573	
2.7k2s^0.16	2.253996427	

Settling velocity equation calculation	
2n	5.532475982
$(1-\Phi)^{2n}$	0.013621214
$(\text{Rho}(L) - \text{Rho}(pf))gD$	93.73065696
$Cd * \text{Rho}(pf)$	40959.54168
main equation	3.11704E-05
$4/3 * \text{main equation}$	4.15605E-05
Settling velocity (ie square root)	0.006446746
Reynolds number	133.9384498

Reynolds number calculation with mudclasts		
	<i>Nomenclature</i>	<i>Equation used</i>
Shape factor (sand)	ks1	$(\pi/6)*(ds^3/dp^3)$
Shape factor (mud clast)	ks2	$(\pi/6)*(ds^2^3/dp^2^3)$
Function of particle shape (mud clast)	n2	2.7k2s^0.16
2n-2		
Drag coefficient (mud clast)	CD2	$CD0/((1-\phi_2)^{2n-2})$
ϕ_1^* (ϕ_s^* Equation 4: Ross et al. 2014)	ϕ_1^*	$\phi_1/(1-\phi_2)$
Pseudofluid density (Eq 3: Ross et al., 2014)	Ppf	$\phi_1^* \times Ps + (1-\phi_1^*) \times Pf$
Settling velocity (mud clast)	Ws2	$((4/3)*(((1-\phi_1-\phi_2)^{2n})*(Ps-Ppf)*g*D^2))^0.5/CD2*Ppf$
Pseudofluid viscosity	μ_{pf}	$\mu_f*(1-\phi_1^*)^{-2.8}$
Reynolds number (Mud clast)	Re	$(Ppf*Ws2*d)/\mu_{pf}$

Equation used	Results
$(\pi/6)*(ds^3/dp^3)$	0.523598776
$(\pi/6)*(ds^2^3/dp2^3)$	1.163552835
$2.7k2s^{0.16}$	2.766237991
	3.532475982
$CD0/((1-\phi_2)^{2n2-2})$	21.74842921
$\phi_1/(1-\phi_2)$	0.535353535
$\phi_1^* \times Ps + (1-\phi_1^*) \times Pf$	1883.333333
$((4/3)*(((1-\phi_1-\phi_2)^{2n})*(Ps-Ppf)*g*D2))^{0.5}/CD2*Ppf)$	0.006446746
$\mu_f*(1-\phi_1^*)^{-2.8}$	0.009064889
$(Ppf*Ws^2*d)/\mu_{pf}$	133.9384498

Tabulated data for D=0.05m			
ϕ	0.54	0.47	0.4
ϕ_1	0.53	0.46	0.39
ϕ_1^*	0.535353535	0.464646	0.393939
P_{fp}	1883.333333	1766.667	1650
$2n$	4.507992853	4.507993	4.507993
$(1-\phi)^{2n}$	0.030179686	0.057153	0.099979
$(\rho(L) - \rho(pf))gD$	93.73065696	144.201	194.6714
$Cd*\rho(pf)$	40959.54168	38422.22	35884.91
main equation	6.90623E-05	0.000214	0.000542
$4/3*main\ equation$	9.20831E-05	0.000286	0.000723
Settling velocity	0.009595995	0.016911	0.026892
μ_{pf}	0.009064889	0.006097	0.004308

Reynolds numbers for 0.05 cm particle				
		ϕ	ϕ	ϕ
		0.54	0.47	0.4
Aperture	0.1	199.3676657	490.0312	1030.01
Aperture	0.15	299.0514986	735.0467	1545.014
Aperture	0.2	398.7353314	980.0623	2060.019
Aperture	0.25	498.4191643	1225.078	2575.024
Aperture	0.3	598.1029972	1470.093	3090.029
Aperture	0.35	697.78683	1715.109	3605.033
Aperture	0.4	797.4706629	1960.125	4120.038
Aperture	0.45	897.1544957	2205.14	4635.043
Aperture	0.5	996.8383286	2450.156	5150.048
Aperture	0.55	1096.522161	2695.171	5665.052
Aperture	0.6	1196.205994	2940.187	6180.057
Aperture	0.65	1295.889827	3185.203	6695.062
Aperture	0.7	1395.57366	3430.218	7210.067
Aperture	0.8	1594.941326	3920.249	8240.076
Aperture	0.9	1794.308991	4410.28	9270.086
Aperture	1	1993.676657	4900.312	10300.1
Aperture	1.2	2392.411989	5880.374	12360.11
Aperture	1.3	2591.779654	6370.405	13390.12
Aperture	1.4	2791.14732	6860.436	14420.13
Aperture	1.5	2990.514986	7350.467	15450.14
Aperture	1.6	3189.882651	7840.499	16480.15
Aperture	1.7	3389.250317	8330.53	17510.16

B.2 Buffels River, Unit A5-A6 orientation data

Locality on panel	Parallel ridge	Plumose	Orientation of injectite
A	106-286		N/A
B		108/90	094/52 S
C	110		094/52 S
D1		45/148	N/A
D2		021/108	N/A
E	084-296		112/45 S
F		106	N/A
G		22/242	N/A
H		007	117/29 S
I		174	102/42 S
J		16/115	090/53 s
K	117		090/53 S
L	028/086-226		087/90
M		024	095/52 S
N	085		113/42 S
O		078	100/30 S

Unit A5 beds: 103/41S

Orientation layout

XXX-XXX bi-direction

XXX unidirection

XX/XXX dip/dip direction

XXX/XX strike/dip

Where parallel ridges have only 1 orientation, hackle marks were used as a direction indicator.

B.3 Zoutkloof orientation data

Bedding 100/10S

<i>Injectite</i>	<i>Type</i>				<i>Size</i>	<i>Direction/ bearing</i>	<i>Strike/dip injectite</i>
	Ridge	Plumose	Step	Dyke			
1		x			L	008	099/43S
	x					352	099/43S
	x					335	099/43S
	x					010	099/43S
	x			x		087/267	099/48S
	x					320/140	106/38S
2				x		110/290	110/90
	x					310/130	
3				x		212/022	022/75NW
		x				025	
1		x				300	098/35S
	x					050/230	098/35S
	x					120/300	115/75S
				x		100/280	
4			x			107/287	
	x					110/290	110/90
5			x			062/242	062/20S
1	x					110/290	horizontal
		x			S	266/086	
	x				L	247/067	
	x					280/100	100/45S
Feeder dyke		x			L	238	
5			x			308/128	
			x			242-062	062/90
	x					242-063	062/91
				x		246-066	
6 (Z30)	x				L	053-233	120/18S

		x			M	076	120/18S
		x			M	140	038/06S
		x			S	190	043/09S
		x			S	076	075/20S
		x			S	099	075/20S
	x					082-262	110/31N
7	x					142-322	142/68S
			x			012/192	012/30SE
	x					005-185	012/30SE
	x					102-282	horizontal
<i>Injectite</i>	<i>Type</i>				<i>Size</i>	<i>Direction/ bearing</i>	<i>Strike/dip injectite</i>
	Ridge	Plumose	Step	Dyke			
		x			VS	100	
	x				L	097-277	
				x		068-248	068/45N
	x					068-249	068/45N
	x					313-133	125/32SW
				x		162-342	
		x			M	311	107/35S
			x			124-304	124/50S
			x			106-286	rounded
	x					089-269	horizontal
			x			110-290	
			x			105-295	
8 (Z47)	x					150-330	060/28S
				x		156-336	156/58E
	x					050-230	156/58E
		x				244	
		x				112	
		x				180	
9	x					022-202	100/57sw
	x					032-212	100/57sw

B.4 Geelbeck data

Locality on panel	What it is	Orientation
A	sill	128/12NE
B	dewatered sands	
C	possible ridges on dykes	064-224
D	dykes connected to E2	155/90
E	possible ridges on dyke	
F	plumose on dyke or dewatering?	145
G	dyke complex	
H	flat sill	120/09NE
I	ridges/ptygmatic folding	078-248
J	mudclast surface	
J	circle dyke thing	
K	dyke complex to sill	
K	dyke complex to E	
L	folded dyke	
L	ridges on dyke?	
M	dyke complex	
M	ridges/plumose/dewatering	226
N	parallel ridges on dyke?	153-333
O	sill step	112-292
P	sill/dyke complex	
Q	sill end	
R	straight dyke	
S	ridges	
T5	base of sill burrows	
T1	burrows on sill with dyke marks	dykes 152-332
T2	burrows with positive relief	
T3	burrow with +ve relief on a dyke	
T4	burrow on dyke	
U1	burrows on sill	
U2	tube in sill	

V	margins	
W	burrows on sill	
W2	"parallel ridges"	027-207
Y-GB3	big vut from beds in E	
X	base of E2 erosive w/ injectites	
Y	erosive base E2 above injectites	
Z	burrows on parallel ridge on dyke	110-290
AA	burrows on injectites >1m below E	
AB	x-cutting burrows	
AB2	Burrows on sill	
AC	Guttermark base E 4 cm wide	124-304
AC2	Guttermark base E 14 cm wide	132-312
AD	Burrows base E	
AE	Burrows on dyke	
AF	Loading base E	
AG	NE pinchout of scour/channel	
AH	Plumose on step	between 182-150
AI	Sample collected	